AN ABSTRACT OF THE THESIS OF

Bohumil Kasal for the degree of Doctor of Philosophy in Forest Products presented on March 10, 1992.

Title: A Nonlinear Three-Dimensional Finite-Element Model of a Light-Frame Wood Structure

Signature redacted for privacy.

Abstract approval: _____
Robert J. Leichti

The light-frame wood structure is an assemblage of several components such as walls, floors and roof connected by intercomponent connections such as nails or metal plates. The behavior of the full-structure is determined by the behavior of the individual components and connections. Whereas individual substructures were investigated both experimentally and analytically, there is a lack of research aimed to incorporate individual components of the light-frame wood building into the full-structure model. This research provides an analytical tool to investigate the behavior of light-frame wood structures loaded by static loads. Special attention is given to load sharing among wall components.

A one story, 16- by 32-ft (4.88- by 9.75-m) wood-frame building was tested under cyclic quasi-static loads. Results of the experiment were used to verify a nonlinear finite-element model of the full building.

Concepts of superelements and substructuring are applied to the finite-element problem. A special quasi-superelement energetically equivalent to a three-dimensional finite-element model of the full substructure was developed to represent the walls. Intercomponent connections were transformed into one-dimensional nonlinear elements, which had properties obtained from experiments and detailed finite-element analyses.

The full structure was an assemblage of the superelements representing floor and roof, and quasi-superelements, which represented walls and intercomponent connections. Boundary conditions and loads used in the experiment were applied to the model, and deformations and reaction forces were compared.

A sensitivity study of the model was performed, and the influences of the properties of substructures and intercomponent connections on the load sharing capability of the model were investigated.

The response of the three-dimensional model of the full-structure to the static wind loads was studied and compared with currently used analytical models. Linear and nonlinear analytical models for computing reaction forces in the shear walls were proposed and their sensitivity studied.

Stress analysis of the three-dimensional substructure was performed when the full model was loaded by a combination of dead, snow and wind load. Use of tensorial strength criteria as a part of the postprocessing procedure was demonstrated on evaluation of stresses in plywood sheathing.

A NONLINEAR THREE-DIMENSIONAL FINITE-ELEMENT MODEL OF A LIGHT-FRAME WOOD STRUCTURE

by

Bohumil Kasal

A THESIS

submitted to

Oregon State University

in partial fulfillment of
the requirements for the
degree of

Doctor of Philosophy

Completed March 10, 1992

Commencement June 1992

APPROVED:

Signature redacted for privacy.

Assistant Professor of Forest Products in charge of major

Signature redacted for privacy.

Chair of Department of Forest Products

Signature redacted for privacy.

Dean of Graduate School

Date thesis is presented March 10, 1992

Typed by Bohumil Kasal for Bohumil Kasal

ACKNOWLEDGMENTS

I wish to express my sincere thanks to my major professor Dr. Robert J. Leichti for his advice, guidance and support. I would like to acknowledge the direction lent by the late Dr. Anton Polensek.

I owe many thanks to my colleagues and friends Min Wang and Kevin and Cath Groom who assisted me in numerous ways.

Finally my love and gratitude are due to my parents Miloslava and Jiri Kasal and to my wife Dana for their support and patience throughout the course of my study.

This research was funded by the Forest Research Laboratory, Oregon State University and by the U.S. Department of Agriculture, Competitive Grants Program in Wood Utilization, Grant No. 88-33521-4079.

TABLE OF CONTENTS

1. INTRODUCTION 1

2. LITERATURE REVIEW 6
   Wood Stud Walls 6
   Floor 10
   Roof 13
   Joints and Intercomponent Connections 15
   Full-Structure Testing and Analysis 17
      Full-Scale Tests 17
      Earlier analytical models 19
   Summary 21

3. THE FULL STRUCTURE 23
   Design of the Structure 23
      Walls 23
         Framing 23
         Sheathing 25
      Floor 25
      Roof 29
   Experimental Investigation 32
      Test Objectives 32
      Testing Procedures 32
   Summary 36

4. FINITE-ELEMENT MODELS OF SUBSTRUCTURES 37
   Background 37
   Walls 42
      Detailed Substructure 43
         Material and Connection Properties . . . 44
         Verification of the Modeling Method . . 51
            Bearing Walls Tested by Polensek . 52
            Nonbearing Walls Tested by Polensek 57
            Experiments Performed in Shear . . 58
      Equivalent Substructure 63
         Shear resistance 65
         Out-Of-Plane Stiffness 70
         Compression in the Stud Direction . . . 75
         Equivalent Model Verification 76
         Generation of the Characteristic Properties for Equivalent Models . 80
            Shear Stiffness 82
            Bending Stiffness 92
            Axial Stiffness 95
            Additional Bending and Axial Stiffness 95
         Comments on Equivalent Model of Walls . 97
   Roof 99

Floor 102
Model of the Orthotropic Plate 102
Summary 108

5. INTERCOMPONENT CONNECTIONS 110
Partition-to-Exterior Wall Connection 112
Connection in the Wall Field 112
Connection Between Top Plate of the Partition Wall and Exterior Wall 117
Corner Connection between Exterior Walls 122
Connection between Sole Plate and Floor 122
Walls 1 through 4 127
Walls 5 and 6 132
Connection Between Walls and Roof Superelement . . 136
Summary 141

6. FULL STRUCTURE MODEL 142
Objectives of the Model 142
Assembly of the System 142
Total Assembly 143
Walls 146
Floor 146
Roof 147
Intercomponent Connections 147
Boundary Conditions 148
Model Verification 148
Loading 148
Case 1: 1200 lb (5.33 kN) on Walls 1 and 2 . 149
Case 2: 1800 lb (8 kN) on Walls 3 and 4 . . . 154
Case 3: 7000 lb (32.0 kN) Applied to Walls 1 through 4 159
Summary 167

7. SENSITIVITY STUDY 168
Influence of Wall Stiffness on Load-Sharing Capability of the Structure 169
Shear Stiffness 169
Bending Stiffness 171
Connection between Roof Diaphragm and Walls . . . 173
Intercomponent Connection between Walls 180
Walls-To-Floor Connection 180
Summary 183

8. SIMPLIFIED ANALYTICAL MODELS FOR COMPUTATION OF SHEAR REACTION FORCES . . . 184
Shear Forces Induced by Wind 185
Analytical Solutions Incorporating Wall Stiffness 188
APA Estimate of Wall Stiffness 188
Development of the Rigid-Beam Model 190
Nonlinear Spring Model 193
Linear Spring Model 197
Summary 200

9. LOAD COMBINATION AND ANALYSIS OF SUBSTRUCTURES . . . 201
Analysis of Wall 1 202
Framing 202
Sheathing 209
Nails 222
Summary 229

13. CONCLUSIONS 230

12. BIBLIOGRAPHY 233

APPENDIX A. Drawings of the Experimental Building . . . 249

APPENDIX B. Finite-Element Meshes of the Sustructures . 275

APPENDIX C. Computer Program for the Solution of
Material Properties of an Orthotropic Plate . . . 295

APPENDIX D. Finite-Element Formulation of Some Elements
Used for the Full Structure Model 302

LIST OF FIGURES

Figure		Page
1	Three-Dimensional View of the Experimental Structure (Philips, 1990).	24
2	Position of the Load Cells Recording Reaction Forces.	26
3	Typical Framing of the Wall in the Experimental Building - Wall 1.	27
4	Construction of Floor (a) Framing, (b) Sheathing.	30
5	A Typical Roof Truss.	31
6	Schematic of the Test Specimen for Nail Connection Tested in Shear.	33
7	Schematic of the Deformation and Force Measurement in a Shear Wall.	35
8	Finite-Element Mesh of the Wall 1, (a) Framing and (b) Sheathing.	45
9	Load-Deformation Characteristics for Nail Connections Loaded in Shear (Phillips, 1990). . .	48
10	Comparison of Load-Deformation Curves for Connection of Plywood 3/8-1/2 in. Thick and Douglas-Fir Wood Loaded in Shear.	49
11	Load-Deformation Characteristics for Nail Connections Loaded in Withdrawal (Groom, 1992). .	50
12	Finite-Element Mesh of the Wall Panel Tested by Polensek (1975) and Used for the Model Verification. The Studs are Shown with Typical Mesh for Sheathing in the Left Corner. (a) Undeformed Mesh and (b) Deformed Mesh.	53
13	Experimental and Analytical Results for Bearing Wall Tested by Polensek (1975), (a) Bending Deformation at the Wall Mid Stud and (b) Shear Deformation at the Top Plate.	55

Figure		Page
14	Stress, σ_y, and Strain, ϵ_y, for a Stud in the Wall Loaded by Axial Force and Pressure, Tested by Polensek (1975) and Modeled by Using Finite-Elements.	56
15	Experimental and Analytical Results for Nonbearing Wall Tested by Polensek (1975); (a) Bending Deformation at the Mid Height of the Center Stud and (b) Shear Deformation at the Top Plate. . . .	59
16	Finite-Element Mesh of Wall Tested by Easley et al (1982) and Used for the Model Verification. (a) Framing, (b) Sheathing.	60
17	Shear-Deformation of the Wall Tested by Easley et al (1982).	61
18	Influence of the Stiffness of Nail Connections and Presence of Gaps on Shear Resistance of Wall 4. .	62
19	Finite-Element Representation of the Equivalent Model of the Wall 1.	64
20	Experimental and Analytical Results for Bearing Wall Tested by Polensek (1976a) and Loaded by Axial Forces and Pressure. Verification of the Equivalent Model.	79
21	Effect of the Finite-Element Mesh Size on the Accuracy of the Equivalent Model Loaded in Bending.	81
22	Example of the Nail Joint Subjected to Cycled Loading (Chou, 1987).	83
23	Generation of the Characteristic Load-Deformation Curves for Shear Stiffness of the Equivalent Models of (a) Wall 1 and (b) Wall 2, where the Envelopes Are Experimental Data by Phillips (1990).	85
24	Generation of the Characteristic Load-Deformation Curves for Shear Stiffness of the Equivalent Models of (a) Wall 2 and (b) Wall 3, where the Envelopes Are Experimental Data by Phillips (1990).	86
25	Characteristic Load-Deformation Curves for Nonlinear Diagonal Springs, (a) Experimental and (b) Analytical.	88

Figure		Page
26	Load-Displacement Curves for (a) Nail Connection Between Sheathing and Studs Used as the Input for Detailed Wall Models and (b) Shear Walls with Different Nail Connections.	90
27	Load-Deformation Curves for Stiffness of the Shear Walls. (a) Walls 1 and 2 and (b) Walls 3 and 4. . .	91
28	Finite-Element Mesh of the Roof Truss. (a) Single Truss and System, (b) Sheathing, (c) Deflected truss.	101
29	Finite-Element Mesh of the Floor Superelement (a) Framing, and (b) Sheathing.	103
30	Composite T-Section Representing an Effective Breadth Approach.	106
31	Detail of the Connection Between Partition Wall and Exterior Walls and its Finite-Element Representation.	113
32	Stiffness in Global X-Direction of the Connection between Partition and Exterior Wall per Unit Height of the Wall. Curves are Identical for Walls 2 and 3 Connected to Walls 5 and 6.	116
33	Stiffness in Global Z-Direction of the Connection between Partition and Exterior Wall per Unit Height of the Wall, (a) Wall 2, and (b) Wall 3. .	118
34	Connection between Top Plates of Partition and Exterior Walls and its Finite-Element Representation. Dimensions are in Inches.	119
35	Load-Displacement Curves for Interior-to-Exterior Wall Connection. (a) Separation Stiffness and (b) Rotational Stiffness (Groom, 1992).	121
36	Connection between Exterior Walls. Test Fragment was 12 in. Deep.	123
37	Finite-Element Mesh of the Model of Corner Connection (Groom, 1992).	124
38	Load-Deformation Curve for the Corner Connection Loaded in (a) x-Direction and (b) z-Direction (Groom, 1992).	125

Figure Page

39 Load-Deformation Curve for the Corner Connection Loaded by Moment (a) Moment-Rotation and, (b) Force-Displacement Relationship (Groom, 1992). . . 126

40 Degrees of Freedom Used to Describe Wall-to-Floor Connection. 128

41 Load-Deformation Characteristics for the Connection Between Walls and Floor Loaded in Shear. 130

42 Load-Deformation Characteristics for Withdrawal Stiffness of the Connection Between Walls and Floor. 131

43 Model of the Rotational Stiffness of the Connection Between Sole Plate of the Interior Wall and Floor. 133

44 Finite-Element Mesh of the Connection between Exterior Walls and Floor. 134

45 Load-Displacement Curves for the Connection between Exterior Wall and Floor for a Segment 12 in. Long (a) Withdrawal and (b) Rotation (Groom, 1992). 135

46 Finite-Element Mesh of the Connection between Roof and Top Plate of the Wall (Groom and Leichti, 1991). 137

47 Load-Deformation Curve for Connection between Roof Truss and Walls. Sliding of the Truss (a) along and (b) across the Top Wall Plate (Groom, 1992). . 138

48 Load-Deformation Curve for Connection between Roof Truss and Walls. Rotation (a) Out-of-Plane and (b) In-Plane of the Truss (Groom, 1992). 139

49 Uplift of the Roof Truss Connected to the Wall Top Plate (Groom, 1992). 140

50 A Conceptual Schematic of the Finite-Element Model of the Full Structure Showing Essential Degrees of Freedom. 144

51 Finite-Element Mesh of the Full-Structure, (a) Mesh 1 with the Roof Truss and (b) Mesh 2 with no Roof Truss Plotted. 145

Figure		Page
52	Full Model Verification with the Load Applied to Walls 1 and 2, (a) Reaction Force and (b) Deformation for Wall 1.	150
53	Full Model Verification with the Load Applied to Walls 1 and 2, (a) Reaction Force and (b) Deformation for Wall 2.	151
54	Full Model Verification with the Load Applied to Walls 1 and 2, (a) Reaction Force and (b) Deformation for Wall 3.	152
55	Full Model Verification with the Load Applied to Walls 1 and 2, (a) Reaction Force and (b) Deformation for Wall 4.	153
56	Full Model Verification with the Load Applied to Walls 3 and 4, (a) Reaction Force and (b) Deformation for Wall 1.	155
57	Full Model Verification with the Load Applied to Walls 3 and 4, (a) Reaction Force and (b) Deformation for Wall 2.	156
58	Full Model Verification with the Load Applied to Walls 3 and 4, (a) Reaction Force and (b) Deformation for Wall 3.	157
59	Full Model Verification with the Load Applied to Walls 3 and 4, (a) Reaction Force and (b) Deformation for Wall 4.	158
60	Full Model Verification with the Load Applied to Walls 1 through 4, (a) Reaction Force and (b) Deformation for Wall 1.	161
61	Full Model Verification with the Load Applied to Walls 1 through 4, (a) Reaction Force and (b) Deformation for Wall 2.	162
62	Full Model Verification with the Load Applied to Walls 1 through 4, (a) Reaction Force and (b) Deformation for Wall 3.	163
63	Full Model Verification with the Load Applied to Walls 1 through 4, (a) Reaction Force and (b) Deformation for Wall 4.	164
64	Deformation of the Top Corners of the Shear Walls Loaded by 7000-lb (32-kN) Force at the Top of Each Wall.	166

Figure		Page
65	Reaction Forces for Different Wall Shear Stiffness Ratios where a 10000-lb Load is Applied at the Top Corner of Wall 1.	170
66	Effect of the Wall Shear Stiffness on Load-Sharing among Shear Walls for the Structure under Wind Load.	172
67	Influence of Bending Stiffness of Long Walls on Load-Sharing Capability of the Structure When a 10000-lb Load is Applied at the Top Corner of Wall 1 in the Finite-Element Model.	174
68	Influence of Bending Stiffness of Long Walls (Walls 5 and 6) on Load-Sharing among Shear Walls when the Model was Loaded by Wind Load (Pressure on Wall 5, Suction on Wall 6).	175
69	Influence of the Roof Connection Stiffness on Load-Sharing among Shear Walls when 10000-lb Load Was Applied to the Top Corner of the Wall 1. . . .	177
70	Influence of the Roof Connection Stiffness on Deformation at the Top Corner when 10000-lb Load Was Applied to the Top Corner of the Wall 1 in the Finite-Element Model.	178
71	Influence of the Roof Connection Stiffness on Load-Sharing among Shear Walls for Wind Load. . .	179
72	Influence of the Different Stiffness of Connections between Walls on Load Sharing for Model Loaded by 10000 lb Applied at the Top Corner of Wall 1.	181
73	Influence of the Connection between Walls and Floor on Load-Sharing Capability of the Model when 10000-lb Load Was Applied at the Top Corner of Wall 1.	182
74	Input Shear Wall Stiffness used for the Analytical Model, (a) Experiment and (b) APA Formula.	191
75	Model of the Rigid Beam on Elastic Supports. . .	195
76	Loads Applied to the Finite-Element Model of the Full Structure.	203
77	Deformed Finite-Element Mesh of the Structure Loaded by a Combination of Wind, Dead, and Snow Load.	204

Figure		Page
78	Stress Contours for σ_y (psi) at the Midpoint of the Stud No. 7 in Wall 1.	206
79	A Vector Representation of the Framing Deformation in Wall 1.	207
80	Deformation of the Framing in Wall 1 (200x). . . .	208
81	Stress σ_x (psi) for the Plywood Sheathing of Wall 1, Stress Contours for (a) Full Wall and (b) Left Lower Window Corner.	210
82	Stress σ_y (psi) for the Plywood Sheathing of Wall 1, Stress Contours for (a) Full Wall and (b) Left Lower Window Corner.	211
83	Stress σ_{xy} (psi) for the Plywood Sheathing of Wall 1, Stress Contours for (a) Full Wall and (b) Left Lower Window Corner.	212
84	Stress σ_x (psi) in Gypsum Sheathing of Wall 1, Stress Contours for (a) Full Wall and (b) Left Upper Window Corner.	213
85	Stress σ_y (psi) in Gypsum Sheathing of Wall 1, Stress Contours for (a) Full Wall and (b) Left Upper Window Corner.	214
86	Stress σ_{xy} (psi) in Gypsum Sheathing of Wall 1, Stress Contours for (a) Full Wall and (b) Left Upper Window Corner.	215
87	Contours for the Values of the Strength Theory Function of the Tensorial Strength Criteria for Plywood Sheathing of the Wall 1.	220
88	Values of the Strength Theory Function for Plywood Sheathing of Wall 1 as a Function of the Position.	221
89	Finite-Element Mesh of (a) Plywood and (b) Gypsum Sheathing of Wall 1.	224
90	Nail Connection Forces in Global X-Direction between Framing and (a) Plywood, (b) Gypsum Sheathing.	225

Figure Page

91 Nail Connection Forces in Global Y-Direction between Framing and (a) Plywood, (b) Gypsum Sheathing. 226

92 Nail Connection Forces in Global Z-Direction between Framing and (a) Plywood, (b) Gypsum Sheathing 227

LIST OF TABLES

Table		Page
1	Nailing Schedules and Sheathing Used for Construction of Walls	28
2	Element Types and Element Material Properties Used for Wall Modeling	46
3	Loading and Boundary Conditions for Plate	72
4	Solutions for the Load Cases given in Table 3	74
5	Input and Results for the Plate 1-in Thick Used to Represent the Nonbearing Stud Wall Tested by Polensek (1975)	77
6	Properties of Orthotropic Plates Representing Wall Bending Stiffness	93
7	Comparison between Properties of a Segment and Full Wall for Wall 4	94
8	Example of the Generation of Geometric Input Parameters for Wall 1	96
9	Elastic Material Properties Used for the Analysis of the Connection Between Partition and Exterior Walls	114
10	Nails Used for Soleplate-to-Floor Connection for Walls	127
11	Shear Capacity for Walls Based on Uniform Building Code	186
12	Wind Load on the Complete Structure according to the Uniform Building Code (ICBO, 1988)	187
13	Wind Pressures on the Building Used for the Design Example	189

Table | Page

14 Comparison between Shear Reaction Forces in Walls Obtained from Proposed Models and Current Design Procedure 192

15 Strength Properties of Douglas-Fir Plywood Estimated from Plywood Design Specifications (APA, 1989) 217

16 Forces and Deformations for Nail Connections between the Framing and Sheathing for Wall 1 . . 229

LIST OF APPENDIX FIGURES

Figure		Page
A1	Three-Dimensional View of the Experimental Structure (Phillips, 1990)	250
A2	Framing of Wall 1	251
A3	Plywood Sheathing of Wall 1	252
A4	Gypsum Sheathing of Wall 1	253
A5	Framing of Walls 2 and 3	254
A6	Plywood Sheathing of Wall 2	255
A7	Gypsum Sheathing of Wall 3	256
A8	Framing of Wall 4	257
A9	Plywood Sheathing of Wall 4	258
A10	Gypsum Sheathing of Wall 4	259
A11	Framing of Wall 5	260
A12	Plywood Sheathing of Wall 5	261
A13	Gypsum Sheathing of Wall 5	262
A14	Framing of Wall 6	263
A15	Plywood Sheathing of Wall 6	264
A16	Gypsum Sheathing of Wall 6	265
A17	Floor, (a) Framing and (b) Sheathing	266
A18	A Typical Roof Truss	267
A19	Plywood Sheathing of the Roof	268
A20	Gypsum Sheathing as Attached to the Bottom Truss Chords	269
A21	Load Cells between Floor and Walls 1 through 4	270
A22	Connection between Walls and Roof	271

Figure		Page
A23	Connection between Floor and Wall 1 and 4	272
A24	Connection between Floor and Partition Walls	273
A25	Connection between Floor and Walls 5 and 6	274
B1	Finite-Element Mesh of Wall 1, (a) Framing and (b) Sheathing.	276
B2	Finite-Element Mesh of Walls 2 and 3, (a) Framing and (b) Sheathing.	277
B3	Finite-Element Mesh of Wall 4, (a) Framing and (b) Sheathing	278
B4	Finite-Element Mesh of the Framing of Wall 5	279
B5	Finite-Element Mesh of the Sheathing of Wall 5, (a) Gypsum and (b) Plywood	280
B6	Finite-Element Model of Framing of Wall 6	281
B7	Finite-Element Mesh of the Sheathing of Wall 6, (a) Plywood and (b) Gypsum	282
B8	Finite-element Mesh of the Roof Truss	283
B9	Finite-element Mesh of the Roof Sheathing	284
B10	Finite-Element Mesh of the Floor Framing	285
B11	Finite-Element Mesh of the Floor Sheathing	286
B12	Finite-Element Mesh of an Equivalent Model of Wall 1	287
B13	Finite-Element Mesh of an Equivalent Model of Walls 2 and 3	288
B14	Finite-Element Mesh of an Equivalent Model of Wall 4	289
B15	Finite-Element Mesh of an Equivalent Model of Wall 5	290

Figure Page

B16 Finite-Element Mesh of an Equivalent Model of Wall 6 291

B17 Coarse Finite-Element Mesh of the Full-Structure 292

B18 Refined Finite-Element Mesh of the Full-Structure 293

B19 Finite-Element Mesh of the Floor Modeled as an Orthotropic Plate 294

A NONLINEAR THREE-DIMENSIONAL FINITE-ELEMENT MODEL OF A LIGHT-FRAME WOOD STRUCTURE

1. INTRODUCTION

Residential and low-rise wood-frame structures represent a large percentage of the total buildings constructed in the United States. In 1989, about 196.0 billion dollars was spent on residential construction, which is about 46% of the total investment for new construction (Anonymous, 1990). According to Haynes (1989) the demand for new housing units steadily increases, although the rate varies from year to year. The statistical surveys and available research results document the importance of light wood-frame structures in the US economy. Furthermore, pressure is continually increasing to effectively utilize the fiber resource through material development and efficient design of wood structures.

The light-frame wood structure is an assemblage of several components - substructures such as walls, floors and roof connected by intercomponent connections such as nails or metal plates. The substructures consist of simple frames made of lumber of differing cross-sections and sheathed with various composite materials such as plywood, oriented strandboard or fiberboard.

Walls transfer vertical loads from the roof and floors above them, bending loads caused by wind pressure or earthquakes, and in-plane shear forces to the foundation. The common cross-section of the wood framing is 2×4 in. nominal (38×89 mm), but other cross-sections are possible. The members, called studs, are usually vertically oriented

and spaced 16 or 24 in. (406 or 610 mm) on center. Nails of different sizes and spacing are used to connect the studs and sheathing to the studs.

Floors are made from wood joists whose size and spacing is designed to sustain expected loads. The joists are sheathed by plywood or wood composites nailed to them. The function of the floor is to support the walls, and transfer all possible lateral loads to the foundation. The stud walls are connected to the floor joists through the lower horizontal member, the sole plate, via nails.

Different roof constructions, ranging from rafter systems to prefabricated trusses are used. The roof is connected to walls through nails or special steel anchors. Loads acting on the roof must be safely transferred into the walls.

Current design procedures for light-frame wood structures are mostly based on test data and knowledge of the behavior of wood and fasteners. Little attention is paid to the interaction between different substructures and consequent load distribution, which is a function of tributary area and the stiffness relationships. The design process is limited to the individual components such as floor joists, or columns, and little attention is paid to the interaction between components. This can lead to a structure with both overdesigned and underdesigned substructures.

To analyze the load distribution within the complete building, an analytical model of the complete structure must be developed because no closed-form solution is available. This requires a three-dimensional model, which may be complex. Use of wood and wood composites along with the metal connections in the light-frame structure creates a system highly influenced by the properties of individual components. The high variability of mechanical properties of wood and their dependency on environmental conditions such as relative humidity and temperature of the air require specific approaches in the analysis and design. Wood as a

heterogeneous material possesses different material properties in different directions. The structure of wood consisting of different cells oriented along as well across the tree axis leads to the anisotropic character of wood. The anisotropy is usually simplified by defining wood as an orthotropic material. This results in different properties with respect to the direction of interest.

The mechanical properties along the fibers can be interpreted as linear, whereas these across the fibers can be regarded linear in tension and can be simplified as bilinear in compression. A similar situation exists in wood composites, where two principal directions in the plane are usually recognized and the change of the properties through the thickness is neglected.

Wood framing is connected to other components via nails or metal connectors. The behavior of the connections is nonlinear and the load-deformation curve varies with the load direction. Moreover, gaps are often present between members in the light-frame wood building. Gaps between any two components of the structure represent another source of nonlinearity. This results in nonlinear behavior of the substructures. The degree of nonlinearity depends on the load orientation with respect to the main source of the nonlinearity as well as boundary conditions (e.g. wood stud wall behaves nonlinearly when loaded by in-plane shear force and approximately linearly when loaded by bending).

Due to the large number of individual connections, the number of unknown degrees of freedom in the structure can be enormous. Furthermore, the load-deflection curve describing the behavior of the connection is a random property and is influenced by different factors such as wood species, load direction with respect to wood fibers and moisture content, as well as testing procedure. Thus, the characteristics of the connections reported in the literature vary considerably.

These factors make the problem of analytical modeling extremely complex and require that certain simplifications are assumed. The assumptions should not violate the structural performance of the system but should result in a problem of a feasible size.

The finite-element method has been successfully used in many different areas of engineering and materials science to solve rather complicated problems. The concept of superelements and substructuring make the analyses of even large systems feasible. The development of verifiable and suitable model was one of the main goals of this research.

The objective of this study was to develop and verify a finite-element model for predicting deformations and load distribution for a light-frame wood building subjected to static loadings. To focus work towards the objective several goals were established.

1. Develop detailed three-dimensional finite-element models of horizontal and vertical substructures (walls, floors and roof) that were verified by data.

2. Transform the three-dimensional models of the substructures into superelements while utilizing only degrees of freedom needed to analyze the interaction and load sharing among subsystems and overall deformations of the full structure.

3. Develop and verify a finite-element model of the full light-frame wood building using the results of 1 and 2, results from the experimental and theoretical work dedicated to intercomponent connections, and results of the testing the full-scale building.

4. Conduct a sensitivity study to analyze the influence of substructures and intercomponent connections on the performance of the building.

2. LITERATURE REVIEW

Wood Stud Walls

Wood-frame walls are widely used in residential and low-rise buildings. The system typically consists of the vertical studs, horizontal upper and lower beams, and sheathing fastened with nails which creates a plate-like structure. The role of the stud wall in structural performance is to transmit the in- and out-of-plane forces to the foundation.

Substructure performance is complex and displacement-dependent, because connections with nonlinear characteristics are used in individual substructures and to connect adjoining substructures. Materials used to create substructures (wood and wood composites) are not isotropic and behave differently in different direction.

Several computational models have been developed to assess the response of the isolated stud wall to various loadings. Models range from explicit formulas relating the load to deformation (Easley et al, 1982) to more complicated stiffness and finite-element analyses. Tests performed in the past (NAHB, 1965; Corder et al, 1966; Polensek, 1975, 1976b; Easley et al, 1982; Tokuda, 1985; and others) showed the nonlinear behavior for shear (in-plane loading). Adams (1972) tested 39 shear walls to establish design criteria. Allowable loads based on the testing of standard wall frames 8×8 ft (2.03×2.03 m) were established. Although nonlinear load-deformation relationship was observed, no attempt was made to define the wall stiffness.

Most of the experiments on wall systems have been conducted in shear, but a few results for bending and compression (NAHB, 1965; Polensek, 1975) indicate that the load-deflection curve is linear until loads become high enough to cause some partial stud failures, whereupon the curve becomes slightly nonlinear (Polensek, 1989).

Polensek (1976a, b) presented a nonlinear finite-element model for walls subjected to bending and compression. I-beams connected to plate elements were used to account for non-uniform stiffness distribution within the wall and composite action of studs and sheathing. A step-by-step linear procedure was used to account for the nonlinear character of nail joints and no openings were included into analysis. Tuomi and McCutcheon (1978) published formulas to compute the strength of the shear wall. In this model, frames were assumed to distort as a parallelogram while the sheet remained rectangular. Several assumptions were employed including that of a linear load-deformation relationship for nail connection (secant stiffness modulus).

Itani et al (1981) studied the performance of diaphragms subjected to in-plane bending. The analytical solution was in good agreement with the experimental results. However, only a simple wall without openings was tested.

Easley et al (1982) published closed-form formulas for wall diaphragms loaded in shear. Their model was based on a steel diaphragm. Experiments and a nonlinear finite-element model were used to verify the equations. The finite-element model consisted of isotropic plane-stress elements for studs and sheathing and nonlinear springs for nails. The fasteners were assumed to be identical and the studs were positioned symmetrically about the centerline. Rigid-body translations in the horizontal planes were observed from the tests and this was used in the model. Allowing vertical motion of the header had negligible effect on shear deformation and nail forces.

Gupta and Kuo (1984, 1985) used strain-energy relationships to derive the solution for the shear wall. A sinusoidal shape of deformed studs was assumed. Their solutions were compared with the results of Easley et al (1982) and satisfactory agreement was reported. A case when studs were considered infinitely rigid in bending was studied and a negligible difference was found in the results between the original and new assumptions. Later, the model was improved by including uplift deformation (Gupta and Kuo, 1987).

Itani and Cheung (1984) developed a finite-element formulation of the nonlinear joint element to model nail connections in wood diaphragms. The element was used as a part of their three-dimensional model of a shear wall. The wall model consisted of beam elements representing studs and two-dimensional plane stress elements representing wall sheathing which were connected by nonlinear joint elements. Model was verified by comparison the analysis with experimental results for walls without openings.

Itani and Robledo (1984) suggested a finite-element model loaded in shear for walls with doors and windows. Nail slip, the main source of the nonlinearity, was modeled by a set of nonlinear springs.

Nelson et al (1985) studied the influence of the position of a non-continuous shear wall on the loading capacity of the building loaded by a wind pressure. A segment of a building with one internal shear wall and two outside walls (windward and leeward) was tested. The highest loading capacity was achieved, when the wall was immediately attached to the loaded windward wall. Since the shear wall was not continuous, considerable vertical reaction force was transferred into the floor joist, causing, in some

instances, joist to fail. This shows the significance of the noncontinuous partition wall, which is sometimes neglected in shear load design, in transferring shear forces.

Koželouh and Najdekr (1986) presented a simplified procedure for the analysis of the forces in the wood diaphragms due to the applied in-plane load.

The dominating influence of the connection properties on the wall stiffness was shown by Cheung et al (1988). The number of nails had an important influence on the racking strength of the walls tested by Okabe et al (1985). Hata and Sasaki (1987) designed a special element to account for the nail behavior, and very good agreement between experimental results and finite-element analysis was found (Hata et al, 1988).

Glos et al (1987) studied the strength of simple wall segments. Simplified formulas for the computation of the racking resistance were presented. The model was empirical and was based on the linear regression between the maximum shear load and wall shear stiffness defined as a function of the elasticity properties of studs and sheathing and their cross-sections. The validity of the results for walls different from those tested is, however, questionable.

Schmidt and Moody (1989) analyzed a full light-frame structure. Only in-plane stiffness of the walls was included and several other restrictions were applied to avoid making the model too complex. Hayashi (1989) derived empirical formulae to compute the shear stiffness and strength of walls sheathed with plywood. Walls with openings were treated and joint stiffness was included into the model. Newton's method for solution of nonlinear equations was used to obtain load-deflection characteristics of walls.

Dolan (1989) developed a finite-element model of the shear wall for static and dynamic analysis. The model was

verified by testing plywood and waferboard sheathed walls. Walls with openings were not included. Recently, Takainagi et al (1990) included the edgewise bending of the shear wall to the total deformation. Oliva (1990) tested gypsum-board sheathed wood-stud walls in shear and suggested a tri-linear model to describe load-deformation behavior. Most recently, Ge et al (1991) presented a finite-element model for walls with openings loaded in shear. An empirical equation to compute the adjusted shear modulus of a panel with an opening was developed based on plane-stress finite-element models.

As it follows from the literature, there exists a number of verified models for wood-stud walls loaded predominantly in shear. However, the models rarely address the problem of openings and act mostly as isolated substructures, and are not incorporated into the full structural models.

Floor

The floor transfers in-plane and out-of-plane forces into the vertical substructures and the foundation. Usually, the floor is designed as a system of independent beams with repetitive use consideration (National Forest Products Association, 1986) without including the contribution of the sheathing to the bending stiffness (Breyer, 1988; APA, 1988). Some European standards have implemented the use of the effective width concept, which acknowledges the increased stiffness of floors with sheathing (Institute for Standardization and Testing, 1984; Deutsche Industrie Norm, 1969).

The diaphragm action of the floor is considered in a similar way as for the wall diaphragm, where a shear force capacity per unit width is established (APA, 1988; Breyer,

1988). A detailed guideline for floor design is available in a publication by the Applied Technology Council (1982). Considerable research effort has been dedicated to the behavior and analysis of wood joist floors. Some of the relevant results are discussed.

Polensek et al (1972) reported very little load sharing in a nailed floor loaded by concentrated load; the point load distributed only to the joists adjacent to the loaded member. This supports the idea of the independent beam action.

Corder and Jordan (1975) tested nailed and nailed-glued joist floors with plywood and particleboard sheathing subjected to uniform pressure. When compared to system of beams, the stiffness was about 50% greater for nailed floors and 80-131% for nailed-glued connections. Thus, when a floor system of joists with attached sheathing is loaded by a uniformly distributed load, composite action is significant.

Dutko (1976) presented a procedure to compute the effective width of the sheathing for floors loaded in bending, but the glued and nailed floors were treated separately and composite action of the joists and sheathing was also assumed for the nailed connections. A problem arises when the sheathing is discontinuous, resulting in the stress distribution in the sheathing which does not follow the theory originally developed for steel beams with rigidly connected continuous metal sheathing. A similar approach was used by Smith (1979) who presented formulae to compute the stiffness of floors subjected to uniform pressure. Theoretical results of both works are verified by experiments and apply only to uniformly distributed loads. Their value is in the recognition of the sheathing contribution to the floor stiffness hence leading to a more efficient design. Since floor loads are mostly approximated

by a uniform loading, the applicability of formulas is obvious.

Sazinski and Vanderbilt (1979) used a finite-element model to analyze floors in bending. Subfloor and sheathing as well as gaps were included into the model but material and connection properties were considered as linear. Wheat et al (1983) introduced the nail joint nonlinearities into Sazinski and Vanderbilt's model. Comparison of the experimental results with the numerical analysis for deformations showed very good agreement. The deflection at failure for the nonlinear model was only 10-15% higher than for linear models, which indicates the usefulness of a linear model for loads required by Uniform Building Code (ICBO, 1988), because of a relatively high safety factors (2.0-3.0). A similar model was proposed by Tsujino (1985). The testing showed only slight nonlinearities in bending deflection, which indicates that linear approximation of nail connection stiffness as well as disregarding gaps in a model can still lead to satisfactory results in deflection analysis. Wheat et al (1986a) reported that the experimental stiffness was greater than the model predicted for 15 test floors. This was attributed to the composite action of sheathing and joists which was excluded from the analytical model. Najdekr (1989) used finite-element analysis to compute deformations and stresses in a wood floor with particleboard sheathing on both sides. The model was linear and rigid connection between sheathing and joists was assumed.

Several models to analyze the joist floor behavior were proposed and verified. The experimental results show that there is a composite action of the floor assembly loaded by a uniform pressure. Significant increase in floor stiffness can be achieved by using continuous sheathing glued to the joists. Closed form formulae have been proposed to compute the stiffness of the floor loaded by a uniform pressure.

Roof

The roof has been considered to be the most engineered part of the light-frame structure. In the past 20 years, metal plate trusses have been widely used for roof systems. Besides transmitting vertical forces into walls, the roof and ceiling act together as a horizontal diaphragm. Truss design is well established and is not discussed here. However, the effect of truss behavior on structural performance is relevant.

Recently probability and load distribution studies have been added to account for the variability of the material and loads (Pierce and Harrod, 1982; Cramer and Wolfe, 1989; Wolfe and McCarthy, 1989). This is resulting from the fact, that the elasticity and strength properties may vary significantly from member to member within a truss influencing the truss performance. The behavior of the truss is considered to be linear. Some researchers do not accept the linearity assumption and apply the nonlinear analysis (Sasaki et al, 1988). However, recent works by Wolfe and McCarthy (1989) showed that the linearity assumption agrees well with the roof performance. Similar conclusions were reached by Lafave (1990) who found that the load-deflection responses were linear up to two times the design loads for 15 tested trusses.

A two-way action of the roof was observed by Nicol-Smith (1977) who tested a roof system under different boundary conditions from continuous support to point support at the corners. This indicates, that the roof assembly with the sheathing present may no longer be simplified using a plane projection of one truss loaded by a tributary load. Also, load sharing between adjacent trusses may contribute to more efficient performance. From the work of Lafave (1990), it follows that the inclusion of the load sharing effect into

the truss analysis leads to better roof performance. The load distribution throughout the roof assembly does not depend on load level, which suggests the justification of linear analysis of the whole roof assembly.

Recent studies in Germany (Glos et al, 1990) demonstrated the possibility of trusses with glued lap joints, which increased the ability of the connection to transfer moments. Several trusses were tested and design procedure for shear and moment resistant joint was discussed. The practical use of the glued truss connection may be, however, questionable due to the sensitivity of the glued joint to the thickness variation of the members, moisture content and grain orientation.

The diaphragm function of the roof sheathing was studied by Turnbull et al (1982). Their study included blocked plywood, unblocked plywood and sheet steel diaphragms. The diaphragms were attached to a relatively stiff glulam beams to simulate connection between walls and the diaphragms. Point loads were applied at the top of each lower truss chord to cause the diaphragm in-plane bending. The blocked plywood diaphragm outperformed the other systems with respect to maximum in-plane load causing diaphragm bending. Although the sheet steel diaphragm was stiffer, its capacity was lower than the one for the plywood diaphragm, which resulted in higher design value for unit shear load for the plywood diaphragm. The relationship between load and bending deformation was nonlinear, but no corrections for slip between the supporting glulam beams and the diaphragm were made.

Joints and Intercomponent Connections

Properties of joints in the wood structure are recognized as one of the key problems in the design of light-frame structures. The early research was mainly focused on the strength rather than stiffness characteristics. The ultimate loading capacity of the nails has been related to the material density and geometrical characteristics of the joint such as diameter and depth of penetration (FPL, 1965; Scholten, 1965).

The NFPA (1986) specification requires the load capacity of the joint based on the specified allowable load per connector. Even the yield model approach for dowel-type connectors, recently adopted by NFPA (McLain, 1991), relies on strength and failure mode of the connection, but no deformation characteristics are calculated or are required. With the latest analysis techniques and the capability to analyze the nonlinear behavior, the research focus has turned towards the deformation characteristics of the joints to provide the necessary input for the analysis.

The importance of full information about the load-displacement relationship was recognized by Polensek (1978), Jenkins et al (1979), Loferski and Polensek (1982) and others. The nonlinear relationship can be approximated by a piece-wise linear curve (Polensek 1978; Polensek and Schimel, 1986) which becomes more accurate with increased number of segments. Pellicane and Bodig (1982) compared the testing techniques for nail-slip moduli measurement. The load-slip characteristics were sensitive to the test configuration mainly for small initial deformation. Thus, the test configuration must properly reflect the final use of the joint. Polensek (1978) studied properties of several joints used in wood stud walls and he used secant moduli to model the nonlinear behavior. Ehlbeck (1979) expressed the

strength of the nail joints as an empirical function of different material and geometrical parameters. He attempted to linearize the load-slip relationship using different secant moduli. Jenkins et al (1979) published the experimental relationship between the load and displacement for Douglas-fir studs and 3/8-in. (9.5 mm) plywood and 1/2-in. (12.7 mm) gypsum wallboard sheathing. The long term-load effects were also included. Three different slopes for the nailed connection between the stud and gypsum board were suggested by Polensek and Bastendorff (1982) and a similar approach was applied by Loferski and Polensek (1982).

Gromala (1985) published data for ten different sheathing materials nailed to southern pine lumber. Curves were approximated by three different slopes. Wheat et al (1986) studied the slip of the nail connection in a wood-joist floor. For the load of 40 psf (59.5 Pa), the measured slip was less than 0.015 in., (0.38 mm), which was considered in the range of proportionality. Tokuda (1983) studied the normal stress on a nail surface as the result of material pressure at a constant moisture content. The stress was found to be rather uniformly distributed along the circumference and decreased as a function of time. The stress rate become constant after 20 days and was low.

Intercomponent connections for light-frame structures have not been widely researched. Polensek and White (1979) published a finite-element model to compute the stiffness of wall-to-floor connection, and a double modulus of connection was reported as a result. A similar connection was analyzed for rotation by Polensek and Schimel (1986) where slightly nonlinear behavior was observed. Recently, Groom (1992) and Groom and Leichti (1991) have examined various intercomponent connections typical of light-frame structures. Their analyses have included partition-to-exterior wall connection, exterior wall-to-exterior wall connection, and several different metal framing anchors.

Full-Structure Testing and Analysis

Full-Scale Tests

The experimental investigations of full-scale structures are limited due to the high costs of the experiments and difficulties with the physical modeling. During the last two decades, several attempts were made to investigate the behavior of the full building.

Tuomi and McCutcheon (1974) performed a series of tests on a simple light-frame building. The building was tested at different stages of construction to determine the influence of the components on the behavior of the structure. The structure was loaded using a uniformly applied pressure until failure, which in this case was splitting of the sill plate. Although no analytical procedure was suggested, the testing showed that the structure was overdesigned at some parts whereas some details were underdesigned.

McCutcheon et al (1979) addressed the integrity of the substructures within the full structure. The intercomponent connections were identified as weak links leading to the overall damage in the structure loaded by wind pressure. A truss-frame system was developed to create more efficient connections.

Tuomi (1980) discussed the need for full-scale tests of wood structures as well as specifics related to wood such as high variability of material and connection properties, orthotropy, relative humidity influence etc. Walker et al (1984) described the testing facility and some tests performed on full houses subjected to wind loads. The need was emphasized for the full assembly design procedure.

Sugiyama et al (1988) performed a full-scale test of a

two story wood-frame house subjected to lateral load. A limited contribution to the wall shear resistance was reported for the wall areas above and below the wall openings. However, the contribution to the overall house shear resistance by the walls perpendicular to the loading (torsional and bending stiffness influences) was negligible. This result may have been due to the small deformations, which could have occurred in the connections. Deformations occur in the connections when the connection stiffness is lower than the bending and torsional stiffness of the walls. Although the configuration, as well as the dimensions of the structural members of the building were different from those currently used in the United States, this work provided an interesting insight into the mechanism of the structural deformation.

Steward et al (1988) tested a 14×66-ft (4.27×20.12-m) house with six internal walls of different length and stiffness. A concentrated force at the top of one wall at a time, as well as uniformly distributed pressure, were applied. Load sharing among the walls was measured via deflection recording. They showed that the amount of load taken by each wall can be controlled through out-of-plane stiffness of floor and roof diaphragms which provides the support against rigid-body rotation. The load sharing was restricted to walls adjacent to the applied force. It was observed, that the diaphragm-shear wall system behaved as a rigid beam on an elastic foundation and the majority of the applied uniform pressure was transferred via end walls. The shear tests up to the ultimate capacity showed high safety factors (2.8 and 3.0) which means that the building was overdesigned.

Reardon (1989) studied the influence of different sheathing materials on diaphragm action of house components. A significant improvement in house stiffness was accomplished by including the wall or roof sheathing into

the model. The weight of the roof improved the resistance of the house against horizontal forces by reducing the uplift component of the deformation.

Full-scale test of the light-frame building was performed by Phillips (1990) who applied point loads at the top corners of the shear walls. The experiment was designed to serve as a tool for the verification of an analytical model and results have been used throughout this work.

Sadakata (1988) subjected a full house to a seismic loading. No analytical procedure was involved. Boughton (1988) performed a series of tests of the house simulating cyclone loading. An equivalent static force was used. Connections were identified as weak points causing failures. The comparison of the test results with the currently available analytical solutions showed lack of the accuracy.

Ohashi and Sakamoto (1988) tested a two-story structure with two partition walls in each story. A horizontally oriented cycled load was applied at the top corner of one wall at a time and deflections were measured. From the load-deflection curves it followed that the structure behaved as a nonlinear system with degrading stiffness. The curves were similar to those reported for individual nail connection (Chou, 1987) which indicated the strong influence of connections on the overall structure behavior.

Earlier analytical models

Gupta and Kuo (1987) analyzed the building tested by Tuomi and McCutcheon (1974). A model of the shear wall which included the wall uplift due to the horizontal load was used as a basic element. The uplift of the wall with respect to the floor was a part of the wall model and not a separate degree of freedom in the model of the full house. A limited number of global degrees of freedom were

identified and used in the analysis. Although several simplifications were involved (bending and axial deformation of studs, as well as shear deformation of the sheathing were ignored) agreement with the test results was achieved. The model, however, was linear and did not predict the entire load-deformation path.

Moody and Schmidt (1988) applied their analytical model for the racking resistance of the wall to the tests of houses performed in Japan. The results were in agreement with experiments for some cases but differed substantially for others. This may be due to an oversimplified analytical model, that included several drastic assumptions such as neglecting the out-of-plane wall stiffness and shear resistance of areas above and below openings.

A three-story building was investigated by Yasumura et al (1988). The configuration of internal walls perpendicular to the load varied for each floor. The house was loaded by point loads applied simultaneously in the plane of the roof diaphragm and the displacements were recorded. The analytical model developed by Tuomi and McCutcheon (1978) was applied to compare the theoretical shear deformation of the isolated wall with the experiment, but the model failed to accurately describe the experimental result. The lack of accuracy of the model was attributed to torsional deformation of the wall, which was not accounted for in the model. Inclusion of uplift deformation into the model brought the analytical results closer to the experiments. As in the test performed by Ohashi and Sakamoto (1988), the load-deformation curves were similar to those reported for individual connections.

Tuomi and McCutcheon's structure (1974) and the Tongan structure tested by Boughton (1988) were analyzed by Schmidt and Moody (1989) who used a nonlinear model for wood stud walls. Their wall model did not account for the areas below and above openings, composite action with adjacent panels as

well as plate action. Thus, the assembled model had a limited number of degrees of freedom. In spite of these simplifications, the model gave relatively good predictions of the wall forces and displacements.

Kataoka (1989) created a nonlinear three-dimensional finite-element model for full-scale structural analysis. Nonlinear springs were used to model shear resistance of the walls as well as intercomponent connections. The building was modeled as a three-dimensional frame with nonlinear diagonals and nonlinear member connections. No bending stiffness of the wall was included into model.

Review of the literature has shown that no tests were designed in conjunction with analytical modeling. Rather, existing results, often incomplete, were analyzed by different authors, using specialized models with limited applications. No attempt was made to measure reaction forces at each vertical substructure to assess the portion of the total load transferred into the foundation.

Summary

From the literature review it follows that more attention has been given to individual substructures then complete buildings. This is due to the experimental and analytical difficulties connected with test or analysis of a full structure.

The properties of the intercomponent connections are an important part of the full structure and not much research has been done in this area. Individual nail connections have been studied rather extensively but only recently a nonlinear load-deformation character of the connection has been recognized. Most of the past studies used linearized model to describe connection behavior.

More research needs to be done in the area of nonlinear

behavior of the connections including cycled loading. The behavior of the connections under combined loading has not yet been reported. This information is important to the analysis of subsystems under general boundary and loading conditions.

3. THE FULL STRUCTURE

As a parallel project, a light-frame wood building 16×32 ft (4.88×9.75 m) was tested at Washington State University (Phillips, 1990). For the first time, the testing was designed not only as an experimental investigation, but as a verification tool for the finite-element model as an integral part of the project. A three-dimensional view of the experimental structure is shown in Figure 1. Detailed drawings of the individual substructures are presented in Appendix A.

Design of the Structure

The experimental building was designed as a simple light-frame structure which included typical materials, substructures and connections. Doors and window openings were included, but windows and doors were not installed. Since the main goal of the experimental research was to provide sufficient information for a subsequent analytical model, the structure had to include load and deformation measuring devices, which lead to some atypical details.

Walls

Framing

Framing was constructed from 2×4-in. (38×89-mm) nominal Douglas-fir stud grade lumber spaced 16 in. (406 mm) on center. No blocking was used for all walls. Double top and

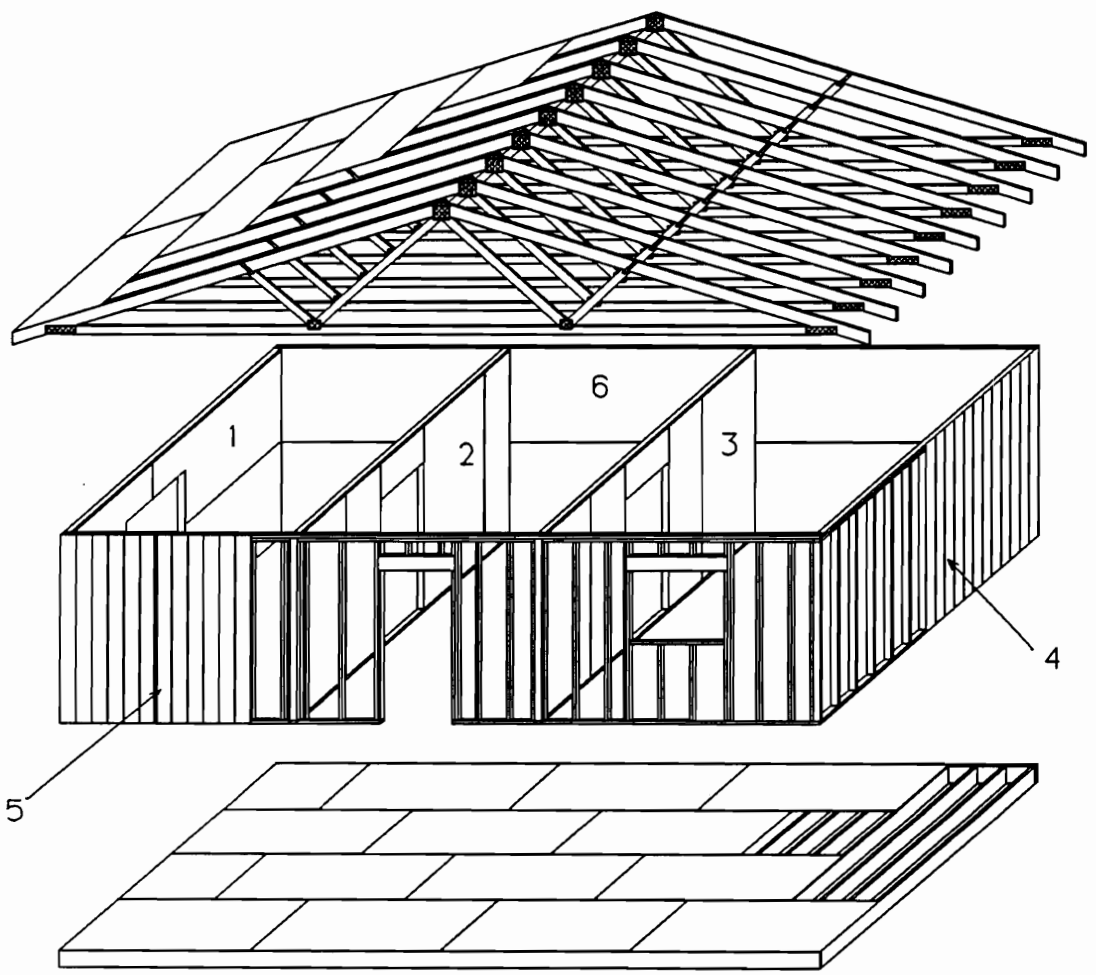

Figure 1. Three-Dimensional View of the Experimental Structure (Philips, 1990).

sole plates were end nailed to the studs. Frames for shear walls (walls 1 through 4 in Figure 1) were shorter to create a space for the load cells which measured reaction forces beneath each shear wall as shown in Figure 2. The typical framing for wall 1 is shown in Figure 3. The detailed drawings are in the Appendix A.

Headers above the door and window were constructed from two 2×4-in. (38×89-mm) horizontally oriented studs. Double studs were used for lower beams.

Sheathing

Plywood and gypsum board were used as wall sheathing. The nails and nail spacing were deliberately different for each wall to create differences in wall stiffness. The construction variables are listed in Table 1. Gaps in the sheathing were oriented differently as shown in the Appendix A.

Wall 1 and wall 4 were constructed of the same materials, but wall 1 included a 3×4-ft (914×1219-mm) window opening. The partition walls (wall 2 and 3) contained 3×6-ft (914×1828-mm) door openings, but wall 2 was sheathed with 0.5-in. (12.7-mm) plywood, while wall 3 was sheathed with 0.5-in (12.7-mm) gypsum board.

Floor

The floor was constructed of 2×10-in. nominal (38×241-mm) Douglas-fir lumber. Joists were spaced 16 in. (406 mm) on center and were sheathed with 5/8-in. (16-mm) plywood. Sheathing was nailed using 8d nails spaced 6 in. (162 mm) on the perimeter and 10 in. (254 mm) on interior. Floor construction was based on the Uniform Building Code (ICBO, 1988) for 16-ft (4.88-m) span and 40-psf (1.92-kPa) live load (Phillips, 1990). Again, no blocking was used. The

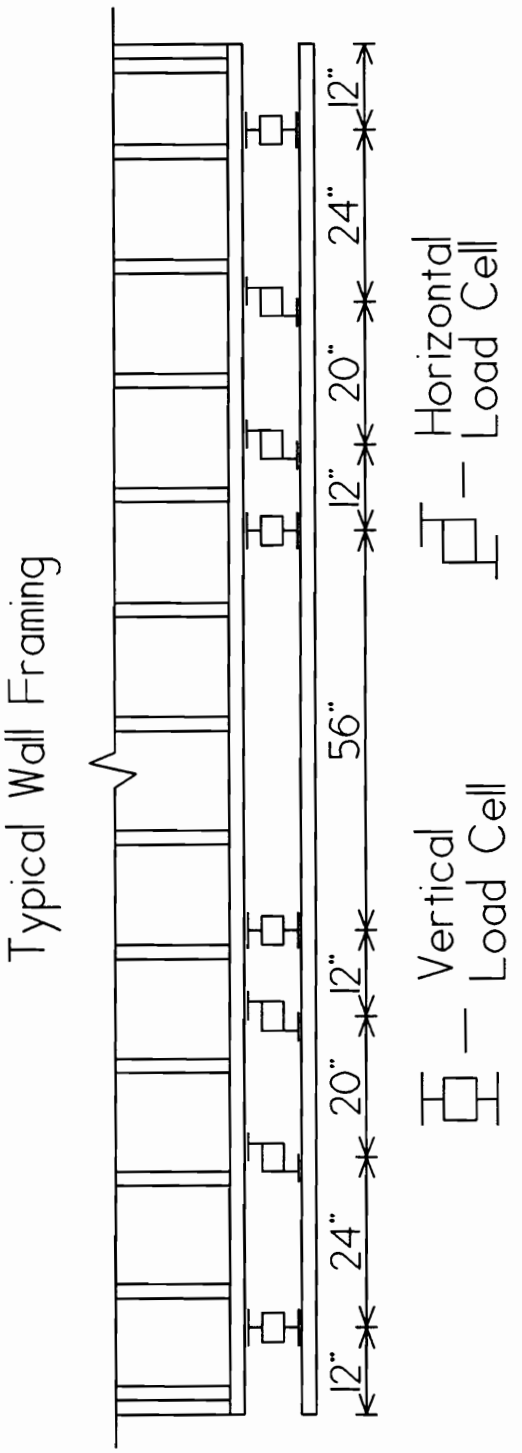

Figure 2. Position of the Load Cells Recording Reaction Forces.

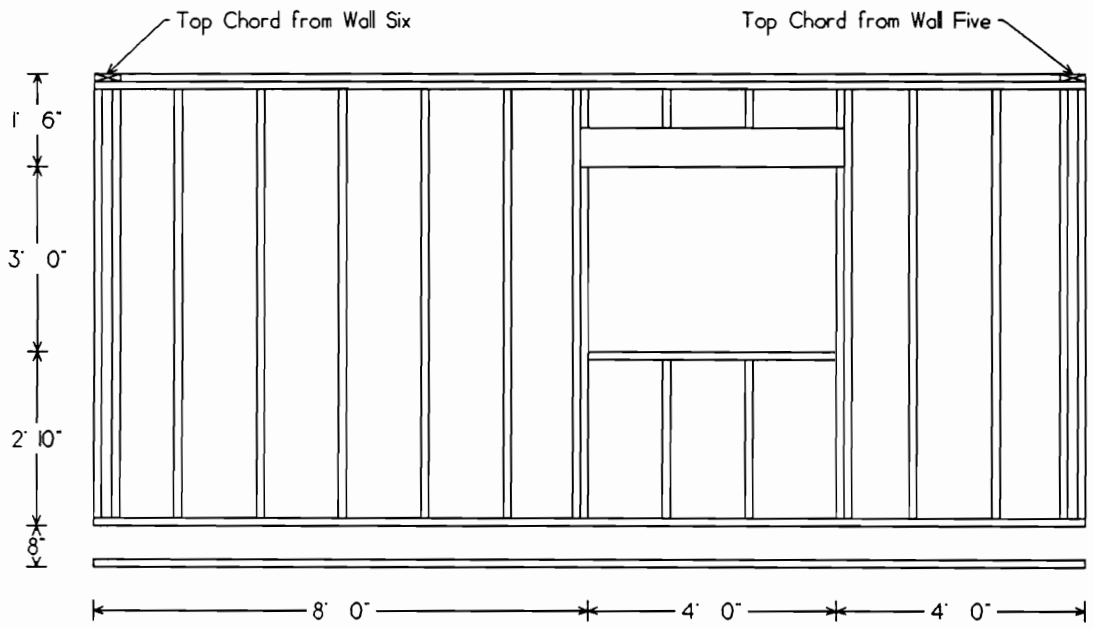

Figure 3. Typical Framing of the Wall in the Experimental Building - Wall 1.

Table 1. Nailing Schedules and Sheathing Materials used for Construction of Walls

Wall	Size	Framing Size	Sheathing	Nail Size	Nail Spacing	
					Perimeter	Interior
	ft (cm)	in. (mm)	in. (mm)	(mm)	in. (mm)	in. (mm)
1	8×16 (244×488)	2×4 (38×89)	T1-11 plywood 0.6 (15) & gypsum 0.5 (13)	6d (2.9) No.11 (2.8)	6 (152) 7 (178)	12 (305) 7 (178)
2	8×10 (244×488)	2×4 (38×89)	gypsum 0.5 (13) on both sides	No.11 (2.8)	7 (178)	7 (178)
3	8×16 (244×488)	2×4 (38×89)	plywood 0.5 (13) on both sides	8d (3.3)	6 (152)	12 (305)
4	8×16 (244×488)	2×4 (38×89)	T1-11 plywood 0.6 (15) & gypsum 0.5 (13)	6d (2.9) No.11 (2.8)	6 (152) 7 (178)	12 (305) 7 (178)
5	16×32 (488×976)	2×4 (38×89)	T1-11 plywood 0.6 (15) & gypsum 0.5 (13)	6d (2.9) No.11 (2.8)	6 (152) 7 (178)	12 (305) 7 (178)
6	16×32 (488×976)	2×4 (38×89)	T1-11 plywood 0.6 (15) & gypsum 0.5 (13)	6d (2.9) No.11 (2.8)	6 (152) 7 (178)	12 (305) 7 (178)

floor was connected on its perimeter by steel T-shape straps, placed 4 ft (1220 mm) apart, to a flatwise oriented 2×6-in. (38×152-mm) plate which was bolted every 2-ft (610-mm) to the to strong-back concrete floor. Moreover, the 2×10-in. (38×241-mm) joists were toe-nailed to the 2×6-in. (38×152-mm) plate. Such a connection was necessary to create boundary conditions preventing the floor from possible uplifting. The floor framing and sheathing is shown in Figure 4a and b.

Roof

The roof was constructed of W-shaped trusses placed 24 in. (610 mm) apart with 32-ft (9.75-m) span. The trusses were made with 2×4-in. (38×89-mm) members except for the top chord, which was made with 2×6-in. (38×152-mm) lumber. The truss was designed for 30-psf (1.44-kPa) live load and 7-psf (0.34-kPa) dead load on the top chord and 10-psf (0.48-kPa) dead load on the bottom chord. The truss is shown in Figure 5 and additional details are in the Appendix A. Nails were spaced 6 in. (152 mm) on the edges and 12 in. (304 mm) over intermediate supports. 8d common nails were used to attach 0.5-in. (12.7-mm) plywood sheathing to the trusses.

The ceiling was 0.5-in. (12.7-mm) gypsum board and was attached by 1-3/8 in. (35 mm) gypsum nails to the bottom chord of the truss.

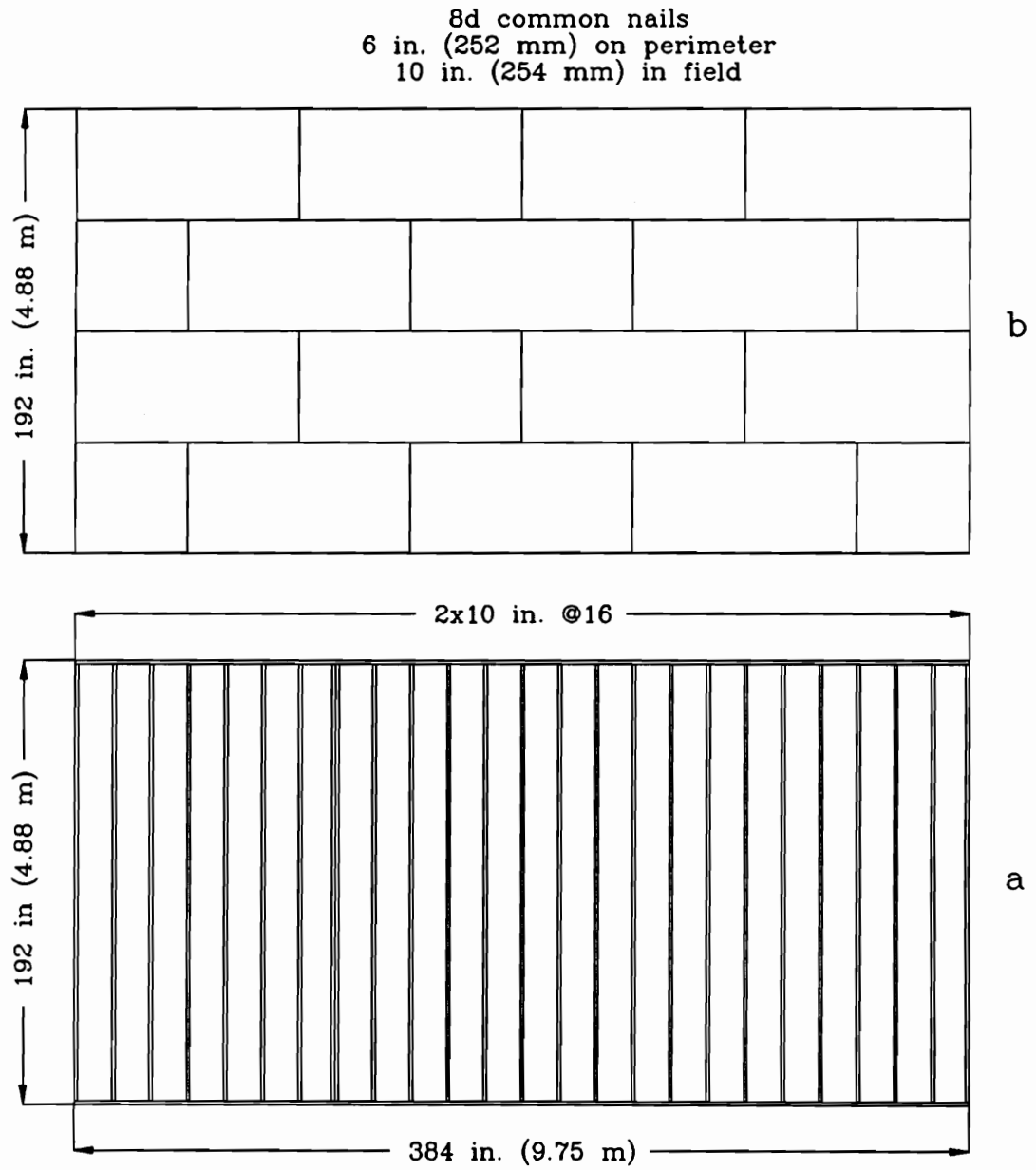

Figure 4. Construction of Floor (a) Framing, (b) Sheathing.

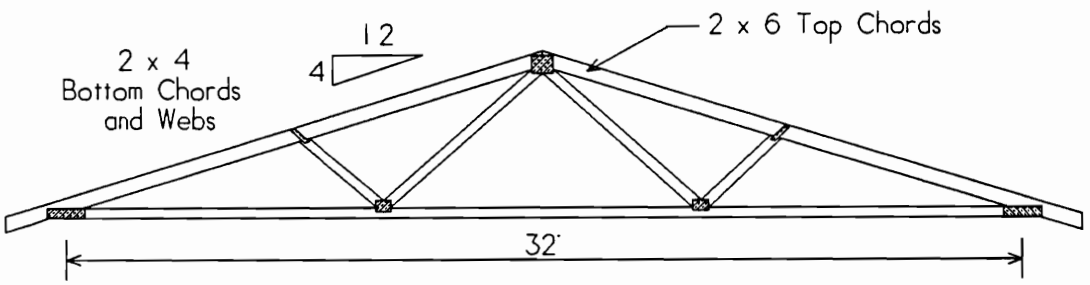

Figure 5. A Typical Roof Truss.

Experimental Investigation

Test Objectives

The objective of the test was to provide the experimental data which can be used to verify a finite-element model of the full light-frame building. The model is expected to be used for the static analysis of the structure and to predict the amount of load being transferred by individual shear walls into the foundation.

Testing Procedures

To provide sufficient information about materials used in the experimental building, elasticity properties of lumber used for the framing and roof trusses were measured using a wave propagation method. Each member was labeled and positioned in the structure such that the modulus of elasticity was known for any individual stud.

The shear load-deformation characteristics of the sheathing were measured using eccentrically loaded shear specimens. American Society for Testing and Materials (ASTM) specification D 1761 (ASTM, 1977) was used as a basis for the testing of nail connections. The specimens were Douglas-fir blocks, 2×4×12 in. (38×89×305 mm), sheathed from one edge by pertinent sheathing material. The sheathing and block overlapped by 4 in. (102 mm) and only one nail was used as shown in Figure 6. The assembly was tested in tension where the load acted at the midpoint of each connected part. Thus, an eccentric loading was applied. The load-slip curves, which were used as the input for a

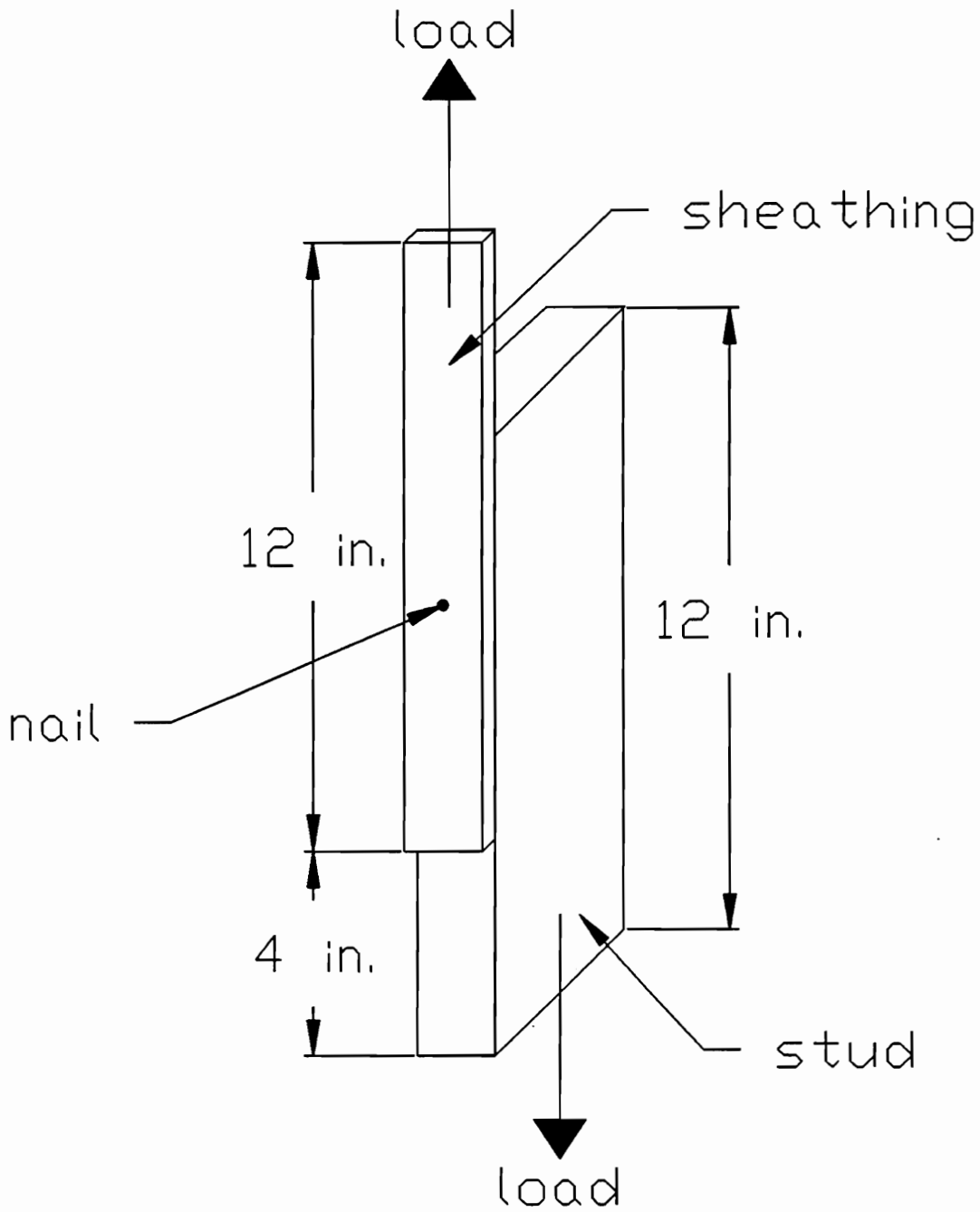

Figure 6. Schematic of the Test Specimen for Nail Connection Tested in Shear.

mathematical modeling are shown later in the text.

The building was constructed and tested in several stages:

1. Only shear walls (wall 1 through 4) were erected and sheathed on one side. Walls were resting on the load cells rigidly connected to the wall sole plate as shown in Figure 7. Each wall was loaded at the top corner by three cycles of ±800 lb (3558 N) except for wall 2 which was loaded by ±400 lb (1779 N). The lower load for wall two was due to the expected low shear stiffness resulting from gypsum board sheathing applied on both sides. Linear variable differential transducers (LVDT) were used to measure horizontal deflection of the top plate and wall uplift, as well as rigid-body translation due to the slip between the sole plate and floor - Figure 7. This information was used to subtract the rigid-body motions from the measured top corner displacement to obtain the deformation due to the shear of the wall.

2. Individual shear walls with sheathing present on both sides were tested in the same manner as previously by a load of ±800 lb (3558 N). This test provided the estimate of the initial wall stiffness. Load levels were low and no irreversible deformation in connections was expected.

3. The long walls (wall 5 and 6) were erected, connected to the shear walls and this assembly was tested by point loads ±800 lb (3558 N) applied simultaneously to walls 1 and 2, then walls 3 and 4, and finally to all four walls simultaneously.

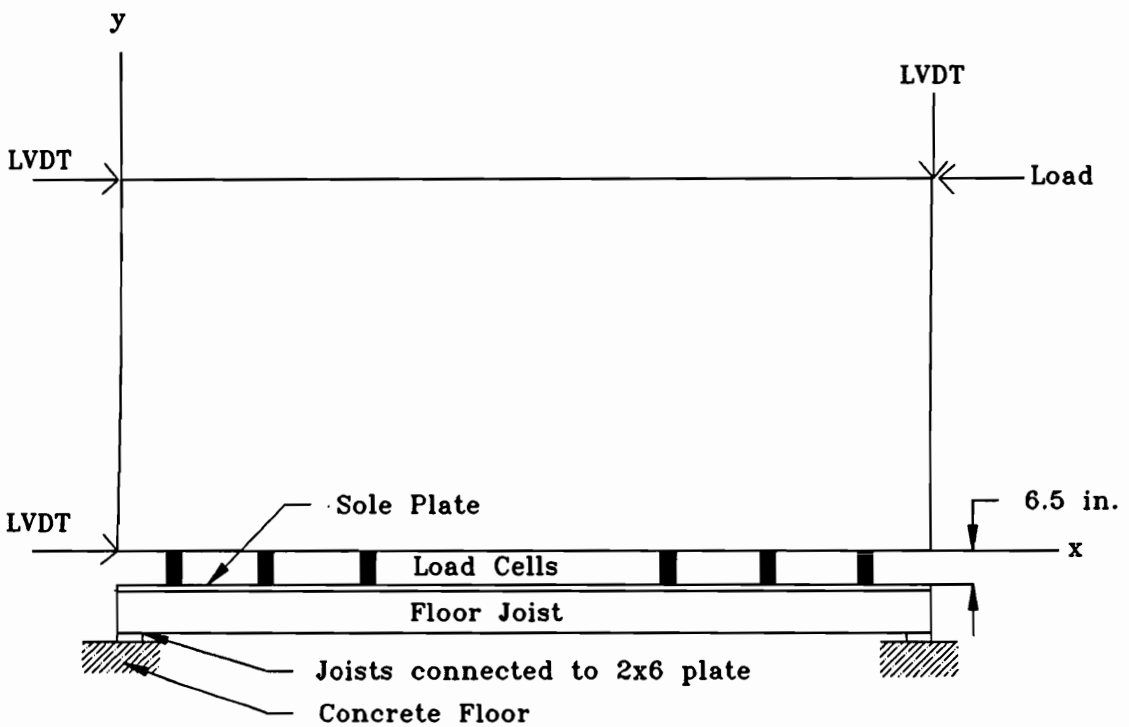

Figure 7. Schematic of the Deformation and Force Measurement in a Shear Wall.

4. The entire structure was completed and loaded in three stages:

(i) ±1200 lb (5338 N) to wall 1 and 2 in three cycles
(ii) ±1800 lb (8006 N) to wall 3 and 4 in three cycles
(iii) ±2000 lb (8896 N) to ±7000 lb (31 136 N) applied to all walls.

Load was applied using hydraulic cylinders attached to the rigid testing frame. Steel plates were bolted to the upper beams of walls 1 through 4 and connected to the loading cylinders, which made it possible to load the structure in both directions. The details of the experiments are discussed in the work of Phillips (1990).

Summary

In this chapter the experimental structure was described and typical substructures were discussed. A complete set of drawings describing the experimental building is in Appendix A.

Tests performed on the materials, connections, subassemblies, and full building including measurements of the load and deformations were described.

4. FINITE-ELEMENT MODELS OF SUBSTRUCTURES

To obtain information about the load distribution within the structure, the full building must be analyzed. However, if all of the details are retained, such a model quickly becomes too large and even a powerful computer system can be overwhelmed. Thus, a reasonable balance between the required accuracy, costs and time must be established. Even the substructure analysis can become too costly if a minimum simplification is not applied.

There has been considerable effort dedicated to modeling isolated substructures of light-frame wood structures. Models for individual walls, floors and roof or ceilings have been documented, and are verified in most cases. The nonlinear behavior has been a concern of many researchers and working models were developed and published. The models of the individual substructures in this work are based on the capabilities of the available software. As long as results obtained from the detailed analysis represent the true behavior of the substructures, the nature of the model is not important from the standpoint of its use to generate the input information for the global model. Finite-element software ANSYS (Kohnke, 1989) was used to conduct the analysis.

Background

Before discussing individual substructures, a general discussion about the three-dimensional finite-element model of the full structure is relevant. As it follows from the literature review, analytical models of the full building had to be significantly simplified or else a computational

solution to the problem may not be feasible. To retain all the structural details in the model is impossible due to the vast number of degrees of freedom and effort to create such detailed model. Therefore, for computational purposes, the building was assumed to be an assembly of substructures.

The following major substructures and components are analyzed:

1. Walls
2. Roof
3. Floor
4. Intercomponent connections

Substructures are connected in the structural system via intercomponent connections. The overall response of the system to an applied load is nonlinear, but some of the substructures retain a linear response while others respond nonlinearly. Intercomponent connections require separate analyses and experiments to determine their behavior. Groom (1992) and Groom and Leichti (1991) showed the nonlinear nature of the intercomponent connections in the structure.

The proposed three-dimensional model was designed as an assembly of walls, roof and floor connected by intercomponent connections. The roof and floor were analyzed as superelements, while a special quasi-superelement was developed for each wall. A model of an orthotropic plate was applied to the floor as an alternative approach.

The concept of superelements and substructuring is employed. The superelement, a part of the structural model, behaves linearly and is connected to the rest of the model via its boundary nodes. Internal degrees of freedom of the superelement are eliminated via the condensation process and do not enter the solution of the global structure.

The concept of substructures has been discussed by several authors (Cook, 1981; Zienkiewicz, 1982; Stasa, 1985); in principle, the large continuous domain is divided into the subdomains and only the degrees of freedom on

boundaries are utilized. The computational subdomain is also called a superelement. The following matrix equations demonstrate the principle of substructuring (Stasa, 1985; Kohnke, 1989). Equations relating the applied forces to the stiffness matrix and displacements are written:

$$\begin{bmatrix} K_{11} & K_{12} \\ K_{21} & K_{22} \end{bmatrix} \begin{bmatrix} a_1 \\ a_2 \end{bmatrix} = \begin{bmatrix} f_1 \\ f_2 \end{bmatrix} \tag{1}$$

Where $\mathbf{a}_1$ = vector of displacements of the nodes at the boundary

$\mathbf{a}_2$ = vector of displacement of the internal nodes

$\mathbf{K}_{ij}$ = partitioned stiffness matrix, i, j=1, 2

$\mathbf{f}_i$ = load vector

Solving the second submatrix of Equation (1) for $\mathbf{a}_2$ we obtain:

$$a_2 = (K_{22})^{-1}[f_2 - K_{21}a_1] \tag{2}$$

Using first matrix Equation of (1) and eliminating $\mathbf{a}_2$ using (2):

$$\begin{aligned} K_{11}a_1 + K_{12}a_2 &= f_1 \\ K_{11}a_1 + K_{12}[(K_{22})^{-1}(f_2 - K_{21}a_1)] &= f_1 \\ [K_{11} - K_{12}(K_{22})^{-1}K_{21}]a_1 &= f_1 - K_{12}(K_{22})^{-1}f_2 \end{aligned} \tag{3}$$

$$or$$

$$K^s a^s = f^s$$

Where $\mathbf{K}^S$ = superelement stiffness matrix

$\mathbf{a}^S$ = superelement displacement vector

$\mathbf{f}^S$ = superelement load vector

One disadvantage of the superelement formulation is that the stiffness matrix must be constant. In the case of nonlinear behavior, the stiffness matrix $\mathbf{K}^s$ is a function of the displacement $\mathbf{a}^s$, and slave (or removed) degrees of freedom inside the boundary have an influence on the global stiffness matrix. Thus, no computational savings are possible because the stiffness matrix must be reevaluated in each load step. This implies that the application of the superelement is meaningful only if the substructure behavior is linear.

As it was shown by Wolfe and McCarthy (1989) and Lafave (1990) the roof behaves linearly when loaded up to twice the design loads. The diaphragm action is often simplified by considering the roof to be a rigid plate or beam (Breyer, 1988; Phillips, 1990). Similarly, the floor systems has been shown to behave linearly (Tsujino, 1985) and nonlinear analysis showed only a slight improvement in the results mainly for loads higher than design loads (Wheat et al, 1983). These facts lead to modeling roof and floor as superelements. However, an alternative approach having the floor modeled as an orthotropic plate is also presented.

Walls are considered to be linear in bending and nonlinear in shear. They also behave quasi-linearly when subjected to a combination of pressure and axial force applied in the vertical direction (Polensek, 1975; 1989). There are no experimental results for a combination of shear, pressure and axial force. Thus, there is no experimental information about the coupling between shear and other two loads. However, Polensek (1975) showed the presence of slip deformation between the sheathing and studs of the wall subjected to bending and axial pressure, which indicates the influence of the lateral load on the shearing stiffness of the wall. This problem is studied analytically later in the text.

The nonlinear character of walls leads to a requirement that the nonlinearity must be represented in the full structure model. However, this will lead to the large number of degrees of freedom and consequently long solution times and extreme computing hardware requirements. The reduction of degrees of freedom for the walls is performed by creating a quasi-superelement which preserves the nonlinearity of the original substructure and condenses the degrees of freedom into a limited number of nodes.

The quasi-superelement is based on the idea that the work done by the external forces on the equivalent model (quasi-superelement) is equal to the work required to deform the original structure under an equivalent load and boundary conditions. Thus, the quasi-superelement is required to undergo the same displacements as the original substructure. These requirements, however, are imposed only to a number of discrete points, element nodes. The total potential energy of the substructure and quasi-superelement are equal, therefore an energetically equivalent model is created.

Intercomponent connections are modeled as nonlinear one-dimensional elements similar to the representation of an individual nail connection in the detailed models. The load-deformation characteristics of the intercomponent connections are obtained from experiments and detailed finite-element models (Groom and Leichti 1991; Groom, 1992).

The full structure analysis requires simplifications based on the literature review and computational resources. The following assumptions are made:

1. The roof behaves linearly when loaded in bending.
2. The diaphragm behavior of the roof is linear.
3. The floor behaves linearly in bending and acts as an orthotropic plate.
4. Shear walls behave nonlinearly in shear and are linear in bending and torsion.
5. Intercomponent connections are nonlinear.

6. Self-weight of the horizontal structures is applied as a dead load.

After the global problem is solved for unknown displacements, the substructure (superelement) can be loaded on its boundary by the displacements resulting from the full-structure analysis and loads applied directly to superelement, and detailed analysis performed. In the substructure analysis the requirement of linearity can be released and the substructure can be analyzed as a nonlinear model.

Walls

Walls are vertical substructures designed to transfer forces to the foundation. The following forces were identified as acting on the walls and were considered when developing the full structure model:

1. Horizontal shear force caused by the reactions due to the wind pressure or earthquake.
2. Bending and torsional moments resulting from the wind pressure or suction and forces acting on the wall boundary connected to other substructures.
3. Axial forces due to the weight of the carried substructures (roof, floor, including dead loads, live loads and other loads resulting from the function of the structure).
4. Body forces due to the self weight.

These forces can act simultaneously and the appropriate load combinations are discussed by ICBO (1988). The wall models consisted of a detailed, three-dimensional, finite-element model and its two-dimensional equivalent, a quasi-superelement.

Detailed Substructure

Two-dimensional, orthotropic, shell elements were used to model studs and sheathing. The two-dimensional shell element is a triangular or rectangular element which is located in three-dimensional space and has six degrees of freedom at each node: three translations in x-, y-, and z-direction, and three rotations around x-, y-, and z-axes. It can be orthotropic or isotropic and linear behavior is assumed. Detailed descriptions are given by Kohnke (1989) and Batoz et al (1980).

The nonlinear character of joints was modeled by one-dimensional springs clustered at common nodes for sheathing and studs (one spring for the withdrawal, and two for shear resistance). The nonlinear load-deflection element is a nonlinear spring with only one degree of freedom (any of the above six can be specified). Elements can have different behavior in tension and compression and nonconservative unloading, which is especially valuable for nail modeling. Contact stiffness between materials in a joint can be modeled by high compression stiffness of the element.

The three-dimensional solid was used to model headers above openings. The three-dimensional solid is a brick-type element with eight nodes and three degrees of freedom at each node.

The element stiffness matrices are available elsewhere (Kohnke, 1989) and are not presented here. The rectangular shape of the studs and sheathing allowed an exact shape modeling. Thus, the error due to the domain approximation tends to zero.

In the model, each nail connection was replaced by three nonlinear load-deflection elements, one for each degree of freedom. Because of the arrangement of nails in a plane, only translational degrees of freedom needed to be modeled.

Rotations of the elements were controlled by translational stiffness of the connections. Each stud and panel of the sheathing had its own node numbering. Thus, each stud was allowed to move and rotate freely unless connected to the rest of the structure. The connection of studs to sole plates and top plates was carried out via nonlinear load-deflection elements representing nails.

Then, sheathing was superimposed on the framing and was connected via nonlinear load-deflection elements. Finally, gap elements were specified to account for the sheathing discontinuities. The number of nodes for large walls was reduced by clustering several nails into one node (4 nails/node for the 16×32-ft (4880×9760-mm) walls). Although the number of nodes was reduced by nail clustering, the models were still rather complicated and expensive in terms of computer time.

Windows, doors and other openings were part of the model. The finite-element mesh for the example model of wall 1 which included an opening, is shown in Figure 8. Heavy lines in Figure 8b show the boundaries of the discontinuous sheathing. Detailed finite-element models of the remaining walls and their equivalents are shown in the Appendix B, while the element stiffness matrices are discussed in Appendix D.

Material and Connection Properties

Material properties and element types used to generate the input for the detailed models are in the Table 2. Phillips (1990) performed nondestructive tests to measure the modulus of elasticity of each framing member used in the experimental building and Table 2 contains averages of these measurements. The remaining orthotropic material properties are based on the work of Bodig and Jayne (1982).

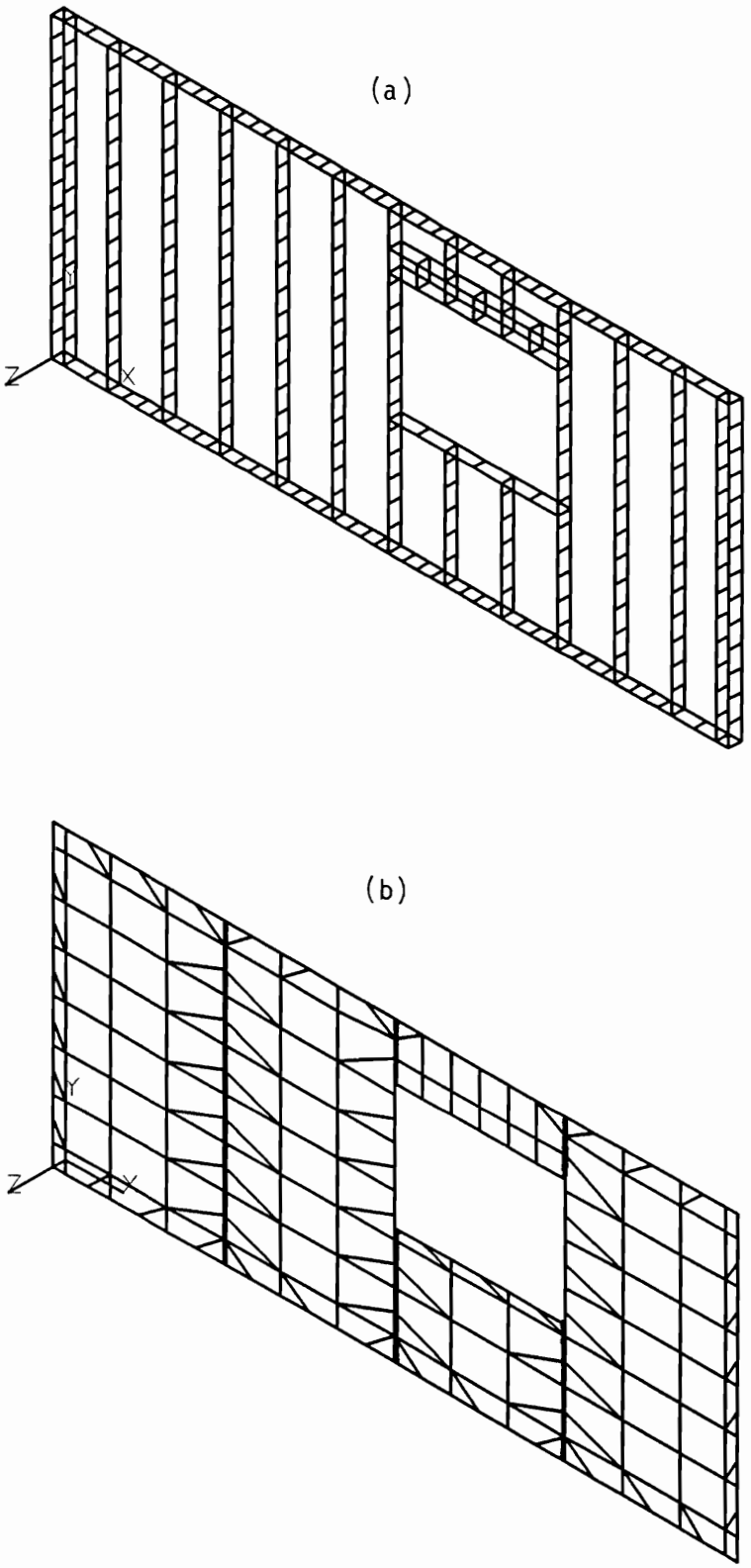

Figure 8. Finite-Element Mesh of the Wall 1, (a) Framing and (b) Sheathing.

Table 2. Element Types and Element Material Properties Used for Wall Modeling.

Element	Element Type	E_x	E_y	G_{xy}	μ_{xy}	DOF	Source
		psi (MPa)	psi (MPa)	psi (MPa)			
Stud	2-D shell	1.88E6 (12962)	0.154E6 (1062)	0.128E6 (883)	0.04	6	Phillips (1990)
Upper beam	2-D shell	1.88E6 (12962)	0.154E6 (1062)	0.128E6 (883)	0.04	6	Phillips (1990)
Lower beam	2-D shell	1.88E6 (12962)	0.154E6 (1062)	0.128E6 (883)	0.04	6	Phillips (1990)
Headers	3-D solid	1.88E6 (12962)	0.154E6 (1062)	0.128E6 (883)	0.04	6	Phillips (1990)
Plywood sheathing	2-D shell	1.73E6 (11928)	0.29E6 (2000)	0.15E6 (1034)	0.08	6	Polensek (1976)
Gypsum sheathing	2-D shell	0.164E6 (1131)	0.094E6 (648)	-	0.07	6	Polensek (1976)
Nails	1-D nonlinear load-deflection	N/A	N/A	N/A	N/A	1	Phillips (1990) Polensek et al (1979)
Gaps	Gap element	N/A	N/A	N/A	N/A	2	N/A

Shear properties of nail connections tested by Phillips (1990) and Polensek (1976b) were used for the load-deformation curves of nonlinear springs representing nail connections. The load-deformation curves for different nail connections loaded in shear are shown in Figure 9. These curves represent the nonlinear regression equations based on 10 specimens. The testing procedure with the load offset of 2 in. (51 mm) generated an eccentricity in the loading resulting in lower stiffness as compared with results published for tests with reduced eccentricity (Gromala, 1985). Load deflection curves can differ substantially as shown in Figure 10. The load-deformation curve for tests with an eccentricity, performed by Phillips (1990), has lower initial stiffness as compared to tests where eccentricity is minimized. Phillips' results were expressed in the form of nonlinear regression equations relating the nail deformation to the shear force. Curves described by these equations never become flat. Extrapolation beyond the data range can lead to an undefined ultimate capacity of the connection and higher connection stiffness for higher loads. Slip between the studs and wall covering was measured by Polensek (1975) who reported a slip of 0.05 in. (1.27 mm) between the stud and plywood sheathing for walls loaded by combination of axial force of 2008 lb (8.93 kN) per stud and pressure of 60 psf (2.87 kPa). The slip is a small value and probably causes difficulties in the experimental measurement. The value of slip is greatly influenced by the testing method as suggested by the results of Figure 10.

Load-deformation curves for nail withdrawal, shown in Figure 11 were obtained from experiments conducted by Groom (1992). This figure illustrates the bilinear character of most curves. Scattered data was typical, but these curves represent the average response. The compressive stiffness of the nail connection is several orders of magnitude higher than the withdrawal stiffness. The magnitude of the

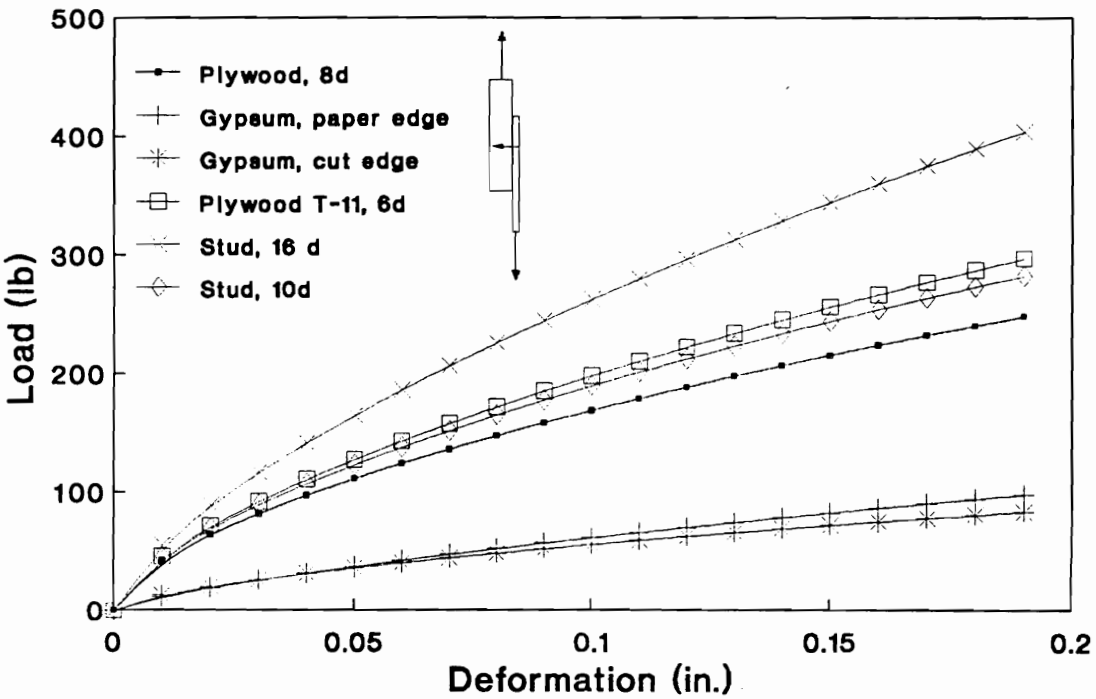

Figure 9. Load-Deformation Characteristics for Nail Connections Loaded in Shear (Phillips, 1990).

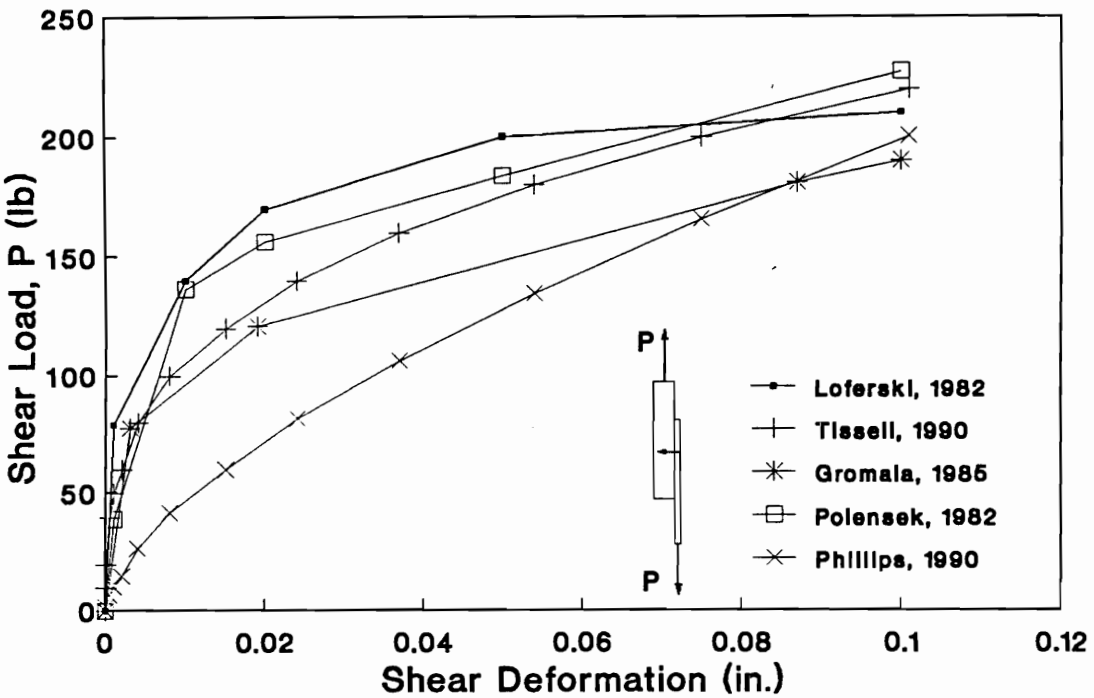

Figure 10. Comparison of Load-Deformation Curves for Connection of Plywood 3/8-1/2 in. Thick and Douglas-Fir Wood Loaded in Shear.

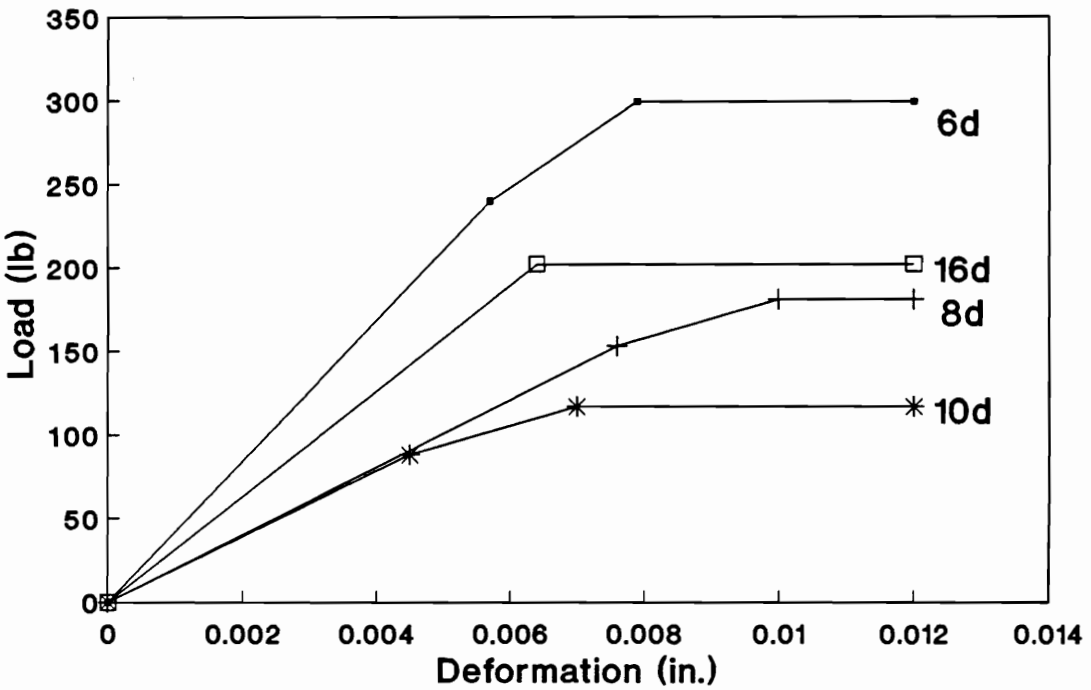

Figure 11. Load-Deformation Characteristics for Nail Connections Loaded in Withdrawal (Groom, 1992).

compressive stiffness is a function of the modulus of elasticity of wood in the direction perpendicular to fibers and the area tributary to one nail connection. The compressive stiffness of the nailed joint is not controlled by nail properties. If higher loads are expected, the stiffness in compression can be modeled as a bilinear material in which the second part of the curve is a horizontal line at the load level corresponding to the crushing strength of the wood.

Verification of the Modeling Method

Results from several experiments were used to verify the modeling method. Results of following experiments were used:

1. Walls tested by Polensek (1975) who applied a combination of axial loads and pressure. Two different wall constructions were tested:
   (a) Bearing wall. The framing was Douglas-fir studs, 2×4 in. (38×89 mm) spaced 24 in. (610 mm) on center, 0.5-in. (13-mm) horizontally oriented gypsum board was used on the tensile side, and 3/8-in. (9.5-mm) plywood vertically oriented was on the compressive side. 6d nails were used to connect the sheathing to the studs. The wall was designated as bearing because of the axial forces applied at the top of each stud. The axial forces simulated the weight of the structure above the wall.
   (b) Nonbearing wall. This wall had the same construction as the bearing wall, except the studs were 2.5-in. (63.5-mm) wide and sheathing was gypsum board on both sides. The nonbearing wall was not loaded by axial forces and only pressure

was applied. The finite-element mesh for the bearing and nonbearing walls is shown in Figure 12.

2. Wall tested in shear by Easley et al (1982). A wall 8×12 ft (2.44×3.66 m) was constructed of 2×4-in. (38×89-mm) Douglas-fir studs spaced 16 in. (406 mm) on center. The stud frame was sheathed from one side with 3/8-in. (9.5-mm) vertically oriented CD exterior plywood. 8d nails spaced 8 in. (203 mm) on the edges and 16 in. (406 mm) in the interior were used to fasten the plywood to studs.

Bearing Walls Tested by Polensek

Polensek (1975) performed combined compression and bending tests for walls without openings such as shown in Figure 12. Walls were subjected to a constant axial force of 884 lb (3.93 kN) on each internal stud and 442 lb (1.97 kN) on the two end studs. The uniform pressure over the plywood face was ramped until the load reached 20 psf (0.96 kPa). This represented the load on a one-story building loaded by dead and snow load combined with wind. Then, the wall was unloaded and loaded by the axial forces to 2008 lb (8.93 kN) per each internal stud (half of the load, 1004 lb (4.47 kN) on the edge studs) and pressure was increased until failure. This axial load simulated the forces resulting from a two-story building.

Polensek (1975, 1976b) measured elasticity properties and strength in bending of each stud and elasticity properties of the gypsum board, which was used on the tensile side. Load-slip curves for nail connections between stud and gypsum board were also experimentally established and were used in the finite-element model. Since the strength of each stud was known, a bilinear material model was used.

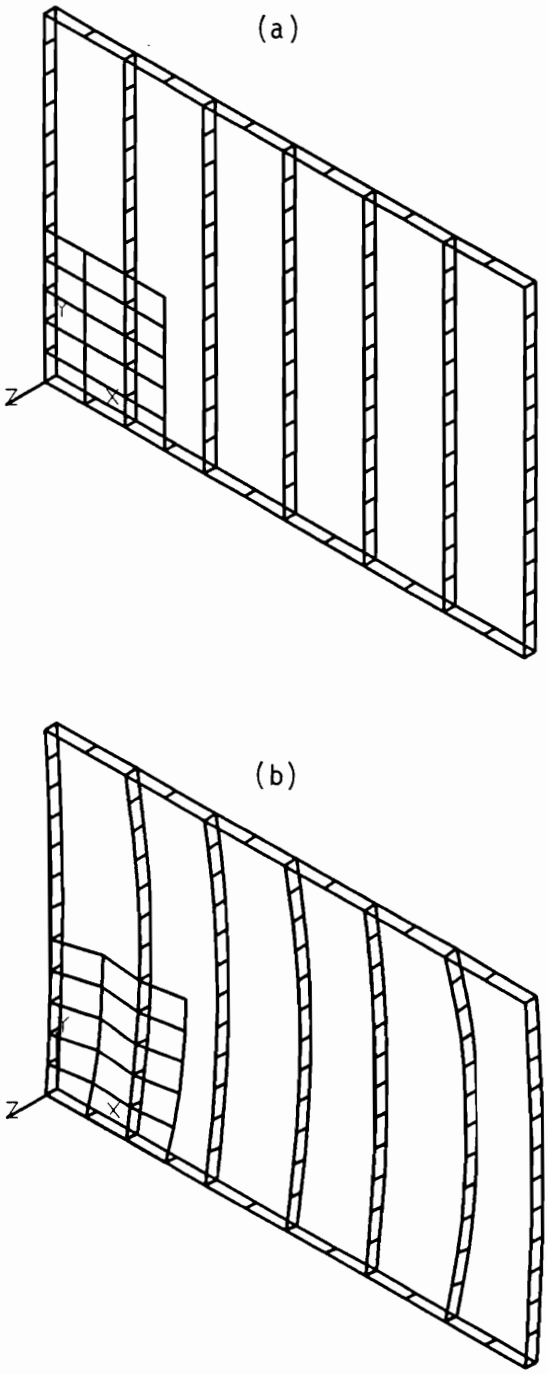

Figure 12. Finite-Element Mesh of the Wall Panel Tested by Polensek (1975) and Used for the Model Verification. The Studs are Shown with Typical Mesh for Sheathing in the Left Corner. (a) Undeformed Mesh and (b) Deformed Mesh.

Thus, the model included partial failures of the studs, a phenomenon observed at higher pressures during the test.

The deformed structure is shown in Figure 12b, while the relationship for the load-deformation is in Figure 13. The offset of the analytical curves in Figure 13a is caused by the axial load, which was applied initially and was followed by a step increase of the lateral pressure and/or shear force. Polensek (1975) used the same sequence except the deflections were zeroed after the axial loading, and therefore, the experimental curve starts from zero. The influence of the axial load to the out-of-plane deformation is, however, small. From Figure 13b, it follows that the shear stiffness of the wall is not influenced by added pressure and/or axial forces. Figure 13b represents analytical results since no experiments were performed for a combination of shear load with an axial load or pressure.

The finite-element model is somewhat stiffer than the tested wall. This may have occurred because only the gypsum properties were measured by Polensek (1975), whereas those of plywood were taken from the literature. The nonlinearity of the experimental curve was not considered to be substantive for pressures up to 40 psf (1.92 kPa) so a linear relationship between pressure and bending deformation was assumed.

The load-stress and load-strain relationship for the wall loaded by a combination of axial load and pressure is shown in Figure 14. The experimental load-strain curve does not include initial strain due to the preapplied axial force. The load increments for a nonlinear analysis had to be reduced after the pressure reached 30 psf (1.44 kPa) which caused a slope change in stress-strain curves for some elements and reduced the convergency rate. Close agreement between experimental and analytical results for strain shows the ability of the three-dimensional finite-element model to be used for the stress analysis of the wall.

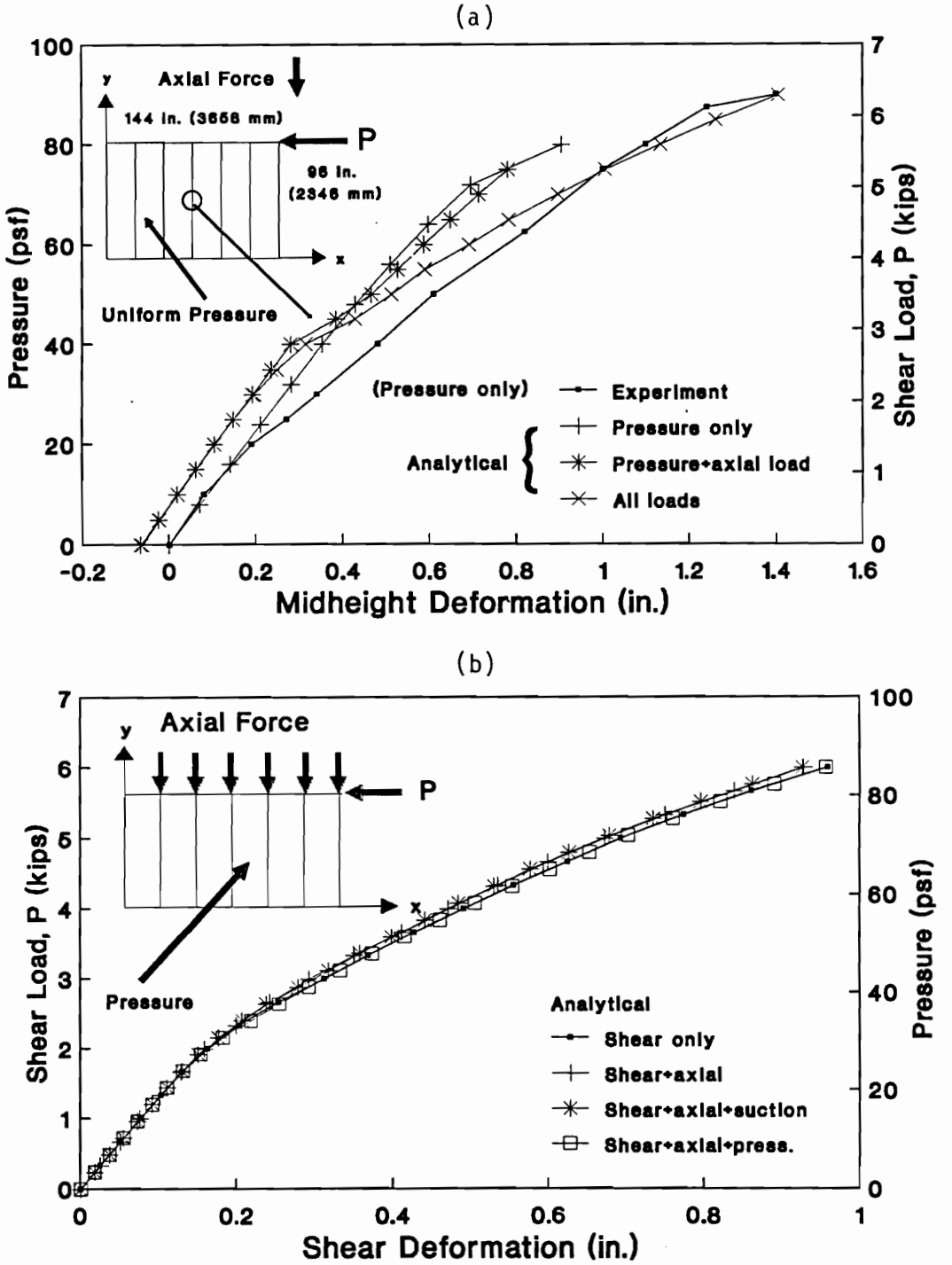

Figure 13. Experimental and Analytical Results for Bearing Wall Tested by Polensek (1975), (a) Bending Deformation at the Wall Mid Stud and (b) Shear Deformation at the Top Plate.

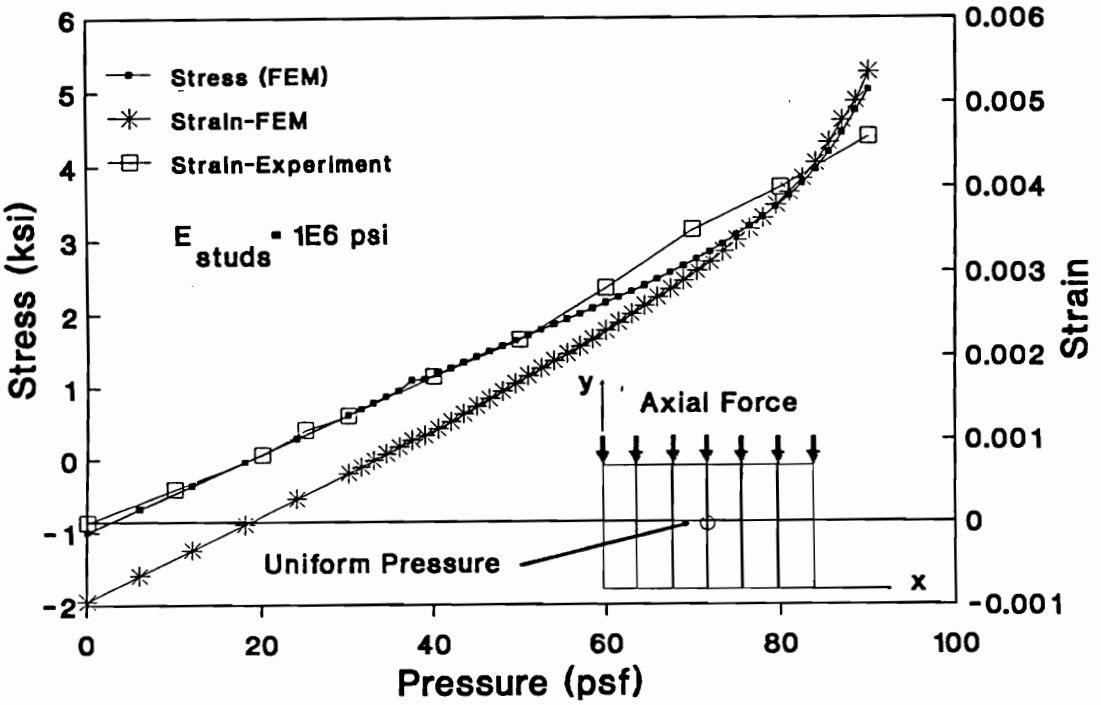

Figure 14. Stress, σ_y, and Strain, ϵ_y, for a Stud in the Wall Loaded by Axial Force and Pressure, Tested by Polensek (1975) and Modeled by Using Finite-Elements.

An important phenomenon which must be investigated is the coupling between bending and shear deformation of the wall. A wall can be loaded by a wind pressure and at the same time can act as a shear diaphragm. The investigated different load combinations showed that there is no strong coupling between bending, shear and axial wall stiffness, unless loads are close to the ultimate failure load for one or more studs. The slip between sheathing and studs during bending load is small, which probably does not cause the joint stiffness degradation. The bending stiffness is predominantly controlled by the stiffness of the studs and sheathing, which results in nearly linear behavior as shown in Figures 13a and 15a, whereas shear stiffness is influenced more by the nail slip resulting in nonlinear behavior-Figures 13b and 15b.

Nonbearing Walls Tested by Polensek

The wall covered on both sides by gypsum board, designated as a nonbearing wall and also tested by Polensek (1975), was analyzed for different load combinations. The construction and finite-element model for this wall was identical to the wall in Figure 12 except the width of the studs (2.5 in.) and sheathing (0.5-in. gypsum board on both sides). The predicted response of the wall to different load combinations is shown in Figure 15. This wall was tested only for pressure loading; the remaining curves in Figure 15 represent the analytical results. The axial and shear loads had no substantial influence on bending performance of wall

loaded by pressure, whereas the shear stiffness decreased as pressure increased. This can be caused by soft nail connections between gypsum and studs and lower bending and shear stiffness of the wall leading to larger deflections and consequently nail shear deformations.

Experiments Performed in Shear

Results of Easley et al (1982) were used to verify the shear wall modeling method. Materials and nail properties reported by them were used to generate the input. They tested the assembly in shear when the bottom plate of the wall was fixed and shear force was applied along the top plate. The three-dimensional finite-element model of the wall is shown in Figure 16 and the experimental and analytical load-deformation curve in Figure 17. Again, the load-deformation relationship for shear was nonlinear and was controlled by the nail connection stiffness. Easley et al (1982) also observed the rigid body rotations of studs for walls loaded in shear. Their analytical model based on this assumption was in a good agreement with the experiments.

The nail shear stiffness is a controlling factor in shear wall performance as documented in Figure 18. In this figure, the shear deformation of wall 4 is compared for two different nail stiffnesses. Also the influence of gaps in sheathing was analyzed for different nail properties reported by Phillips (1990) and Polensek (1976b). Difference in wall stiffness with and without specified gaps between panels was not large. The model with no gaps was somewhat softer because the rigid-body rotation of the panels was not prevented by the contact with the adjacent panels. The advantage of the model without gaps is that a smaller stiffness matrix is formulated and is less demanding

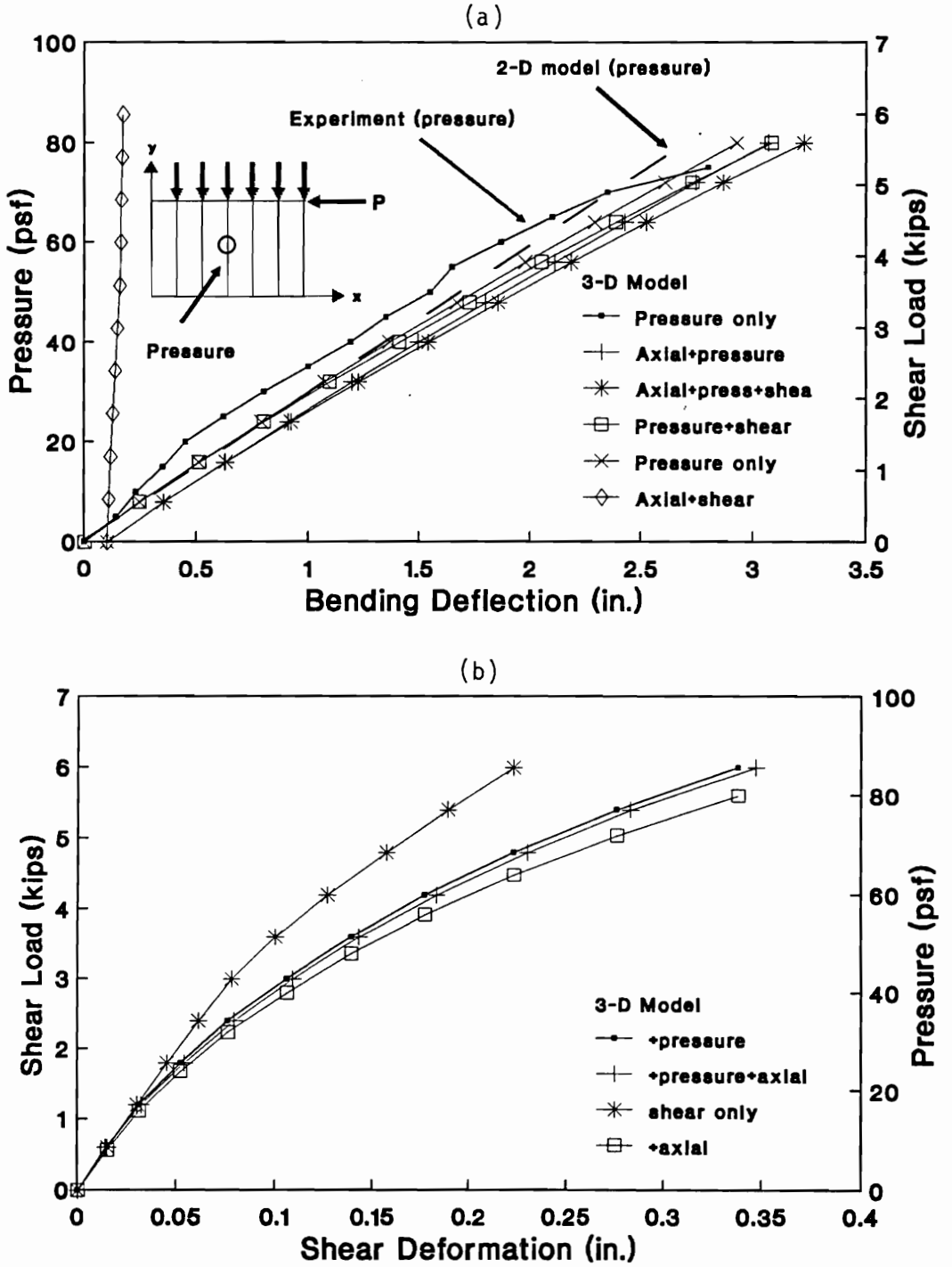

Figure 15. Experimental and Analytical Results for Nonbearing Wall Tested by Polensek (1975); (a) Bending Deformation at the Mid Height of the Center Stud and (b) Shear Deformation at the Top Plate.

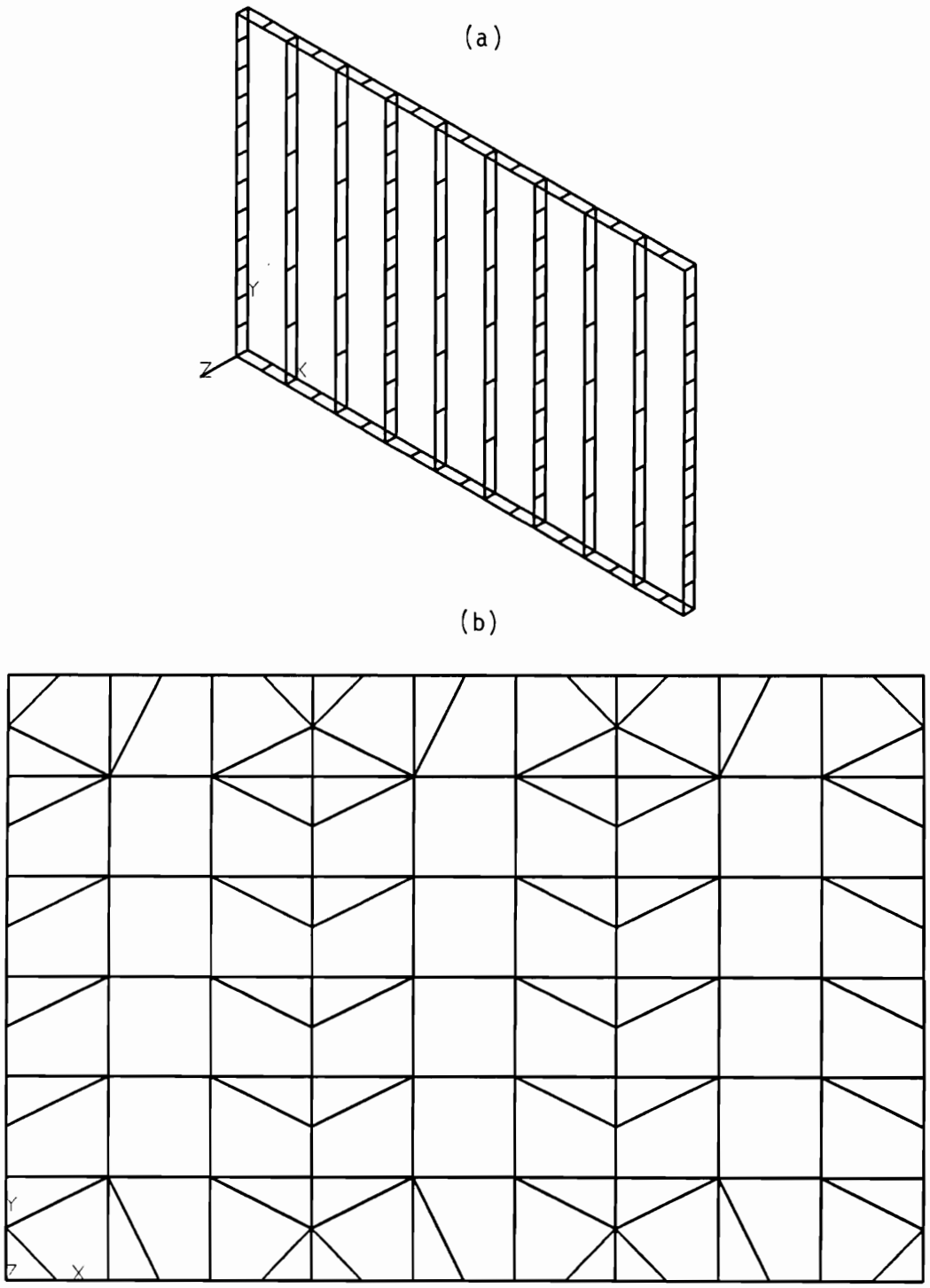

Figure 16. Finite-Element Mesh of Wall Tested by Easley et al (1982) and Used for the Model Verification. (a) Framing, (b) Sheathing.

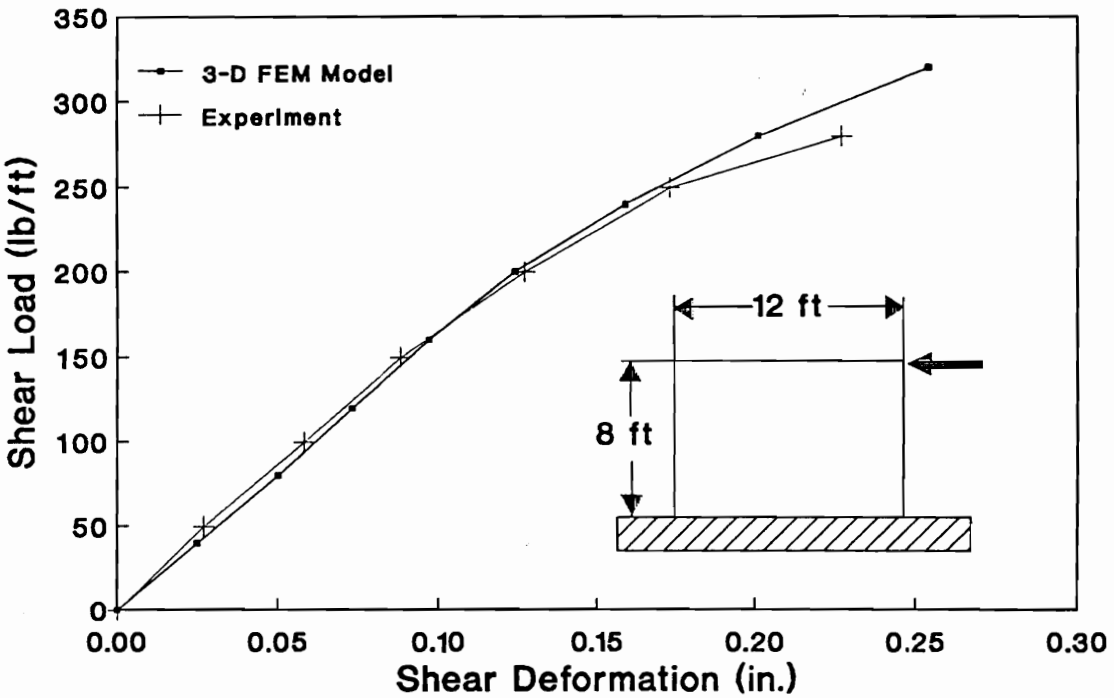

Figure 17. Shear-Deformation of the Wall Tested by Easley et al (1982).

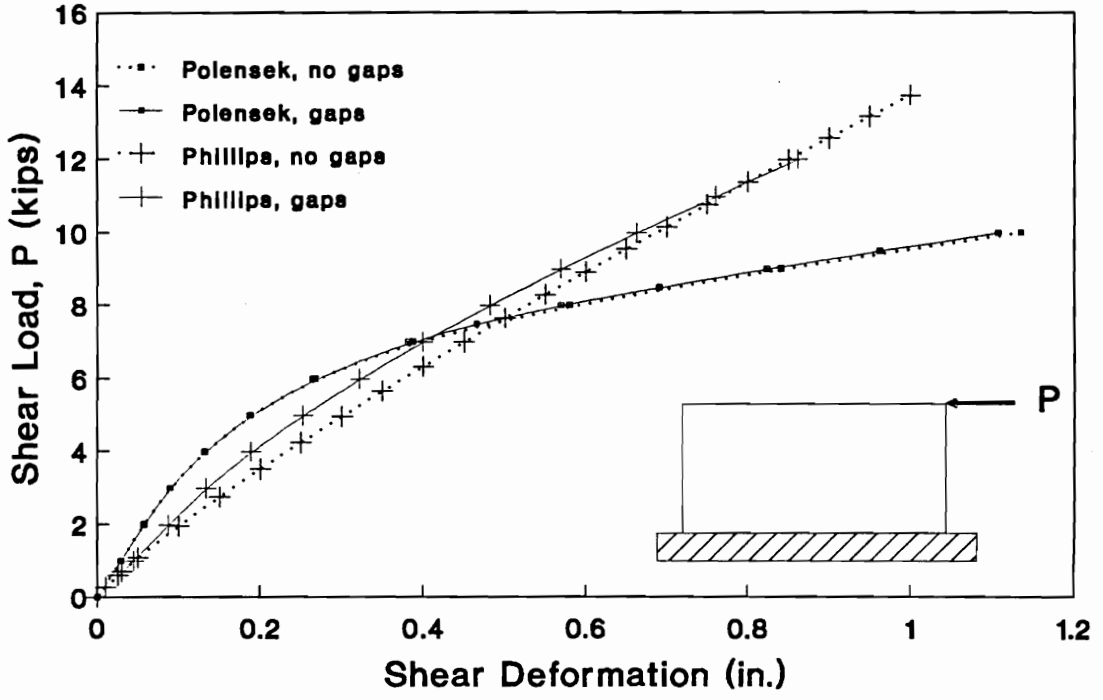

Figure 18. Influence of the Stiffness of Nail Connections and Presence of Gaps on Shear Resistance of Wall 4.

on computational time. However, caution must be exercised, when a stress analysis of the wall is performed. The model without gaps may lead to a distortion of the results.

Equivalent Substructure

The equivalent substructure was required to give the same response as the detailed substructure only with a minimum number of degrees of freedom (the number of equations assembled and solved is to be a minimum). Since in the full structure, reaction forces and the deflections (on the boundaries) were the principal concerns, the focus was on the boundaries where the substructures are connected.

The initial step in the process of developing an equivalent model was to identify primary or master degrees of freedom. These degrees of freedom controlled the behavior of the structure. For example, the rotational degree of freedom of the wall in its own plane is sufficiently defined by the translational stiffness of the connections laying in this plane (two adjacent nodes restrained against translation prevent a rotation of any intermediate point). Thus, master degrees of freedom for the sole plate of the wall in Figure 19 were three translations and one rotation, the rotation around Z-axis (ROTZ). ROTZ must be included because the model is two-dimensional and out-of-plane rotation must be restrained. Therefore, only four out of six possible global degrees of freedom were recognized since the other two rotational degrees of freedom (around x and y-axes) were represented by translation of nodes laying in line. This means that four nonlinear spring elements were needed on each boundary node to create the connection with the rest of the structure.

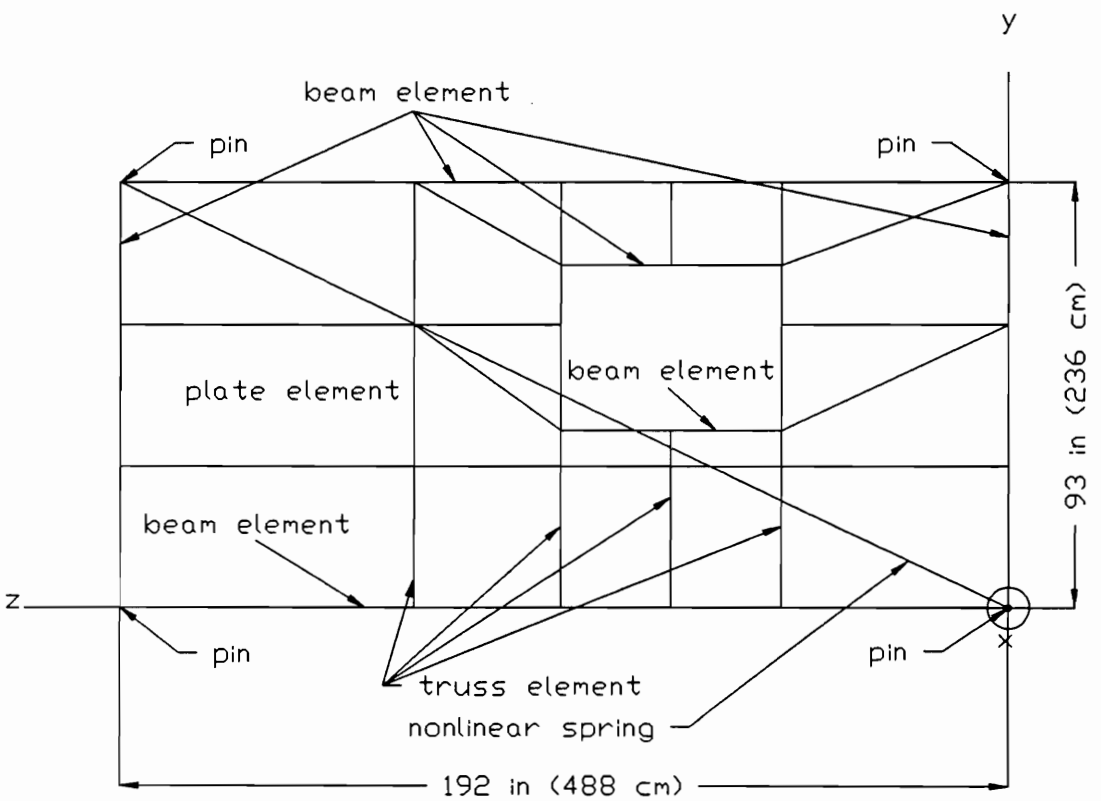

Figure 19. Finite-Element Representation of the Equivalent Model of the Wall 1.

Shear resistance

The shear stiffness was modelled by a nonlinear and nonconservative diagonal spring and a three-dimensional truss created by beam elements pinned at the corners. The use of beam elements made it possible to include additional nodes at the boundary and these nodes were used to connect the wall to the rest of the structure. Also, constraint equations were defined to ensure a rigid-body rotation of the studs in the plane of the wall. Constraint equations express the degree of freedom at one primary node as a linear combination of degrees of freedom at some other nodes. The equation corresponding to the primary degree of freedom is removed from the system. The upper beam undergoes a rigid-body motion in the load direction. This mechanism of shear wall deformation has been documented by several researchers (Tuomi and McCutcheon, 1978; Easley et al, 1982). The nonrigid stud-to-sheathing connection may allow some minor flexure of the studs. This was studied by Gupta and Kuo (1987) who assumed a sinusoidal deformation of the stud. Based on the literature study as well as the observations, it is believed that neglecting possible flex of the stud in in-plane direction of the wall does not constitute a significant error. The model, however, is capable of accommodating the flexibility requirement by adjusting the bending stiffness of the edge studs. To assume a particular shape (such as sinusoidal) may be justified in cases where some additional constraints exist such as blocking in the center of the studs. The upper beam has bending properties equal to the top plate of the real wall. This follows from the continuum approach to the bending and torsional properties of the wall as discussed later.

The edge beams have negligible out-of-plane bending stiffness, infinitely large stiffness for in-plane direction and area equivalent to the area of studs lumped into the edge beam. If double studs on the wall edge are used, the out-of-plane bending stiffness is equal to the bending stiffness of the additional stud. Using this configuration, the only contribution to the global stiffness matrix is the translation in the z-direction and additional bending stiffness in the out-of-plane direction as dictated by double edge studs (if any) and horizontal beams. The load-deflection curve from the shear analysis of the detailed model is the spring stiffness for the equivalent model, or it can be the result from experiment or any other suitable model.

From the analytical investigation of the coupling between bending and shear loads, it follows that shear stiffness may be reduced when the wall is loaded by pressure. To account for the influence of the wall bending on the shear stiffness, the load-deformation curve of the wall in shear can be obtained by analyzing the three-dimensional model for a combination of wind pressure and shear instead of for the simple shear. This can be easily performed since wind pressure (suction) on the outside walls is known from the Uniform Building Code (ICBO, 1988). The pressure and shear must be incremented simultaneously to account for the simultaneous effect of the wind load. Since the walls in the building mostly loaded in shear are not at the same time subjected to high wind pressure (shear walls are located in the direction parallel to the wind direction usually resulting in suction considerably lower than wind pressure on a windward side of the building), the analysis for simultaneous effect will not lead to substantial change in the wall shear stiffness.

The spring element is the diagonal connecting two opposite corners in Figure 19. The stiffness of the nonlinear spring

represented the global shear stiffness of the wall including openings. Using the spring element for shear stiffness significantly reduced the number of the degrees of freedom since no nails are modelled and only global in-plane response is input. Furthermore, the constraint equations specified for internal nodes reduced the total number of degrees of freedom (Kohnke, 1989) given a set of L linear, simultaneous equations.

$$\sum_{j=1}^{L} K_{ij}u_j=F_k \quad (1\leq k\leq L) \tag{4}$$

Where u_j = unknown deformations
K_{ij} = stiffness matrix
F_k = load vector

Constraint equations are in the form

$$\sum_{j=1}^{L} C_j u_j=C_0 \tag{5}$$

The primary degree of freedom is denoted u_i and (5) is normalized by dividing by C_i

$$\sum_{j=1}^{L} C_j^* u_j=C_0^* \tag{6}$$

where

$$C_j^*=\frac{C_j}{C_i} \quad \textit{and} \quad C_0^*=\frac{C_0}{C_i}$$

Since $C_i^*=1$, Equation (6) can be written in the form

$$u_i+\sum_{j=1}^{L} C_j^* u_j=C_0^* \quad for \quad j\neq i \tag{7}$$

$$K_{ki}u_i+\sum_{j=1}^{L} K_{kj}u_j=F_k \quad for \quad j\neq i \tag{8}$$

Multiplying Equation (7) by K_{ki} and subtracting from Equation (8) the following expression is obtained

$$\sum_{j=1}^{L} (K_{kj}-C_j^*K_{ki})\, u_j=F_k-C_0^*K_{ki} \quad for \quad j\neq i$$

$$and\ for\ k=i \tag{9}$$

$$\sum_{j=1}^{L} (K_{ij}-C_j^*K_{ii})\, u_j=F_i-C_0^*K_{ii}$$

Now a Lagrangian multiplier λ_k is introduced

$$\lambda_k=\frac{\partial u_i}{\partial u_k} \tag{10}$$

and Equation (9) is rewritten

$$\sum_{j=1}^{L} (K_{kj}-C_j^*K_{ki})\, u_j-F_k+C_0^*K_{ki}+\lambda_k\sum_{j=1}^{L} (K_{ij}-C_j^*K_{ii})\, u_j-F_i+C_0^*K_{ii}=0 \tag{11}$$

$$for\ j\neq i$$

From Equation (7) by solving for u_j and computing the partial derivative with respect to u_k

$$\lambda_k=-C_k^* \tag{12}$$

and substituting into Equation (11)

$$\sum_{j=1}^{L} (K_{ij}-C_j^*K_{ki}-C_k^*K_{ij}+C_k^*C_j^*K_{ii})\,u_j=F_k-C_0^*K_{ki}-C_k^*F_i+C_k^*C_0^*K_{ii} \qquad \textbf{(13)}$$

$$for\ j\neq i$$

Which can be written in the form

$$\sum_{j=1}^{L-1} K_{kj}^*u_j=F_k^* \qquad for\ (1\leq k\leq L-1) \qquad \textbf{(14)}$$

This is the new matrix equation relating loads to displacements.

$$K_{kj}^*=K_{kj}-C_j^*K_{ki}-C_k^*K_{ij}+C_k^*C_j^*K_{ii}$$

$$and \qquad \textbf{(15)}$$

$$F_k^*=F_k-C_0^*K_{ki}-C_k^*F_i+C_k^*C_0^*K_{ii}$$

and the i-th equation

$$K_{ij}^*=K_{ij}-C_j^*K_{ii}-C_i^*K_{ij}+C_i^*C_j^*K_{ii}$$

$$but\ since \quad C_i^*=1 \qquad \textbf{(16)}$$

$$K_{ij}^*=0$$

and similarly $K_{ki}^*=0$ and $F_i^*=0$. Thus, the i-th equation, with primary degree of freedom u_i drops out of the system and L-1 equations are solved. The force applied to the primary degree of freedom is redistributed into the remaining nodes in the constraint equation. However, this would mean that the intercomponent forces are not transmitted through the

boundary if constraint equations are specified there. Thus, a beam element with an infinite stiffness in the in-plane direction of the wall is used to ensure a rigid-body rotation of the edge stud (instead of constraint equations) and this ultimately leads to proper force redistribution along the wall edge.

Out-Of-Plane Stiffness

Wind pressure and reaction forces from perpendicular walls and diaphragms cause bending and torsional moments. These forces are resisted by the wall which can act as a bending member.

The bending stiffness is modeled by superimposing a two-dimensional plate element with the membrane stiffness removed. The plate is orthotropic to account for different stiffnesses of the wall in the height and width of the wall. An iterative solution for the orthotropic plate under different boundary and loading conditions is used to establish the plate stiffness. An equation of the orthotropic plate (Lekhnitskii, 1987) is solved for the displacements

$$D_{11}\frac{\partial^4 w}{\partial x^4}+2D_3\frac{\partial^4 w}{\partial x^2\partial y^2}+D_{22}\frac{\partial^4 w}{\partial y^4}=p(x,y) \qquad (17)$$

Where D_{11}, D_{22}, D_3=bending stiffnesses and combined stiffness

$D_3=D_{11}\nu_{21}+2D_k$

$D_k=Gh^3/12$

G = shear modulus

ν_{21} = Poisson's ratio of the plate

h = plate thickness

w=w(x,y) deflection at point x,y
p(x,y)=load

The general solution can be expressed in the form of the double Fourier series as (Lekhnitskii, 1987)

$$w=\sum_{m}^{\infty}\sum_{n}^{\infty} A_{mn}\sin\left(\frac{m\pi x}{a}\right)\sin\left(\frac{n\pi y}{b}\right) \qquad (18)$$

Where A_{mn} = Fourier coefficient
a = length of the plate
b = width of the plate
m,n=1,3,5,7...,∞

Solutions of the equation (17) depend on the loading and boundary conditions and are available in the literature (see e.g. Lekhnitskii, 1987). For pure torsion of the plate loaded at opposite corners by force 2P, Lekhnitskii (1987) proposed a general solution in the form

$$w(x,y)=Ax^2+Bxy+Cy^2+C_1x+C_2y+C_0 \qquad (19)$$

Bending moments M_x, M_y, and normal forces N_x, N_y are zero and torsional moment M_{xy}=P. For moments, the following hold

$$M_x=-D_{11}\left(\frac{\partial^2 w}{\partial x^2}+\nu_{21}\frac{\partial^2 w}{\partial y^2}\right)$$
$$M_y=-D_{22}\left(\frac{\partial^2 w}{\partial y^2}+\nu_{12}\frac{\partial^2 w}{\partial x^2}\right) \qquad (20)$$
$$M_{xy}=-D_k\frac{\partial^2 w}{\partial x\partial y}$$

Using Equation (19) and (20), and applying boundary conditions w(0,b)=0, w(a,0)=0 and symmetry condition w(0,0)=w(a,b) leads to a solution in the form

$$w(x,y) = -\frac{P}{2D_k}\left(xy - \frac{b}{2}x - \frac{a}{2}y + \frac{ab}{2}\right) \quad (21)$$

and the deflection at the corners is

$$w(a,b) = w(0,0) = -\frac{P}{4D_k}ab \quad (22)$$

from which torsional stiffness D_k can be easily computed

$$D_k = -P\frac{ab}{4w(0,0)} \quad (23)$$

Loading and boundary conditions used to obtain finite-

Table 3. Loading and Boundary Conditions for Plate.

Load	Case	Boundary conditions
Uniformly distributed pressure over the wall surface	1	4 edges simply supported
	2	2 short-edges simply supported
	3	2 long-edges simply supported
Pure torsion	4	2 opposite-corners simply supported

element solutions of the global model are given in Table 3. These finite-element solutions represent values of deformations for given loading and boundary conditions. Using the deflections from the numerical solutions and applying known analytical solutions plate stiffnesses can be estimated as follows.

First, the initial estimates of D_{11} and D_{22} are obtained from the condition having the two opposite edges simply supported which corresponds to the simple beam case. The torsional stiffness D_k is calculated from the pure torsional case. Then, the case of 4-edges simply supported is utilized and the solution published by Lekhnitskii (1987) is used to refine the estimate of D_{11}, D_{22} and D_3 stiffness. An iterative procedure was used to calculate the plate stiffnesses. Solutions for the deflections for the tested load cases are in Table 4. A program for the calculation of the orthotropic elasticity properties of a plate continuum is in Appendix C.

The values of the plate stiffnesses were used to obtain the orthotropic material properties of the fictitious plate having only bending stiffness. For the wall in Figures 8 and 19, a segment on the left of the window was analyzed, which was defined as basic structural unit of the wall; a segment of seven studs spaced 16 in. (406 mm) on center, sheathed on both sides, and with no horizontal beams. Thus, an analysis of a representative segment was performed as a three-dimensional finite-element analysis using the procedure as outlined. The representative segment, variable in size and sheathing orientation, is dependent on the wall being analyzed. The resulting orthotropic material properties were assigned to all areas around the window. Continuity conditions of the finite-element formulation ensured common displacements for the boundaries of the areas. Headers and horizontal plates around openings stiffened the performance of the basic structural segment. This effect was achieved by superimposing beam elements representing the stiffness of the headers and upper and lower beam into the equivalent model as shown in the model in Figure 19.

Table 4. Solutions for the Load Cases given in Table 3.

Case	Deflection at point x,y, w(x,y)
1	$w=b^4/\pi^4 \sum_m \sum_n a_{mn} [\sin(m\pi x/a) \sin(n\pi y/b)]/D$ where $D=D_{11}(m/c)^4+2D_3n^2(m/c)^2+D_{22}n^4$ $a_{mn}=16p/mn\pi^2$ $m,n=1,3,5,7...\infty$
2	$w=5pb^4/384\ D_{22}$
3	$w=5pa^4/384\ D_{11}$
4	$w=[-P/(2D_k)](xy-bx/2-ay/2+ab/2)$ $P=H/2$

Where a=width of the
b=height of the wall
p=uniform pressure per unit area
c=a/b
H=force applied at the opposite corners, two other corners supported
x,y=points for which the deflection w is calculated

Compression in the Stud Direction

So far, the continuum had bending and torsional stiffness equal to that of the wall superimposed on the truss giving the model in-plane stiffness. Compression stiffness was added by superimposing truss elements in the direction of the studs. These truss elements represented the capacity of the wall to resist vertical loading. Double studs at the corners and window framing studs were included into the model via corresponding cross-sectional properties. The total cross-sectional area of the truss elements was equal to the total cross-sectional area of the vertical studs minus the area already defined by the vertical beams. For the coarse mesh in Figure 19, several studs were lumped into one element, thus the area of an individual truss element was larger than the area of a single stud.

The cross-sectional properties of the vertical elements which represented studs were different for each finite-element mesh. The total cross-sectional area, however, was independent of mesh size. The following calculation illustrates the principle used in the calculation of the cross-sectional area of the vertical truss elements:

$$A_{tot} = (n-2)\,A_{stud} \tag{24}$$

$$A_{truss} = \frac{A_{tot}}{N_{truss}} \tag{25}$$

Where: A_{stud} = cross-sectional area of one stud
A_{tot} = cross-sectional area of all studs minus the area of two edge studs if double edge studs are used
A_{truss} = cross-sectional area of one vertical truss
n = total number of vertical studs

N_{truss} = number of vertical truss elements

However, the area of the edge studs was a function of the mesh size and was calculated as follows:

$$A_{edge}=A_{truss}+A_{stud} \quad (26)$$

Where: A_{edge} = cross-sectional area of the edge beam

The area of the edge beam was the area of the truss element plus the area of the additional edge stud if double edge studs were used. The moments of inertia depended on the thicknesses of the beam. The beam must have an "infinite" stiffness in the in-plane direction and "zero" stiffness in out-of-plane direction to ensure the rigid body rotation of the edge studs and to eliminate the use of constraint equations. In fact, the stiffness was finite, but greater than an order of magnitude than it would be if real stud properties were used.

Rigid-body motion constraints were imposed on all internal nodes laying in line parallel with the z-axis. The requirement for rigid-body motion was based on observation of experimental tests and results.

Equivalent Model Verification

The equivalent wall model was verified using results of Polensek (1975) for nonbearing and bearing walls. Bending and torsional loads were applied to the three-dimensional detailed model and plate stiffnesses were computed using solutions presented in Table 4. Values of deflections obtained from finite-element analysis and corresponding elasticity properties for the plate 1 in. (25.4 mm) thick are in Table 5 (a unit thickness of the plate was chosen).

Table 5. Input and Results for the Plate 1-in. Thick Used to Represent the Nonbearing Stud Wall Tested by Polensek (1975).

Item	Unit	Bearing Wall	Nonbearing Wall
Height	in. (cm)	96 (244)	96 (244)
Length	in. (cm)	144 (610)	144 (610)
Thickness	in. (mm)	1 (25.4)	1 (25.4)
Testing pressure	psf (Pa)	20 (958)	20 (958)
Stiff bending deflection	in. (mm)	0.17831	0.6521 (16.6)
Soft bending deflection	in. (mm)	60 (1524)	75 (1950)
4 sides supported deflection	in. (mm)	0.1741	0.58 (14.7)
Reaction for 1 in. (25.4 mm) torsional deflection	lb (N)	7.1 (31.6)	10.1 (44.9)
E_x	psi (MPa)	0.160E6 (1103)	0.138E6 (952)
E_y	psi (MPa)	0.107E6 (73776)	0.315E7 (21719)
G_{xy}	psi (MPa)	0.151E6 (1041)	0.233E6 (1606)
μ_{xy}	-	0.001	0.02

Note the large deflection of the panel in the soft direction (only the two end studs are supported) which means that there was a very low stiffness in that direction. Truly, such a deflection is unrealistic and a lower load should be used to avoid the geometry change. In this case, the value of the deflection for a given pressure was extrapolated from lower pressure value to demonstrate the difference in the stiffness along and across studs. The orthotropic plate 1 in. (25.4 mm) thick was superimposed over the truss system representing shear and axial resistance of the wall, and the resulting model was loaded by pressure, 20 psf (956 Pa), and axial force, 884 lb (3.932 kN), on the top of internal studs and 442 lb (1.97 kN) on the top of end studs.

The equivalent model mesh was 4×6 elements, each stud was represented by its true cross section. The resulting deflection for the nonbearing wall as compared to the three-dimensional finite-element model and experimental result is shown in Figure 15. The differences among the equivalent model, detailed model and experiment were caused by modeling simplifications. For example, the bending properties of the orthotropic plate were obtained from the iterative solution while the plate stiffnesses were adjusted until the analytical solution of the orthotropic plate with 4-sides supported case matched the finite-element solution for the three-dimensional model. This means that the three-dimensional structure was modeled by the two-dimensional continuum, which is an approximation.

A comparison of the models to the bearing wall tested by Polensek (1975) is in Figure 20. The finite-element mesh and loads were the same as for the nonbearing wall except that axial forces were 1004 lb (4.47 kN) and 2008 lb (8.97 kN) on end and internal studs, respectively. The equivalent linear model was sufficiently accurate for pressures up to 20 psf (958 Pa). Then both three-dimensional (nonlinear) and equivalent (linear) models become stiffer than the

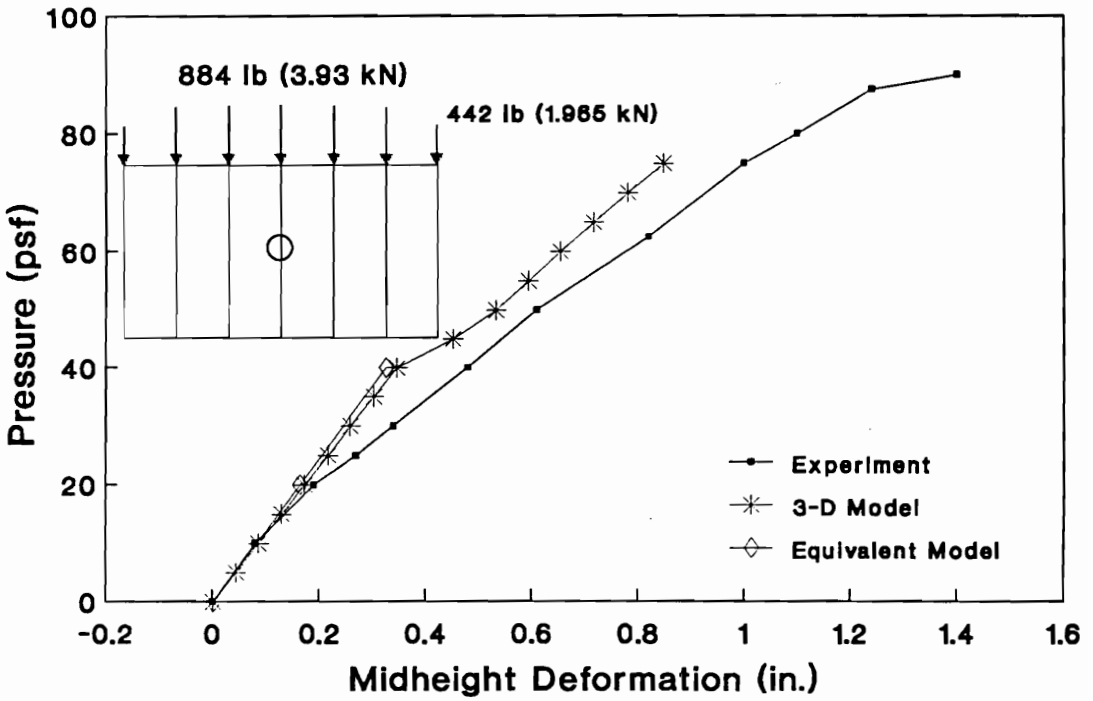

Figure 20. Experimental and Analytical Results for Bearing Wall Tested by Polensek (1976a) and Loaded by Axial Forces and Pressure. Verification of the Equivalent Model.

experimental wall. For most cases, a pressure of about 20 psf (958 Pa) is sufficiently high. As an example, a wind velocity of 90 mph (144 km/h) causes the wind pressure of approximately 21 psf (1005 Pa) on the windward wall of low-rise building. This, however, represents rather severe conditions.

The study of the mesh size on the resulting deflection of the equivalent model of the experimental wall is shown in Figure 21. A simply supported orthotropic plate loaded by uniform pressure was analyzed analytically using solutions given in Table 4. A 2×2 element mesh gives an error already less than 2.5% at the middle nodal point and the error decreases rapidly with increased number of elements. Thus, rather small numbers of elements yield satisfactory results for deflections. This would not be the case if internal forces due to the bending were of interest. However, only boundary deformations and reaction forces are of interest. If the stress analysis is required, it can be pursued as the analysis of the three-dimensional model of the substructure.

Generation of the Characteristic Properties for Equivalent Models

The equivalent models represent their three-dimensional counterparts in a three-dimensional full-structure model. The input characteristics which are represented by geometrical (thickness, depth, area, moment of inertia) and physical properties (modulus of elasticity, Poisson's ratio) of different elements must be generated from three-dimensional models, experiments and geometrical and physical characteristics of real substructures.

In this work, two approaches were used and combined:

(1) shear stiffness of the shear walls was based on the experimental results given by Phillips (1990) who

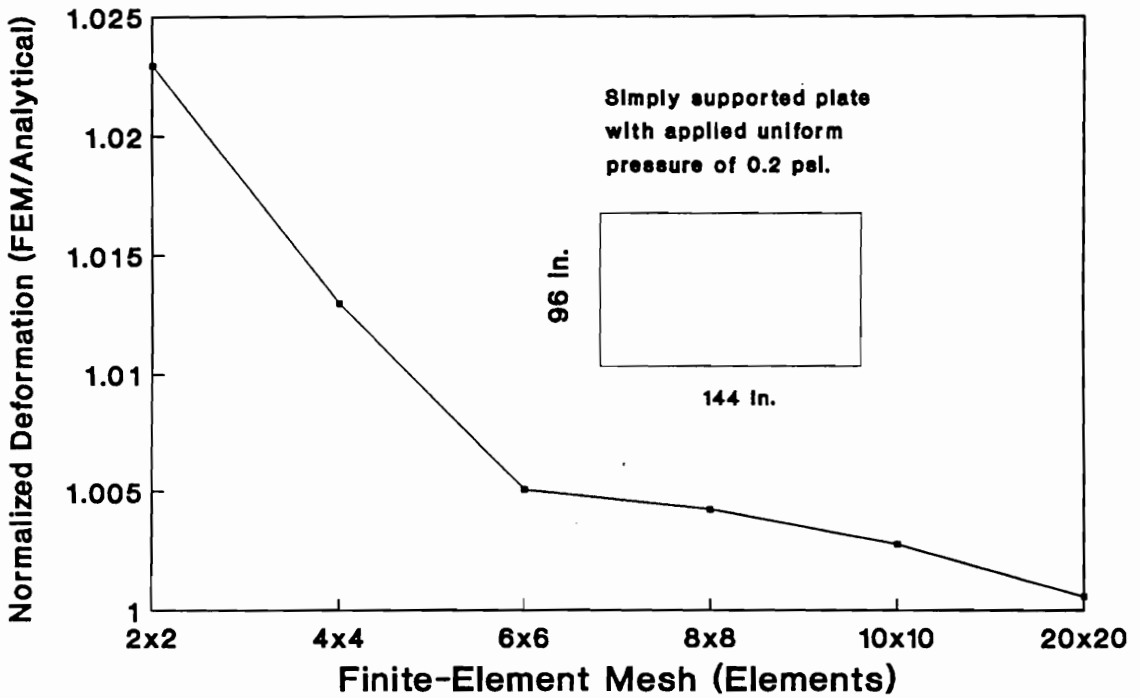

Figure 21. Effect of the Finite-Element Mesh Size on the Accuracy of the Equivalent Model Loaded in Bending.

measured net shear deformation of each shear wall as a function of the cycling shear force. This led to a gradual deterioration of the shear wall stiffness due to the nail stiffness degradation as observed by Polensek and Schimmel (1991). However, the load-deformation curves available for the nail connections, describe only one loading, which will lead to a stiffer three-dimensional model of the wall. Thus, the experimental load-deformation curves for the walls were used to define the stiffness of the diagonal nonlinear spring in the equivalent model.

(2) all other parameters of the equivalent models were generated from the three-dimensional wall finite-element models as described earlier.

Shear Stiffness

The shear stiffness of the wall is controlled by the shear stiffness of the connections between the wall covering and the studs. This connection is nonlinear and nonconservative and its stiffness changes with the load history, number of cycles and load level.

The example of the nail joint subjected to cyclic loading is in Figure 22 (Chou, 1987). The envelope (backbone) curve describes the joint behavior rather well and has been used by several researchers to simplify joint behavior (Chou, 1987; Dolan, 1989; Polensek and Schimmel, 1991) who even linearized the curve by using several secant lines. Successive loadings cause the largest displacements due to the gradual stiffness degrade of the joint. Thus, the envelope (or backbone) curve for the wall will result in less stiff load-deformation characteristics as compared to the static loading with no cycling.

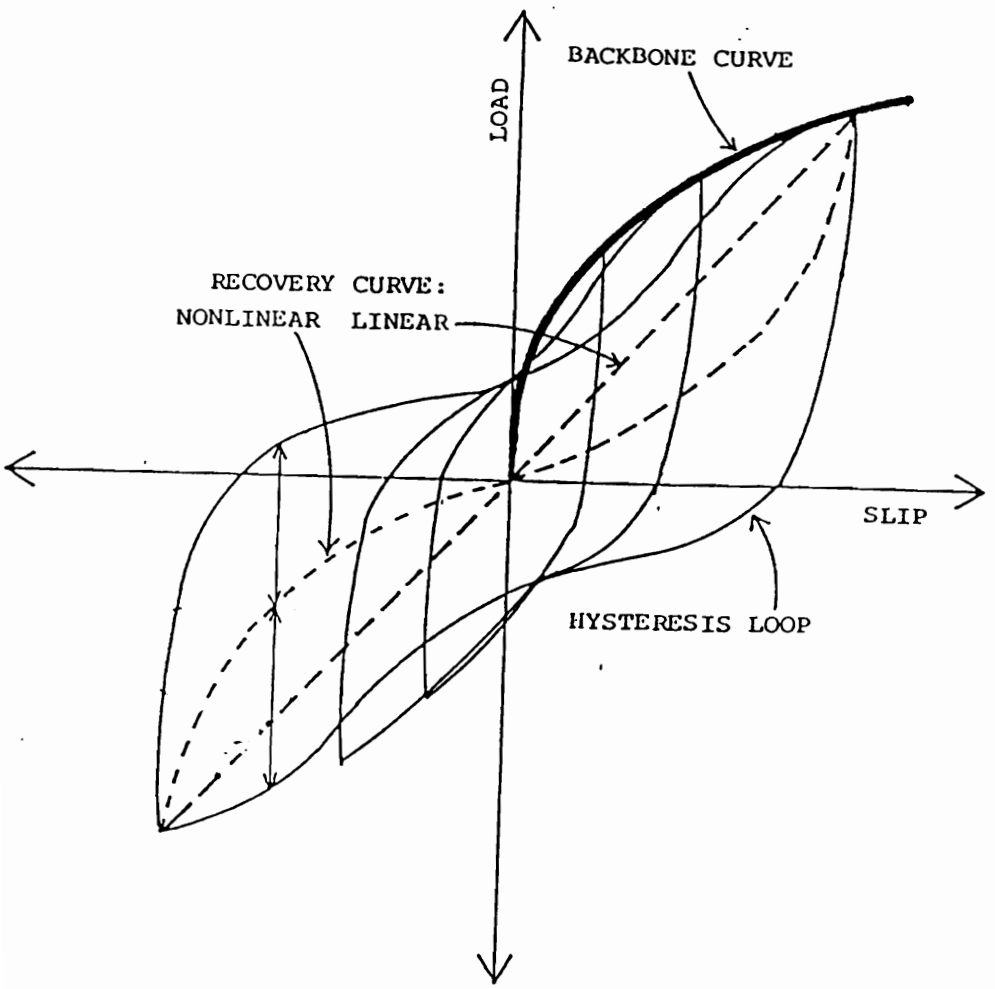

Figure 22. Example of the Nail Joint Subjected to Cycled Loading (Chou, 1987).

The backbone-curve-approach shown in Figure 22, was used to obtain load-deformation characteristics for walls. This procedure is shown in Figures 23 and 24. The nonlinear regression model shown in Figure 23 was used to approximate the relationship between load and deformation of the wall. The regression curve plotted as a thick line represents a least-square approximation of the shear load-deformation relationship experimentally obtained by Phillips (1990). High regression coefficients shown in Figures 23 and 24 support the suitability of the regression model.

Another problem arising from reversible loading in light-frame wood buildings is that the unloading path of the structure may not follow the loading path, thus yielding a nonconservative system. If the unloading path follows the loading path, the system is conservative and no energy loss occurs. With the nonconservative system, the unloading path must be specified and this is defined by an unloading modulus. However, to address this problem is beyond the scope of this research, and, therefore, simplifications were made.

From Figures 23 and 24 it follows that either the tangent or chord modulus can be used to linearize the unloading path. None of the lines has constant slope which indicates that the unloading path is a function of load level and, most likely, load history (number of cycles, frequency, load level, previous loading etc.). The tangent to an unloading curve changes with decreasing load, whereas the chord connecting the peak and zero load for a given wall and cycle does not change significantly as shown in Figure 23. This lead to an approximation of the unloading path via chord modulus.

For the nonlinear nonconservative element used to model shear resistance of the wall, the unloading path followed the first defined slope (initial slope). The initial slope of the load-deformation curve for the wall had the form

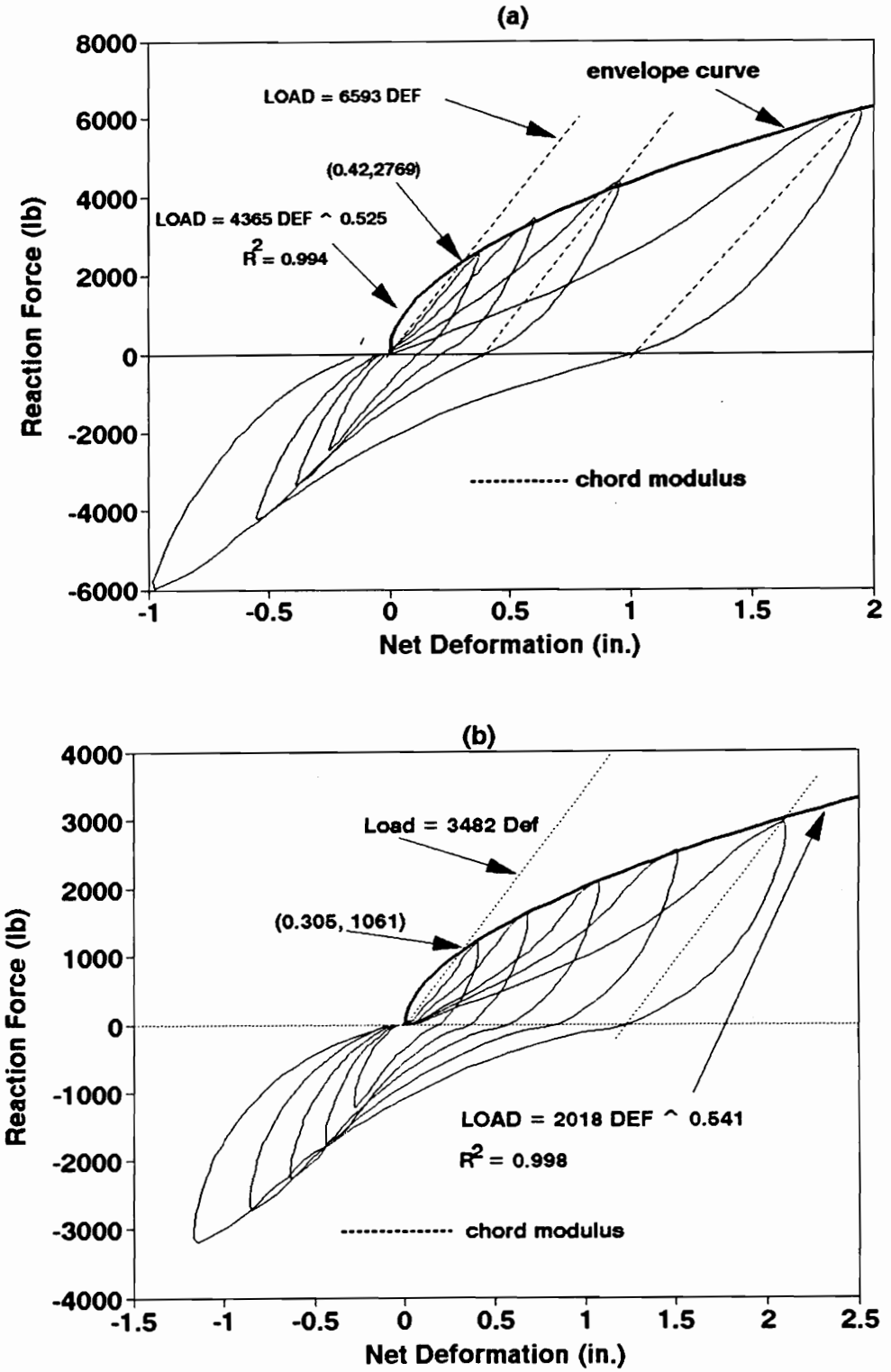

Figure 23. Generation of the Characteristic Load-Deformation Curves for Shear Stiffness of the Equivalent Models of (a) Wall 1 and (b) Wall 2, where the Envelopes Are Experimental Data by Phillips (1990).

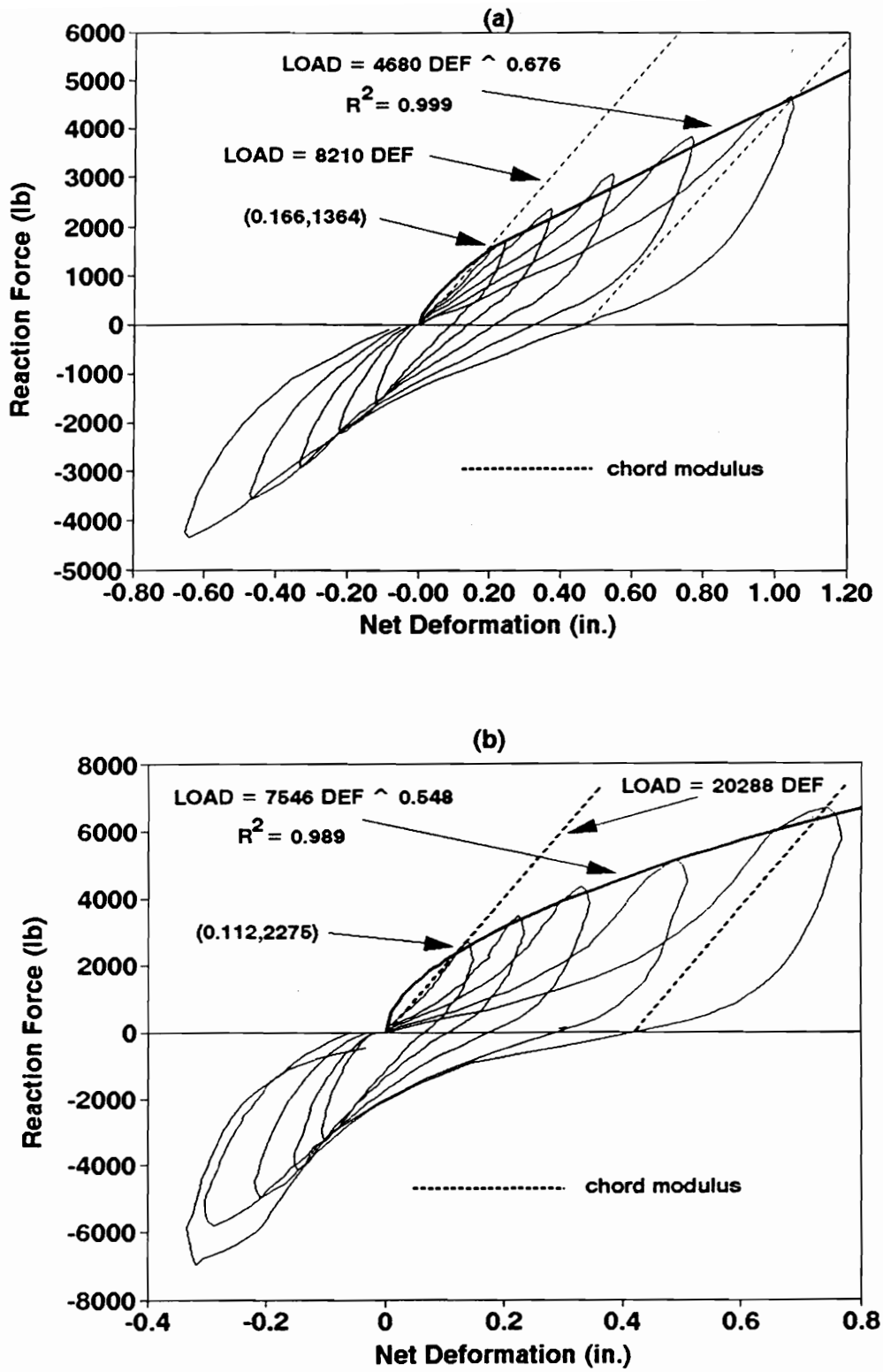

Figure 24. Generation of the Characteristic Load-Deformation Curves for Shear Stiffness of the Equivalent Models of (a) Wall 2 and (b) Wall 3, where the Envelopes Are Experimental Data by Phillips (1990).

LOAD=k*DEFORMATION, where k is the initial slope. The wall load-deformation curve is a power function of the form LOAD=a*DEFORMATION^b, where a and b are constants. The intersection of the straight line passing through the origin with the curve defined by power function is $x_{int}=(\frac{a}{k})^{\frac{1}{1-b}}$,

where a and b are coefficients of the power function above. The intersection defines the point on the nonlinear curve from which every slope is smaller than the initial one. This is important since unique slopes are defined throughout the whole load-deformation path. However, an initial error is introduced due to the linearization because the relationship between load and deformation is linear up to the deformation designated as x_{int}. Thus, the wall behaves in linear manner until a deformation x_{int} is reached. If no unloading is studied (for example in the case of a structure analyzed for static loads), the original envelope curve without a linear portion can be used and wall behaves in a nonlinear fashion throughout the whole course of loading.

The functions used to model the nonlinear springs representing wall shear stiffness were developed from the experiments as well as finite-element analyses and are shown in Figure 25. The analytical curves were stiffer because a non-degraded nail load-deformation curve was used as the input for the three-dimensional models. The experimental curves represent approximate values, since they were obtained from the full structure testing and relate the internal wall reaction as measured by the load cells and horizontal wall displacement after subtracting the rigid body motions (Phillips, 1990). However, in the real design situation only analytical curves will be available. Thus, one must recognize that the wall shear stiffness depends not only on the magnitude of the wall deformation but also on

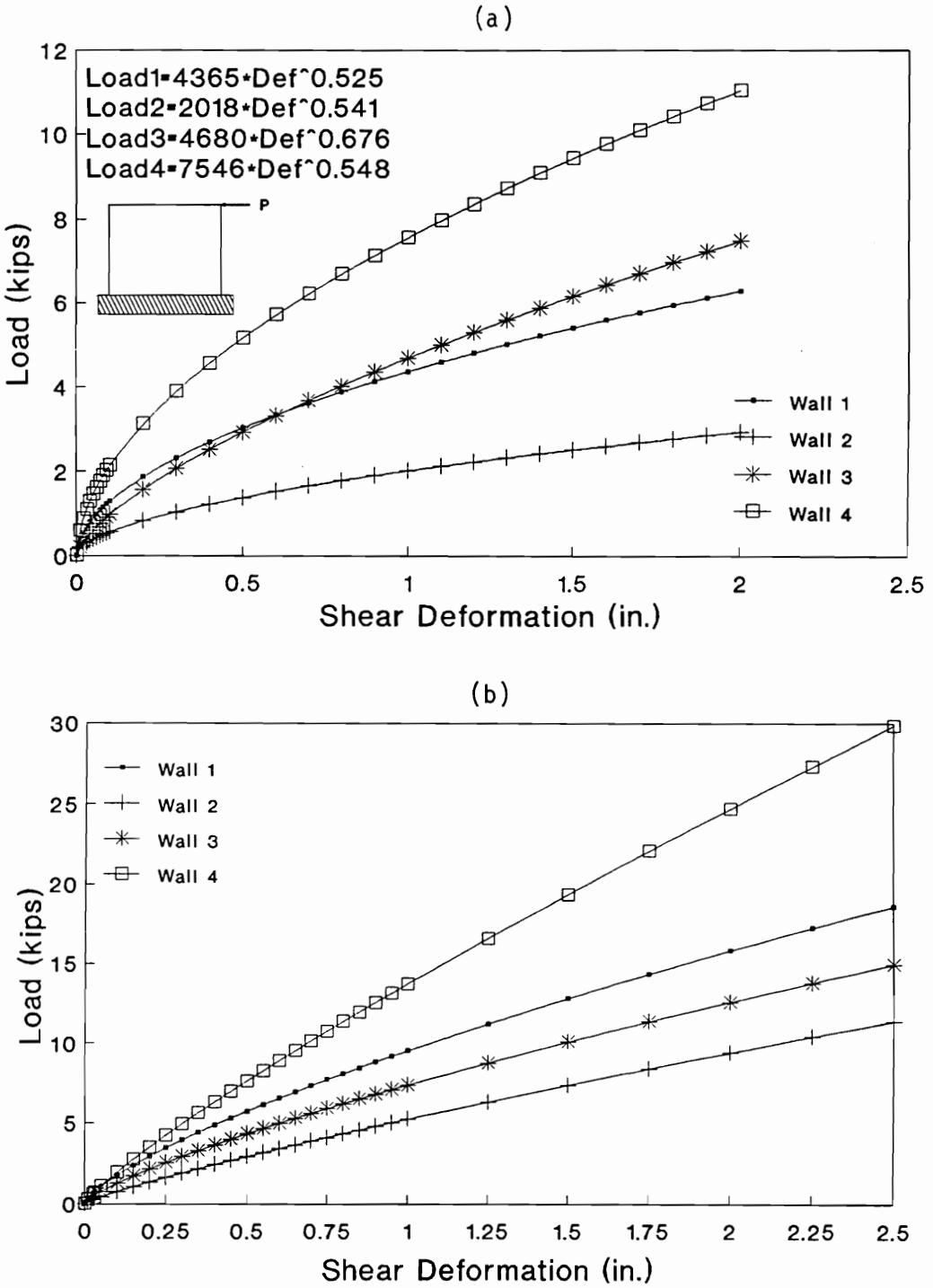

Figure 25. Characteristic Load-Deformation Curves for Nonlinear Diagonal Springs, (a) Experimental and (b) Analytical.

the load history. Also the regression curves obtained from experiments are valid only for the range of the load tested. A significant error can be introduced by extrapolating the data beyond the experimental limits.

The higher stiffness of the analytical curves result from the nail load-deformation curves used for the nonlinear load-deformation elements representing the nails. Figure 26a shows the input characteristics for nails connecting sheathing with Douglas-fir studs as reported by Polensek et al (1979) and Phillips (1990). The influence of the nail connection stiffness is documented in Figure 26b where load-displacement curves for individual shear walls 1 through 4 loaded by shear are shown. The connection stiffness controls the wall behavior. The initially stiff nail connection (Polensek, 1975) causes higher initial wall stiffness which decreases as the nail stiffness changes.

The load-deformation envelope curves for shear walls (from experiments conducted by Phillips, 1990) along with their stiffness are shown in Figure 27. Here, the first slope is equal to an unloading path which means that the walls behave linearly up to the upper bound of the first slope. The change in stiffness at the point where a linear load-deformation curve becomes exponential can be quite abrupt, a phenomenon not to be expected in a real situation.

Since the main experiment was conducted for much larger loads, the early portions of the curves were modeled with a smaller number of points. Also, the experimental results reported by Phillips (1990) did not contain the values of connection deformation for small loads. Similarly, the experimental results for individual wall stiffness made it difficult to compute the shear wall stiffness for loads below 1000 lb (4.48 kN).

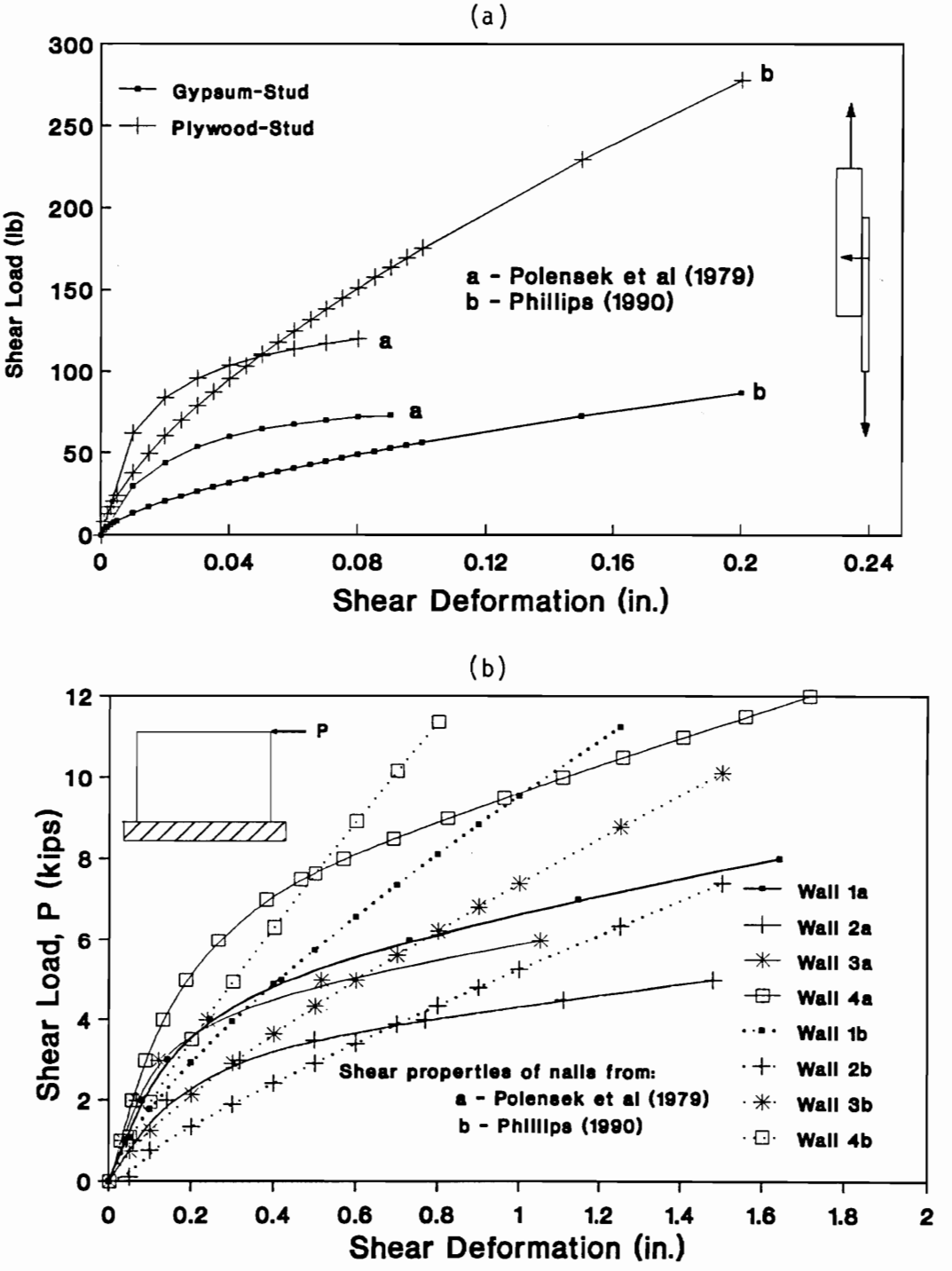

Figure 26. Load-Displacement Curves for (a) Nail Connection Between Sheathing and Studs Used as the Input for Detailed Wall Models and (b) Shear Walls with Different Nail Connections.

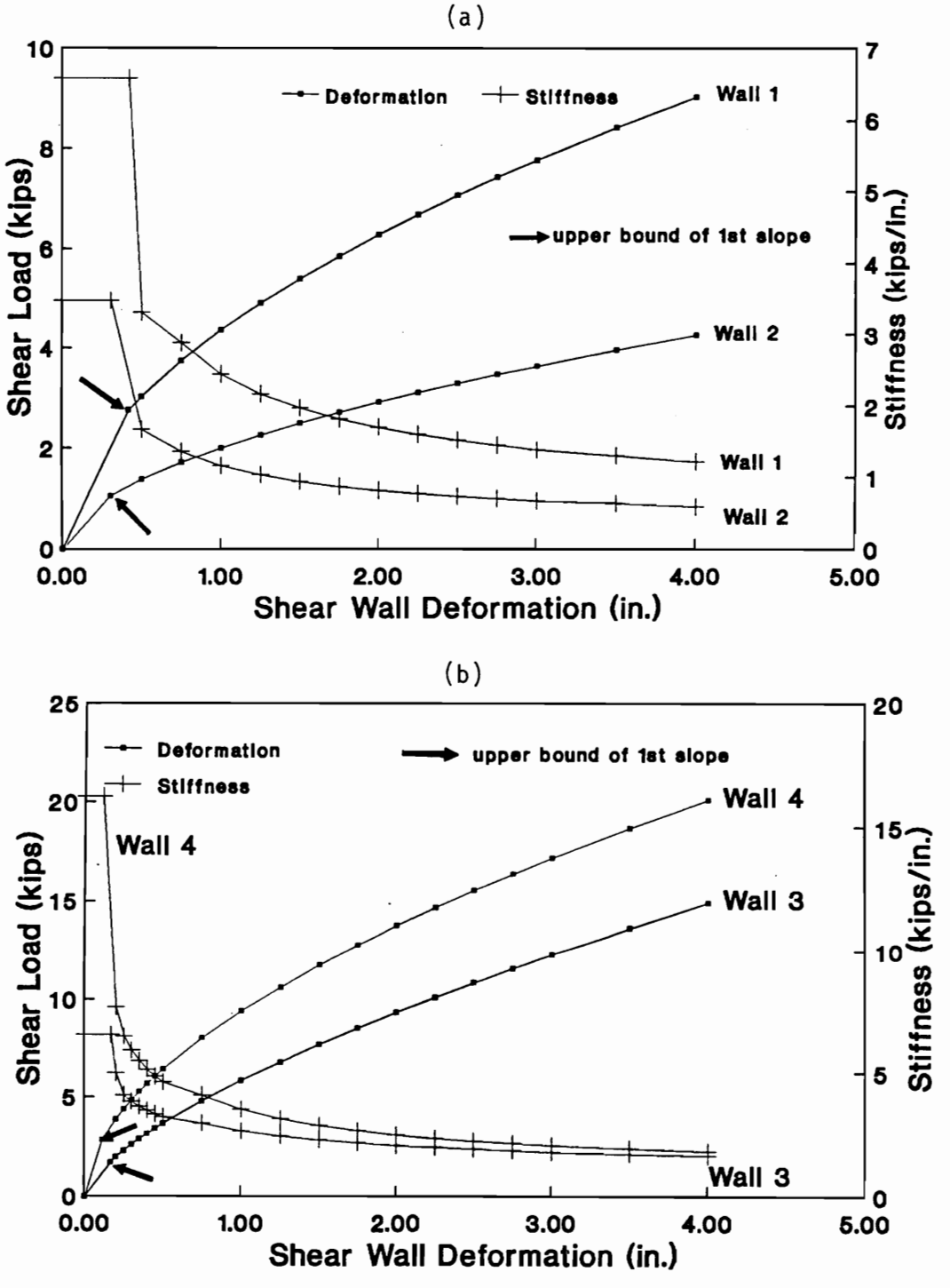

Figure 27. Load-Deformation Curves for Stiffness of the Shear Walls. (a) Walls 1 and 2 and (b) Walls 3 and 4.

Bending Stiffness

The values of deformations as computed from three-dimensional detailed finite-element models for different boundary conditions and loads as well as properties from elastic solution are in Table 6. Segments of different sizes were used to obtain wall properties. The size of the segment was the largest available area without an opening.

The Poisson's ratios were chosen small to account for the high contraction stiffness of box-like structures. Values close to zero were assumed in the finite-element analysis to avoid a contradiction in material properties leading to an incompressible material. This is not a crucial problem since no stress analysis is performed for the global case but neglecting the Poisson ratio magnitude may lead to an error in the computation depending upon software used.

For wall 4, the wall segment and the full wall were analyzed to assess the error in the estimate of bending properties. The results in Table 7 show that the segment analysis is different from the analysis of the full wall. This can be expected, since the sheathing arrangement is not identical for each segment. Thus, error in deformation is always introduced by the segment approach. The differences, although not negligible are not large, and as shown in the sensitivity study, they have negligible influence on the load sharing capability of the full structure. Also, the plate continuum idealization of a three-dimensional structure, although routinely done, brings about some questions arising from the nonuniform stress distributions and gaps in the sheathing.

Table 6. Properties of Orthotropic Plates Representing Wall Bending Stiffness.

Characteristic	Wall 1	Wall 2	Wall 3	Wall 4	Wall 5 and 6
Length-in. (cm)	96.5 (245)	74.5 (189)	74.5 (189)	96.5 (245)	116 (295)
Height-in. (cm)	84.5 (215)	84.5 (215)	84.5 (215)	84.5 (215)	92.5 (233)
Thickness-in. (mm)	1 (25.4)	1 (25.4)	1 (25.4)	1 (25.4)	1 (25.4)
Stiff bending deflection-in. (mm)	0.0874 (2.22)	0.116 (2.94)	0.0671 (1.7)	0.0874 (2.22)	0.1099 (2.8)
Soft bending deflection-in. (mm)	6.3 (160)	9.6 (244)	4.1 (104)	6.3 (160)	5.6 (142)
4-sides supported-in. (mm)	0.0634 (1.61)	0.111 (2.82)	0.0303 (0.8)	0.0634 (1.61)	0.1026 (2.6)
Torsion-reaction for 1 in. deflection-lb (N)	375 (1667)	77.5 (345)	600 (2667)	375 (1667)	224 (996)
E_x-psi (MPa)	0.136E6 (938)	0.398E5 (272)	0.904E5 (623)	0.136E6 (938)	0.341E6 (2351)
E_y-psi (MPa)	0.589E7 (46606)	0.545E7 (37572)	0.914E7 (63011)	0.589E7 (40606)	0.700E7 (48258)
G_{xy}-psi (MPa)	0.297E7 (20475)	0.585E6 (4033)	0.439E7 (30265)	0.297E7 (20475)	0.245E7 (16890)
μ_{xy}	0.01	0.03	0.04	0.01	0.02

Table 7. Comparison between Properties of a Segment and Full Wall for Wall 4.

Characteristic	Wall 4 segment	Wall 4 full size
Length-in. (cm)	96.5 (245)	192 (488)
Height-in. (cm)	84.5 (215)	84.5 (215)
Thickness-in. (mm)	1 (25.4)	1 (25.4)
Stiff bending deflection-in. (mm)	0.0874 (2.22)	0.0943 (2.4)
Soft bending deflection-in. (mm)	6.3 (160)	91 (2311)
4-sides supported-in. (mm)	0.0634 (1.61)	0.0942 (2.4)
Torsion-reaction for 1 in. deflection-lb (N)	375 (1667)	240 (1067)
E_x-psi (MPa)	0.136E6 (938)	0.178E6 (1227)
E_y-psi (MPa)	0.589E7 (40606)	0.645E7 (44466)
G_{xy}-psi (MPa)	0.297E7 (20475)	0.448E7 (30885)
μ_{xy}	0.011	0.014

Axial Stiffness

Axial stiffness of one vertical element is based on the number of studs in the real wall and number of vertical elements in the equivalent wall model (truss elements for internal elements and beam elements for edge studs). The elasticity properties are equal to that of the experimental material (Douglas-fir) whereas the cross-sectional properties reflect the size of the finite-element model. The total cross-sectional area of the vertical truss elements is equal to the total cross-sectional area of the wall studs, but the area of an individual truss element in the finite-element model is not necessarily equal to the area of an individual stud. A simple computation for the equivalent model of wall 4 demonstrates the principle used for all walls.

Wall 4 contained 15 vertical studs including doubled edge studs. For the equivalent model with 4 vertical truss elements, the area of the truss will be Area=13×(Area of one stud)/4. The two edge studs are not included into the equivalent area since they are expressed as the area of the edge beam with high in-plane stiffness. The example of the cross-sectional properties generation for wall 1 is in Table 8.

Additional Bending and Axial Stiffness

Openings in a real wall are restrained by additional framing members to ensure stable dimensions. This additional framing is not a part of the representative segment used to obtain plate properties of an equivalent model. However, the contribution of the additional framing

Table 8. Example of the Generation of Geometric Parameters for Wall 1.

Element	Area-in.^{2} (cm^2)	Thickness -in. (mm)	Width -in. (mm)	I_i-in.^{4} (cm^4)	I_o-in.^{4} (cm^4)
1	5.25 (13.3)	0.1 (2.54)	52.5 (1334)	1206 (50198)	4.375E-4 (0.0183)
2,3	10.5 (67.7)	3.5 (89)	3 (76)	7.875 (328)	10.72 (446)
4	5.25 (13.3)	3.5 (89)	1.5 (38)	0.984 (41)	5.36 (223)
5	10.5 (67.7)	3.5 (89)	1.5 (38)	N/A	N/A
6	19.25 (124)	N/A	N/A	N/A	N/A

I_i = moment of innertia in in-plane direction
I_o = moment of innertia in out-of-plane direction
N/A = not applicable to this type of element

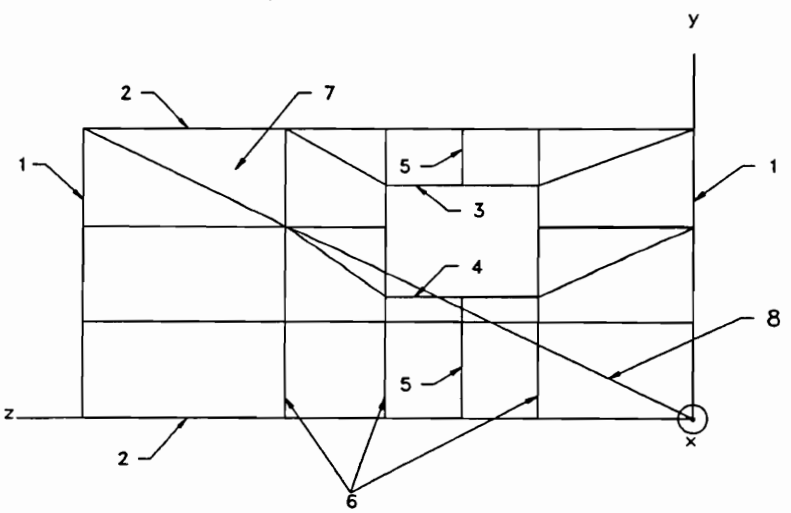

1 = edge studs (beam element)
2 = top and sole plate (beam element)
3 = window header (beam element)
4 = window sill plate (beam element)
5 = studs above and below the window (truss element)
6 = studs (truss element)
7 = plate element
8 = nonlinear spring

must be included in the equivalent model. This is achieved by specifying horizontal members as beam elements and vertical members as truss elements. This introduces a slight error due to the fact that the vertical members increase the wall bending stiffness as well. The vertical framing can be specified as beam elements and pinned to the upper and lower horizontal members (members 2 in Table 8) to account for the contribution to the bending stiffness. In this work, the contribution to bending stiffness by vertical framing members above an opening was neglected and only axial stiffness was included. The error due to this approximation is negligible as shown in the sensitivity study.

The average properties specified for Douglas-fir wood were used for the modulus of elasticity and Poisson's ratios (Bodig and Jayne, 1982).

Comments on Equivalent Model of Walls

The quasi-superelement represents a significant reduction of computational time. For example, the detailed model of wall 1 had 2506 elements, 1292 nodes, and 5554 degrees of freedom. The nonlinear analysis took more than 843 sec. of CPU time when a CRAY-YM supercomputer was used and 26878 sec. CPU time for 486/33 MHz computer. The equivalent model had 55 elements and 29 nodes. The CPU time to analyze the equivalent model for the same loading and boundary conditions was 40 sec. and 366 sec. for CRAY-YM and 486/33 MHz, respectively.

Since the response of walls to the bending load was nearly linear within the investigated range (up to a pressure of 40 psf (1.92 kPa)), linear bending properties were used. The error in bending and torsional deflection was 5 to 10% depending upon the mesh size and accuracy of

the iterative procedure to compute plate properties. Also, the fact that a three-dimensional real structure is replaced by a two-dimensional continuum introduces error, which increases as the conditions depart from the assumptions of a plate. For example, the wall segment when loaded as a simple beam in the soft direction (two vertical edge studs simply supported, upper and lower edge free) can develop kinks as a result of gaps and non-rigid nail connections. Kinks are not admissible for the plate continuum. In fact, the wall when loaded in the soft direction behaves nonlinearly at higher pressures. The stiffness in the soft direction is lower by an order of magnitude than in the stiff direction therefore, the influence on the overall plate behavior is small and is neglected.

The elements of the equivalent model are superimposed at the identical nodal locations (truss for shear, orthotropic plate for bending and torsion, truss elements for vertical studs, and beam elements for the edge studs and headers and horizontal studs around openings). This creates a two-dimensional structure energetically equivalent to a three-dimensional detailed model. Therefore, the equivalent model is giving the same global response as the complicated detailed model. The degrees of freedom associated with the equivalent model are global degrees of freedom and correspond to the equivalent geometrical locations of the real structure. Hence, displacements at the boundary of the equivalent model are the displacements at the centerpoints of the studs in the three-dimensional detailed substructure.

Reduced number of degrees of freedom makes it possible to use the equivalent model in the analysis of the full structure and to obtain the deformation and internal forces on the panel boundaries. These results are used as the input for the substructures to examine the wall behavior using the detailed model. The approach is similar to the known superelement analysis. However, unlike a

superelement, which uses a fixed stiffness matrix and master degrees of freedom, the equivalent model is nonlinear and represents a transformation into the system with equivalent external energy. The input for the model can be generated by any admissible means. However, if the same software is used, a convenient way of reloading the substructure by the output from the global analysis may be possible.

Comparison of the equivalent model with the experimental results and the finite-element analysis of the three-dimensional substructure showed good agreement. Therefore, the equivalent model can be used as a part of the full structure analysis when predicting the global response of the real structure. Characteristic properties for the equivalent model can be generated by any acceptable means, including experiment. The equivalent model can be used for walls with or without openings in a similar manner. A large opening, such as a door, can be easily incorporated by establishing the areas around the opening as separate plate continua and imposing continuity conditions at the substructure boundaries. The shear resisting truss remains unchanged despite the presence of openings.

Roof

The roof was modeled as a three-dimensional substructure with the nodes connecting roof to walls specified as master nodes. Truss elements were used to model the members of each truss except for the lower chord where beam elements are used. Beam elements were necessary in order to facilitate the connection between the roof and the top beams of the walls at points other than truss nodes. Pin connection between truss members was assumed.

A two-dimensional orthotropic shell (3 or 4 nodes) was used for the plywood roof sheathing and for the gypsum board

ceiling. This allowed both in-plane and bending loading. Nonlinear load-deflection elements were used to model the nails. The roof was modeled as a superelement and master degrees of freedom were defined on the boundary connected to the walls. The various components for the roof superelement are shown in Figure 28.

The average elasticity modulus reported for the roof truss members (Lafave, 1990) was used in the model. The geometry was same as shown in the Appendix A. Nail properties given by Phillips (1990) were used for characteristics of nonlinear load-deformation elements used to model connections between the truss members and covering. Since roof truss models have been well documented, no verification of this model has been carried out. The testing load applied to the model revealed linear behavior of the truss which is with agreement with the literature (Lafave, 1990). The deflected shape of the truss is in Figure 28c.

Although a nonlinear roof model was created for substructure analysis the linear superelement was used in the full building analysis. A full structure analysis with a nonlinear roof system may be useful if analyzing roof behavior beyond the range of loads prescribed by the UBC (ICBO, 1988). This, for example, may be useful in reliability studies when load can be increased until some truss members fail and load is redistributed to remaining members. However, in this work, only the linear region was assumed as justified in the literature review.

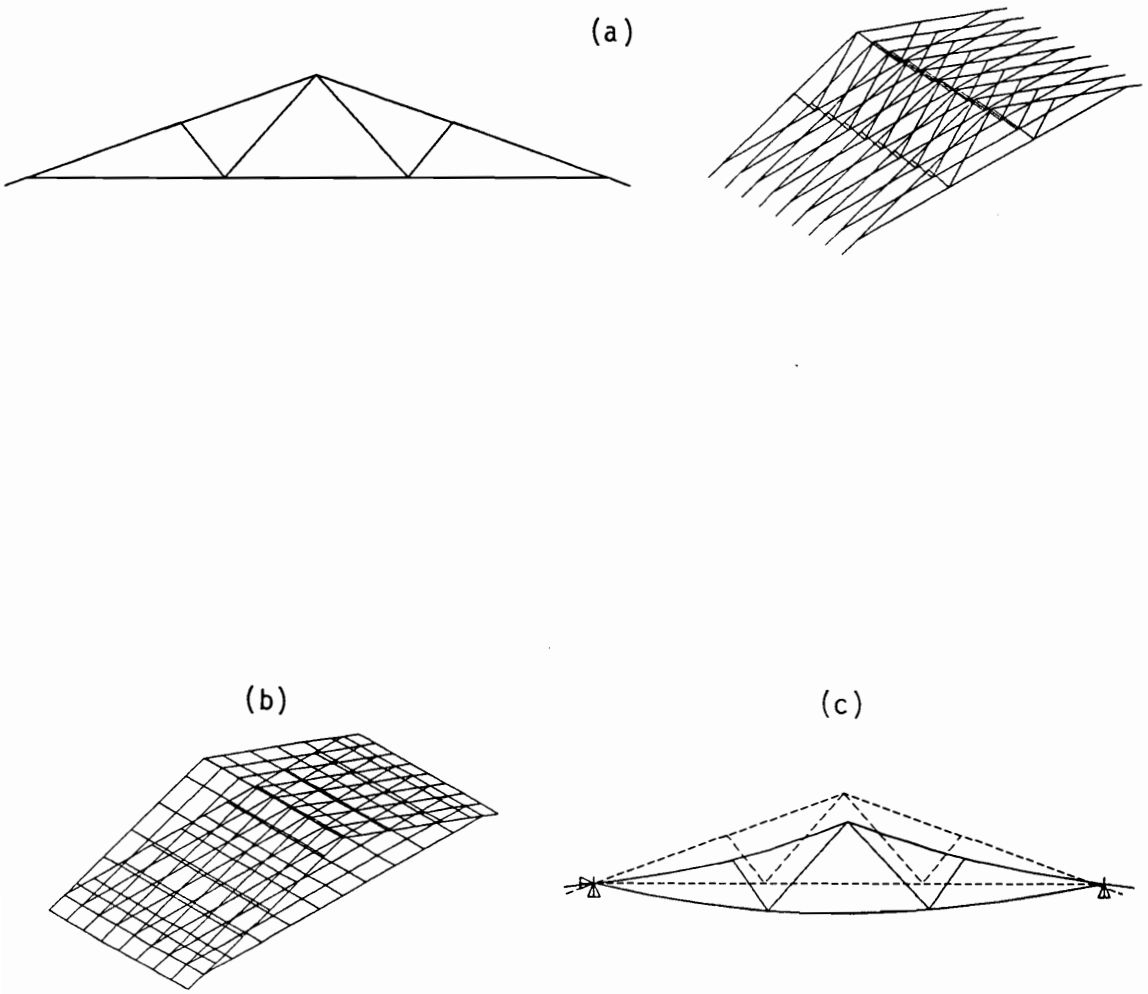

Figure 28. Finite-Element Mesh of the Roof Truss. (a) Single Truss and System, (b) Sheathing, (c) Deflected truss.

Floor

The detailed finite-element model used two-dimensional orthotropic shell elements for joists and sheathing. Joists and sheathing had independent node numbering and were connected via nonlinear load-deflection elements representing nails. For simplicity, gaps were not included into the model and discontinuities in the sheathing were incorporated by different node numbers for each plywood panel. The finite-element mesh for the framing and shearing of the floor is shown in Figure 29.

The elasticity properties of floor joists given by Phillips (1990) were used as the characteristic properties for the detailed finite-element model. Characteristic properties of nonlinear load-deformation elements representing the nail connections between the sheathing and floor joists were based on the results reported by Phillips (1990).

Model of the Orthotropic Plate

The floor can be represented by an orthotropic plate with its principal directions along and perpendicular to joists. The geometrical orthotropy caused by the joist orientation can be transformed into a physical orthotropy and the structure is then represented by the orthotropic plate continuum. The advantages of this approach are a simpler finite-element mesh and less "bookkeeping" resulting from the use of superelement.

The work published by the Institute for Standardization and Testing (1984) implemented the composite action of the

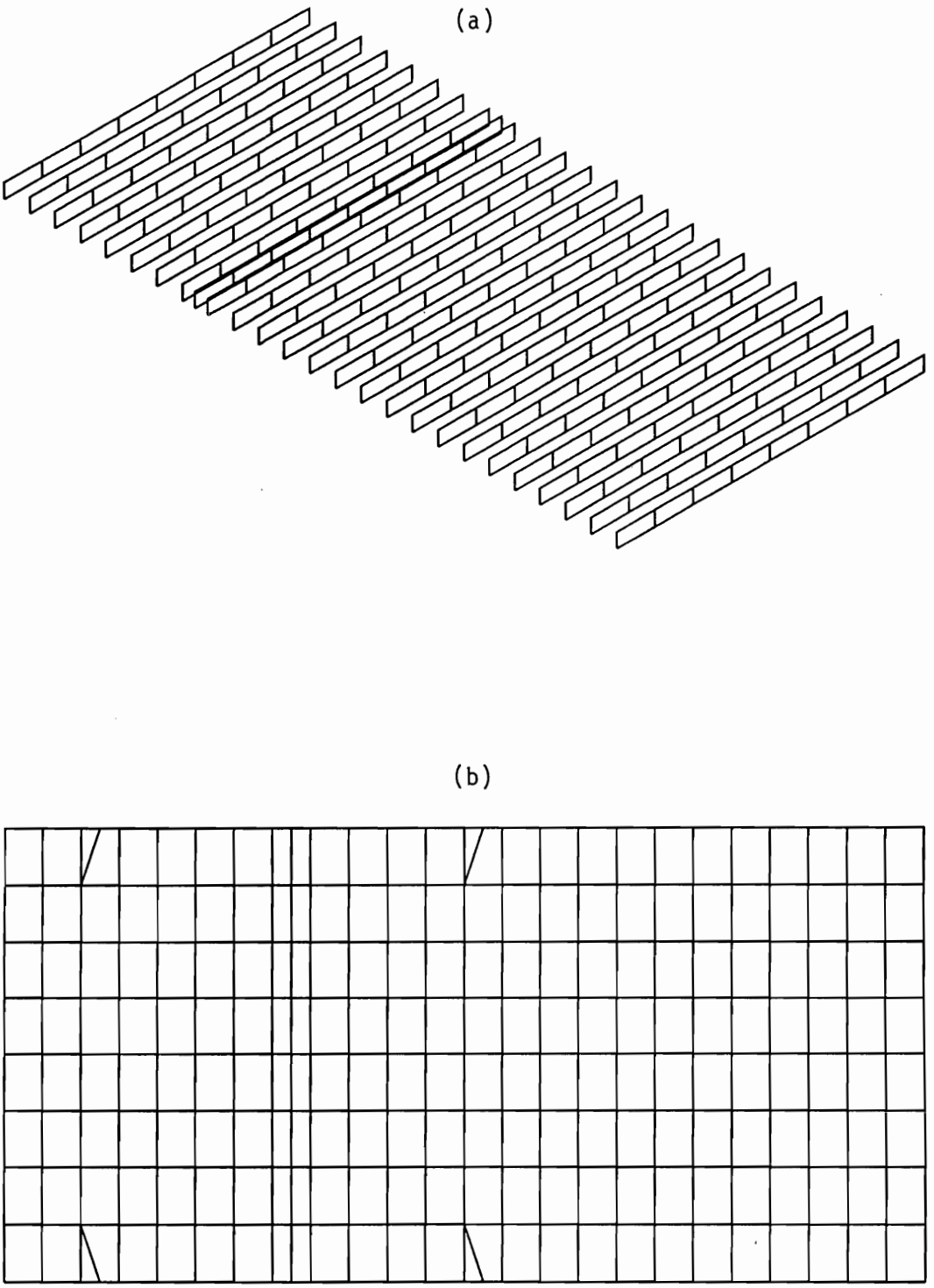

Figure 29. Finite-Element Mesh of the Floor Superelement (a) Framing, and (b) Sheathing.

sheathing and joists. The procedure yields an approximate solution and relies on the following assumptions:

1. Only uniformly distributed transverse load is allowed.
2. Fasteners have constant spacing throughout the length of the panel.
3. All joists have the same spacing.
4. Floor is simply supported.
5. Sheathing is continuous along the joists or is effectively connected.

From these assumptions it follows that the floor stiffness will be somewhat overestimated if the butt joints of the plywood sheathing are not blocked.

The floor joists and sheathing are replaced by a system of T-sections in which the flange width, called effective breadth is defined as

$$b_{ef}=0.9b_s \qquad for \quad \frac{l}{b_s}>6$$

$$b_{ef}=0.15l \qquad for \quad \frac{l}{b_s}\leq 6 \tag{27}$$

Where b_s = joist spacing between internal faces of the joists

l = floor span

b_{ef} = effective breath

The joists spacing must be less than

$$b_s \leq 1.25 t \sqrt{\frac{\sqrt{E_{\parallel} E_{\perp}}}{\sigma_{c\parallel}}} \qquad (28)$$

or

$$b_s \leq 50 t$$

Where t = thickness of sheathing

$E_{\parallel}$ = modulus of elasticity of the sheathing in the joist direction

$E_{\perp}$ = modulus of elasticity of the sheathing in the direction perpendicular to the joists

$\sigma_{c\parallel}$ = compressive stress in the sheathing in the joist direction

The moment of inertia of the floor is then calculated as an assembly of T-sections and the contribution of the sheathing represented by the effective breath is further reduced by 60% to account for nonrigid connections between joists and the covering. The stiffness in the direction perpendicular to the joists is calculated as the stiffness of the sheathing with respect to the neutral axes of the composite section. The moment of inertia is again reduced by 60% to account for nail joints.

From equations (27) and (28), it follows that the contribution of the sheathing to the floor bending stiffness in the direction along the joists is less than 6%.

For this floor model T-section is shown in Figure 30. Thus, the floor longitudinal stiffness can be represented by 24 T-sections 192 in. (4.88 m) long.

Using the described procedure, the total stiffness EI of the floor is calculated and divided by the width to compute the stiffness per unit width, $(EI)_{unit}$, from which the

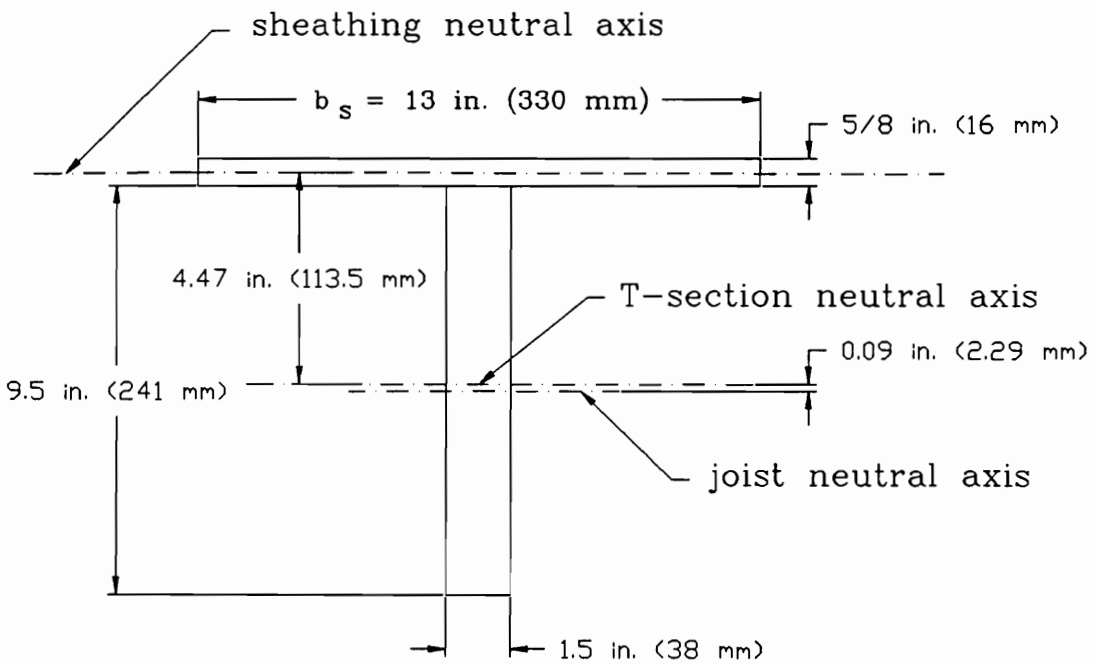

Figure 30. Composite T-Section Representing an Effective Breadth Approach.

modulus of elasticity of a fictitious orthotropic plate, E', of the thickness h is calculated as

$$E' = \frac{12\,(EI)_{unit}}{h^3} \qquad (29)$$

As an example, a fictitious plate is considered to have a thickness h=1 in. (25.4 mm), b=1 in., the moduli are 169.32E6 psi (1.167 MPa) and 62.22E6 psi (0.432 MPa) for stiff and flexible directions, respectively. The shear modulus, G_{12}, can be estimated from the formula used for channel concrete cross-sections (Kolar, 1982)

$$G_{12} \approx \frac{\sqrt{E_1 E_2}}{2\,(1+\sqrt{\mu_{12}\mu_{21}})} \qquad (30)$$

Where E_1 = modulus of elasticity in strong direction
E_2 = modulus of elasticity in weak direction
μ_{12}, μ_{21} = Poisson's ratios of the whole plate

Poisson's ratios must be estimated, because they represent the behavior of the whole floor and not the material from which the plate is made. The logical choice is a very small value for μ_{21} (such as 0.1 or smaller) which represents a contraction in the strong direction when the plate is loaded in tension in the weak direction. The argument for this choice is that channel and box-like cross-sections undergo very small transverse deformation in the channel direction when loaded in the direction perpendicular to the channels (Kolar, 1982). The second Poisson's ratio must be calculated from the reciprocity theorem

$$E_1\mu_{21} = E_2\mu_{12} \qquad (31)$$

The method of establishing plate stiffness is approximate and most likely overestimates the transverse stiffness despite the fact that this value is reduced by 60% as

suggested by Institute for Standardization and Testing (1984). The overestimation results from the gaps in sheathing which are not considered in the stiffness calculation. However, as shown later, the floor stiffness has little influence on the performance of the full structure. Thus, the orthotropic plate can be used as the floor in the full structure analysis.

Summary

In this chapter detailed and equivalent models of substructures were discussed. The equivalent models are necessary to reduce the computational size of the problem to a feasible level. Walls are modeled via quasi-superelements whereas roof and floor are modeled as superelements.

Three-dimensional models of the walls were verified using experimental results and the characteristic properties for substructures were given. The experimental load-deformation curves for shear walls are different from the analytical results based on the three-dimensional finite-element models. The differences vary due to the nonlinear behavior of walls loaded in shear. The ratio between analytical and experimental shear loads for a given shear deformation of the walls varied from 1.0 to 2.5 and was dependent on imposed deformation.

The lower stiffness obtained from the experiments is due to the gradual degradation of the nail connection stiffness resulting from cycled loading. Properties of nail connections were found to be a controlling phenomenon in shear wall behavior.

The roof was modeled as a truss except the lower chord which can be subjected to bending. This made possible to

specify nodes at locations other than intersections of truss members. Modeling the lower chord of the truss as a beam allowed the truss to be connected to walls at any point along the chord.

An alternative approach for modeling the floor as an orthotropic plate was also presented. This model is approximate due to the effective width definition and assumptions made to compute it.

5. INTERCOMPONENT CONNECTIONS

There are a number of different intercomponent connections in a light-frame wood building. Connections range from simple nailing of two adjacent members to specially designed metal-plate connectors such as hangers or T-straps. The connections are an integral part of the building, and their function is to hold the individual substructures together and to transfer forces between substructures.

The response of the intercomponent connection to the load is in most cases nonlinear and is a function of many parameters such as wood species, wood density, load-to-grain direction and moisture content of the wood. It is also greatly influenced by variability of the materials. Thus, experimental results will be different even for the same connection type and same wood species.

To include each individual connection in the full-structure model will result in an enormous number of degrees of freedom due to the necessity of refining the finite-element mesh at the vicinity of connection points. Moreover, this would require that all of the substructures in the model exist in their three-dimensional form, which will lead to an extremely large problem.

A large group of the intercomponent connections in the light-frame wood structure is composed of the nail connections. Nails are used as connecting elements and properties of the individual nail connection determine the behavior of the whole subassembly. Also, the connections repeat at certain prescribed frequencies (such as truss connected to wall every 24 in. (610 mm)). Thus, the

intercomponent connection can be isolated from the structure and analyzed as a separate substructure. This substructure can be subjected to load and boundary conditions simulating the actual physical test, which would be employed to determine the connection stiffness in translation and rotation. Finally, load-deformation curves for the subassembly are constructed and used as the characteristic properties of a one-dimensional nonlinear load-deflection element subsequently used to connect the boundaries of quasi-superelements and superelements in the full-structure model.

This process is similar to the quasi-superelement analysis. For example, the corner connection between two external walls is analyzed as a typical segment of unit width. Load-deformation characteristics in shear and torsion are obtained in the form of force-deflection or moment-rotation relationships and these serve as a direct input for a global model.

The following intercomponent connections were defined:

1. Partition-to-exterior wall connection.
2. Corner connection between exterior walls.
3. Connection between floor and partition walls.
4. Connection between floor and exterior walls.
5. Connection between walls and roof.

For each of the defined connections, master degrees of freedom were identified, and detailed three- or two-dimensional finite-element models created and analyzed (Groom, 1992; Groom and Leichti, 1991). Several connections were tested and results of the analysis compared with experiments. In such cases, experimental results were used as the input for the intercomponent connection properties.

Partition-to-Exterior Wall Connections

Partition-to-exterior wall connections transfer forces between exterior walls loaded by pressure, axial and shear force (isolated or combined) and partition walls which are not loaded by a lateral load.

The connection between partition walls (walls 2 and 3) was designed so that walls 1 through wall 4 could be tested prior to walls 5 and 6 being erected. This resulted in the connection detail as shown in Figure 31. Partition walls were connected to walls 5 and 6 via an overlapping top plate of the exterior walls.

Connection in the Wall Field

The connection in the wall field is the connection along the vertical edges of partition walls and intermediate studs of walls 5 and 6, except the top plates, which were analyzed separately.

The connection in the wall field was realized only by contact between the sheathing of the exterior and partition walls. The edge stud of the partition wall was not nailed to the stud of the exterior wall due to the testing arrangement. This resulted in no separation stiffness of the connection for points other than top and bottom. Also, only forces (translations) and no rotations (moments) were transferred between the partition and exterior walls in the nodes other than top and bottom.

The contact (compressive) stiffness of the connection in the x- and z-direction was computed by modelling the connection as a series of nonlinear springs as shown in

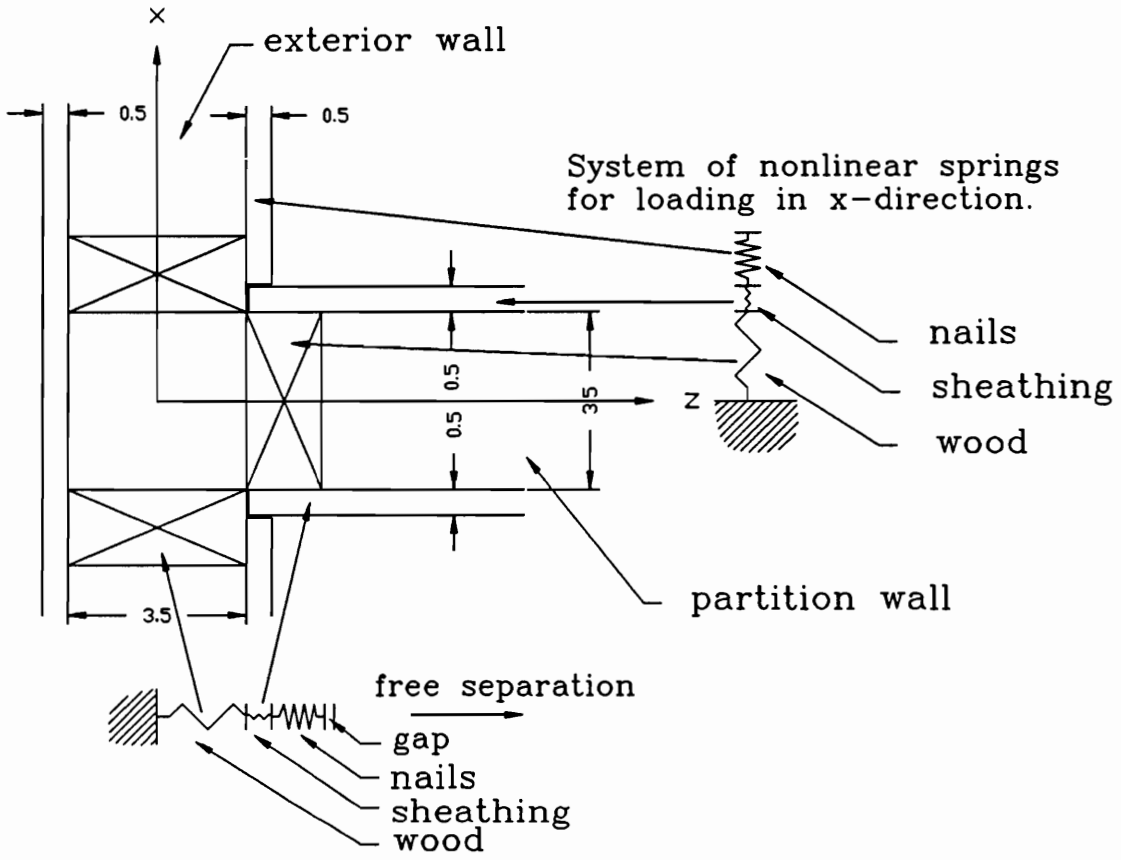

Figure 31. Detail of the Connection Between Partition Wall and Exterior Walls and its Finite-Element Representation.

Figure 31. The wood was represented as a one-dimensional elastic spar (or spring) having plastic capability, which represented crushing strength of wood perpendicular to fibers. Similarly, gypsum board sheathing was modeled in the same way (Polensek, 1976a). Plywood sheathing was considered as wood perpendicular to fibers for load perpendicular to the plywood plane and plywood properties for in-plane loading (APA, 1989) were used otherwise. Material properties are in Table 9.

When the partition wall in Figure 31 was loaded in the

Table 9. Elastic Material Properties Used for the Analysis of the Connection Between Partition and Exterior Walls

Material	E_8	σ_{yield}	E_4	σ_{yield}
	ksi (MPa)	psi (MPa)	ksi (Mpa)	psi (MPa)
Gypsum board 1/2 in.	101[a] (697)	480[a] (3.31)	91[a] (628)	359[a] (2.48)
Plywood 1/2 in.	1000[d] (6897)	290[d] (2.69)	1000[d] (6897)	290[d] (2.69)
Douglas-fir	90[c,e] (621)	380[b,e] (2.62)		

[a] Polensek (1976)
[b] Wood Handbook (1987)
[c] Bodig and Jayne (1982)
[d] APA (1989)
[e] perpendicular to fibers
E_8, E_4 = modulus of elasticity in 8 ft and 4 ft direction

positive x-direction, the wood and sheathing were assumed to deform elastically until the material crushing strength was reached. From that point, further increase of deformation

did not require additional load. However, the sheathing oriented parallel to the acting force (sheathing of the exterior wall parallel to x-direction) is not supported and is connected to the adjacent studs via nonlinear nail connections. This means that along with the elastic, or plastic deformation of materials, nail slip takes place. In addition, neither the area of contact is known nor the number of nails being engaged during the loading. It is assumed that the number of nails per contact area as well as the area itself change as the load proceeds. To investigate this problem in detail is beyond the scope of this work. Thus, several simplifications were made to obtain approximate results:

(1) domain of a unit depth with the attributed area was analyzed, (2) no initial gap existed, (3) the number of nails per unit depth was based on the assumption that only the first two rows participate in the force distribution. The work of Hata and Sasaki (1987) indicates that nails far from the applied load do not significantly participate in the load transfer.

The number of nails per unit depth was calculated as the total number of nails in two rows parallel to the wall edge divided by height of the wall. Slip curves generated by Philips (1990) were used as the characteristic properties for nail connection stiffness. To investigate the influence of nail stiffness, the number of nails was varied. The number of nails per 1-in. (25.4-mm) depth shown in Figure 32 represents nails attributed to 1-in. segment cut from the wall. E.g. 1 nail/1-in. depth means that an 8-ft tall wall will have total of 96 nails engaged into transfer of the contact force (1×96=96). If only 2 rows of nails are assumed to be affected by the acting load, nails will be spaced 2 in. apart (48 nails in each row). Clearly, such spacing is impossible and represents a theoretical quantity. To obtain a stiffness per node, the load was multiplied by

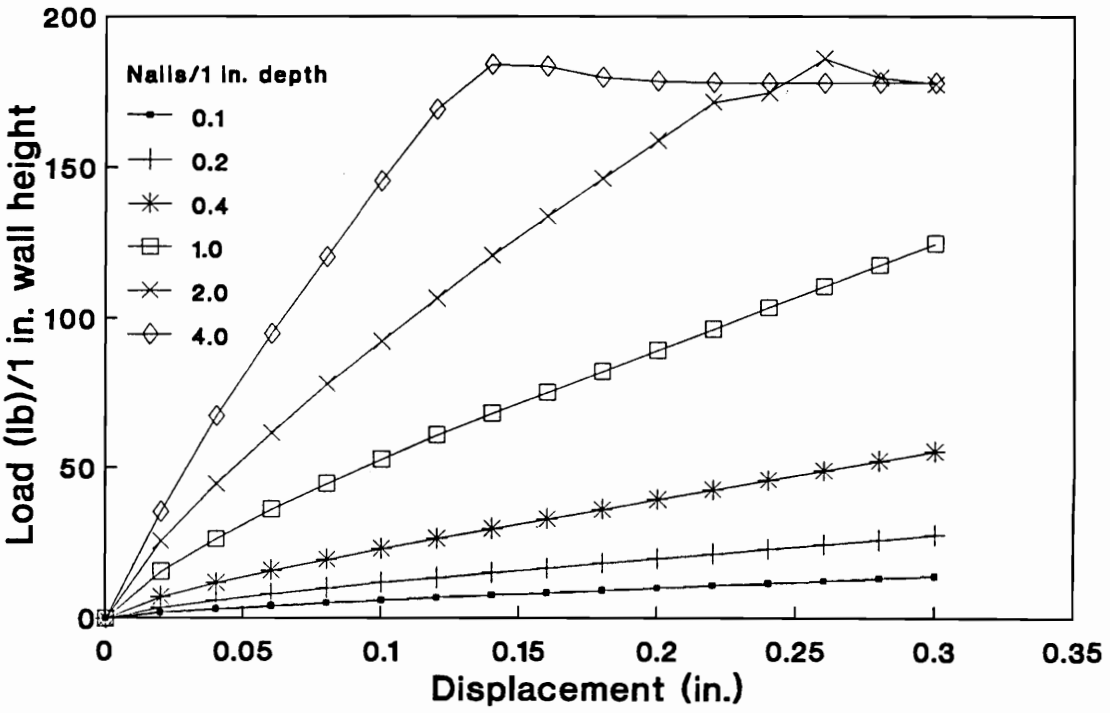

Figure 32. Stiffness in Global X-Direction of the Connection between Partition and Exterior Wall per Unit Height of the Wall. Curves are Identical for Walls 2 and 3 Connected to Walls 5 and 6.

the total contact length and divided by the number of nodes.

Plastic deformation of wood perpendicular to the fibers was attained after a rather large number of nails was involved. This is shown in Figures 32 and 33. In order to yield wood, the connection between the sheathing and stud must be sufficiently stiff. The total deformation of the connection was controlled by the nail slip combined with the compressive deformation of wood and sheathing. The resulting stiffness of the segment of a unit depth is in Figures 32 and 33. Given the fact, that the contact stiffness is largely controlled by nails, no difference can be expected for walls 2 and 3 as shown in Figure 33.

Nails connecting gypsum sheathing to studs of the exterior wall transfer the load in x-direction and different sheathing of the partition wall has little influence on the deformation. The yield load is affected by the strength of the sheathing material, but this difference was negligible for walls 2 and 3.

The connection between the partition walls and the exterior walls behave differently when loaded in z-direction as shown in Figure 33. When connection is loaded in z-direction, nails of the partition wall are loaded in shear. Since the nailing schedules as well as the sheathing are different for walls 2 and 3, different curves are obtained.

Connection Between Top Plate of the Partition Wall and Exterior Wall

Top plates of the walls were connected by nails to ensure force transfer at the wall corners. The top plate of walls 5 and 6 was continuous and was overlapping the top plates of the partition walls as shown in Figure 34. Four 16d nails were driven from the top of the continuous plate.

A two-dimensional finite-element model of the connection

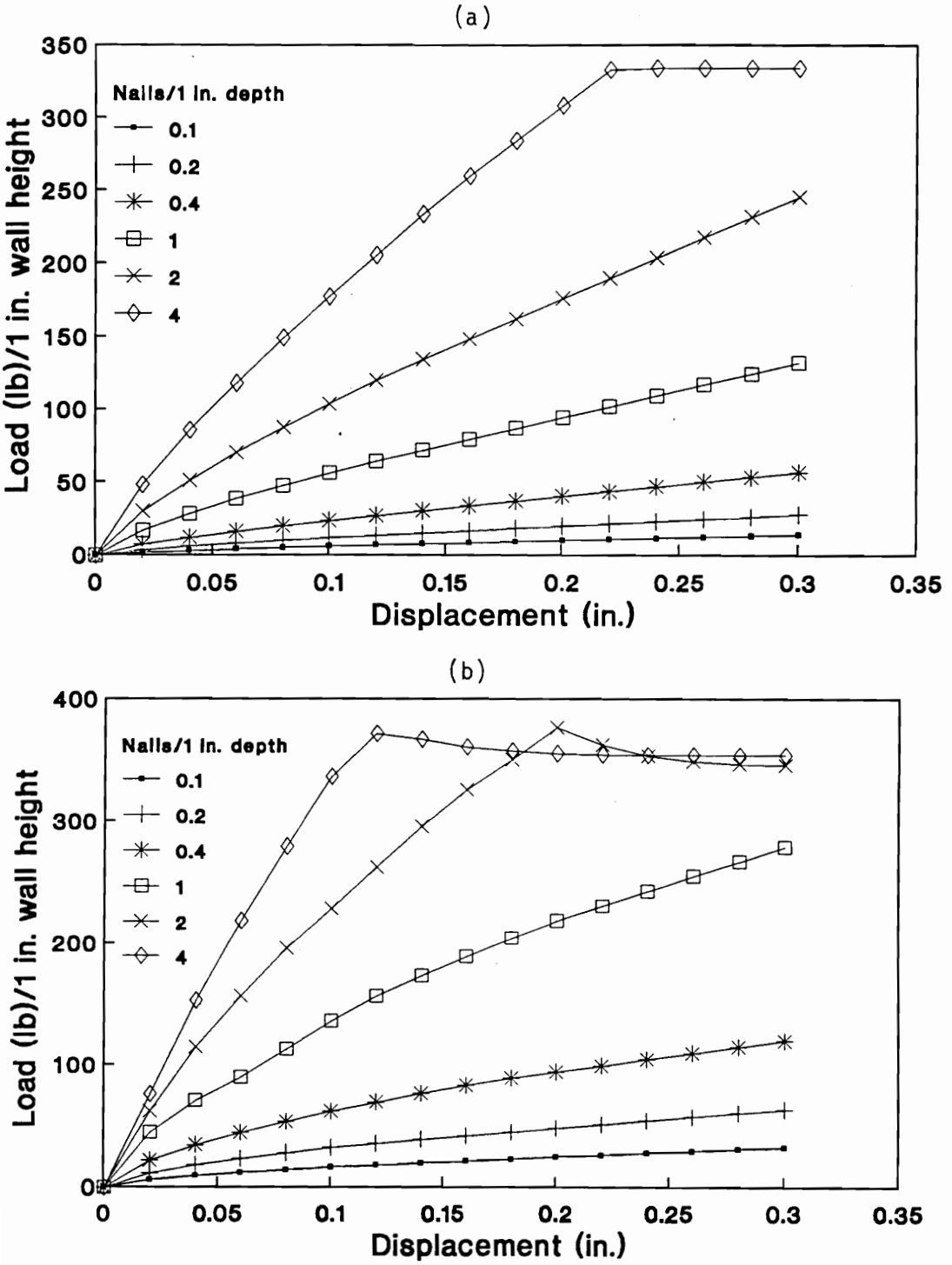

Figure 33. Stiffness in Global Z-Direction of the Connection between Partition and Exterior Wall per Unit Height of the Wall, (a) Wall 2, and (b) Wall 3.

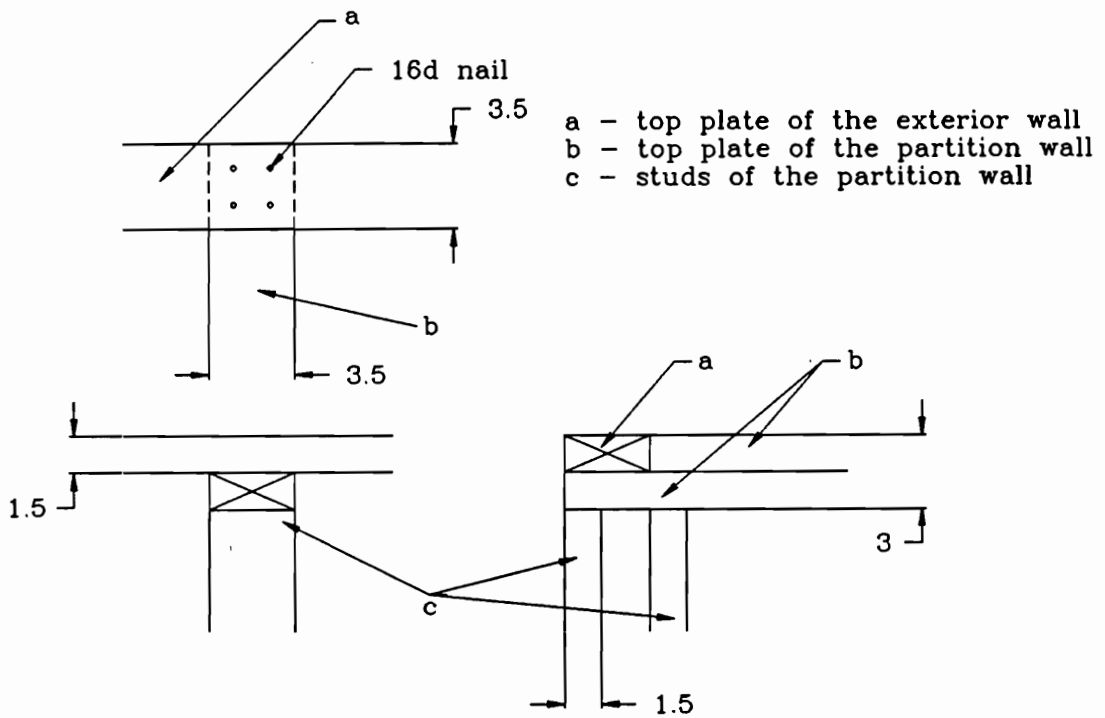

Finite-Element Representation

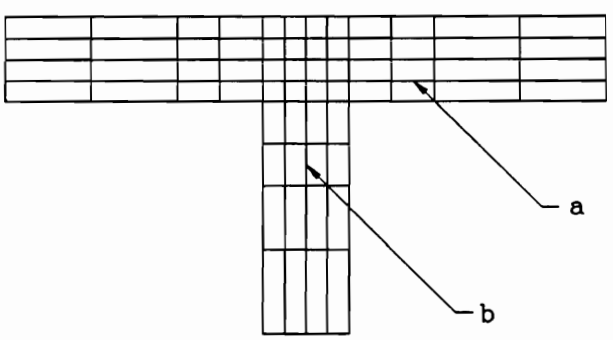

Figure 34. Connection between Top Plates of Partition and Exterior Walls and its Finite-Element Representation. Dimensions are in Inches.

was created and loaded by several different loads and boundary conditions to simulate an actual test. The model consisted of two segments representing the wall plates. The segments were numbered independently and were connected at four common points by nonlinear load-deformation elements representing nails (Groom, 1992). In this way load-deformation characteristics of the connection for shear, withdrawal and moment loading were obtained (Groom, 1992).

A two-dimensional finite-element model of the connection is shown in Figure 34 and load-displacement characteristics are given in Figure 35. Whereas the separation stiffness was nonlinear due to the nonlinear shear behavior of nails, rotational behavior was close to linear.

Withdrawal stiffness is calculated as a multiple of the withdrawal stiffness of one nail (in this case, the connection had four nails) whereas compressive stiffness is expressed as a function of the modulus of elasticity of wood in compression and area in contact (Stiffness = Area × Modulus/Length). This value is several orders of magnitude higher than the withdrawal stiffness.

For this particular case the stiffness in compression was calculated as 0.572×10^6 lb/in. (100 kN/mm) which represents the force necessary to deform the connection of an area 3.5×3.5 in. (89×89 mm) and length 3 in. (76 mm) by 1. This value is not an exact representation of the compressive contact stiffness between the top plates of interior and exterior walls since the boundary conditions, and consequently the compressed length, are not known. The mere fact, however, that this stiffness is much larger than other stiffnesses controlled by nails indicates that the estimated values will cause a negligible error in the full-structure analysis. In most cases, it is sufficient to guess the compressive stiffness as one or two orders of magnitude higher than the withdrawal or shear stiffness.

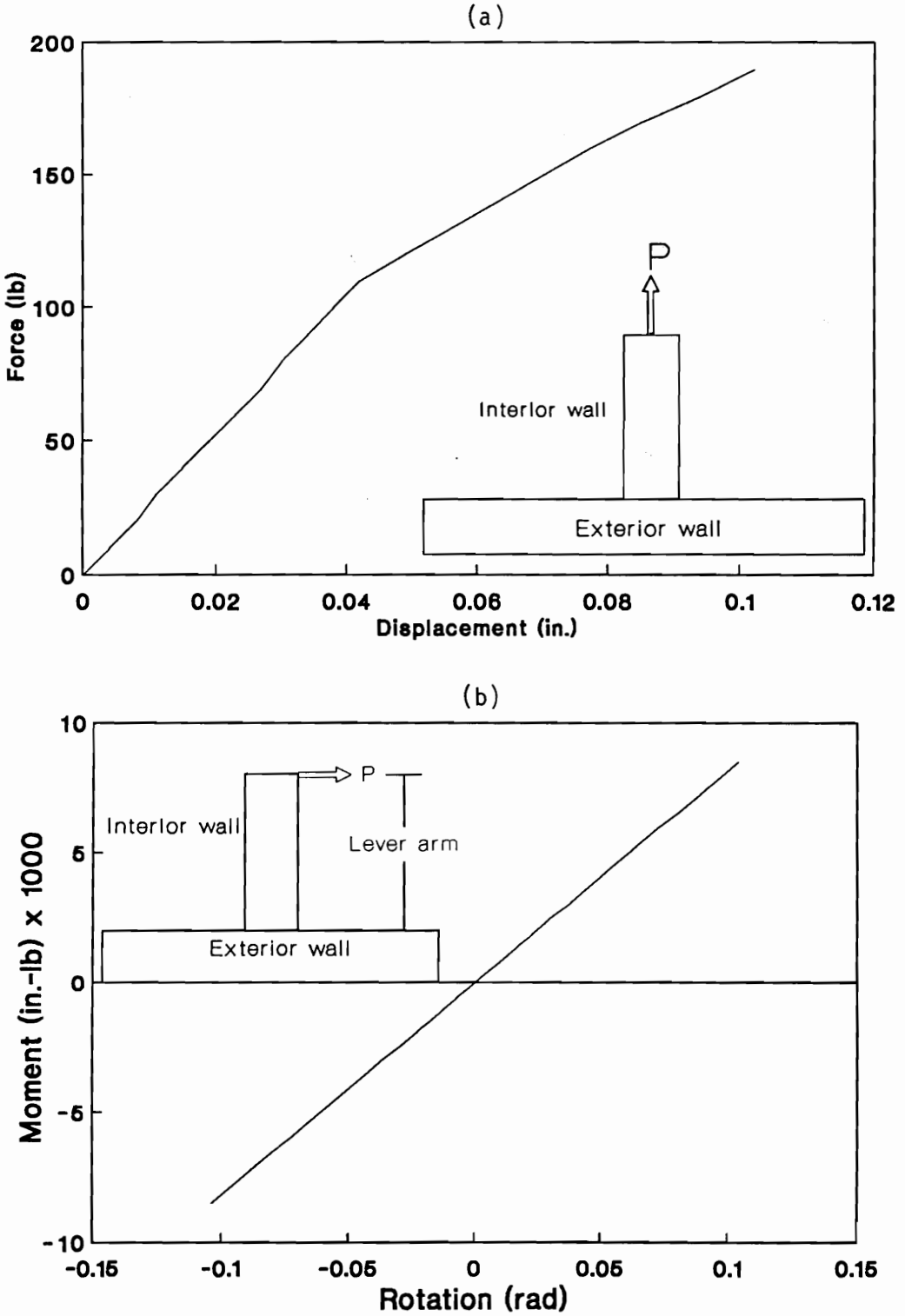

Figure 35. Load-Displacement Curves for Interior-to-Exterior Wall Connection. (a) Separation Stiffness and (b) Rotational Stiffness (Groom, 1992).

Corner Connection between Exterior Walls

The corner connection between exterior walls was created by overlapping the sheathing and nailing as shown in Figure 36. Experiments were performed to measure the rotational stiffness of the segment 12-in. (354-mm) deep and the results were used to verify the finite-element model (Groom, 1992). The finite-element model was two-dimensional using plane-stress elements. Nails were modeled via nonlinear load-deflection elements and a segment of 6-in. (152-mm) depth was analyzed. The finite-element mesh is in Figure 37.

From Figure 38, it follows that the corner has different stiffnesses for closing and opening. This is due to the non-symmetric construction and different sheathing materials and nailing schedules used for the interior and exterior wall coverings.

The load-deformation curves describing separation stiffness are shown in Figure 39. Again, direction of the force must be recognized due to the difference in the stiffness. Only separation load-deformation relationship is shown. The compressive stiffness of the connection is high and can be estimated as several orders of magnitude higher then separation stiffness.

Connection between Sole Plate and Floor

The connection between the sole plate and floor was formed by 10d and 16d nails driven to the floor joists. The stiffness per one finite-element node in translation was calculated as a ratio of the total stiffness (stiffness of one nail × number of nails in the sole plate) and number of nodes connected wall to floor.

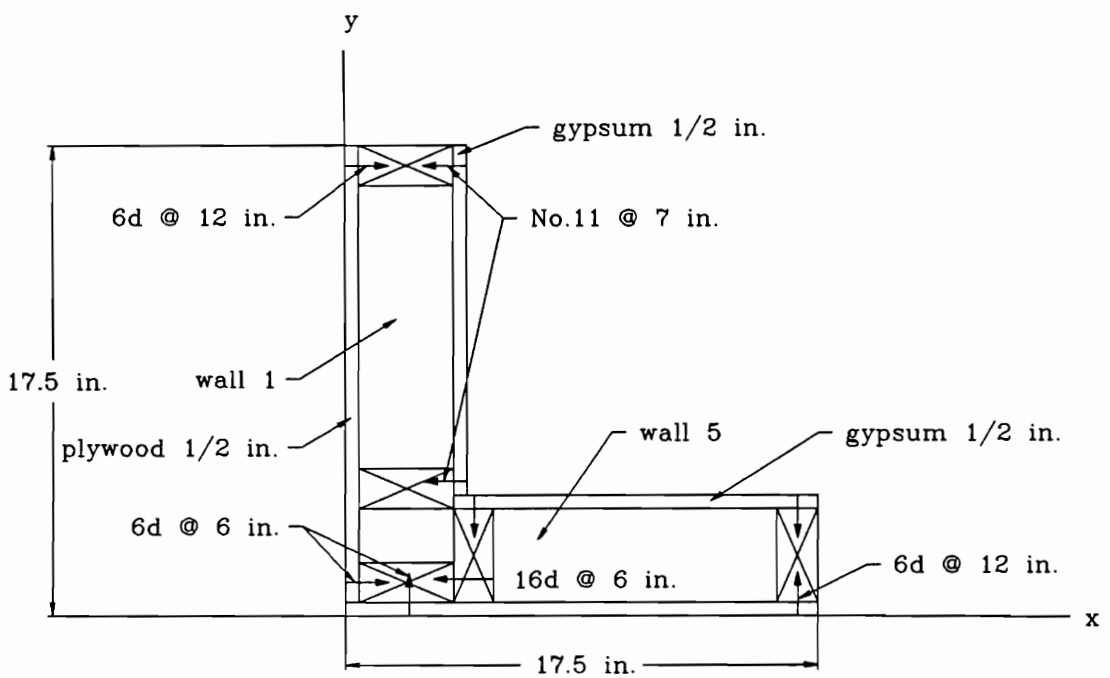

Figure 36. Connection between Exterior Walls. Test Fragment was 12 in. Deep.

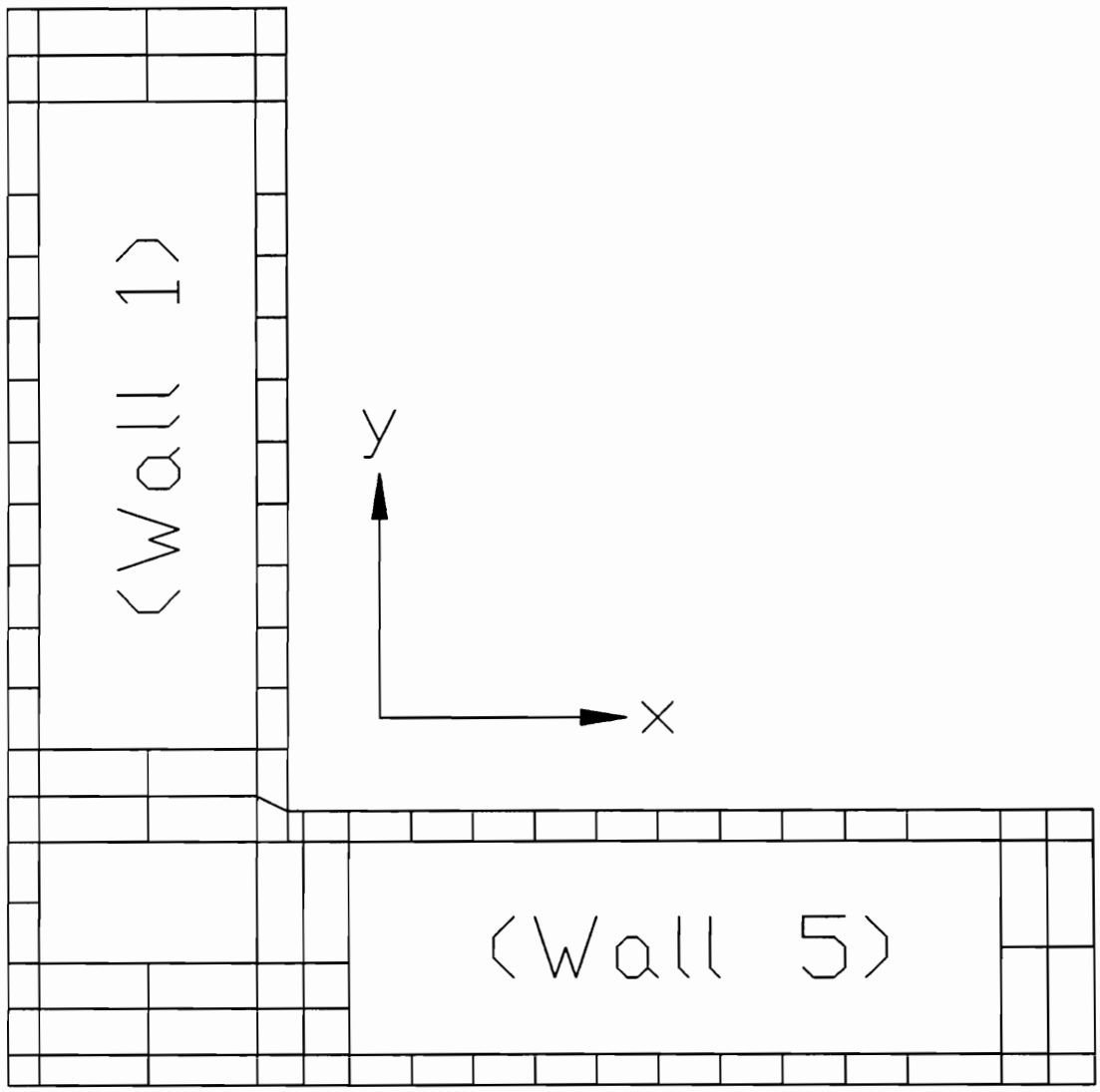

Figure 37. Finite-Element Mesh of the Model of Corner Connection (Groom, 1992).

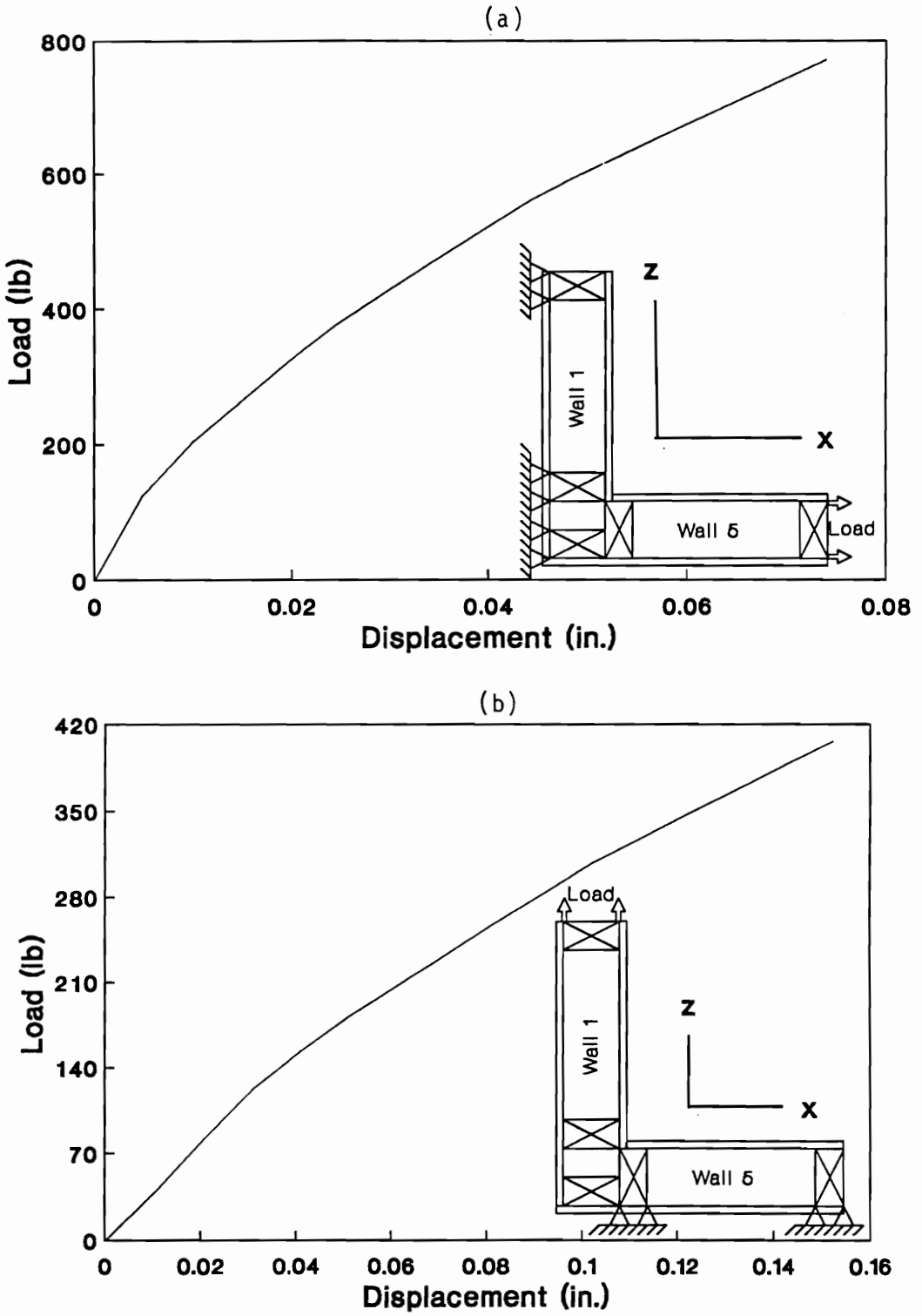

Figure 38. Load-Deformation Curve for the Corner Connection Loaded in (a) x-Direction and (b) z-Direction (Groom, 1992).

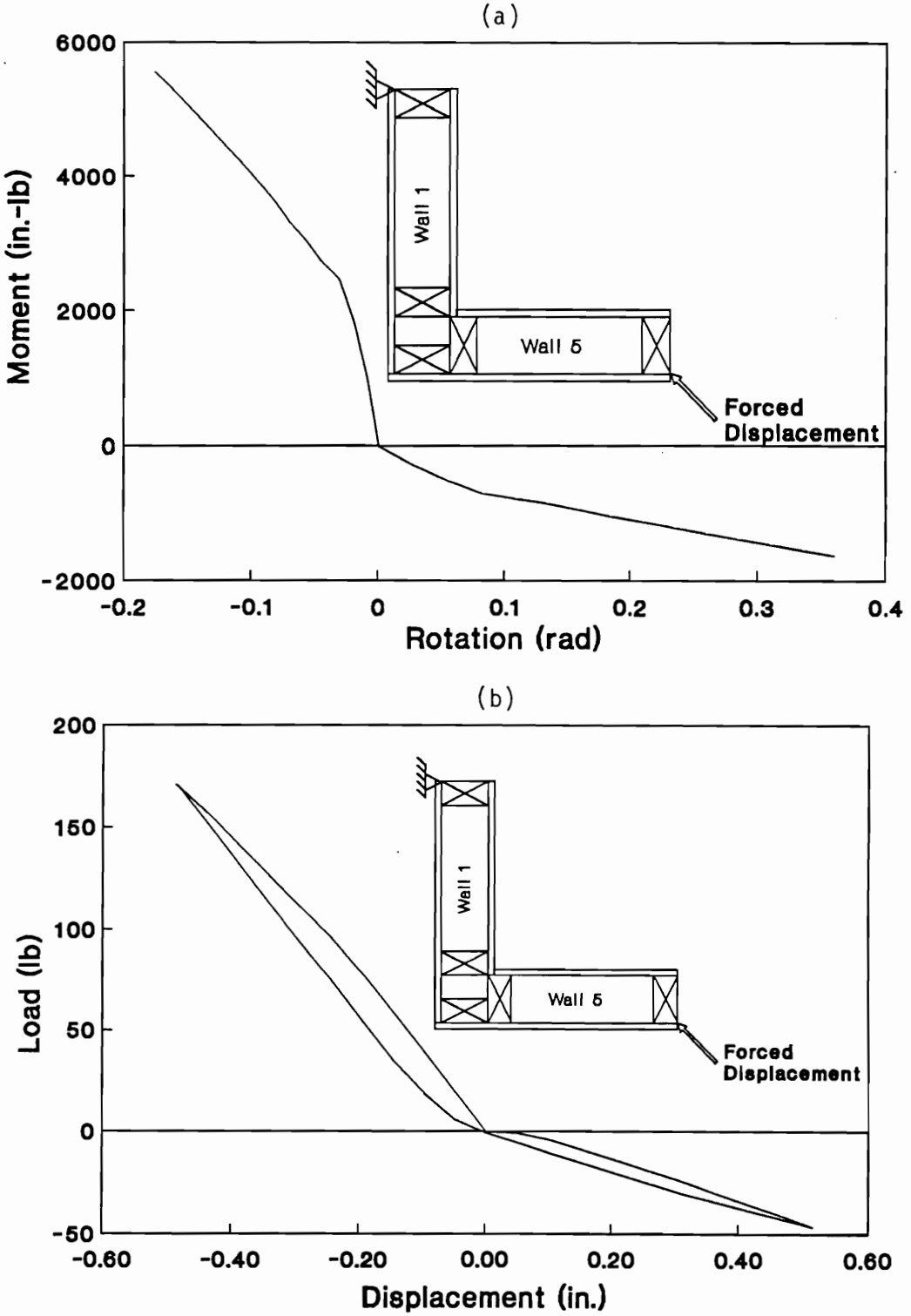

Figure 39. Load-Deformation Curve for the Corner Connection Loaded by Moment (a) Moment-Rotation and, (b) Force-Displacement Relationship (Groom, 1992).

Only four of the six degrees of freedom were neded to describe the wall-to-floor connection - three translations

Table 10. Nails Used for Soleplate-to-Floor Connection for Walls.

Wall	Nails	Spacing in. (mm)	Total nails
1	16 d	6 (152)	32
2	10 d	6 (152)	32
3	16 d	3 (76)	64
4	16 d	3 (76)	64
5	16 d	8 (203)	48
6	16 d	8 (203)	48

and one rotation. Figure 40 shows that the remaining two rotations were defined by the translation of aligned nodes. In fact, even rotation around the z-axis shown in Figure 40 can be described as a function of withdrawal nail stiffness, which is the translation in y-direction.

Walls 1 through 4

The wall must transfer reaction forces to the floor, which is connected to the foundation. These forces are transferred via connection points between walls and floor.

Each wall was connected to the floor via 10d (3.8 mm) or 16d (4.0 mm) nails as listed in Table 10. Walls 1 through 4 were resting on a series of load cells, which were bolted to the sole plate and lower beam of the wall frame. The connection was considered to be rigid (Phillips 1990), but

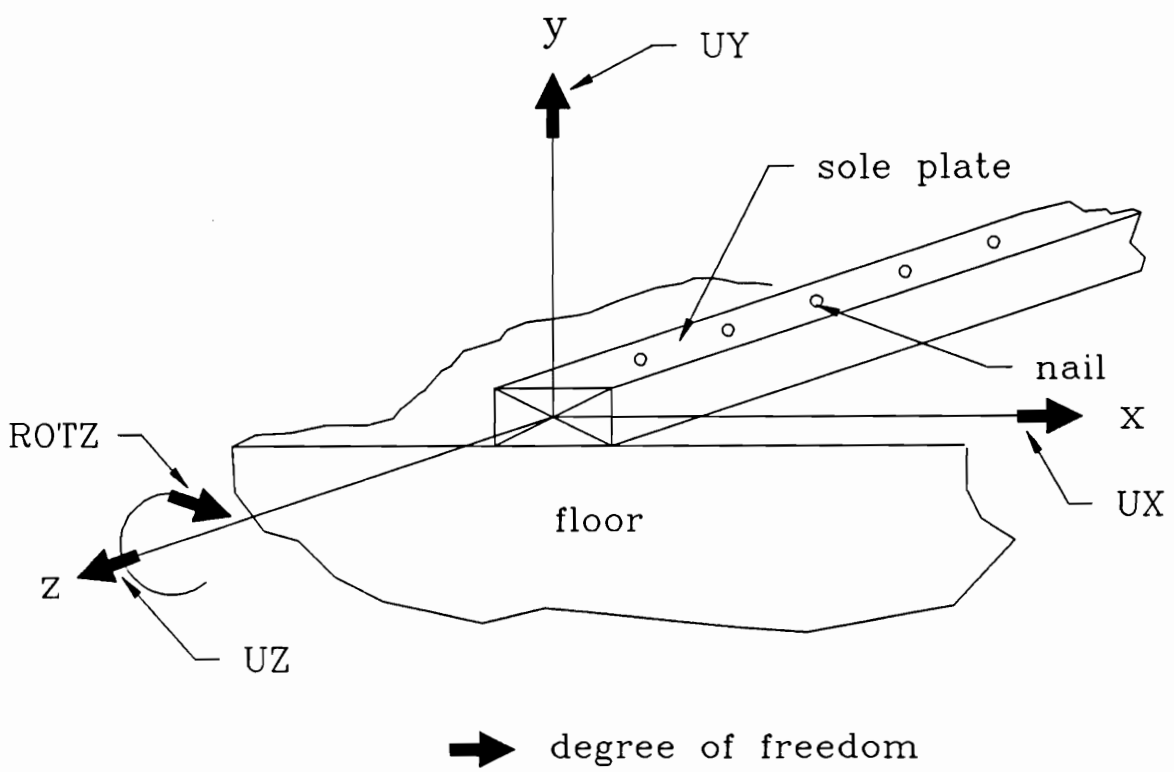

Figure 40. Degrees of Freedom Used to Describe Wall-to-Floor Connection.

the rigidity of the bolted connection was not verified. In this model, the gap necessary to place the load cells between the walls and sole plate was neglected. A theoretical connection stiffness was calculated, which represented the slip resistance of the sole plate-to-floor connection. The stiffness was expressed as the ratio of total stiffness of all nails connecting the sole plate to floor and the number of nodes on the boundary.

However, the total stiffness was smaller due to the connections between load cells and walls and sole plates. Thus, the stiffness of the connection as measured by Phillips (1990) rather then the analytical stiffness, was used as the characteristic property, and this is shown in Figure 41.

It has been observed that shear walls of light-frame structures tend to uplift when loaded by in-plane shear. The uplift is resisted by the weight of the structure above the walls, body weight of the wall and the withdrawal resistance of the connection between the wall sole plate and the floor. Thus, the stiffness of the nail connection in withdrawal is important to the finite-element model.

The withdrawal tests were performed at the Forest Research Laboratory at Oregon State University and are documented by Groom (1992). Tests of the nail withdrawal stiffness from the side grain were performed such that 2 in. (50 mm) of the nail were exposed (not embedded). This accounted for the fact that sole plate and plywood embedment does not contribute to the connection withdrawal stiffness (Groom, 1992).

The withdrawal curves for full walls are in Figure 42. The total withdrawal stiffness of the wall is the product of the number of nails and individual nail stiffness.

The rotational stiffness of the wall out of the wall plane was computed as a function of the withdrawal stiffness of the nail connecting the sole plate and floor joist. The

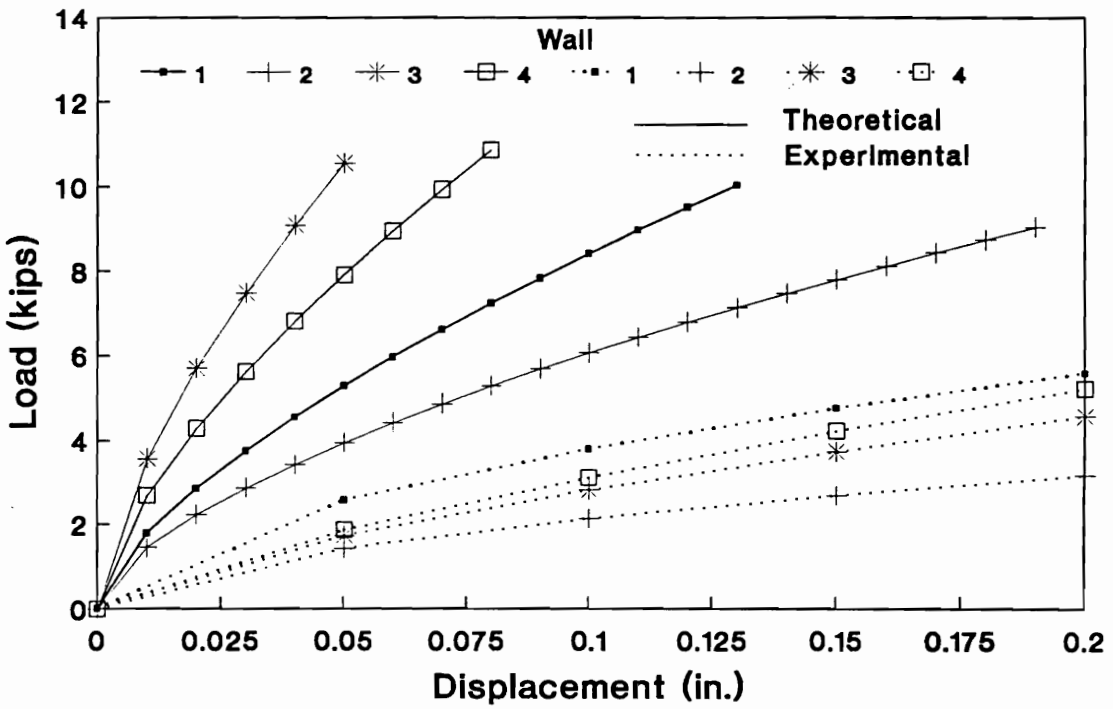

Figure 41. Load-Deformation Characteristics for the Connection Between Walls and Floor Loaded in Shear.

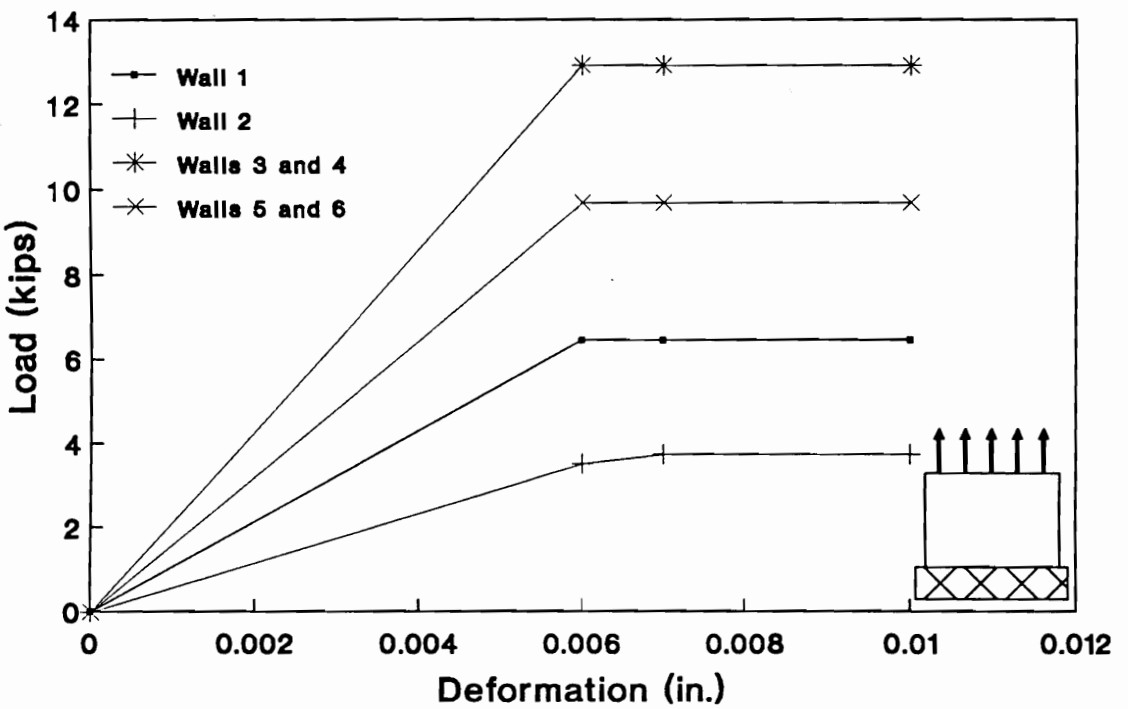

Figure 42. Load-Deformation Characteristics for Withdrawal Stiffness of the Connection Between Walls and Floor.

pivot point was chosen at the sole plate edge and the lever arm was equal to 1/2 of the plate width. The stiffness was computed according to equation (32)

$$\alpha \approx 2\frac{\Delta}{b} \qquad M = F\frac{b}{2} \tag{32}$$

where M=moment necessary to cause a rotation α
Δ=withdrawal deformation of the nail caused by force F

The derivation follows from Figure 43. The horizontal displacement of the nail δ was neglected. Rotation is controlled by withdrawal stiffness of the nail connection between sole plate and floor joists.

Even if the nails were staggered, the assumption of the centroidal nail placement is reasonable since it averages the total wall response.

Walls 5 and 6

The stiffness of the connection between walls 5 and 6 and floor was analyzed by Groom (1992). The finite-element mesh of the connection is in Figure 44. The model contained a rim joist, part of the floor joist and wall connected by nonlinear elements representing nails. A plane stress model took into account the nail stiffness in shear and withdrawal, as well as the gap effects. The resulting uplift and rotational resistance is shown in Figure 45. The compressive stiffness of the connection Figure 32a is high and is represented by contact stiffness between the sole plate and plywood sheathing of the floor. This value is several orders of magnitude larger than the separation stiffness and was calculated as the force necessary to compress the area tributary to one node by unit

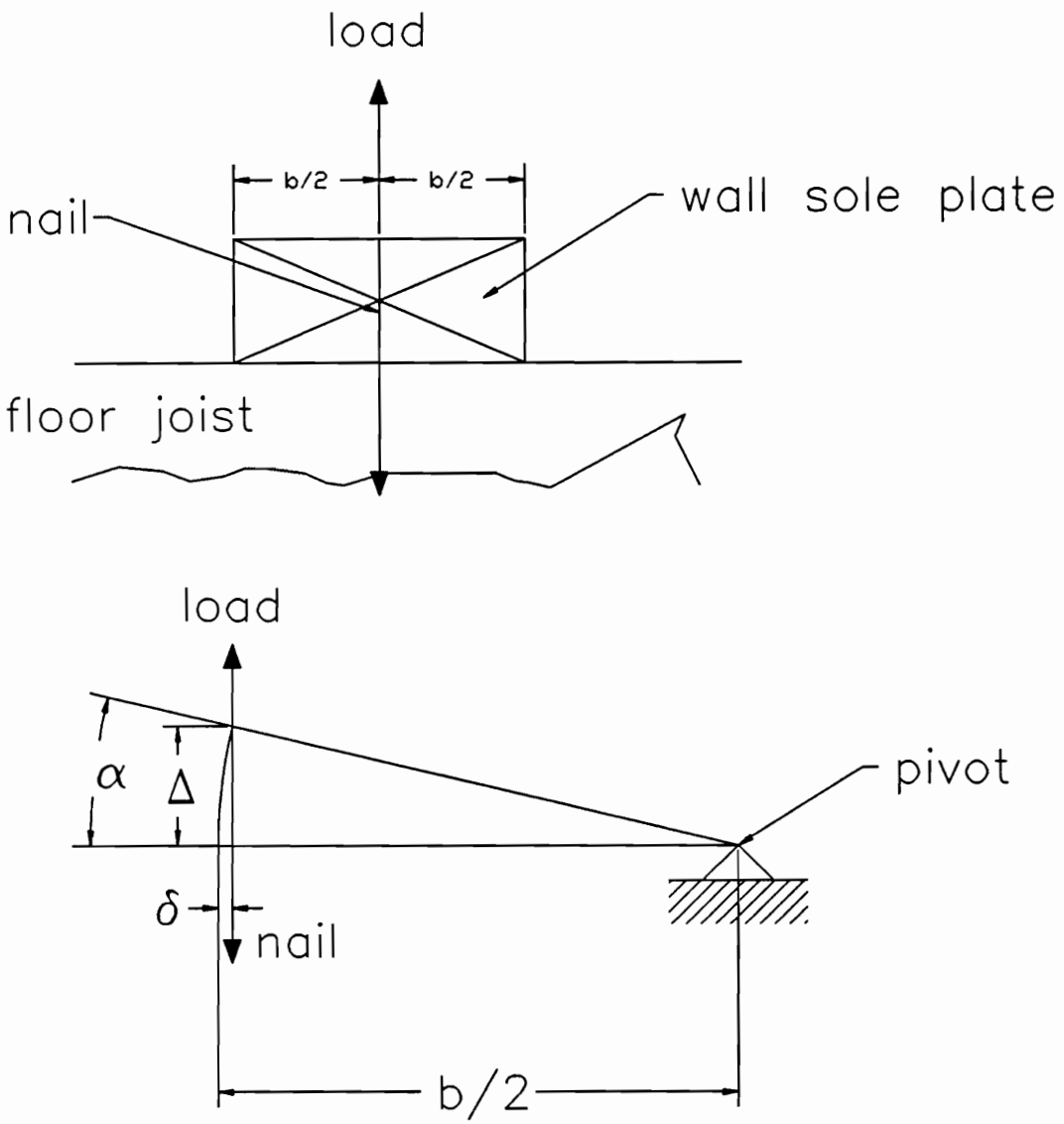

Figure 43. Model of the Rotational Stiffness of the Connection Between Sole Plate of the Interior Wall and Floor.

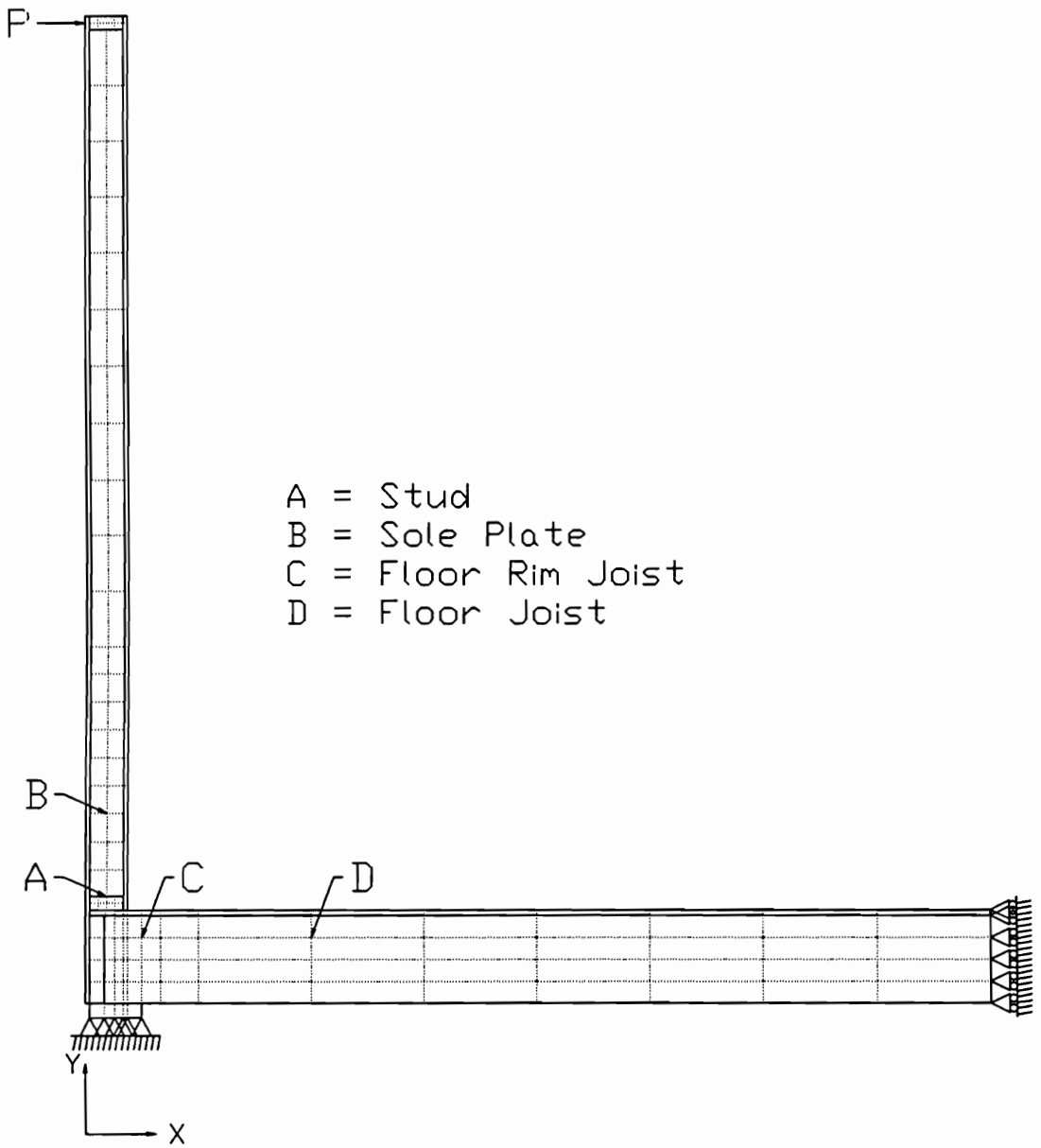

Figure 44. Finite-Element Mesh of the Connection between Exterior Walls and Floor.

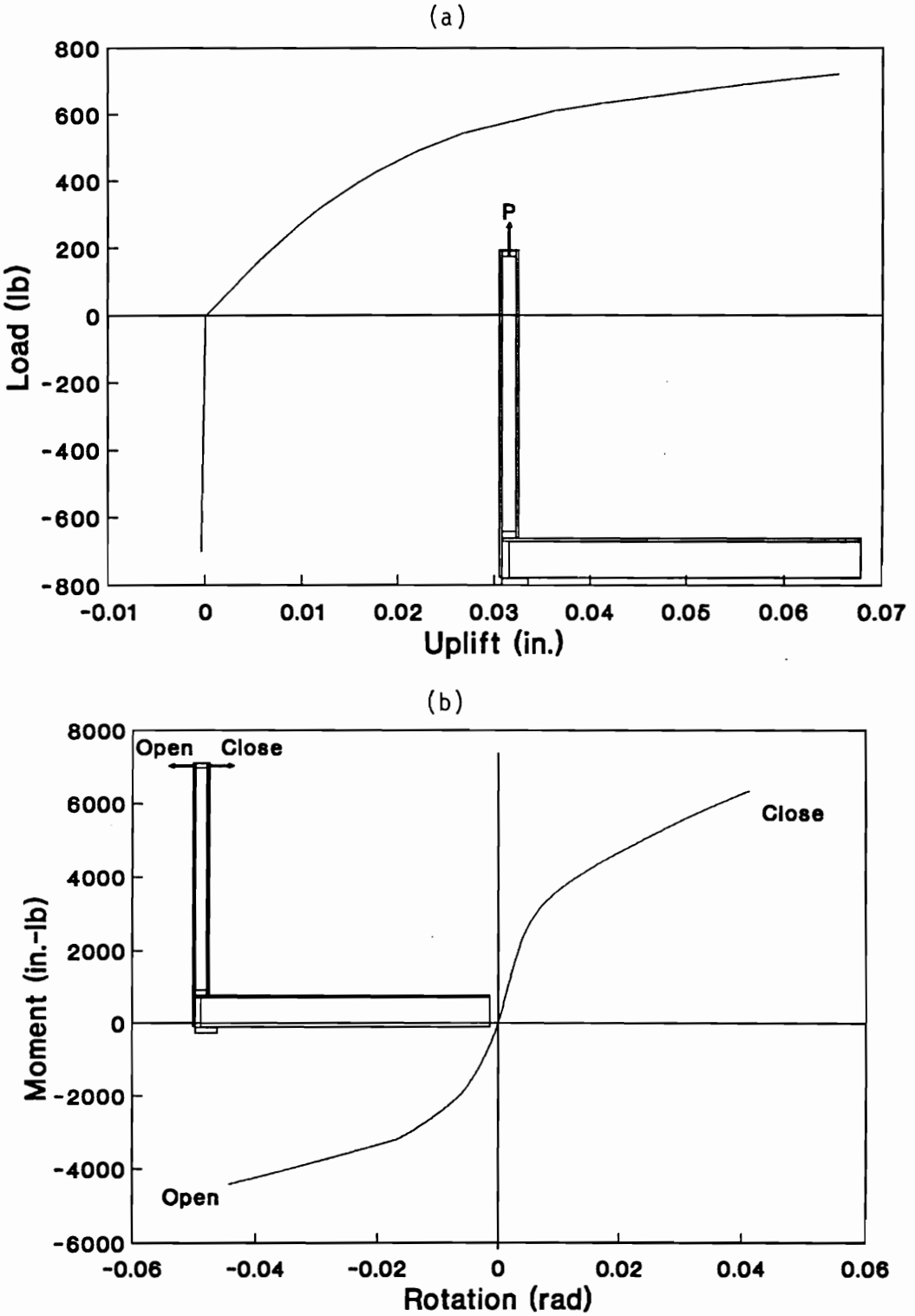

Figure 45. Load-Displacement Curves for the Connection between Exterior Wall and Floor for a Segment 12 in. Long (a) Withdrawal and (b) Rotation (Groom, 1992).

displacement. No plastic deformation of the local area around the contact point between the wall and floor was considered, due to the negligible influence on the total wall deformation.

The analytical results obtained for walls 5 and 6 are applicable to walls 1 and 4. For walls 1 and 4, experimental results were used instead of the analytical.

Connection Between Walls and Roof Superelement

Metal framing anchors shown in Appendix A were used to connect the lower chord of the truss to a top plate of the wall. The anchors were nailed to the lower chord of the truss and top plate of the wall.

The stiffness was analyzed via nonlinear finite-element models (Groom and Leichti, 1991). Shear and withdrawal characteristics of the nail connection were measured in the laboratory and the experimental curves were used as the input. Nonlinear regression analysis was used to obtain the average response of the nail to the load.

The finite-element mesh is shown in Figure 46. A three-dimensional model was used to analyze a fragment of the connection 24-in. (610-mm) long. The model was subjected to loads and boundary conditions simulating the actual test.

The load-deformation curves are shown in Figure 47 through Figure 49. The curves represent the stiffness of the connection point between the wall and roof truss. Displacements are relative displacements between top plate of the wall and lower chord of the truss. These characteristic load-deformation relationships were used for global model analysis since the number of superelement master degrees of freedom coincided with the number of hangers used. However, for the truss above walls 5 and 6, fewer nodes were available. In this case, the stiffness of

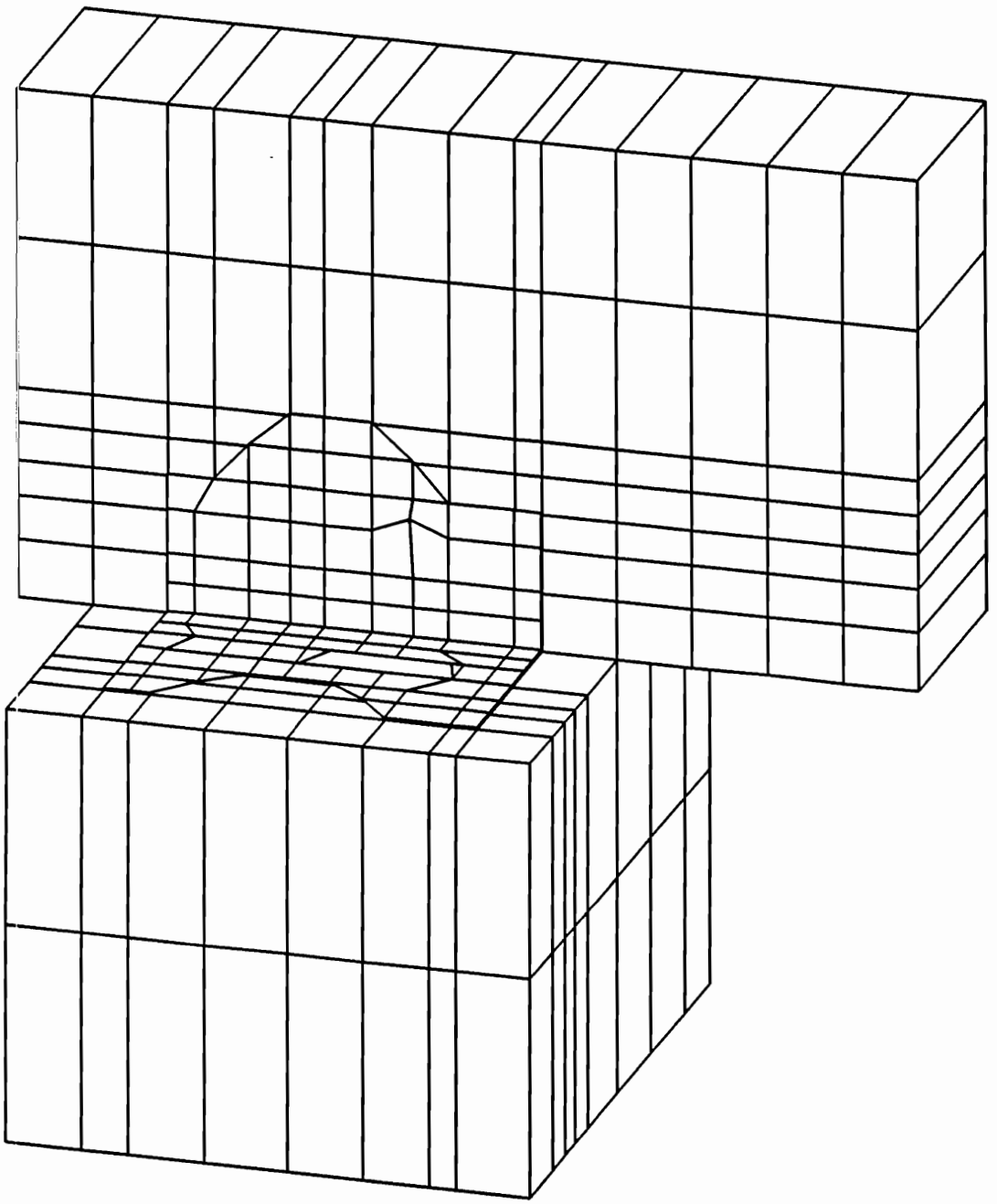

Figure 46. Finite-Element Mesh of the Connection between Roof and Top Plate of the Wall (Groom and Leichti, 1991).

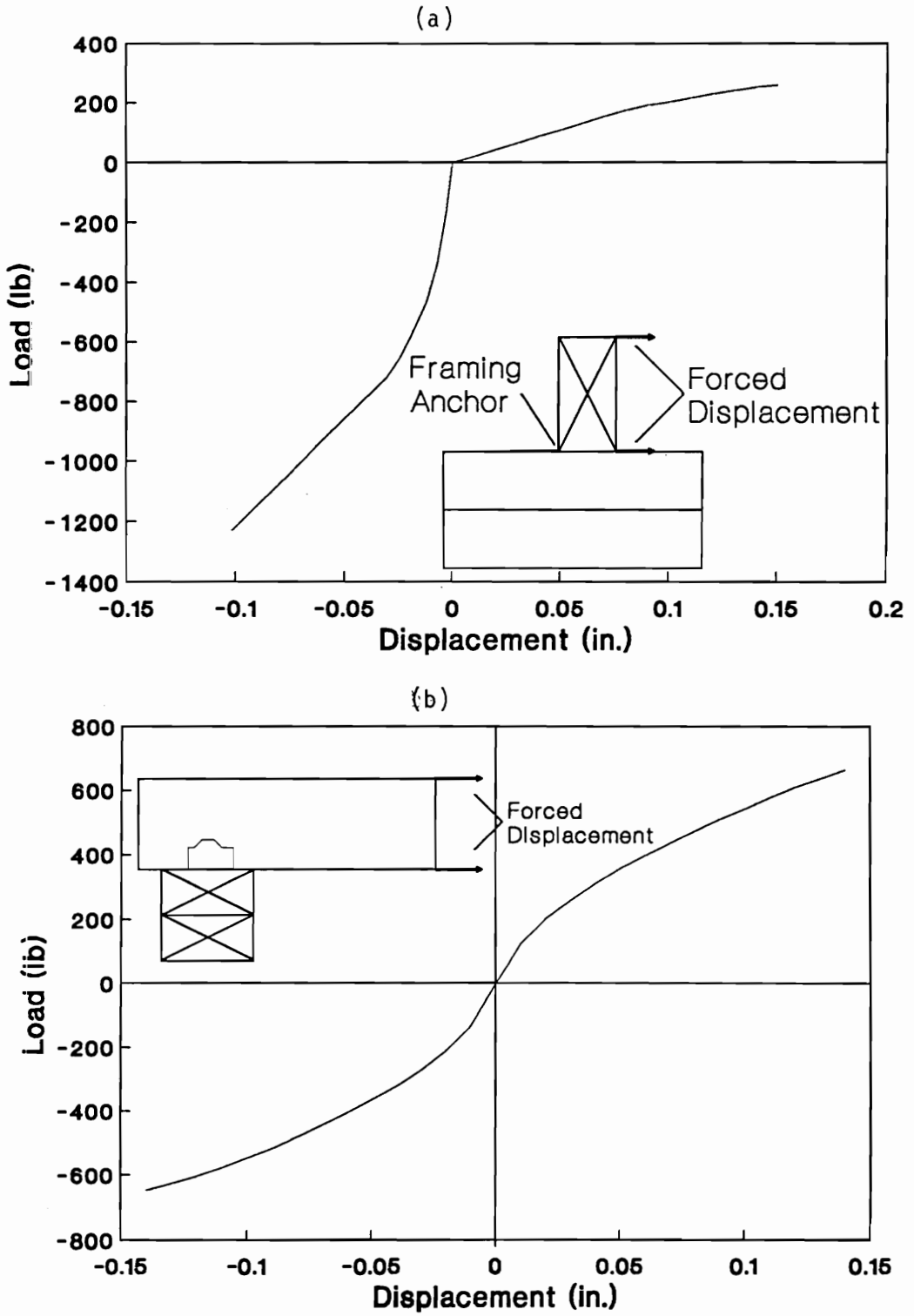

Figure 47. Load-Deformation Curve for Connection between Roof Truss and Walls. Sliding of the Truss (a) along and (b) across the Top Wall Plate (Groom, 1992).

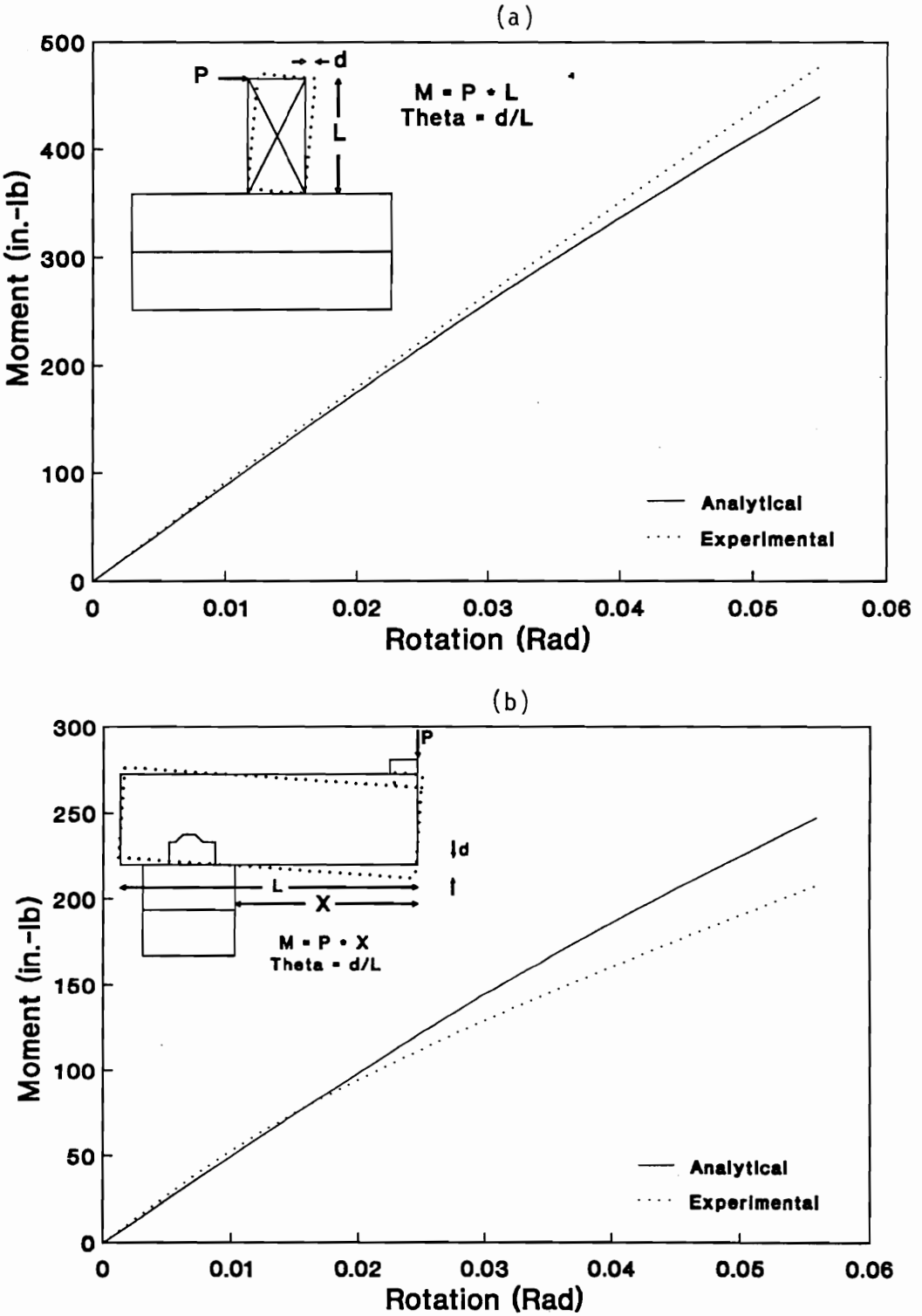

Figure 48. Load-Deformation Curve for Connection between Roof Truss and Walls. Rotation (a) Out-of-Plane and (b) In-Plane of the Truss (Groom, 1992).

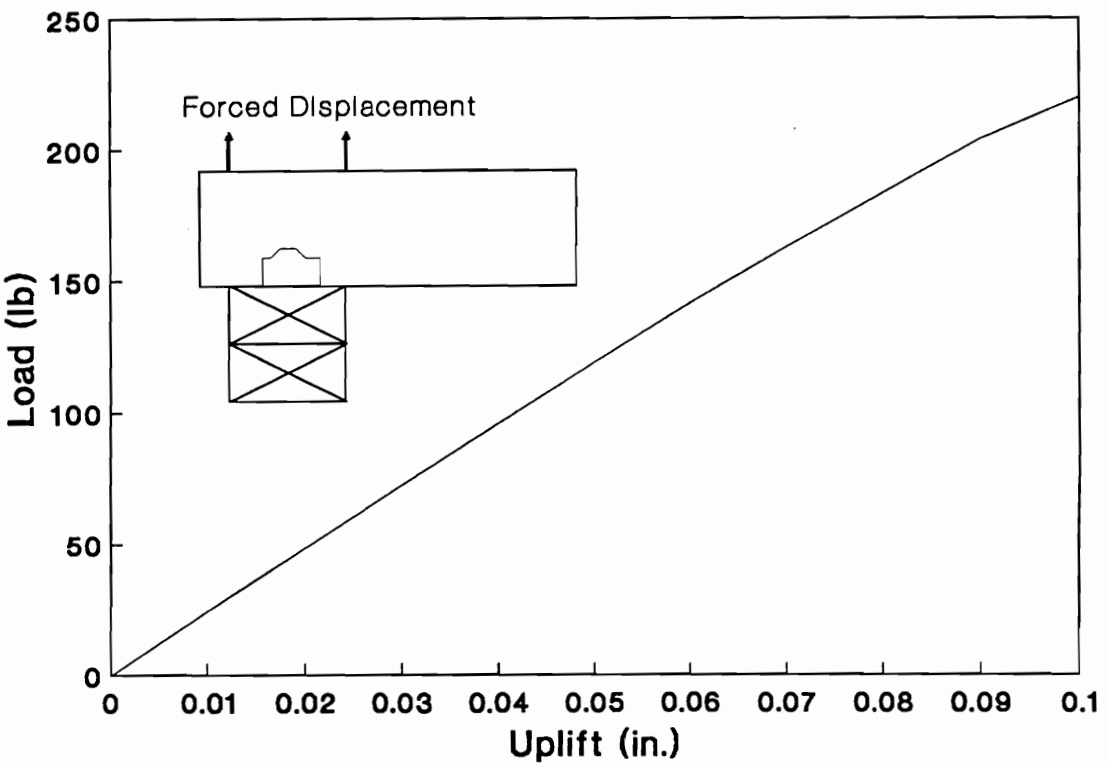

Figure 49. Uplift of the Roof Truss Connected to the Wall Top Plate (Groom, 1992).

the element associated with the nodes connecting walls 5 and 6 to the truss was increased by the ratio of hangers and nodes.

The load deformation curves are nonlinear and load-direction dependent. This is due to the asymmetry of the L-shaped steel connector, which was attached on one side of the truss bottom chord. However, the connectors in the experimental building were oriented randomly thus yielding an average response regardless the load direction. The alternating anchor detail was incorporated into the full-structure model by alternating the connector orientation.

Summary

The characteristic properties of the intercomponent connections were established by evaluating the load-deformation relationship of a representative finite-element model for each intercomponent connection. Certain of these models were verified experimentally by others.

6. FULL STRUCTURE MODEL

Objectives of the Model

The analytical model is required to yield reaction forces and deformations for each shear wall when the structure is loaded by horizontal forces such as the static equivalent of wind pressure. Further, the reactions and deformations should approach the experimental results. In this study, only static loading is of interest.

The model of the full building is an assembly of superelements representing both, the floor and roof, and quasi-superelements representing the walls and intercomponent connections. The quasi-superelements for the walls and intercomponent connections behave nonlinearly, whereas superelements are linear. Moreover, the behavior of the quasi-superelements can be nonconservative, which makes the structural response to the cyclic loading potential study area.

Assembly of the System

The full model is an assembly of the superelements and quasi-superelements, and no rigid connections are used between these macro-elements. The principle of the model is shown in Figure 50.

Nonlinear springs representing intercomponent connections are one-dimensional elements. Thus, for each degree of freedom one spring is specified. The stiffness of the

spring (or characteristic load-deflection curve) depends on the substructure representation and number of nodes connecting substructures. For example, if the total stiffness of connection between the floor and wall for withdrawal in the positive y-direction was known to be 10000 lb/in. (1751 N/mm) and there were 10 nodes connecting the wall to floor, the stiffness of one spring would be 1000 lb/in. (175.1 N/mm).

As shown in Figure 50, not all possible degrees of freedom for each node on the substructure boundaries are necessary. Translational degrees of freedom represented by springs relating force to deflection are always specified. One degree of freedom represented by a rotational spring describing moment to rotation is added to prevent the out-of-plane rotation of the substructure. The load-deformation elements (springs) have no physical dimension that is both nodes have identical locations, which implies that there is no initial gap between substructures.

The size of the finite-element mesh depends on the capability of the computer as well as required accuracy. As shown in the quasi-superelement example, a rather coarse mesh yields satisfactory results for deformations. Since no stress analysis is performed on the full-structure model, the mesh can be coarse as shown in Figure 51.

Total Assembly

The finite-element meshes shown in Figure 51 were created to compare the influence of the mesh size on the results. Mesh in Figure 51a has fewer elements than mesh in Figure 51b. Moreover, mesh (a) contained nonrectangular elements which were necessary to create areas around openings. The mesh size is an important factor influencing the accuracy of a finite-element analysis (Kikuchi, 1986).

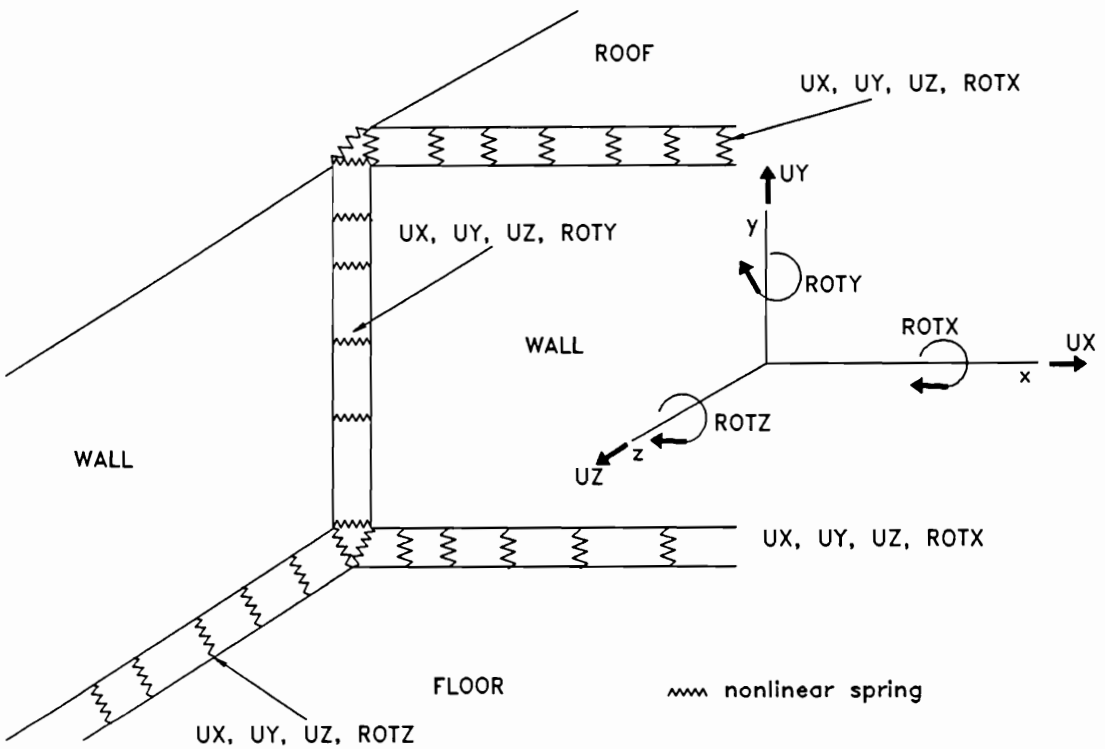

Figure 50. A Conceptual Schematic of the Finite-Element Model of the Full Structure Showing Essential Degrees of Freedom.

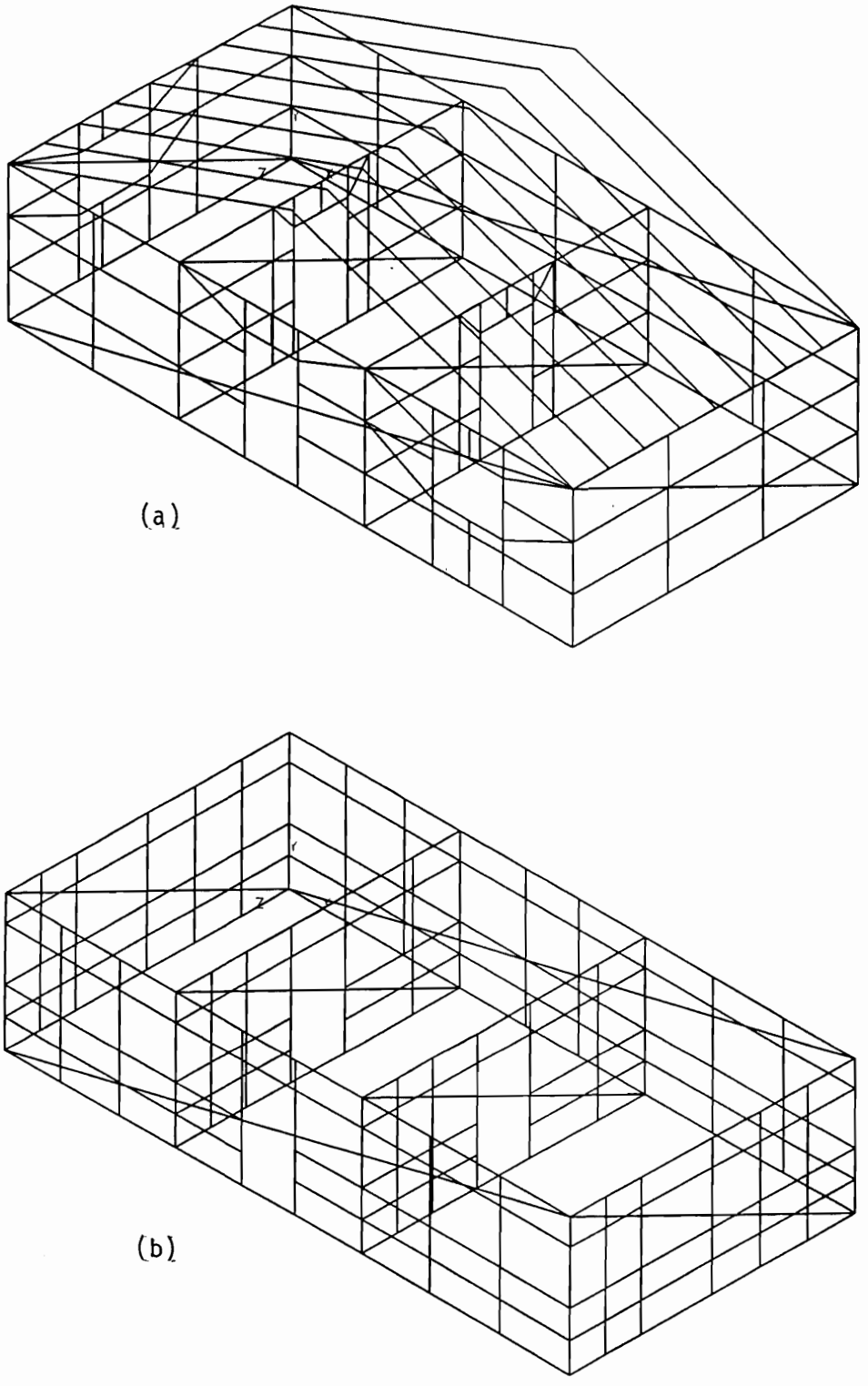

Figure 51. Finite-Element Mesh of the Full-Structure, (a) Mesh 1 with the Roof Truss and (b) Mesh 2 with no Roof Truss Plotted.

Thus, it is necessary to analyze a possible effect of mesh size on the accuracy of the results. Further mesh refinement was not possible due to the hardware and software limitations. However, as shown in following chapters, analyzed models yielded satisfactory results.

The properties of individual elements in the substructures and intercomponent connections were used as described in pertinent chapters.

Walls

The stiffness of the diagonal springs for walls 1 through 4 was based on the experimental results obtained by Phillips (1990), whereas analytical results were used for walls 5 and 6 (no experimental measurements were available). This does not cause a significant error in the verification of the model since walls 5 and 6 were not loaded in shear during the experiment.

The bending properties of the wall represented by an orthotropic plate model do not depend on the mesh size and were used as shown in Table 6.

Floor

The floor superelement was described in Chapter 4 and is shown in Figure 29. Master degrees of freedom were specified at points where the walls were connected to the floor. Nodes associated with master degrees of freedom are called master modes. The nodal locations of master degrees of freedom in the superelement must match those of the full model. Also, the node numbers used as master nodes must be unique to the superelement and full model.

Roof

Incorporating the roof into the full building model was similar to the process used with the floor. Master degrees of freedom were specified at master nodes on the bottom chord of the truss. These master nodes were connected to the top plate of the walls via nonlinear load-deformation elements representing the metal framing anchors studied by Groom and Leichti (1991) and Groom (1992). Thus, depending on the stiffness of the connection, the walls could deform somewhat independently of each other.

Intercomponent Connections

The properties of the nonlinear load-deformation elements representing intercomponent connections were discussed in Chapter 5. Results from both experiments and finite-element analyses were used to model the connections.

The nonlinear nature of the intercomponent connections contributes to the nonlinear behavior of the full structure model. The models of intercomponent connections, however, introduce some error into the full-structure model due to the unknown mechanism of some details such as number of connections engaged into the transfer of shear load from the sheathing to the framing. This would require an extensive research program so an estimated value was used. However, the sensitivity study of Chapter 7 revealed that system was robust with respect to the error in the stiffness of the intercomponent connections.

Boundary Conditions

During the experiments, floor joists and rim joist were toe-nailed to the 2×6-in. (38×140-mm) plate, which was bolted to the concrete foundation. Steel connections were used to prevent possible floor uplift. This connection was represented by specifying zero translations of the nodes at the bottom perimeter of the floor superelement in x-, y-, and z-direction. No boundary conditions were specified elsewhere.

Model Verification

The verification of the model was based on the experimental results obtained by Phillips (1990) for the full-scale building. The measurements obtained from the fully assembled structure loaded by point loads at the top of each wall were compared with the analytical results. Both displacements and reaction forces were compared.

Loading

First, a load of 1200 lb (5.33 kN) was applied to walls 1 and 2 and reaction forces and displacements for each shear wall computed. Then, 1800 lb (8.0 kN) was applied to walls 3 and 4. One full load cycle was analyzed for 1200- and 1800-lb applied loads. These loads were relatively small, producing small deformations. Finally, load of up to 7200 lb (32.0 kN) on each wall was applied. Only load from 0 to 7200 lb was analyzed which lead to an envelope load-deformation curve.

Case 1: 1200 lb (5.33 kN) on Walls 1 and 2

In the experiment, three slow cycles of ±1200 lb (5.33 kN) were applied to each of the walls 1 and 2 of a fully assembled building. The finite-element analysis was conducted for one full cycle as shown in Figure 52 through Figure 55. The results of the analysis are more accurate for the directly loaded walls (walls 1 and 2) than for the walls sharing the load due to the transfer via roof diaphragm and intercomponent connections (wall 3 and 4). The later two walls are given in Figures 54 and 55.

The largest error in reactions and deformations is for wall 4, which is far away from the applied load. However, the magnitudes of the measured displacements and reaction forces are very small.

To properly model the full cycle, the unloading path must be accurately defined. The intersection between the initial linear load-deformation path for the walls loaded in shear (chord modulus representing unloading path as defined in Chapter 4) with the exponential function describing the wall nonlinear behavior represents relatively high load and deformation (Figures 23 and 24) for most walls. This means a linear response is likely from the wall quasi-superelements for small loads. Thus, for this loading, the initial portion of the curve describing properties of the diagonal spring was modeled with more segments. However, this created a steeper unloading path and consequently larger hysteresis for the loading and unloading curve as shown in Figure 52. Since the main objective of this research was to establish the reaction forces for loading between zero and maximum load, no another effort was extended to better model the unloading path.

The change of the slope of the loading path for individual walls is controlled by the nonlinear load-deformation characteristics of intercomponent connections

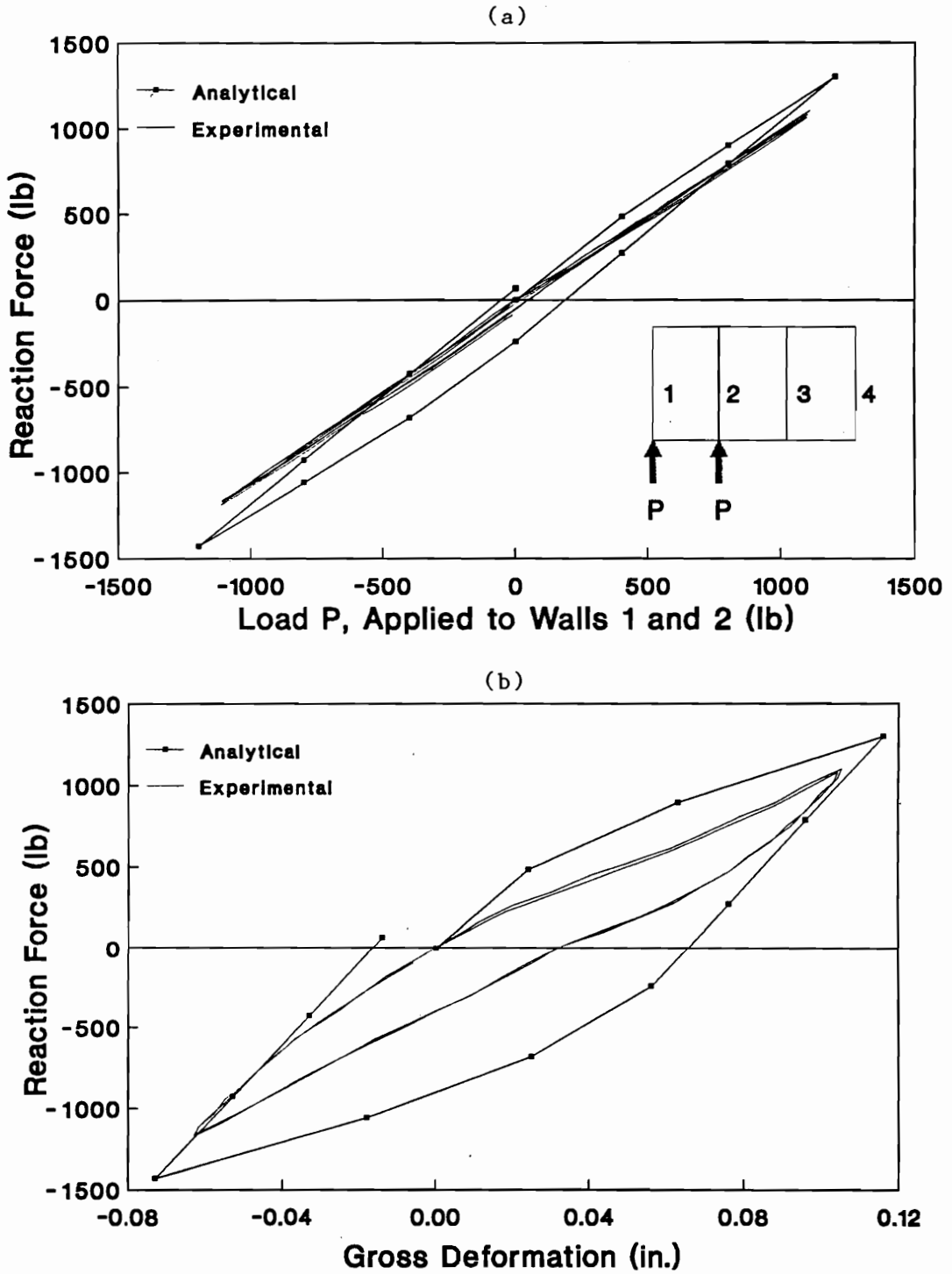

Figure 52. Full Model Verification with the Load Applied to Walls 1 and 2, (a) Reaction Force and (b) Deformation for Wall 1.

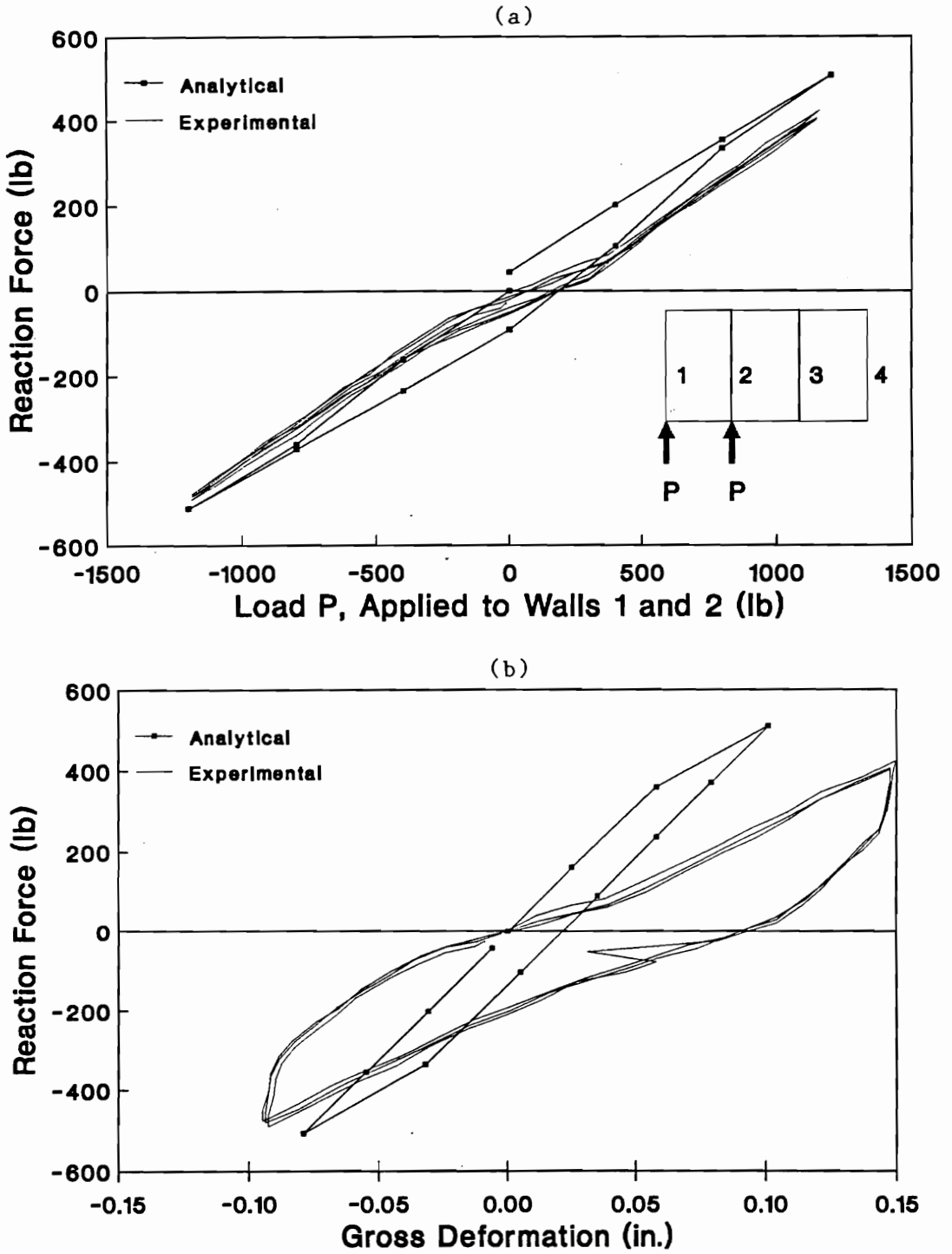

Figure 53. Full Model Verification with the Load Applied to Walls 1 and 2, (a) Reaction Force and (b) Deformation for Wall 2.

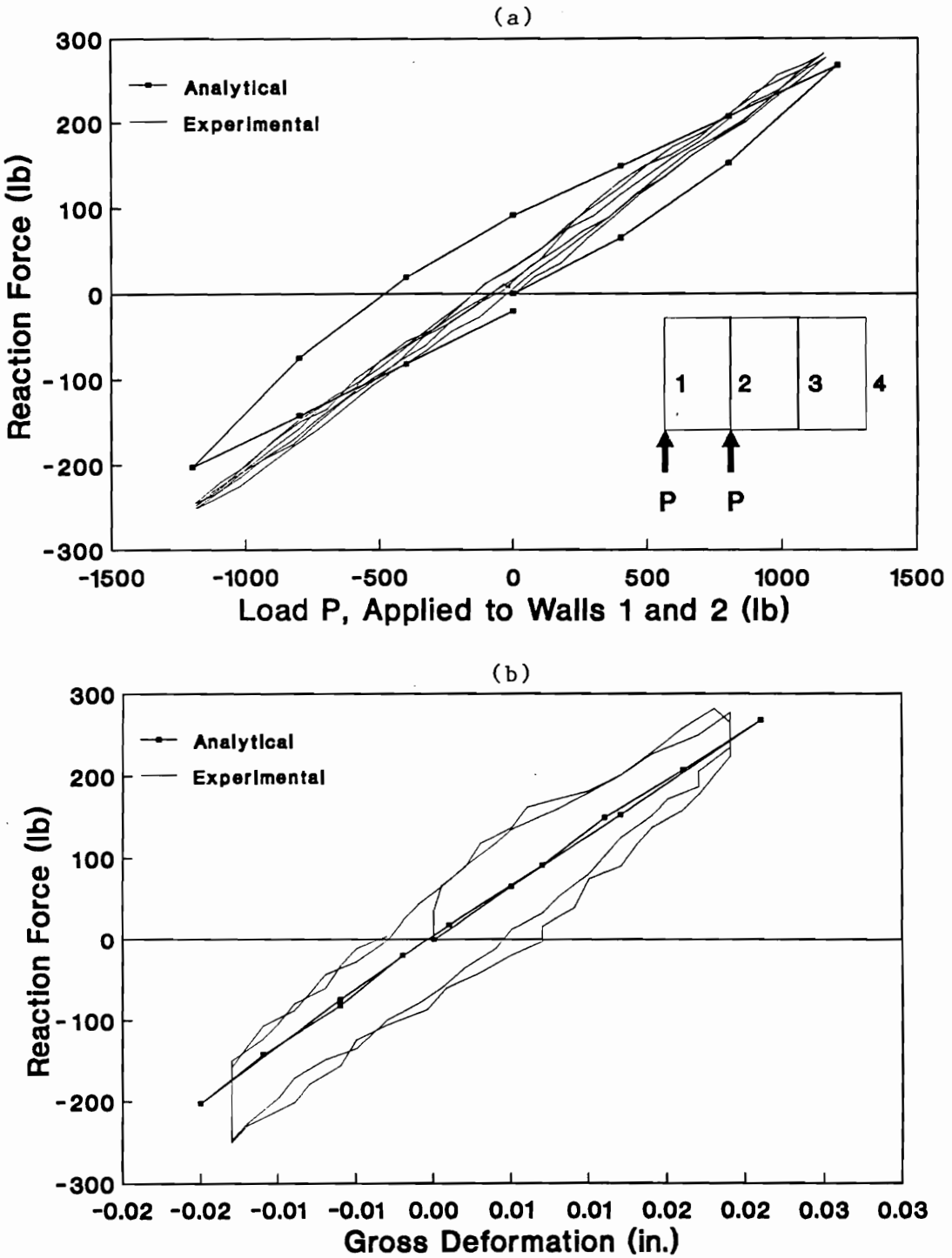

Figure 54. Full Model Verification with the Load Applied to Walls 1 and 2, (a) Reaction Force and (b) Deformation for Wall 3.

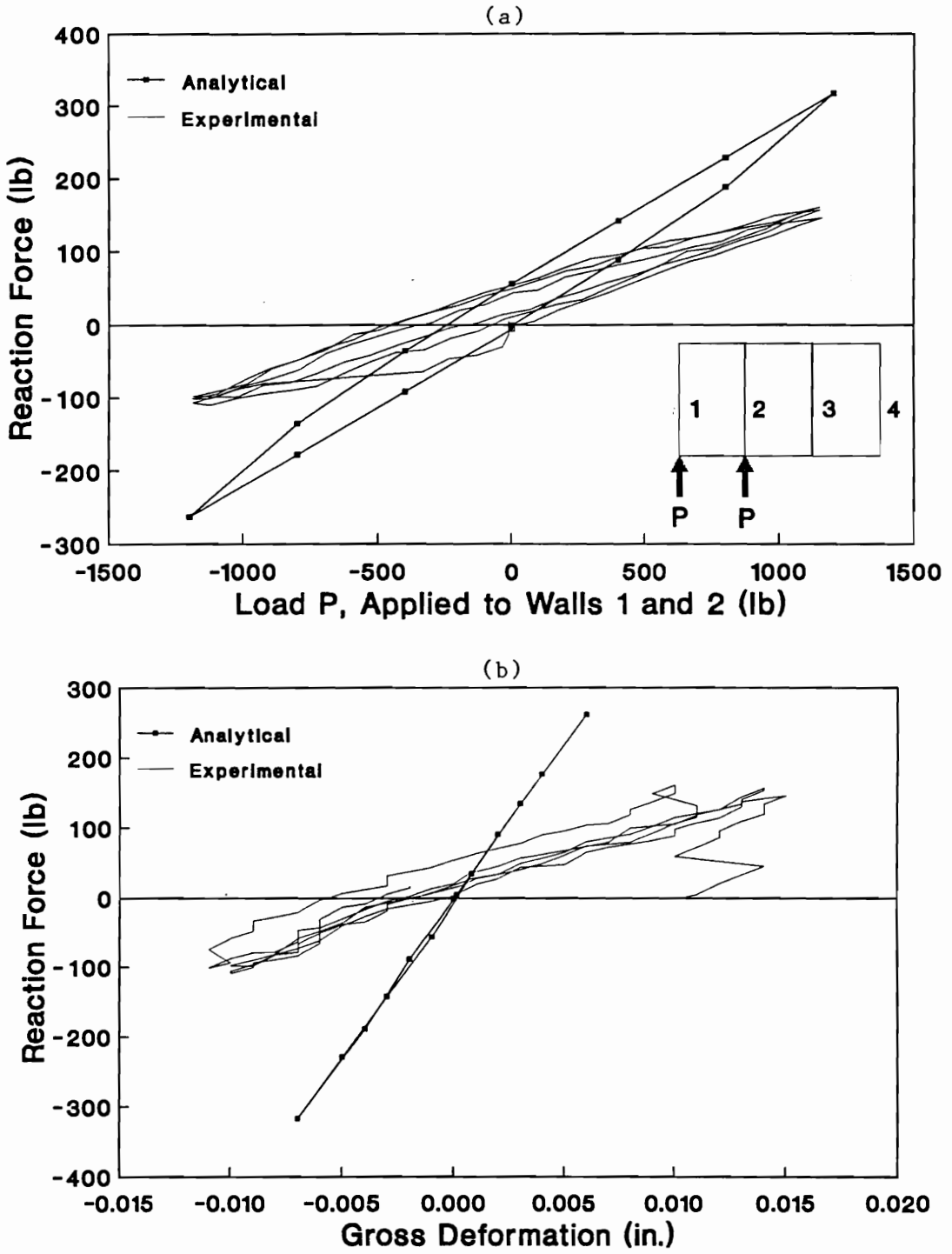

Figure 55. Full Model Verification with the Load Applied to Walls 1 and 2, (a) Reaction Force and (b) Deformation for Wall 4.

and quasi-superelements representing walls. Individual segments can be easily recognized. The segments are straight lines, which are a result of the number of load steps as well as the characteristics of the nonlinear elements for which the nonlinear curve is modeled from discrete points connected by straight lines. Thus, the gross deformation can even be linear for small loads, as shown in Figure 54b. In this case, the experiment revealed similar relationships as the analytical solution. The hysteresis in the experimental loading-unloading curves is most likely due to measurement errors caused by the delayed response of the displacement transducer or hysteresis of the load cell.

Case 2: 1800 lb (8 kN) on Walls 3 and 4

In this phase of the experiment three slow cycles of ±1800 lb (±8 kN) were simultaneously applied to each of the walls 3 and 4. A larger load was applied here because these walls were constructed to be stiffer. The relationships between applied load and reaction forces and applied load and displacements for individual shear walls are shown in Figure 56 through Figure 59.

As in the previous case, the error in reactions and deformations tends to increase with increased distance from the applied load. It may be that the error arises because the deformation of the walls to which the load is applied directly is mostly controlled by the stiffness of the wall and less by the load transferring capability of the full system. The load-deformation curves for walls loaded by shear was experimentally established (Phillips, 1990), whereas the stiffness properties of the elements controlling the load transfer (such as intercomponent connections, and bending of walls 5 and 6) resulted in most cases from

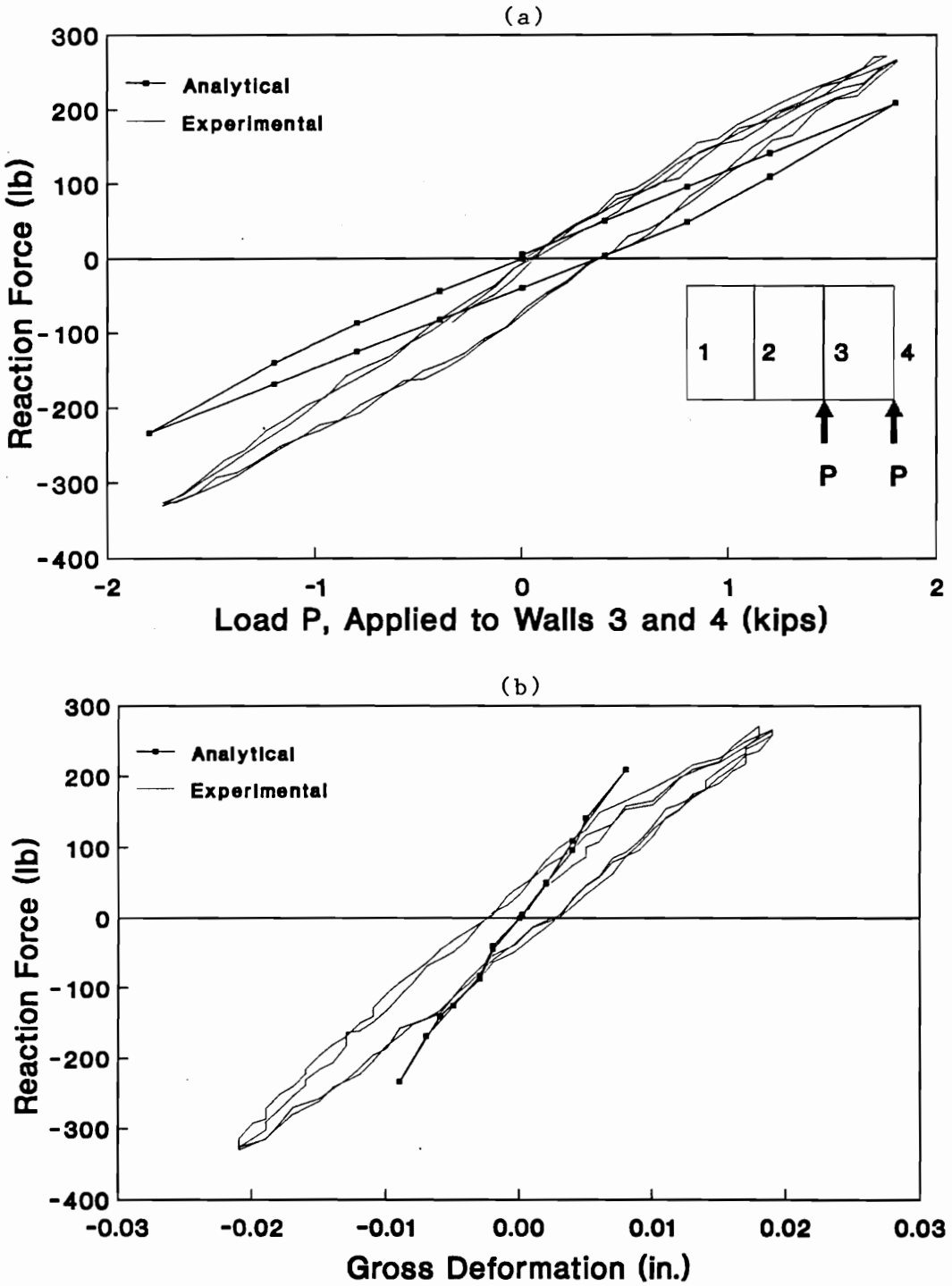

Figure 56. Full Model Verification with the Load Applied to Walls 3 and 4, (a) Reaction Force and (b) Deformation for Wall 1.

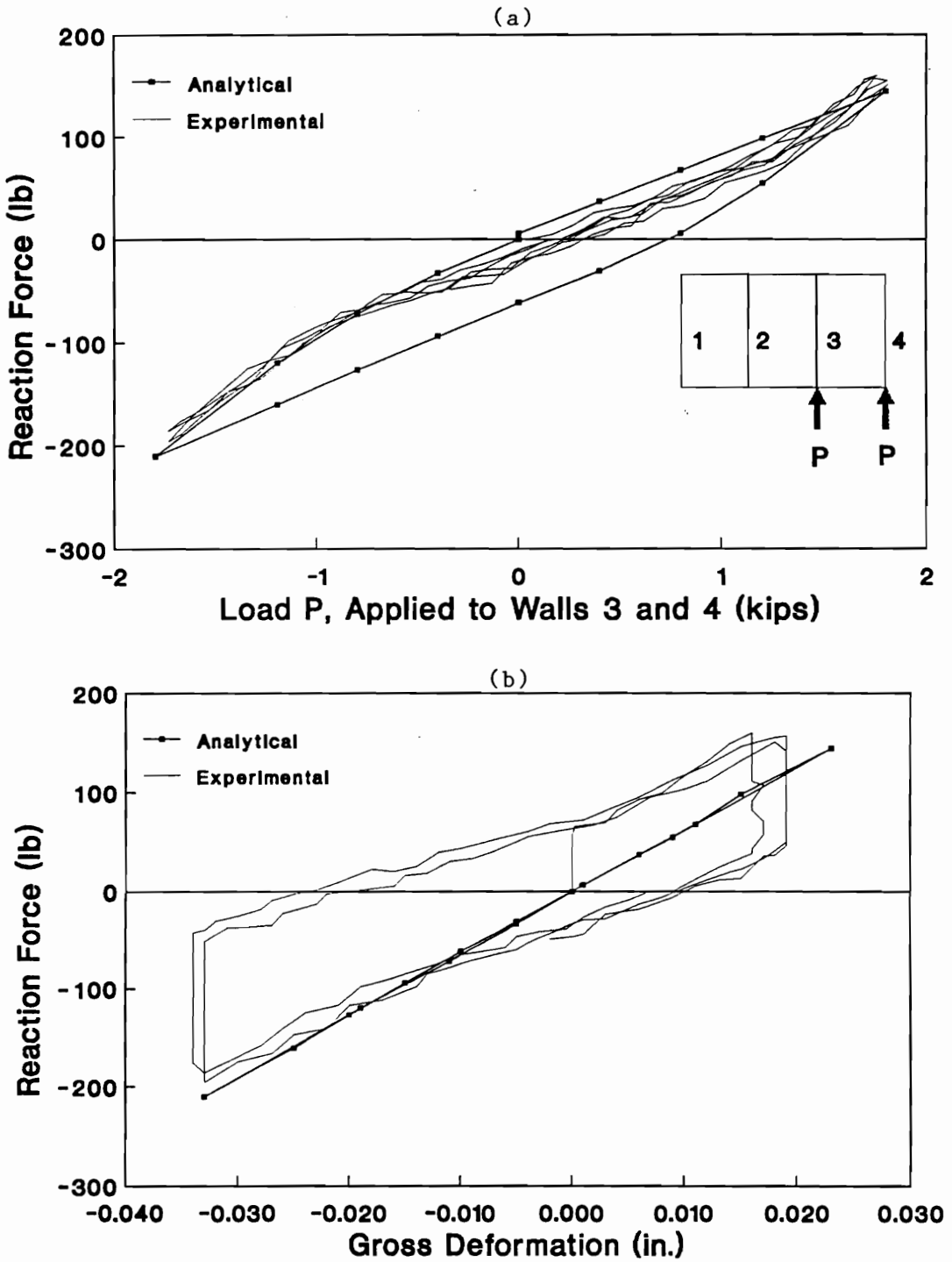

Figure 57. Full Model Verification with the Load Applied to Walls 3 and 4, (a) Reaction Force and (b) Deformation for Wall 2.

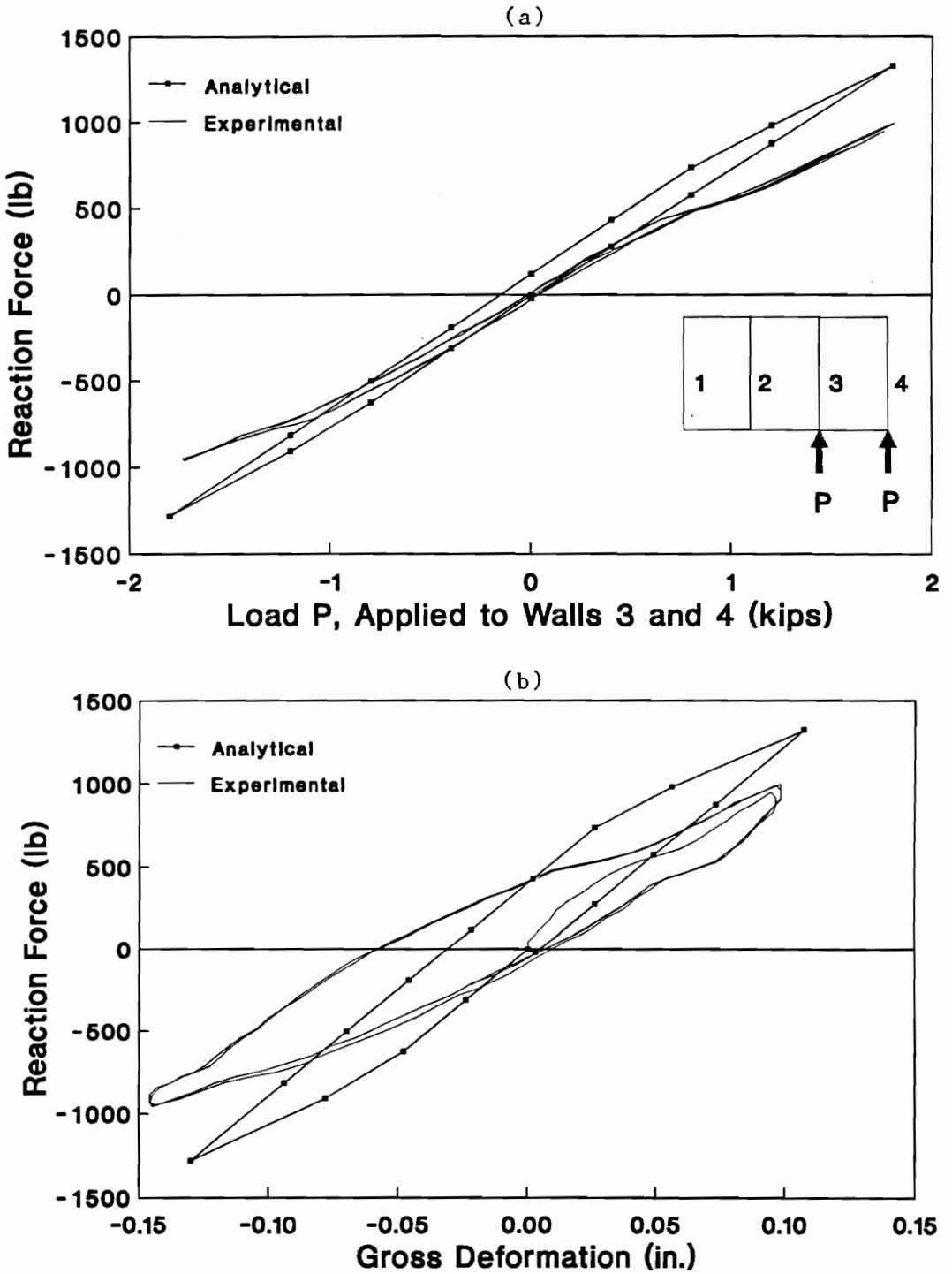

Figure 58. Full Model Verification with the Load Applied to Walls 3 and 4, (a) Reaction Force and (b) Deformation for Wall 3.

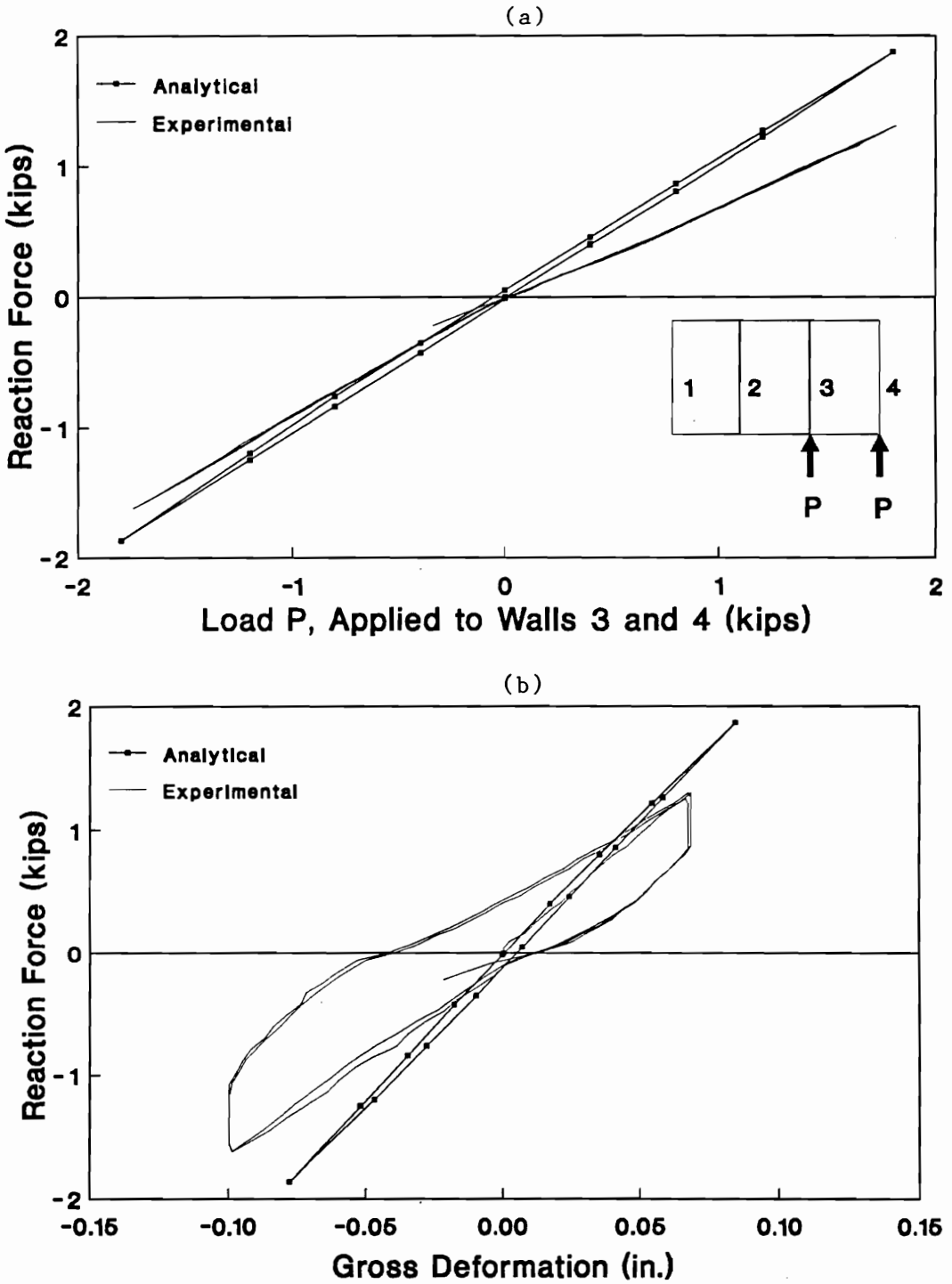

Figure 59. Full Model Verification with the Load Applied to Walls 3 and 4, (a) Reaction Force and (b) Deformation for Wall 4.

substructure finite-element models. These models are subjected to inherent errors stemming from the stochastic character of the input parameters such as moduli of elasticity or load-deformation curves for nail connections. Thus, the error tends to increase as the number of connecting elements and substructures involved with load transfer increases.

Generally, the analytical model gives better predictions for reaction forces than for deformations. It seems, that the deformations due to the moderate loads were relatively small and did not cause the change of the slope in most nonlinear load-deformation elements, and this lead to a stiffer structure. Modeling the early portions of the load-deformation curves more accurately would allow a slope change for small loads. However, this would require a much smaller load step to ensure faster convergence and would consequently lead to unacceptable computational time.

Case 3: 7000 lb (32.0 kN) Applied to Walls 1 through 4

The main test consisted of the cycled load starting at ±2200 lb (±9.8 kN) and going to ±7000 lb (32 kN) in 800 lb (3.6 kN) steps applied to the top corner of each shear wall. Thus, the first cycle was between ±2200 lb (±9.8 kN), second between ±3000 lb (±13.3 kN) etc. The curves relating net shear deformation to reaction force for each shear wall (walls 1 through 4) are in Figure 23 through 25. The envelope curves for gross wall deformation were constructed in the same manner as for the net wall deformation.

The load in the analytical solution was applied in steps of 1000 lb (4.48 kN) to the top corner node of each shear wall as a full cycle between ±8000 lb (35.6 kN). The load is somewhat higher than in the experiment.

Only one cycle corresponding to the last experimental

cycle was applied in the analysis. This was due to the following reasons:

(1) The model is not capable of accommodating the gradual deterioration of the stiffness of the structure which results in loose connections and almost zero initial stiffness when the structure is reloaded. This is a rather complicated phenomenon, modeling of which would require the knowledge of a complete load history because the load level at which the structure starts to stiffen is a function of previous load step. The load history, however, is almost never known.

(2) The envelope curve can describe the load-deformation path of the substructure with sufficient accuracy. The envelope curves can be relatively easy to establish experimentally. If the envelope curves for individual nail connections are known the load-deformation characteristics for the diagonal spring of the wall quasi-superelement can be computed from the detailed three-dimensional models loaded by one loading cycle.

(3) The unloading path of the structure is a function of the unloading paths of all nonlinear elements which behave nonconservatively. There has been no experimental results for cycled loading of individual nail connections, as well as metal connectors, used in the structure. However, the unloading path of shear walls was obtained from the experiments which gave results of a limited accuracy. The error in unloading is the result of the unknown unloading path of the connections used in the model, which were modeled by assuming a straight line following the first slope of the nonlinear element.

Comparisons between experiments and the analytical solution is shown in Figure 60 through 63. Deformations are compared for two different meshes shown in Figure 51. Coarse mesh gives a slightly stiffer structure, but the difference is considered to be nonsignificant.

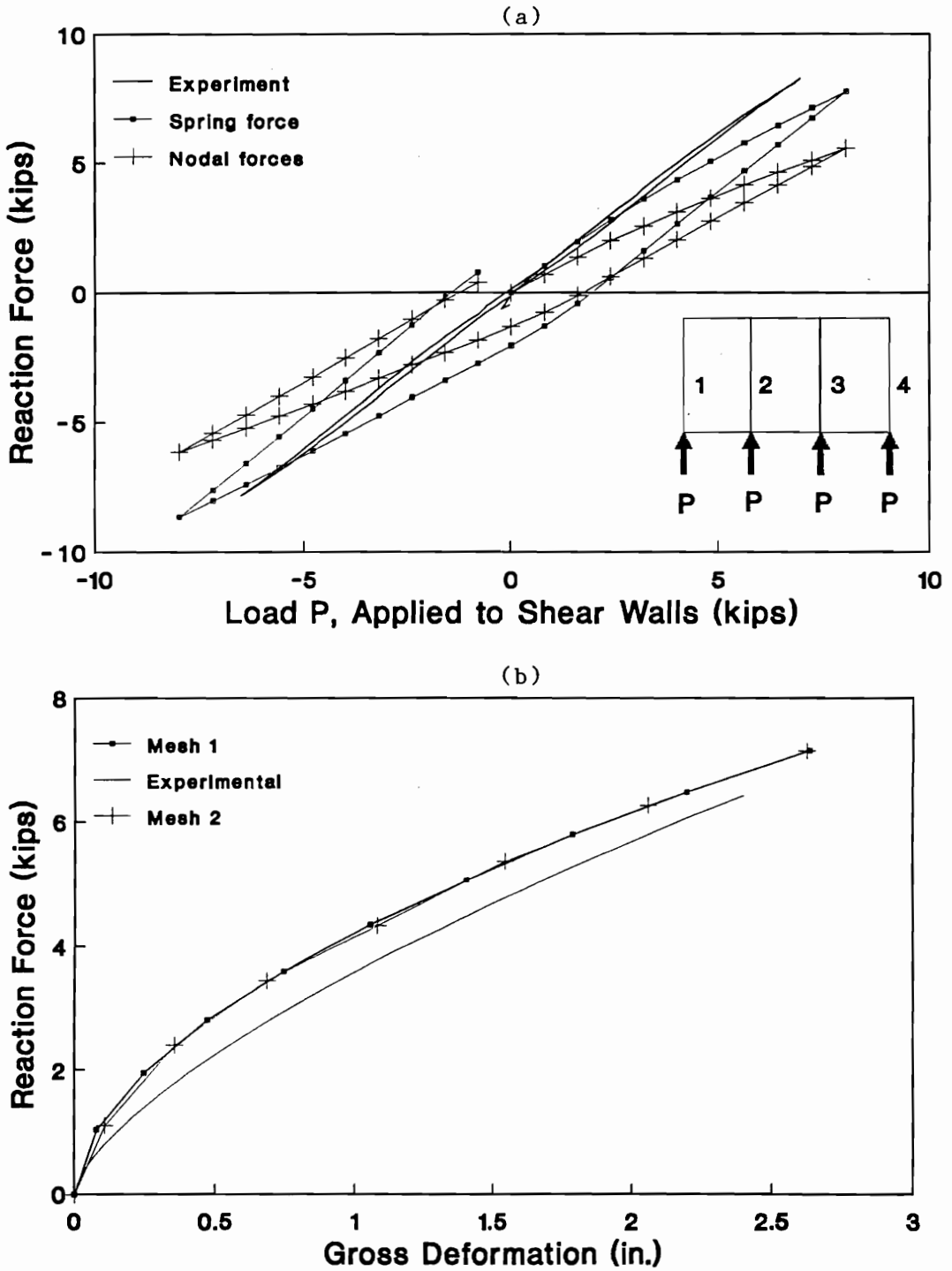

Figure 60. Full Model Verification with the Load Applied to Walls 1 through 4, (a) Reaction Force and (b) Deformation for Wall 1.

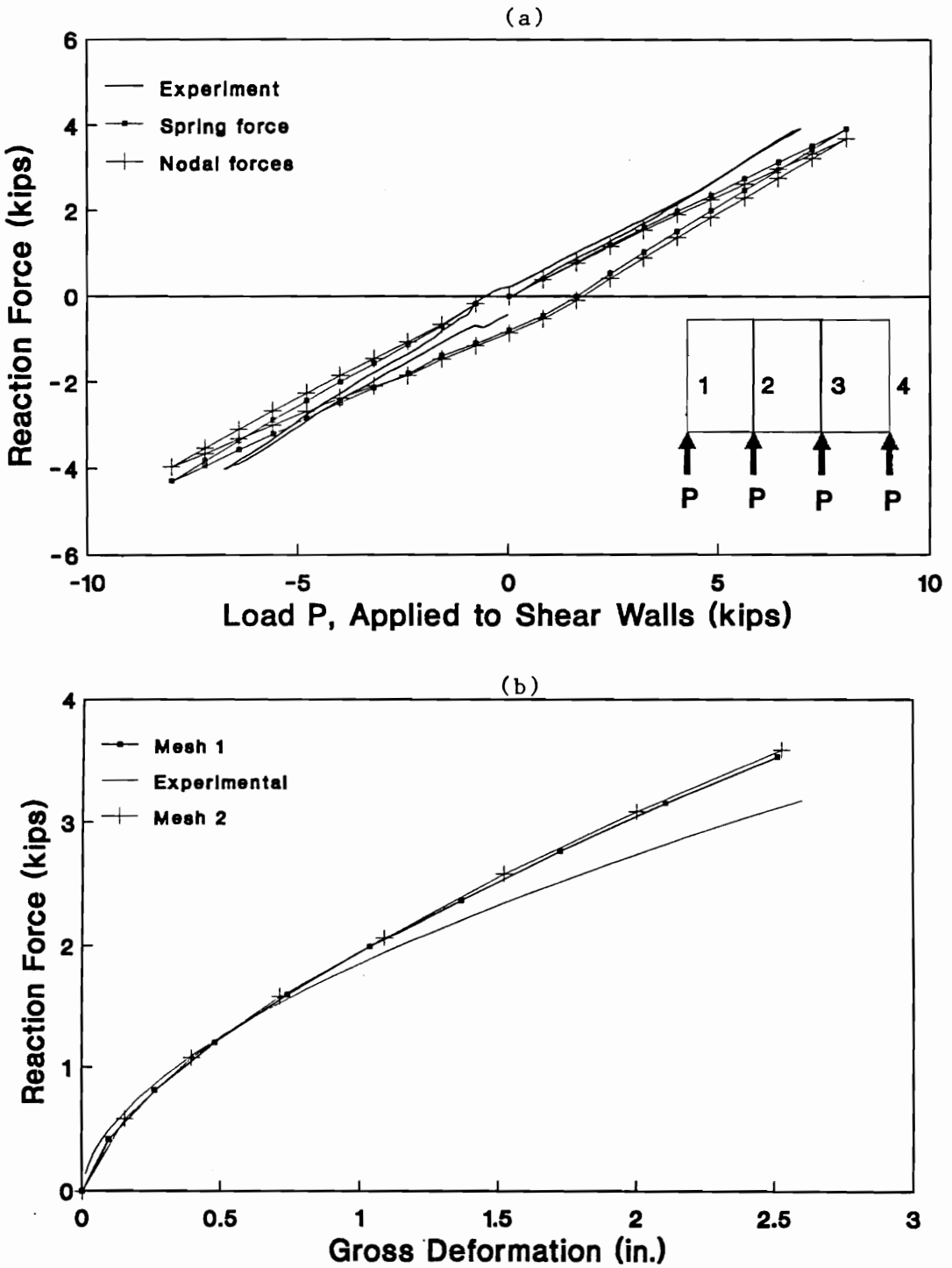

Figure 61. Full Model Verification with the Load Applied to Walls 1 through 4, (a) Reaction Force and (b) Deformation for Wall 2.

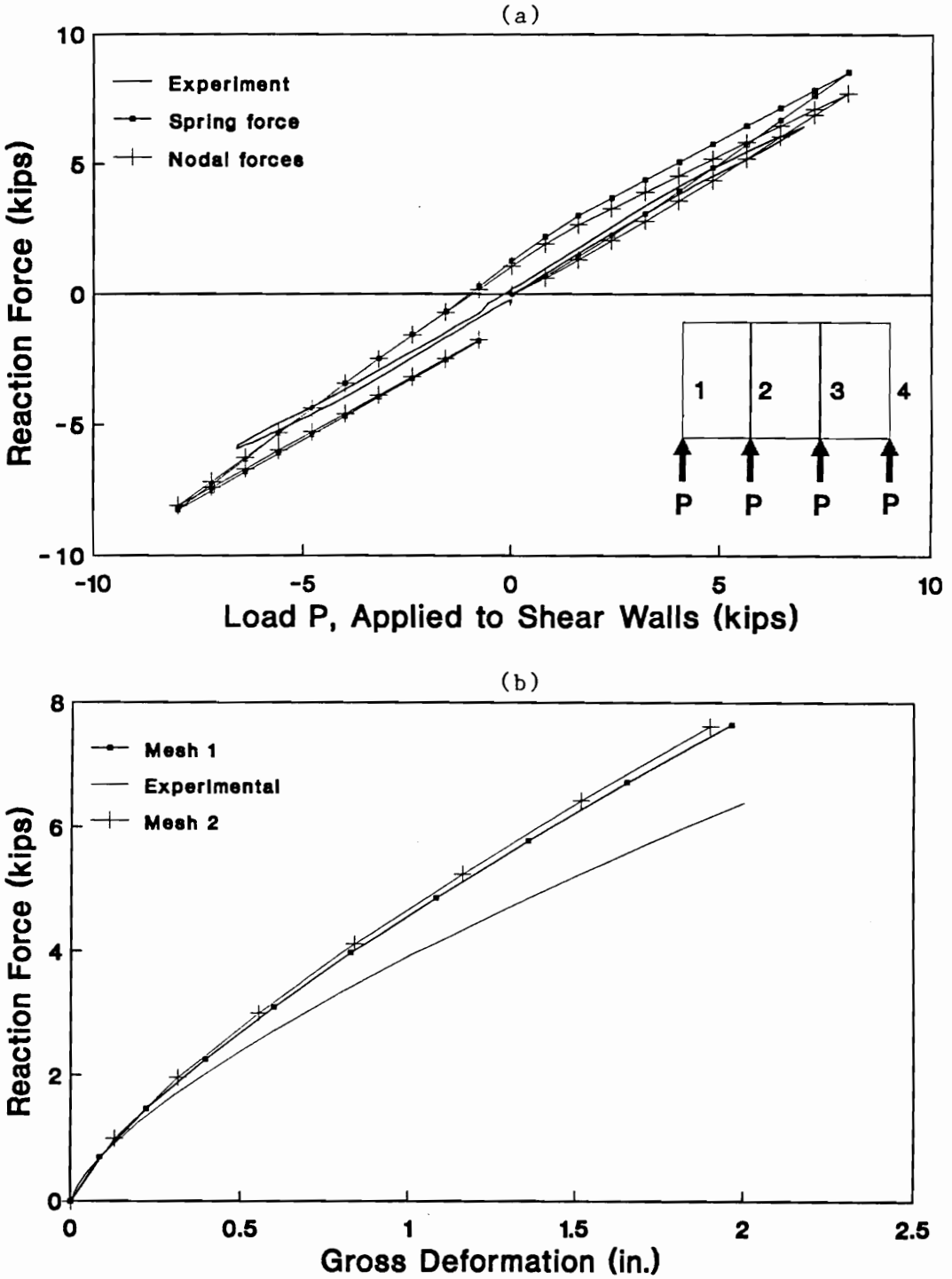

Figure 62. Full Model Verification with the Load Applied to Walls 1 through 4, (a) Reaction Force and (b) Deformation for Wall 3.

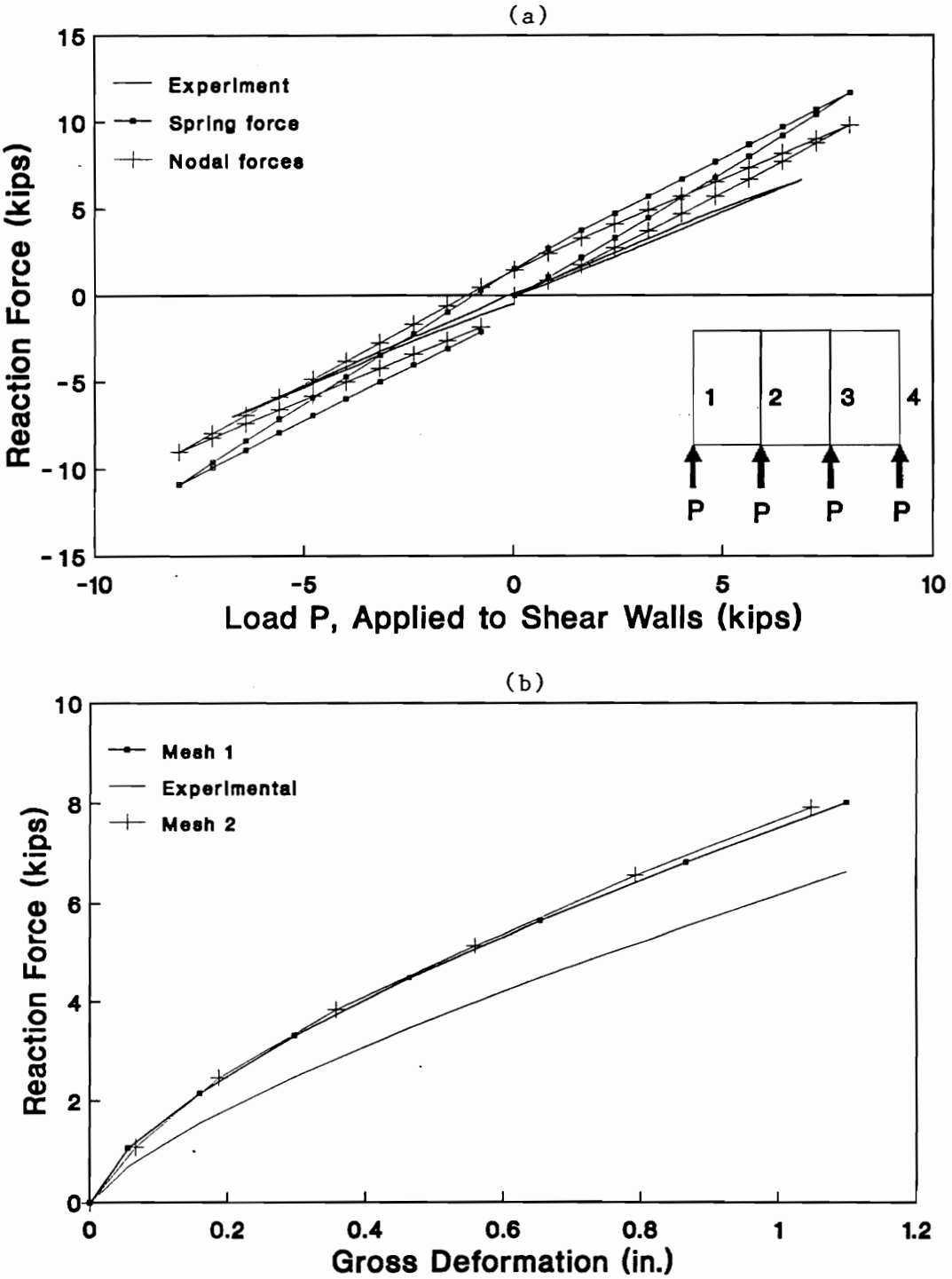

Figure 63. Full Model Verification with the Load Applied to Walls 1 through 4, (a) Reaction Force and (b) Deformation for Wall 4.

The analytical curve relates the reaction force represented by the horizontal component of the axial force in the diagonal spring and the nodal reaction. The nodal force means a sum of the nodal reaction forces beneath each shear wall. For every wall this sum is smaller than the force acting in the diagonal spring. The difference is caused by additional springs connecting the shear walls to walls 5 and 6. These nodal forces were not included into the sum and were attributed to the reaction transferred by walls 5 and 6.

The loading path for the full-structure model loaded stepwise from zero to +7000 lb (32 kN) was compared with the envelope curve obtained from the experiments. Results are in Figure 60b through Figure 63b. Deformations were measured at the top corner of each wall opposite to the acting force as shown in Figure 7. The experimental results are represented by the envelope curves relating gross deformation to the reaction force measured beneath each wall.

The deformations of each wall are not identical, which is caused by the slip deformation between substructures. Deformations of the top corners for the applied load are shown in Figure 64. A certain level of independent horizontal motion of each wall is apparent from the experiment as well as analytical solution.

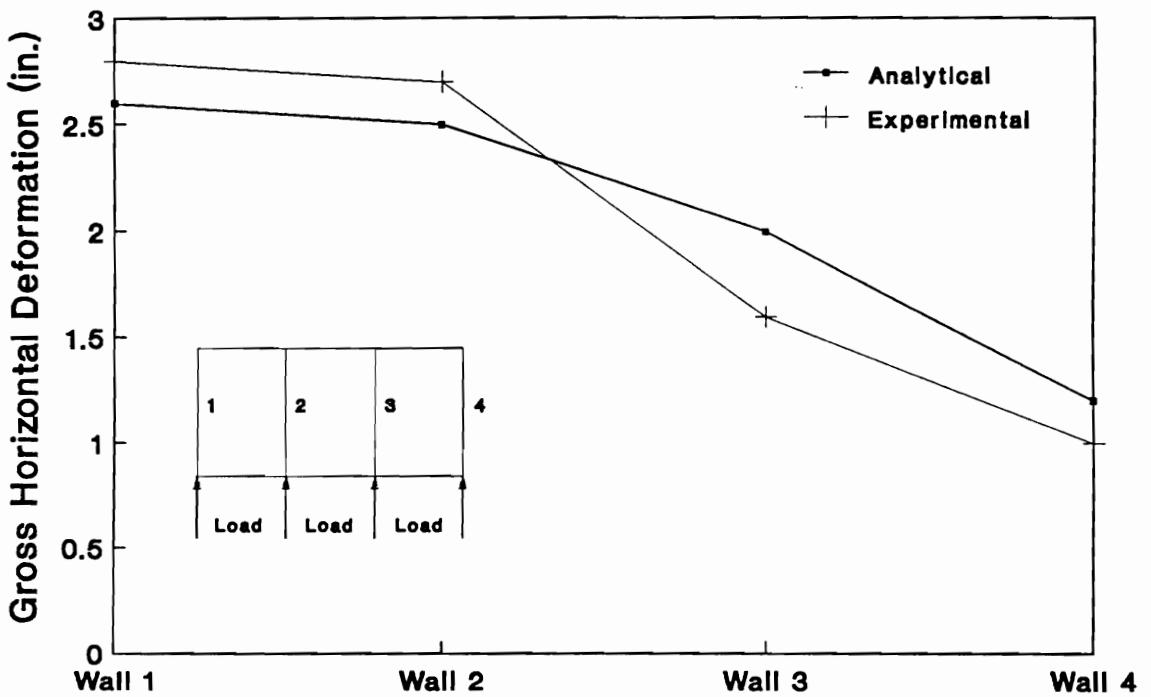

Figure 64. Deformation of the Top Corners of the Shear Walls Loaded by 7000-lb (32-kN) Force at the Top of Each Wall.

Summary

The full-structure finite-element model was created as an assembly of superelements, quasi-superelements and intercomponent connections. Two different mesh sizes were studied and no significant difference between the models was found. This suggests that the coarse mesh designated as (a) in Figure 51 can be applied without a significant error. Since the computation for the coarse mesh was somewhat faster, the coarser mesh is the basis of the subsequent analyses.

The model gives a good prediction of reaction forces and deformations but is less accurate for small loads and walls far away from the acting force.

In spite of the fact that many variables controlling the behavior of the full building were measured, properties for a significant number of substructures were obtained from analytical models. This may be the cause of the departure from the experimental measurements.

7. SENSITIVITY STUDY

To investigate the influence of individual substructures and intercomponent connections on the performance of the full-structure model, a sensitivity study was performed. Since the accuracy of the input, such as intercomponent connection stiffness or bending stiffness of the wall quasi-superelement may be limited, it is important to know what impact the perturbation of the input has on the value on the overall building performance.

The main concern of this research was the shear force within each shear wall, which must be known in order to design the wall. The load sharing among substructures makes it possible to incorporate weak elements such as walls with large openings into the system, without overdesigning others. It is anticipated that load applied to flexible elements is partially transferred into adjacent substructures and this increases the overall loading capacity of the system. Thus, the load sharing capability must be studied. The model allows the simulation of a virtually infinite number of different combinations of component stiffnesses. To narrow the large number of combinations extreme cases were studied first, which lead to the elimination of "mild" differences in stiffness.

Influence of Wall Stiffness on Load-Sharing Capability of the Structure

The stiffness of walls may vary considerably within a given building. Large openings such as doors or windows degrade the wall capability to resist shear loads. Such walls are, in current design practice, ignored or attributed a limited stiffness. Moreover, no load sharing among substructures is considered, which leads to the overdesigned system.

Bending and torsional stiffness of the wall can also be different due to the variety of different materials, stud spacing, nailing schedules and sheathing orientation. Controlling the bending stiffness of the walls may lead to a better load distribution within the building.

Shear Stiffness

To investigate the influence of wall stiffness on load-sharing capability of the structure several ratios of wall stiffness were studied. A wall stiffness of 10000 lb/in. (1.851 MN/m) was chosen as a basis for comparison because this value represents an intermediate magnitude of wall stiffness. The stiffness of walls was linear to keep the ratio of wall stiffnesses independent of load (constant). Thus, if a stiffness ratio was 1:1:1:10 (stiffness ratio of wall 1:wall 2:wall 3:wall 4), wall 4 had stiffness 10×1E4 lb/in. (18.51 MN/m) whereas walls 1 through 3 had stiffness 1E4 lb/in. (1.851 MN/m), and this did not change during the course of loading. The finite-element model of the structure was loaded by 10000 lb (44.48 kN) at the top corner of wall 1.

Reaction forces for each transverse wall were recorded and normalized. The comparison of the reaction forces for different wall stiffness ratios is in Figure 65. It can be

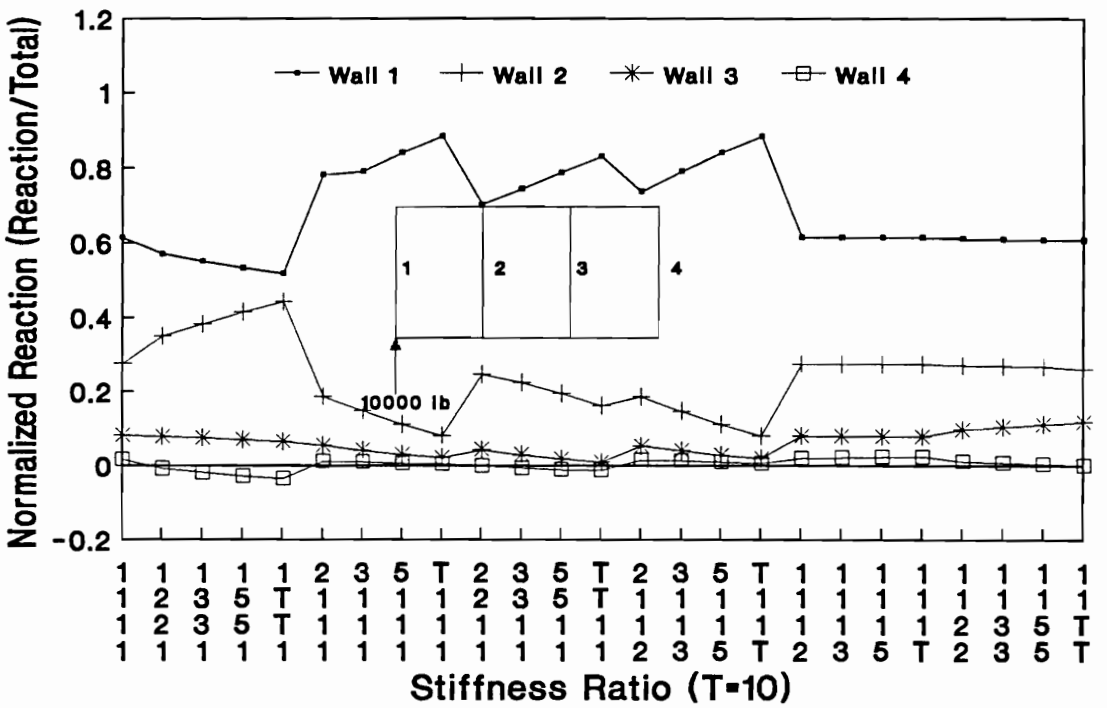

Figure 65. Reaction Forces for Different Wall Shear Stiffness Ratios where a 10000-lb Load is Applied at the Top Corner of Wall 1.

observed that only the adjacent wall is significantly affected by the stiffness ratio change. Reactions in walls 3 and 4 do not change significantly with the stiffness ratio change. Also, the increase of the stiffness of walls far from the point load (wall 3 and 4) does not affect the reaction in the wall at the load point.

The connection between the walls and roof diaphragm and diaphragm flexibility permits the walls to deform independently to certain extent. Therefore, the edges of the deformed walls are not located on the straight line.

The wind effect is usually represented by a uniformly distributed pressure over the wall face. This effect is shown in Figure 66. A rigid beam model, described in Chapter 8, is also shown in the figure. For stiffness ratio 1:1:1:1, the load is distributed almost evenly among the shear walls, which contradicts the tributary area concept; the tributary area concept distributes the load such that internal shear walls will carry twice as much load as external walls. In general, the redistribution of load is more effective for the uniform pressure than for the concentrated force. This will have an effect on the earthquake design if an equivalent shear force concept is applied.

Although the load sharing for point load is smaller then for uniformly distributed load, the error resulting from considering shear walls as independent entities may be large as shown in Figure 65.

Bending Stiffness

The bending and torsional stiffness of the long walls (walls 5 and 6) were multiplied simultaneously by the factors given in Figures 67 and 68. There was no significant change in load distribution for small values of

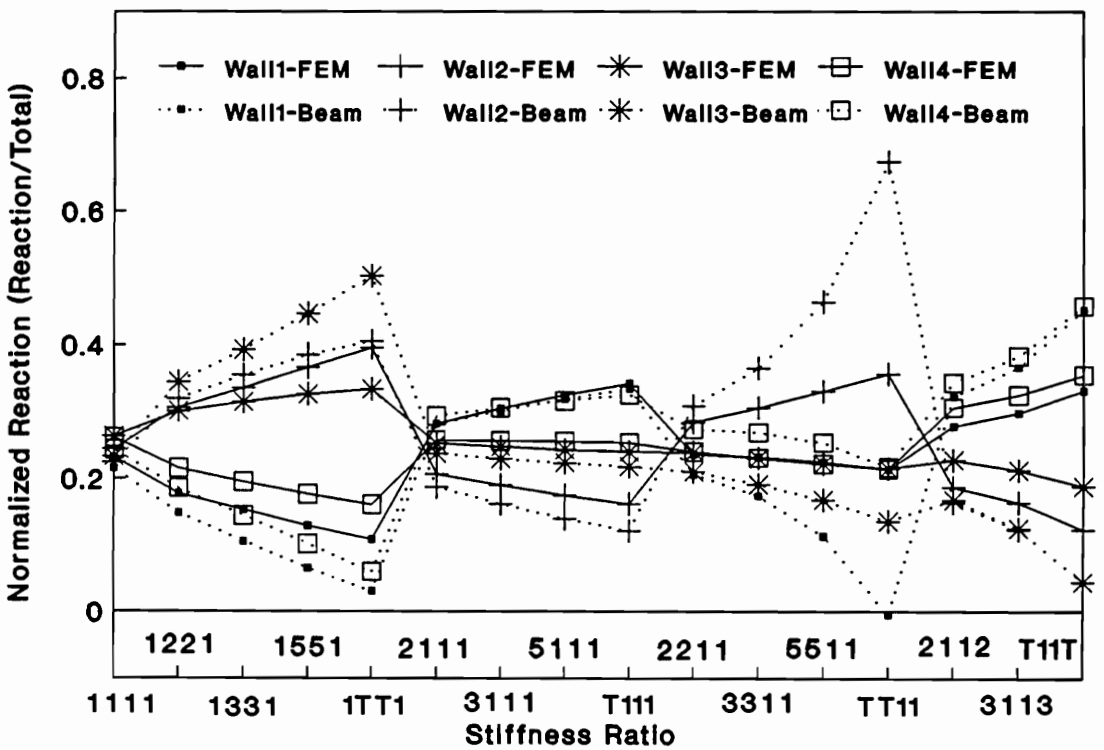

Figure 66. Effect of the Wall Shear Stiffness on Load-Sharing among Shear Walls for the Structure under Wind Load.

the multiplying factor. On the abscissa of Figures 67 and 68 coefficient of 0.001 means no transverse wall is present and shear walls (wall 1 through 4) act as individual substructures connected only via the roof diaphragm. However, very large factors cause a significant shift in the distribution of reaction forces. This can be expected because stiff transverse walls are capable of load redistribution. This is a desirable property of the system because it prevents the overload the weaker shear walls. However, stiffness coefficients in Figures 67 and 68, leading to significant influence of the transverse wall stiffness on load distribution, are too large to be achieved. For the sheathing rigidly connected to studs (labeled "glue" in Figure 67 and Figure 68), the stiffness factor is about 7, as compared to the nailed connection. Thus, higher factors will have to be achieved by increasing the thickness of the wall. This is practically not possible because of the requirements on wall thickness. For example, 2×10-in. (38×241-mm) studs would increase the bending stiffness by a factor of 50 as compared to 2×4-in. (38×89-mm) studs.

Connection between Roof Diaphragm and Walls

The roof diaphragm is very rigid in its own plane (Breyer, 1988) and can transfer the load between shear walls very effectively. To utilize the diaphragm, connections between walls and roof trusses must be sufficiently rigid.

To study the influence of different connection stiffnesses on the load sharing, a stiffness ratio 1:1:1:10 and a load of 10000 lb on wall one were used as a basis. This represents the least sensitive case according to Figure 65. For the given roof connection stiffness, the load 10000 lb (44.48 kN) applied to wall 1 is not

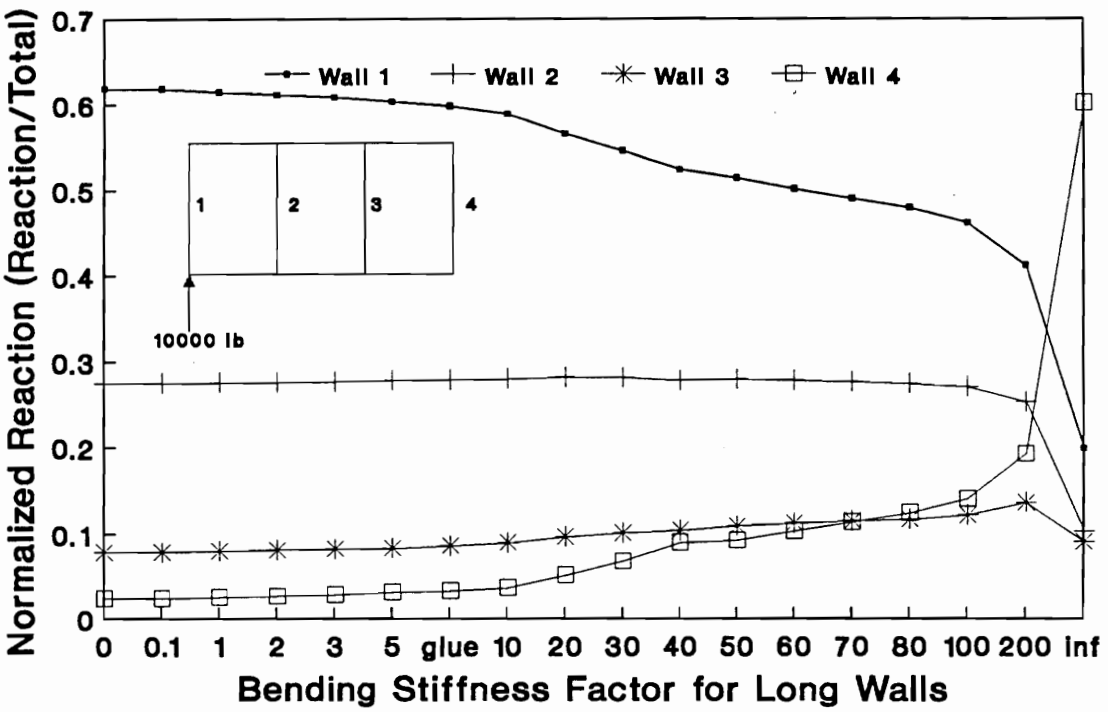

Figure 67. Influence of Bending Stiffness of Long Walls on Load-Sharing Capability of the Structure When a 10000-lb Load is Applied at the Top Corner of Wall 1 in the Finite-Element Model.

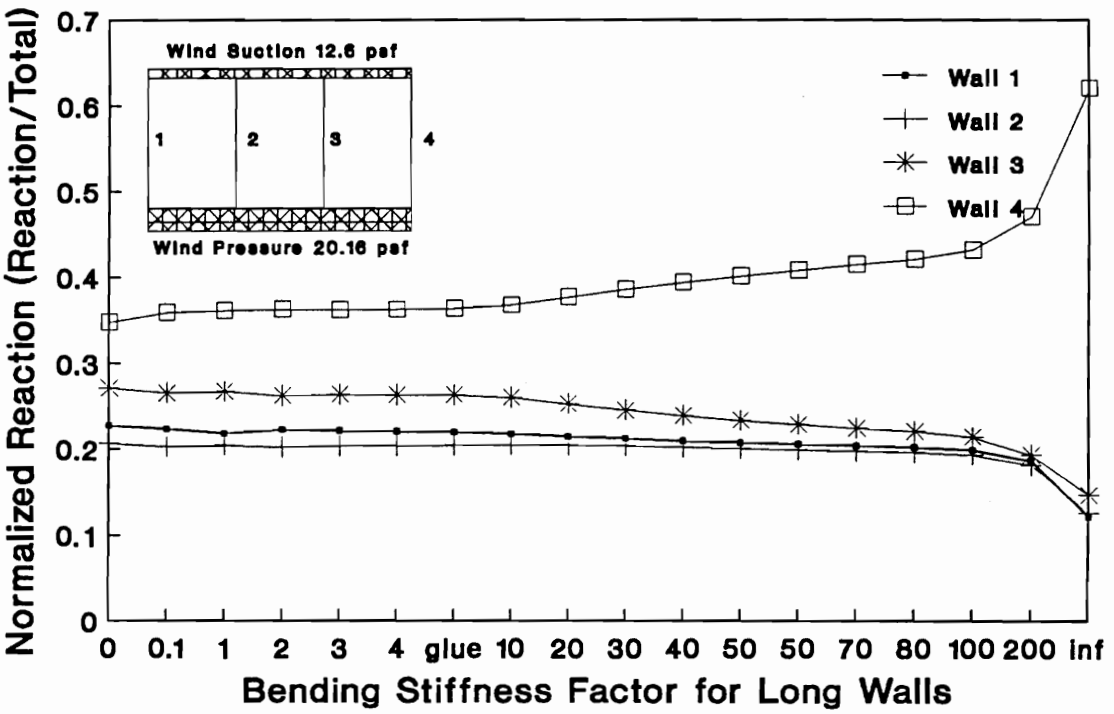

Figure 68. Influence of Bending Stiffness of Long Walls (Walls 5 and 6) on Load-Sharing among Shear Walls when the Model was Loaded by Wind Load (Pressure on Wall 5, Suction on Wall 6).

transferred by wall 4 regardless of its significantly higher stiffness. Both the point load and wind load were applied to the structure. No roof means that almost 100% load is transferred by wall 1 as shown in Figure 69. This indicates that the long walls do not play a significant role in load transferring from wall to wall. Only wall 2, which was adjacent to the applied force received less than 5% load when roof was absent. Very slight change in the deformation of walls can be seen in Figure 70 for the increased wall-to-roof connection stiffness.

Without a roof, shear walls can deform almost independently from each other which results in low sharing. Figure 70 shows the normalized deformation at the top of each shear wall as a function of the roof connection stiffness factor. After the roof connection stiffness factor reached unity, no significant change in reaction redistribution took place. This means that the currently used connectors between walls and roof diaphragm have optimal stiffness.

Similarly, when wind pressure is applied, the stiffening of the wall-to-roof connection does not yield significant improvement in load sharing once the factor 1 is achieved- Figure 71. Here, however, wall 4 took 40% of the total reaction, whereas the remaining walls were almost evenly loaded which is a consequence of their identical shear stiffness. Slightly higher load in wall 1 may be due to the distance from wall 4, (which was 10 times stiffer) resulting in a negligible load transfer.

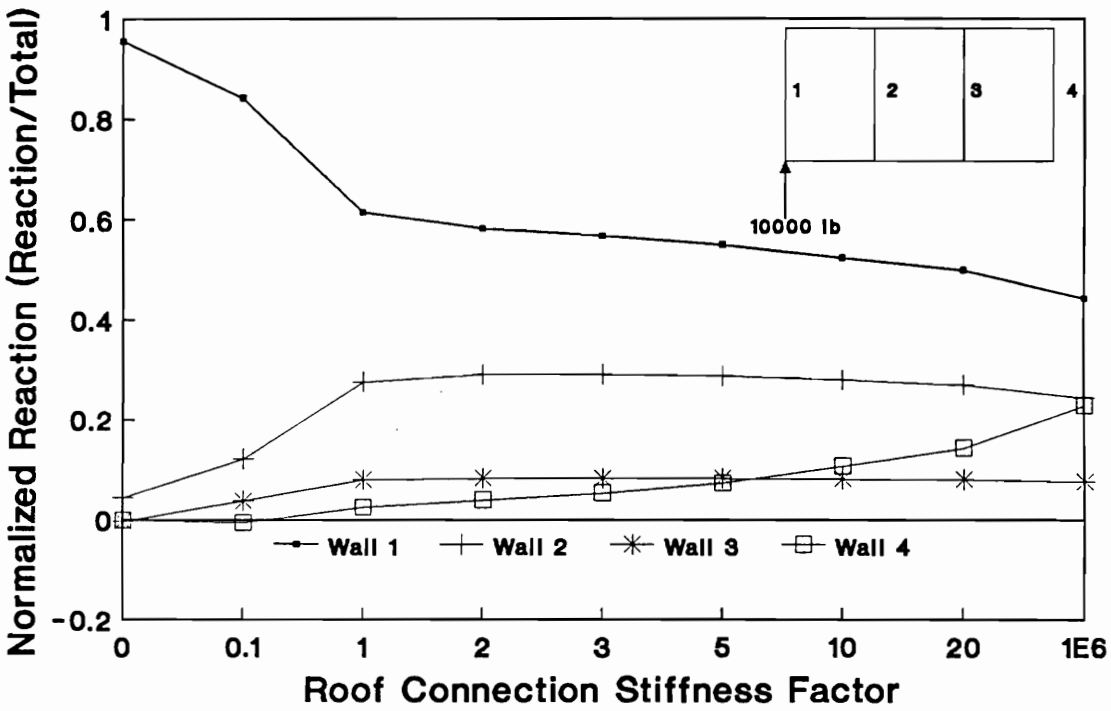

Figure 69. Influence of the Roof Connection Stiffness on Load-Sharing among Shear Walls when 10000-lb Load Was Applied to the Top Corner of the Wall 1.

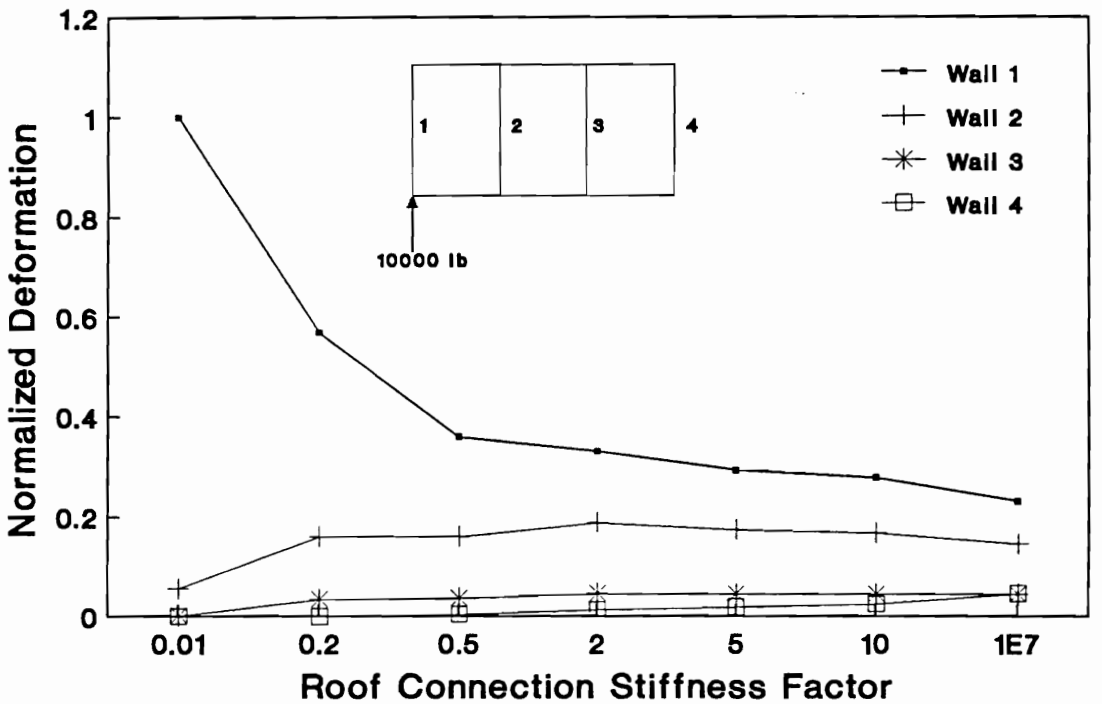

Figure 70. Influence of the Roof Connection Stiffness on Deformation at the Top Corner when 10000-lb Load Was Applied to the Top Corner of the Wall 1 in the Finite-Element Model.

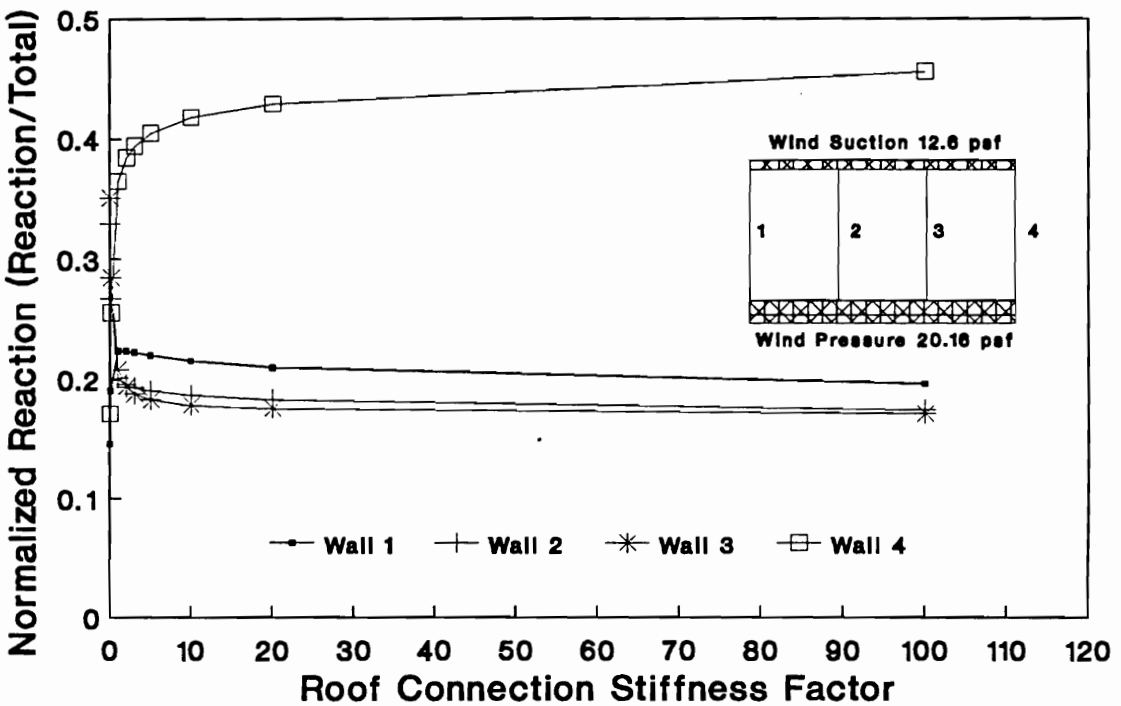

Figure 71. Influence of the Roof Connection Stiffness on Load-Sharing among Shear Walls for Wind Load.

Intercomponent Connection between Walls

The stiffness of the intercomponent connections between all walls (partition and exterior and exterior-to-exterior) was varied by multiplying the original stiffness by the factor shown in Figure 72.

The connection between walls has negligible influence on load redistribution as documented in Figure 72. This indicates that, given the intercomponent properties as defined earlier, connections along the wall edges (excluding corners, where walls are connected to floor and roof) do not influence the load sharing capability of the structure.

The stiffness of intercomponent connections was varied for all connections simultaneously. This kept the stiffness ratio for different locations constant. It is anticipated, that the ratio change will not result in substantially different results.

Walls-To-Floor Connection

The connection between the walls and floor, as represented by stiffness of the nail connection between the wall sole plate and floor joists, has very little effect on reaction force redistribution as shown in Figure 73. Although stiffer connection reduces the slip between the floor and shear wall, no improvement in load sharing is achieved by increasing the connection stiffness.

Results for point load are only shown; two extreme cases (factors 0.01 and 1E6) studied for wind load did not reveale any difference in load sharing among the walls.

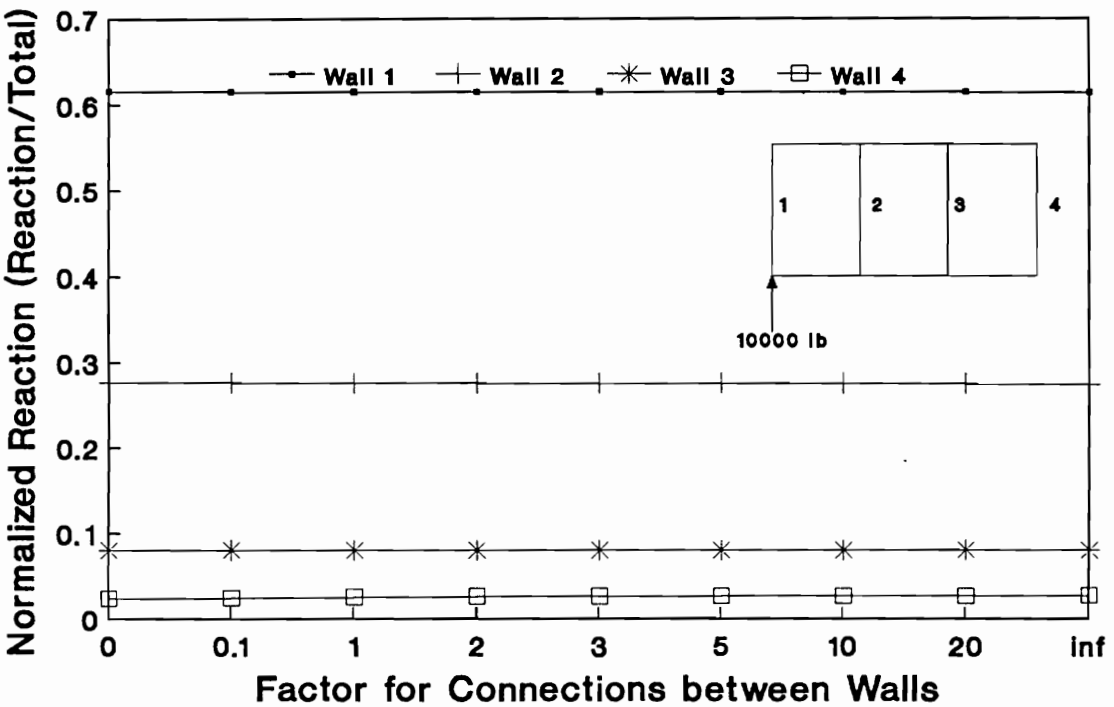

Figure 72. Influence of the Different Stiffness of Connections between Walls on Load Sharing for Model Loaded by 10000 lb Applied at the Top Corner of Wall 1.

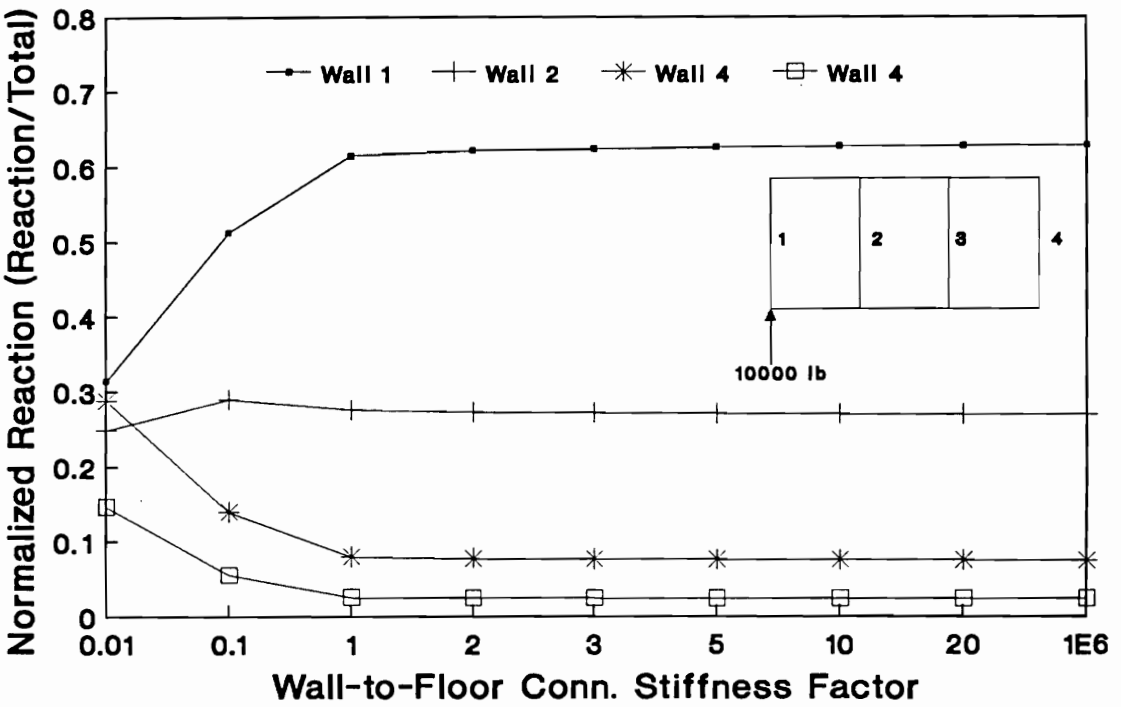

Figure 73. Influence of the Connection between Walls and Floor on Load-Sharing Capability of the Model when 10000-lb Load Was Applied at the Top Corner of Wall 1.

Summary

The sensitivity study was limited to cases where the most significant influence of the property change could be expected. There is an infinite number of possible combinations of different stiffness ratios, and such selection is necessary to make the study feasible. Also, some combinations are beyond the practical range (such as infinite or zero stiffness of the connection) and serve solely as an upper or lower bound.

The "infinite" as used here means a very large stiffness factor, such as 1E6, which makes the connection or component relatively stiff as compared to the rest of the model. "Zero" means element removed from the system. In some cases no zero stiffness is possible without encountering a rigid body motion. In such instance, a low coefficient, such as 0.001, was chosen.

The wall stiffness has a decisive influence on the load sharing capability of the building. Better sharing is achieved for applied pressure than point load. This suggests that neglecting the sharing phenomenon and shear wall stiffness effect may lead to significant error in predicting the shear force in the wall (such as using a beam analogy where support reactions are then applied as wall shear forces).

Generally, it can be stated that the intercomponent connections commonly used in wood-framed structures serve well, and that no significant improvement in load sharing among the shear walls can be expected by increasing the stiffness of any of these components. Increased stiffness of wall-to-roof connection leads to slightly improved load distribution among the walls.

8. SIMPLIFIED ANALYTICAL MODELS FOR COMPUTATION OF SHEAR REACTION FORCES

The three-dimensional finite-element model of the full structure can be used for analysis of the building subjected to static loads. This allows the computation of the reaction forces in the shear walls with regard to the overall performance of the system. The nonlinear character of the structure does not allow the use of a principle of superposition and all loads must be applied simultaneously. This is often violated in the design practice where linear models are used. In the following paragraphs the current design procedure is compared with the finite-element solution and simplified analytical procedure is developed to estimate the shear forces in the light-frame wood structure subjected to wind pressure.

The capacity of a light-frame building with respect to wind loads is entirely dependent on the shear strength of the diaphragms. According to the current design practice, each loaded wall is considered as a separate element (Breyer, 1988). The shear force transferred by each wall is calculated from a series of simple beam solutions in which the beam span equals the distance between the walls. This approach disregards the load sharing and redistribution resulting from the different stiffness of the walls. In the case of a rigid diaphragm, a continuous-beam analogy is used to solve for the unknown reaction forces. The active length engaged in the shear transfer is the total length of the wall less the width of the openings. The proportion of the load transferred is a function of the building geometry, wall stiffness, and other construction details, such as

intercomponent connections. Breyer (1988) suggests neglecting the contribution of gypsum sheathing to shear wall strength making the design more conservative.

The American Plywood Association (APA, 1989a,b) has published the value of wall shear capacity in force per unit wall length for each combination of stud spacing, nail type and spacing, sheathing thickness, and orientation. Similar tables have been published in the Uniform Building Code (International Council of Building Officials (ICBO), 1988) for gypsum wallboard sheathing.

When a building is loaded by a horizontal force, such as wind pressure, the load is carried by each wall to the shear walls and through them to the foundation. Reaction forces in the shear walls can be obtained by analysis of a full structure, which is analytically difficult and requires a verified model.

Shear Forces Induced by Wind

The shear capacity of the walls based on the current design procedure is shown in column 9 of Table 11. The allowable force represents the maximum load allowed per wall as computed from the tables given in the Uniform Building Code (ICBO, 1988) and American Plywood Association design procedures (APA, 1989a,b).

For certain wind loads exerted on the building subjected to the conditions given in Table 12, the pressure p on each surface is (ICBO, 1988):

$$p=q_s C_e C_q \tag{33}$$

where q_s=wind stagnation pressure
C_e=combined height, exposure and gust factor coefficient, and C_q=pressure coefficient

Table 11. Shear Capacity for Walls Based on Uniform Building Code (ICBO, 1988).

Wall	Sheathing		Nails and spacing on perimeter-all unblocked		Length	Shear capacity lb/ft (kN/m)		Allowable force
(1)	interior layer (2)	exterior layer (3)	interior layer (4)	exterior layer (4)	ft (m) (6)	interior layer (7)	exterior layer (8)	lb (kN) (9)
1	gypsum 1/2 in	plywood 1/2 in	No.11 7 in	6d 6 in	12 (3.66)	100 (1.46)	140 (2.04)	2880 (12.81)
2	gypsum 1/2 in	gypsum 1/2 in	No.11 7 in	No.11 7 in	13 (3.96)	100 (1.46)	100 (1.46)	2600 (11.56)
3	plywood 1/2 in	plywood 1/2 in	8d 6 in	8d 6 in	13 (3.96)	280 (4.08)	280 (4.08)	7820 (34.78)
4	gypsum 1/2 in	plywood 1/2 in	No.11 7 in	6 d 6 in	16 (4.88)	100 (1.46)	140 (2.04)	3840 (17.08)
5	gypsum 1/2 in	plywood 1/2 in	No.11 7 in	6 d 6 in	23.8 (725)	100 (1.46)	140 (2.04)	5712 (25.41)
6	gypsum 1/2 in	plywood 1/2 in	No.11 7 in	6 d 6 in	30.8 (939)	100 (1.46)	140 (2.04)	7392 (32.88)

Note: Exterior plywood: APA Exterior siding. For interior walls "interior layer" is defined as a layer facing wall 1.

Table 12. Wind Load on the Complete Structure according to the Uniform Building Code (ICBO, 1988).

Factor (1)		Factor value (2)	Exposure (3)
Wind speed Wind pressure	q_s	90 mph (144 km/h) 21 psf (1 kPa)	Exposure C Open, flat terrain
Gust factor	C_e	1.2	
Pressure coefficients for entire building	C_q	0.8 inward	windward wall
	C_q	0.5 outward	leeward wall
	C_q	0.9 outward	windward roof
	C_q	0.3 inward	leeward roof

The pressures in Table 13 were applied to the finite-element model of the full building and reaction forces for each shear wall were computed. Pressures were applied only to walls 5 and 6 because the current design practice assumes these are the only surfaces distributing the loads to the shear walls 1 through 4. Current design procedure also assumes a series of simple beams between the shear walls or a continuous beam across them; the reaction forces are the loads applied to the shear walls.

The shear forces obtained from the finite-element analysis and analysis based on simple beam approach are compared in Table 14. The sum of the reaction forces is relatively close for the three approaches, and the assumption that one-half of the wind pressure is transferred directly to the foundation is verified. However, while the total reaction forces for the three methods are essentially

the same, a substantial difference in load distribution is evident. The simple beam approach gives unrealistic forces in walls, and the continuous-beam approach yields no improvement. Difference between the simple or continuous beam approach and the finite-element solution can be expected due to the different stiffness of the walls, which is neglected by the former. Furthermore, although the roof diaphragm can be considered as a beam of infinite stiffness, deflections between the walls demonstrated the influence of a non-rigid wall-to-diaphragm connection, which allows some localized deformations.

Analytical Solutions Incorporating Wall Stiffness

The current design procedure (ICBO, 1988) for computation of shear forces in the transverse walls due to wind pressure overestimated reaction forces for internal walls and underestimated forces acting on external shear walls. Moreover, the reaction forces will change as a function of the shear wall stiffness. A method of distributing the reaction forces that incorporates wall stiffness is needed.

APA Estimate of Wall Stiffness

The following procedure for calculating shear wall deflection can be used to estimate the wall stiffness (APA, 1989a; APA, 1989b):

$$\Delta = \frac{8vh^3}{EAb} + \frac{vh}{Gt} + 0.75\delta_n + d_a \qquad (34)$$

Where Δ = deformation of the wall (length)

v = shear load (force/length)

Table 13. Wind Pressures on the Building Used for the Design Example.

surface (1)	pressure, psf (kPa) (2)	direction (3)
wall 1	12.6 (0.6)	outward
wall 4	12.6 (0.6)	outward
wall 5	20.16 (0.97)	inward
wall 6	12.6 (0.6)	outward
roof leeward	17.64 (0.84)	outward
roof windward	22.68 (1.1)	outward
or	7.56 (0.36)	inward

A = area of boundary-element cross section (length^2)

h = wall height (length)

b = wall width (length)

d_a = deflection due to the anchorage detail (length)

E = elasticity modulus of boundary element (vertical member at shear wall boundary) (force/length^2)

G = shear modulus of sheathing (force/length^2)

t = thickness of sheathing (length)

$$\delta_n = \left(\frac{Load}{a}\right)^b \qquad (35)$$

δ_n = nail deformation (length)

Tissel and Elliott (1990) have determined coefficients a and b for plywood nailed to Douglas-fir studs. Values for gypsum board, however, must be obtained from experiments. Deflection resulting from the anchorage detail d_a was not included in the values shown in the column 4 of Table 14 because it is determined by the construction detail, rather than by the property of the wall. Shear wall stiffness based on APA procedure is compared with the test results (Phillips, 1990) in Figure 74. Nail slip was computed from experimental results obtained by Phillips (1990). In the APA formula, only the perimeter nails on the sheathing are considered, which makes the result conservative; each nail is assumed to carry the same load; and openings and gaps in the sheathing make the application of the formulas questionable. Therefore, the results obtained with the formula differ from those obtained experimentally. Furthermore, it follows from equation (34) that equation (35), which determines the magnitude of nail slip, is critical in estimating wall stiffness.

Development of the Rigid-Beam Model

The wind load can be distributed by using one of several different analogies in either a nonlinear or linear form. The rigid-beam analogies account for stiffness of the walls by assuming the roof diaphragm is a rigid continuous beam on elastic supports, or springs. The stiffness of each wall

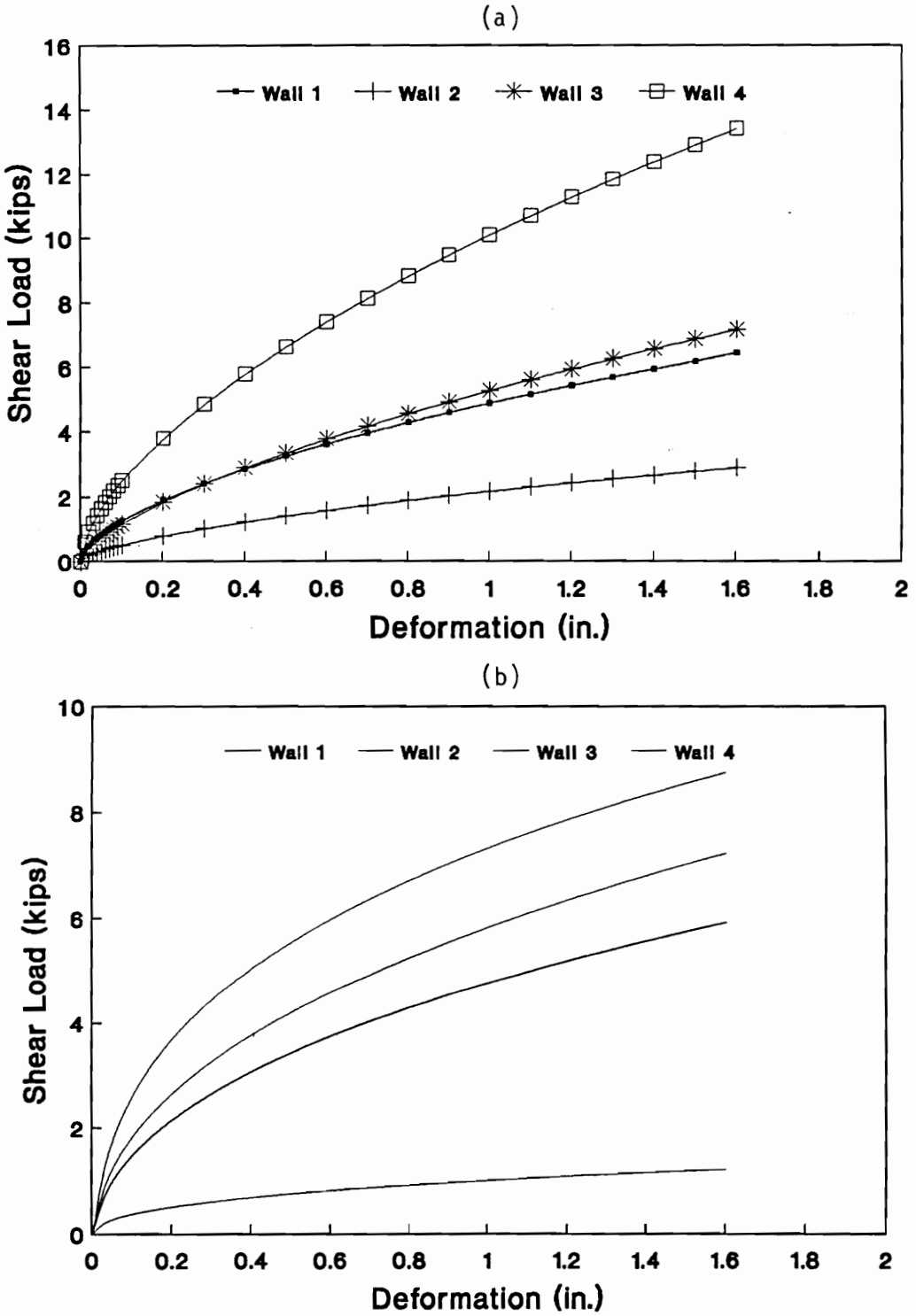

Figure 74. Input Shear Wall Stiffness used for the Analytical Model, (a) Experiment and (b) APA Formula.

Table 14. Comparison between Shear Reaction Forces in Walls Obtained from Proposed Models and Current Design Procedure.

Shear Wall	Shear Force, lb (kN)					
	Current Design Procedure (1)	Continuous Beam Model (2)	Finite-Element Model (3)	APA Shear Wall Formula (4)	Nonlinear Spring Model (5)	Linear Spring Model (6)
1	614 (2.73)	493 (2.19)	1242 (5.52)	1208 (5.37)	1361 (6.05)	1373 (6.11)
2	1280 (5.69)	1351 (6.00)	570 (2.54)	303 (1.35)	498 (2.22)	487 (2.17)
3	1423 (6.33)	1618 (7.20)	1095 (4.87)	1662 (7.39)	879 (3.91)	868 (3.86)
4	751 (3.34)	606 (2.70)	1540 (6.35)	895 (3.93)	1330 (5.92)	1340 (5.96)
Total	4068 (18.09)	4068 (18.09)	4447 (19.78)	4068 (18.09)	4068 (18.09)	4068 (18.09)

can be estimated analytically using a procedure outlined by Easley et al (1982), Tissel and Elliott (1990), or Hayashi (1989), wherein shear deformation is attributed to some shear force and stiffness is estimated as a ratio of the force and deformation. Herein, the analyses assume the roof diaphragm acts as a rigid beam, no slip occurs between the walls and roof diaphragm, and the roof diaphragm can rotate.

Nonlinear Spring Model

The nonlinear spring model is based on a rigid-beam analogy with the center of rotation at some distance x from the member: a beam of length L supported by elastic springs at points a_1, a_2,..,a_n such that a_1=0 and a_n=L such as in Figure 75. The spring deformation and stiffness are designated Δ_i and k_i respectively, and the beam is loaded by a uniformly distributed load of an intensity w (e.g. lb/in.). Then referring to the Figure 75,
(1) the forces in the y-direction are summed:

$$\sum F_y=0$$
$$R_1+R_2+\ldots+R_n-wL=0 \qquad (36)$$
$$\sum_{i=1}^{n} R_i-wL=0$$

where $R_i=R_i(\Delta_i)$ represents reaction or spring force which is a function of the spring deformation Δ_i.
(2) Then, by eq. (37) the moments about the pivot, 0, are summed:

$$\sum M_0 = 0$$

$$R_1(a_1 - x) + R_2(a_2 - x) + \ldots + R_n(a_n - x) - wL\left(\frac{L}{2} - x\right) = 0 \qquad (37)$$

$$\sum_{i=1}^{n} R_i(a_i - x) - wL\left(\frac{L}{2} - x\right) = 0$$

in which $R_i = R(\Delta_i)$.

(3) By geometry:

$$\frac{\Delta_1}{a_1 - x} = \frac{\Delta_2}{a_2 - x} = \ldots = \frac{\Delta_n}{a_n - x} \qquad (38)$$

or

$$\Delta_1(a_i - x) + \Delta_i x = 0 \qquad i = 2, 3, 4, \ldots, n$$

Thus, N=n+1 nonlinear equations of N unknowns (Δ_i, i=1,2,3,..,n and x) are obtained with unknowns Δ_i and x:

$$F(1) = \sum_{i=1}^{n} R_i(\Delta_i) - wL = 0$$

$$F(N) = \sum_{i=1}^{n} R_i(\Delta_i)\,(a_i - x) - wL\left(\frac{L}{2} - x\right) = 0 \qquad (39)$$

$$F(j) = \Delta_1(a_j - x) + \Delta_j x = 0 \qquad j = 2, 3, \ldots, n$$

The system of nonlinear equations can be solved by Newton's method (e.g. Gerald and Wheatley, 1984), in which a set of linear equations is solved repeatedly to obtain a new guess vector for unknown displacements $\Delta_i = x_i$ (i=1,2,..N-1) and pivot location x_N:

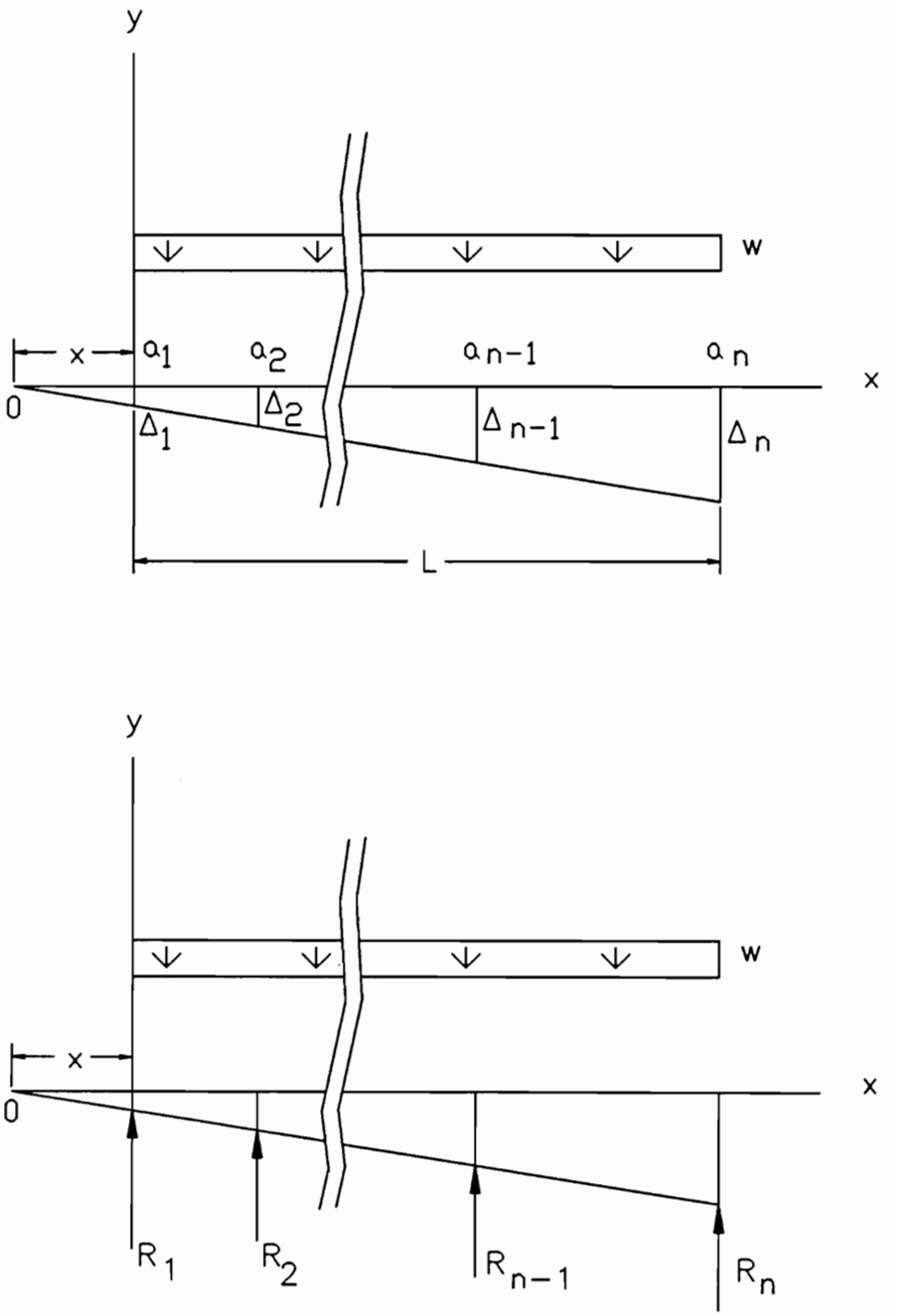

Figure 75. Model of the Rigid Beam on Elastic Supports.

$$[J]\,|_{x=x^{(k)}}\{g\} = -\{F(x^k)\} \qquad (40)$$

Where [J] = Jacobian matrix

{g} = corrector

(x^k) = initial guess of the displacements and pivot which is obtained from a linear model discussed later

superscript ^{k} = k-th guess of the unknown variables

A new guess vector ((k+1-th) guess) of unknown variables ($x^{(k+1)}$) is obtained as the sum of the old guess ($x^{(k)}$) and corrector ($g^{(k)}$).

$$x_i^{(k+1)} = x_i^{(k)} + g_i^{(k)} \qquad i=1,2,3,..,N \qquad (41)$$

The Jacobian matrix of a size NxN has the following form:

$$J_{ij} = \frac{\partial F_i}{\partial x_j} \qquad (42)$$

$$J_{ij} = \begin{bmatrix} -\frac{\partial R_1}{\partial x_1} & -\frac{\partial R_2}{\partial x_2} & -\frac{\partial R_3}{\partial x_3} & \cdots -\frac{\partial R_n}{\partial x_n} & 0 \\ a_2 - x_N & x_N & 0 & \cdots 0 & x_2 - x_1 \\ a_3 - x_N & 0 & x_N & \cdots 0 & x_3 - x_1 \\ \cdot & \cdot & \cdot & \cdots & \cdot \\ -\frac{\partial R_1}{\partial x_1}(a_1 - x_N) & -\frac{\partial R_2}{\partial x_2}(a_2 - x_N) & -\frac{\partial R_3}{\partial x_3}(a_3 - x_N) & \cdots -\frac{\partial R_n}{\partial x_n}(a_n - x_N) & \sum_{i=1}^{n} R_i - wL \end{bmatrix} \qquad (43)$$

where R_i = spring (reaction) force in the form $R_i = ax_i^b$

a,b = constants

x_i = deformation of spring i due to the reaction R_i

N = n+1

$i,j=1,2,3,\ldots,N$

A computer program using the IMSL (IMSL, 1989) procedure for a nonlinear equation solution was developed to compute unknown displacements, pivot location and reaction forces for the beam on elastic supports assuming no rigid-body motion. Experimental load-deformation characteristics obtained by Phillips (1990) for walls loaded in shear were used for the analysis.

Results are given in Table 14. The estimate of the reaction forces is much closer to the "real situation" represented by the finite-element model. The difference between the finite-element solution and the nonlinear spring model is caused by the model simplifications. Although it is quite realistic to consider the roof diaphragm as a rigid beam in a plane, the roof diaphragm is flexible when loaded laterally and in torsion. The flexibility of intercomponent connections allows some relative motion of the walls, so actual displacements deviate slightly from the assumed geometry given in Figure 75. The transverse walls (wall 5 and 6) also contribute to the load redistribution among the walls, which is disregarded in the rigid-beam model.

A shortcoming of this approach is that the model is rather sensitive to the initial guess vector. Given a poor initial guess, the Jacobian matrix J_{ij} can become ill-conditioned due to the large differences in magnitudes of its entries.

Linear Spring Model

The rigid-beam model as given in Figure 75 is easily linearized by shifting the origin from point 0 to position 1; the center of rotation is located on the beam rather than at a distance x from it. Then the total deformation of the

beam is decomposed into rigid-body translation and rotation. This has certain numerical advantage, especially if the rotation is small.

The equilibrium equation take the form:

$$\sum_{i=1}^{n} k_i \Delta_i - w a_n = 0$$

$$\sum_{j=2}^{n} \Delta_j k_j a_j - w \frac{a_n^2}{2} = 0 \qquad (44)$$

Then, from the geometry:

$$\frac{\Delta_2-\Delta_1}{a_2} = \frac{\Delta_3-\Delta_1}{a_3} = \ldots = \frac{\Delta_n-\Delta_1}{a_n}$$

$$or \qquad (45)$$

$$(\Delta_2-\Delta_1)\, a_j - (\Delta_j-\Delta_1)\, a_2 = 0 \qquad j=3,4,\ldots,n$$

This leads to a system of linear equations in the form:

$$\begin{bmatrix} k_1 & k_2 & k_3 & k_4 & \ldots & k_n \\ 0 & k_2 a_2 & k_3 a_3 & k_4 a_4 & \ldots & k_n a_n \\ a_3-a_2 & -a_3 & a_2 & 0 & \ldots & 0 \\ a_4-a_2 & -a_4 & 0 & a_2 & 0 \ldots & 0 \\ \cdot & \cdot & \cdot & \cdot & \ldots & \cdot \\ a_{n-1}-a_2 & -a_{n-1} & 0 & 0 & 0 \ldots a_2 & \cdot \\ a_n-a_2 & -a_n & 0 & 0 & 0 \ldots & a_2 \end{bmatrix} \begin{bmatrix} \Delta_1 \\ \Delta_2 \\ \Delta_3 \\ \Delta_4 \\ \cdot \\ \Delta_{n-1} \\ \Delta_n \end{bmatrix} = \begin{bmatrix} wa_n \\ \frac{a_n^2}{2} \\ 0 \\ \cdot \\ \cdot \\ 0 \\ 0 \end{bmatrix} \qquad (46)$$

where Δ_1 represents a displacement due to the rigid-body translation and $\Delta_i-\Delta_1$, i=2,3,...,n are displacements due to

the rigid-body rotation. Reaction forces can be easily computed as:

$$R_i = k_i \Delta_1 \tag{47}$$

The eq. (46) represents a set of linear equations since spring stiffness k_i is not a function of unknown displacements Δ_i, and therefore eq. (46) can be used to obtain an initial guess for nonlinear case.

When stiffness k_i is a function of the displacement Δ_i, Newton's method can be used for the solution. If the spring load-deformation relationship $R_i=f(\Delta_i)$ is used in the derivation, Jacobian matrix takes the form

$$J_{ij}=\begin{bmatrix} -\frac{\partial R_1}{x_1} & -\frac{\partial R_2}{x_2} & -\frac{\partial R_3}{x_3} & -\frac{\partial R_4}{x_4} & \cdots -\frac{\partial R_n}{x_n} \\ -a_3+a_2 & a_3 & -a_2 & 0 & \cdots 0 \\ -a_4+a_2 & a_n & 0 & -a_2 & \cdots 0 \\ \cdot & \cdot & \cdot & \cdot & \cdots \\ 0 & -a_2\frac{\partial R_2}{\partial x_2} & -a_3\frac{\partial R_3}{\partial x_3} & -a_4\frac{\partial R_4}{\partial x_4} & \cdots -a_n\frac{\partial R_n}{\partial x_n} \end{bmatrix} \tag{48}$$

and the reaction forces R_i are computed from the relationship $R_i=f(x_i)$ which for the exponential form gives $R_i=ax_i^b$, where a and b are constants.

Calculated reaction forces for linear and nonlinear spring stiffness are given in Table 14. The linear and nonlinear spring models distribute the applied load with similar effectiveness. This may not always be true, however. A principal difference between the linear and nonlinear-spring models is that for the nonlinear case spring stiffness k_i is a function of the displacement Δ_i.

For load combinations such as snow and earthquake loadings, slope of the nonlinear load-deflection relationship can change dramatically as a result of larger deflection. Hence, the difference may intensify.

Summary

The finite-element solution shows that current design procedure gives erroneous results since it does not take the load-sharing capability of the structure into account. Simplifying the problem by assuming that the roof diaphragm behaves as a rigid-beam and neglecting slips between substructures leads to satisfactory results, provided that the load-deformation curve for the shear wall is known. This curve can be estimated by using the APA formula, but use of the closed-form solution to obtain wall stiffness requires caution.

Alternative methods to compute reaction forces within the shear walls are proposed in the form of an analogy to a rigid-beam on elastic supports. These are shown to produce good results for lateral load distribution in light-frame structures. It is more accurate and realistic to analyze the structural system as a rigid beam on elastic supports than to use the current design procedure, which does not necessarily lead to conservative results.

It is necessary to note that the simplified analytical approach has limited applicability. For a nonlinear system, the principle of superposition does not hold, which implies that all possible load combinations (such as wind pressure and dead load) must be applied simultaneously. However, using the rigid beam on elastic springs analogy leads to a more accurate estimate of reactions in the individual shear walls than does the model of simple or continuous beam on rigid supports.

9. LOAD COMBINATION AND ANALYSIS OF SUBSTRUCTURES

The finite-element model of the full structure gives the information about the displacements and forces for substructures as well as for intercomponent connections. These results can be used directly to design the particular element such as shear walls or intercomponent connections by applying currently valid design specifications such as the National Design Specification (NFPA, 1986) or APA methods (APA, 1989a,b). This approach represents a combination of analytical and empirical procedures. The advantage is that the design procedure is based upon more accurate information about substructure and connection loading.

Design practice requires consideration of several different load combinations. Due to the nonlinear character of the light-frame wood structure superposition of the load cases and consequently superposition of the internal forces and displacements will yield erroneous results. Thus, the analysis must be performed on the structure subjected to the pertinent load combination. The full-structure model can be utilized for such a case.

As an example, the structure was loaded by a combination of wind, dead and snow load as shown in Figure 76. Wind pressure specified by Uniform Building Code (ICBO, 1988) was also applied to the roof. All external walls were loaded by a wind pressure or suction as required for the whole building design. The weight of the roof was included, but no body forces representing wall weight were applied. Body forces are usually neglected in the static analysis of light-frame wood buildings but may be included as a part of

the dead load, as in the case of roof.

The finite-element mesh of the full structure as deformed by the given wind and snow loads is shown in Figure 77. Deformations on the boundaries of the superelements combined with the applied loads can be used for the stress analysis of the substructures.

Analysis of Wall 1

The detailed finite-element model of wall 1 was loaded on its boundary by the displacements obtained from the finite-element model of the full structure. This represents the deformation caused by the non-rigid character of intercomponent connections as well as by the axial force due to the roof load. Only translations were applied as boundary conditions. Since the number of boundary nodes as well as their location on the finite-element model of full structure does not coincide with these on the three-dimensional wall model, boundary conditions do not exactly match. Deformations were applied to the nodes geometrically closest on both two-dimensional global wall model and three-dimensional detailed model. The rest of the nodes on the three-dimensional model were allowed to deform freely.

The wind suction of 12.6 psf (0.6 kPa) was applied as the load on the external (plywood) wall surface which represented external pressure identical to one used in the analysis of the full structure.

Framing

Stresses in the framing are affected by loading and boundary conditions. According to Saint Venant's Principle, the stresses in the perimeter framing members, such as sole and top plates as well as left and right end studs will be

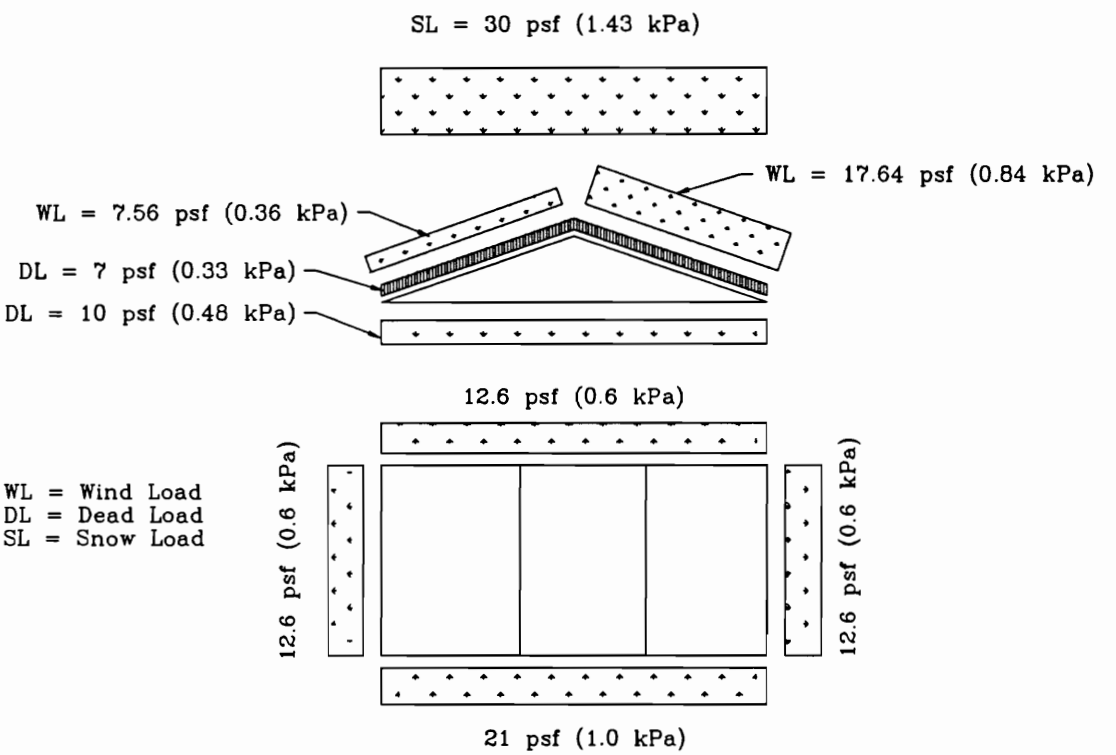

Figure 76. Loads Applied to the Finite-Element Model of the Full Structure.

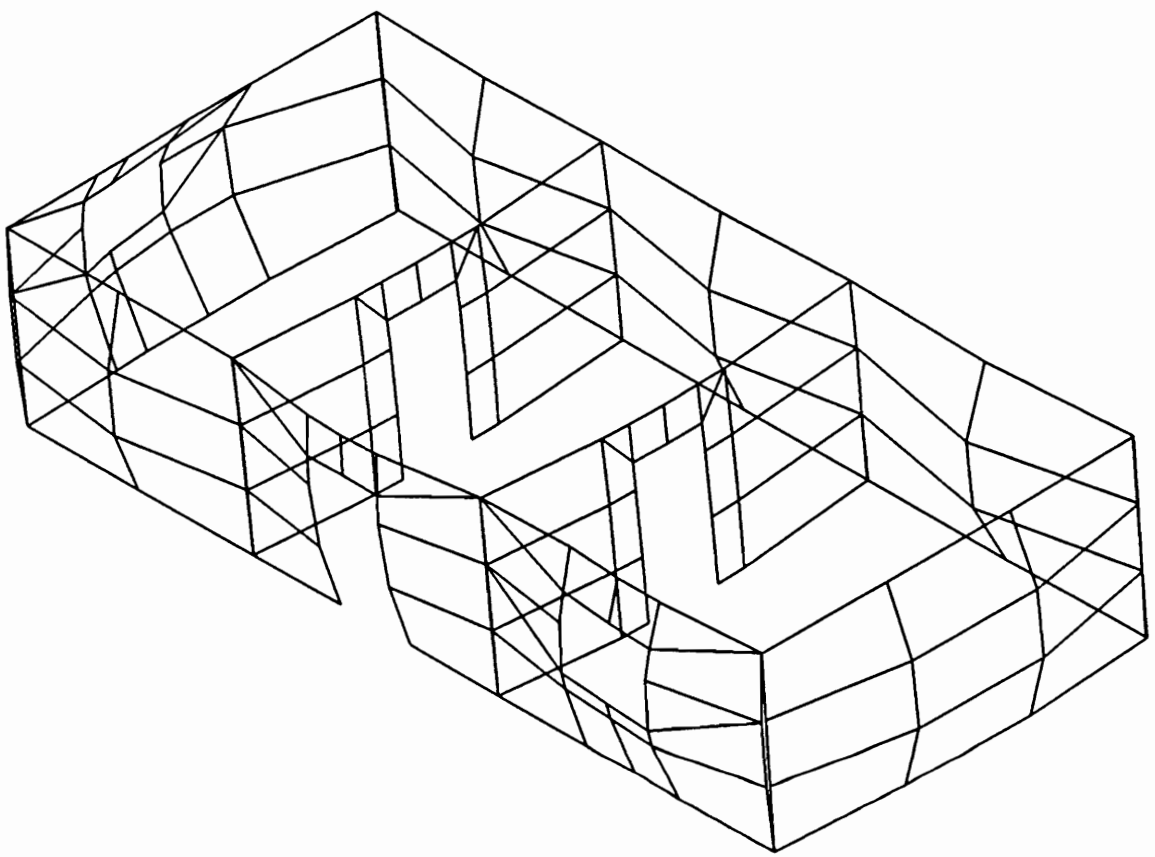

Figure 77. Deformed Finite-Element Mesh of the Structure Loaded by a Combination of Wind, Dead, and Snow Load.

affected because the detailed wall model was loaded by the displacements on the boundary. If the stresses in these elements are important, more boundary nodes at the full-house model will be required for the analysis. Also, direct application of boundary displacements on the members of the interest will no longer be suitable, and a larger portion of the full building model will have to be "cut" and boundaries sufficiently far from the analyzed region loaded. However, for this case, the edge studs as well as top and bottom plate were not critical and thus, the deformations as boundary conditions were applied directly to them.

Example of stress contours for a stud is shown in Figure 78. The normal stress in the midpoint of the stud adjacent to the window is shown. Although the axial load due to the roof weight and roof load is applied via wall axial deformation, there is no substantial asymmetry in the stress distribution. Relatively low normal stress in the stud indicates that the stud strength is not a critical factor.

The finite-element representation of the portion of the wall 1 framing with the sheathing and nails removed is given in Figure 79. The superimposed vectors identify the magnitude and direction of the displacements. The end studs which connect wall 1 to the longitudinal walls (wall 5 and 6) are not affected by wall bending which is documented by vectors remaining in the plane of the wall. The slip of the sole plate increases in the direction towards the center of the wall. The complex deformation of the wall frame is apparent from Figure 80. Deformations are highly exaggerated (200x) for clarity of presentation of torsional as well as axial deformations of the studs.

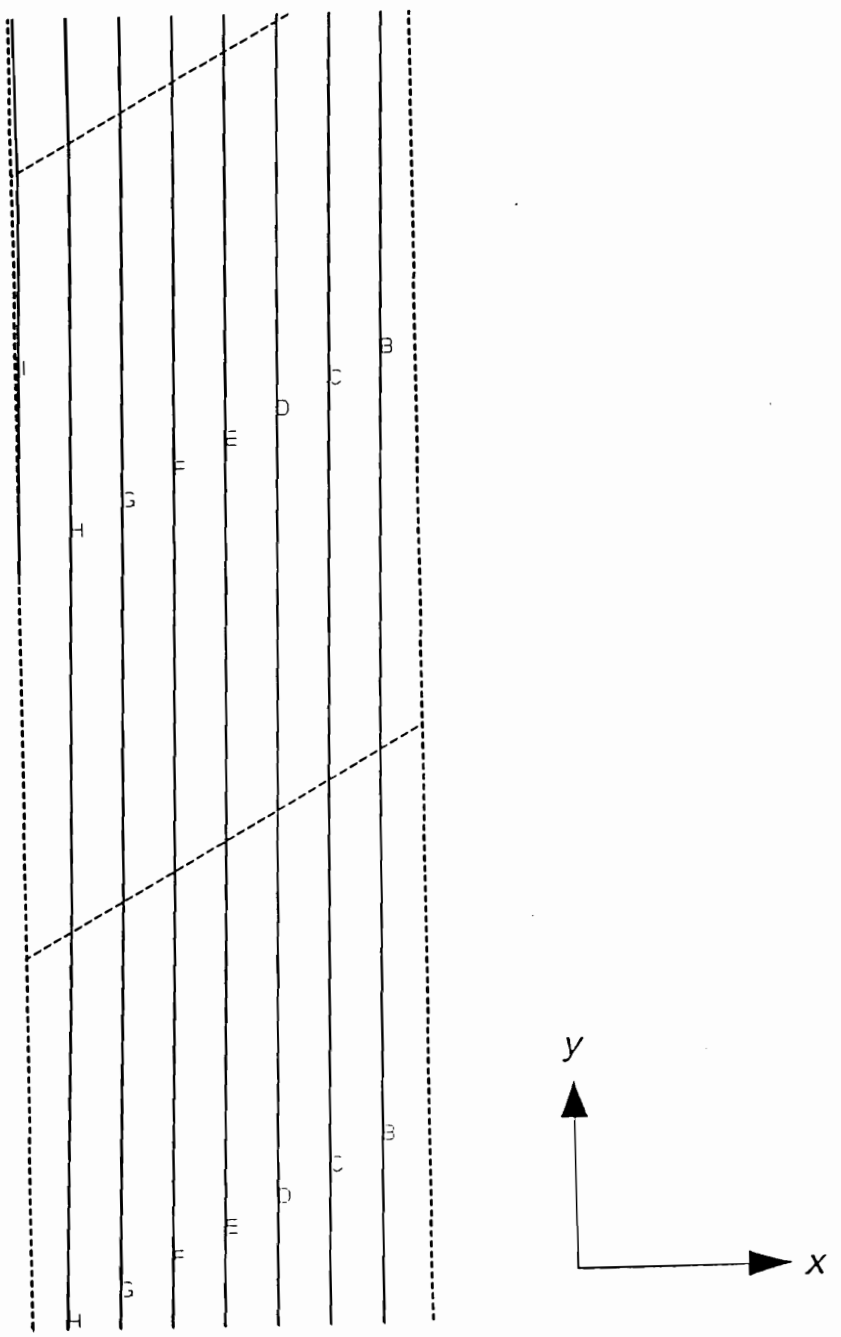

Figure 78. Stress Contours for σ_y (psi) at the Midpoint of the Stud No. 7 in Wall 1.

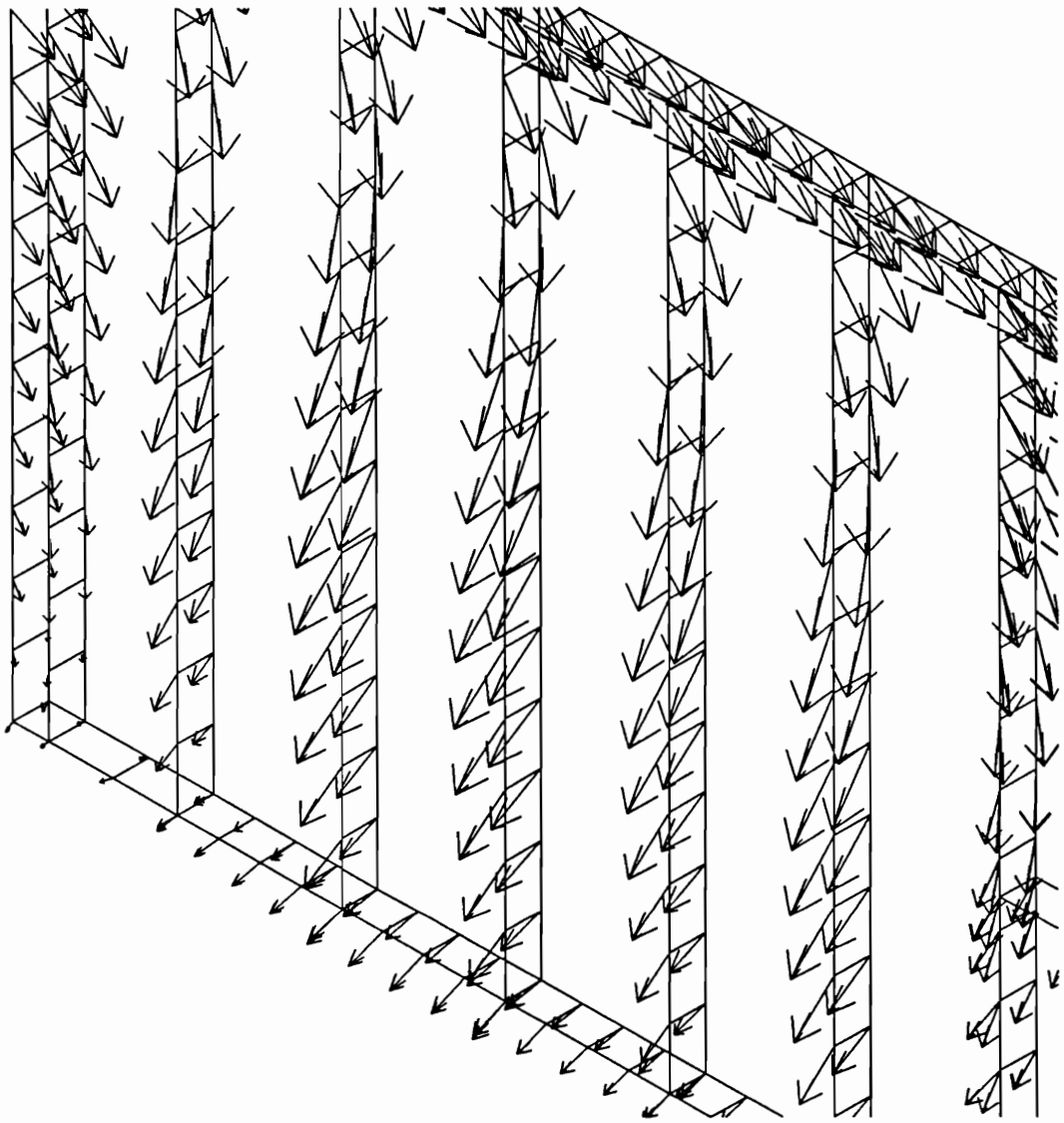

Figure 79. A Vector Representation of the Framing Deformation in Wall 1.

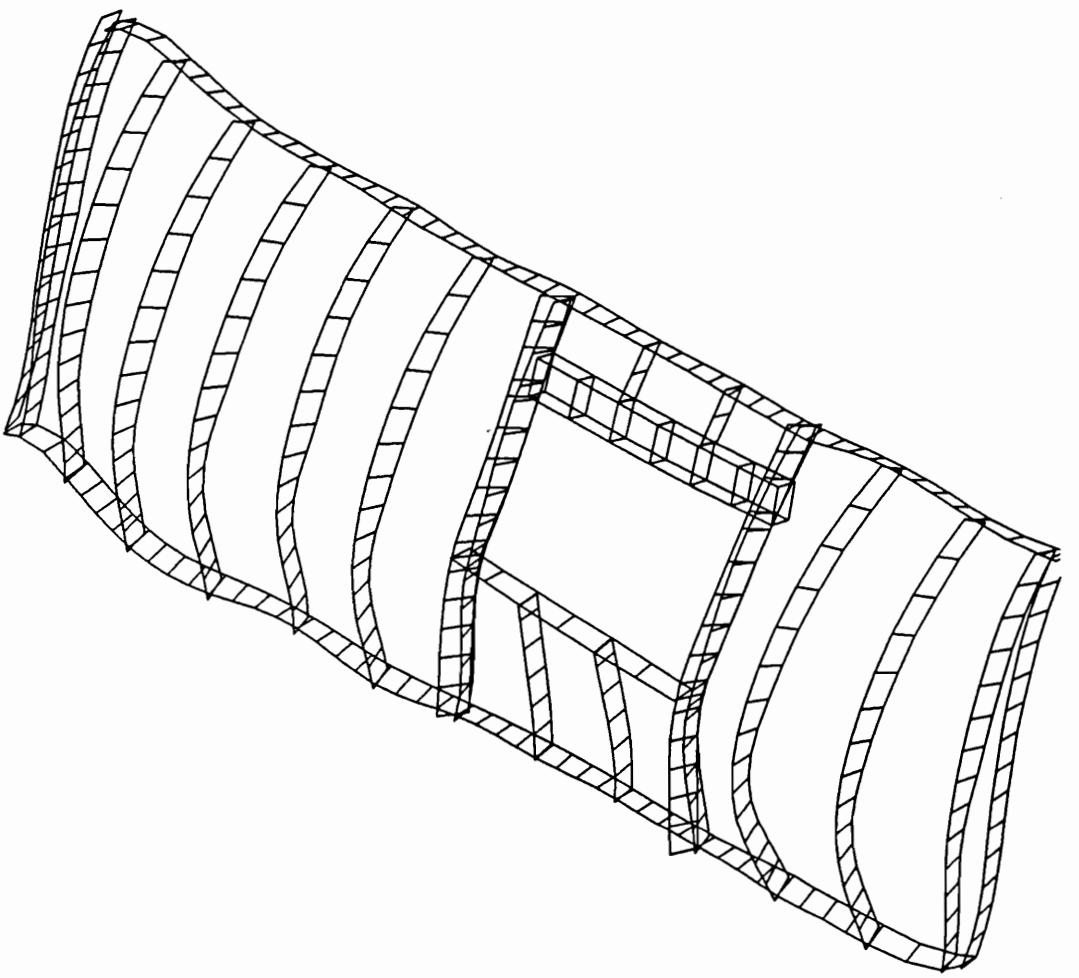

Figure 80. Deformation of the Framing in Wall 1 (200x).

Sheathing

The stress distributions in the sheathing were affected by the joints between studs, location in the wall, and the presence of openings.

Figure 81 through Figure 86 show that stresses are concentrated on the boundary and at the sharp edges around openings. The stress concentration due to the contact effect can be seen in Figure 81b through Figure 83b where the area around left bottom corner of the window is shown. The top corner of the plywood panel below the window is pushed against the continuous sheet causing compressive stress indicated by negative values in the legend. Rapid stress decay is caused by the low elasticity modulus of the material as well as element size.

Stresses in the gypsum sheathing are concentrated at the areas around top corners of the window. This is caused by the horizontal orientation of the panels as well as the panel continuity around the top window corners. This causes a stress concentration which is not interrupted by the presence of gap as it would be in tension. When a gap can open, no stress is transferred from panel to panel. The corner detail of gypsum sheathing in Figure 84b while loaded in tension indicates that the corner tends to open. This coincides with the overall wall shear deformation as shown in Figure 84a through Figure 86a.

The stress evaluation and consequent sheathing design is complicated by orthotopic character of the material. Interpretation of multiaxial stress requires the application of a suitable strength theory.

A tensorial strength criterion proposed by Malmeister (1966, 1972) and Tsai and Wu (1971) is appropriate. This phenomenological strength criterion defines the strength envelope as an ellipsoidal hyperplane in n-dimensional space in which the number of "coordinate axes" is given as a

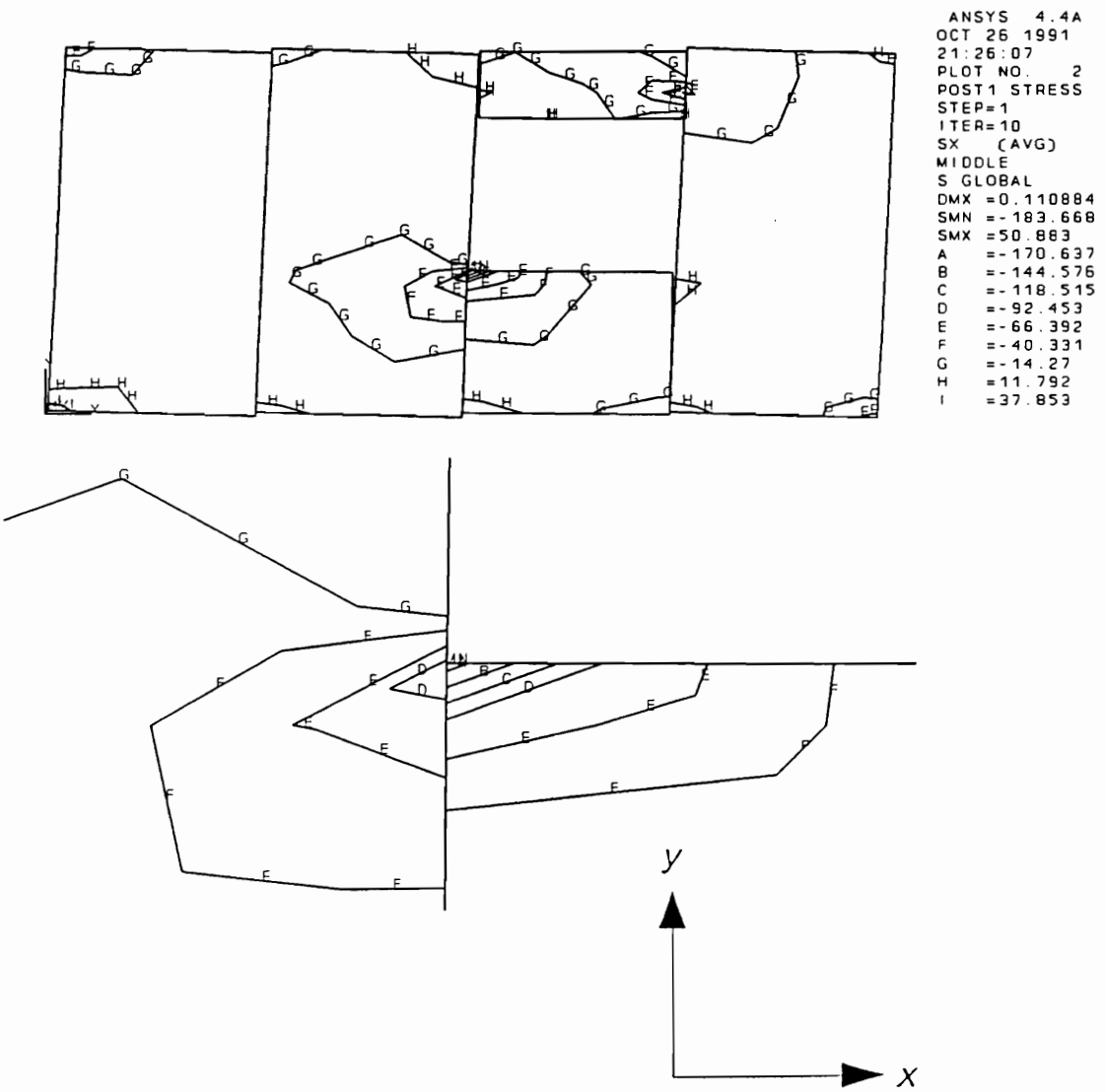

Figure 81. Stress σ_x (psi) for the Plywood Sheathing of Wall 1, Stress Contours for (a) Full Wall and (b) Left Lower Window Corner.

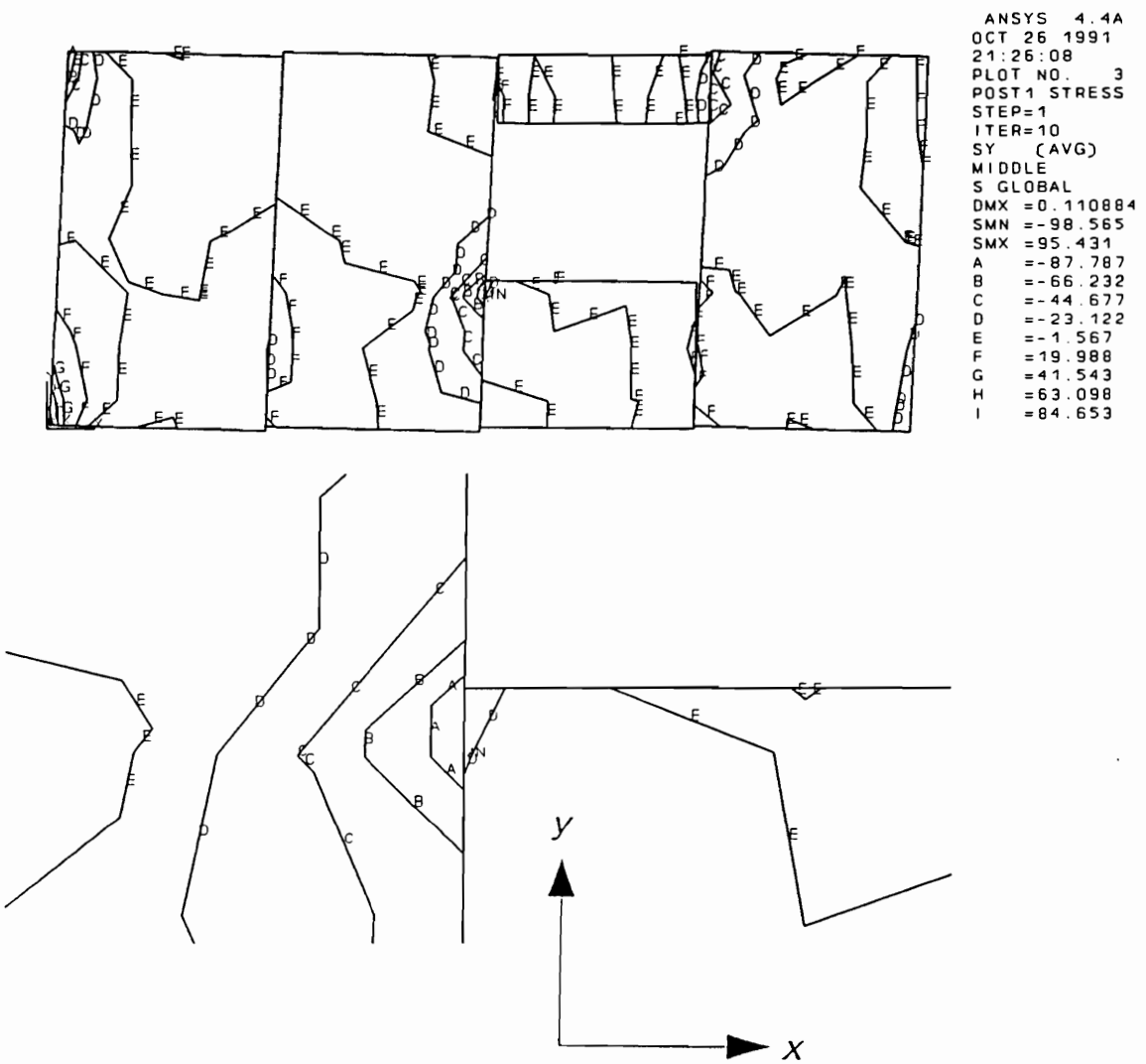

Figure 82. Stress σ_y (psi) for the Plywood Sheathing of Wall 1, Stress Contours for (a) Full Wall and (b) Left Lower Window Corner.

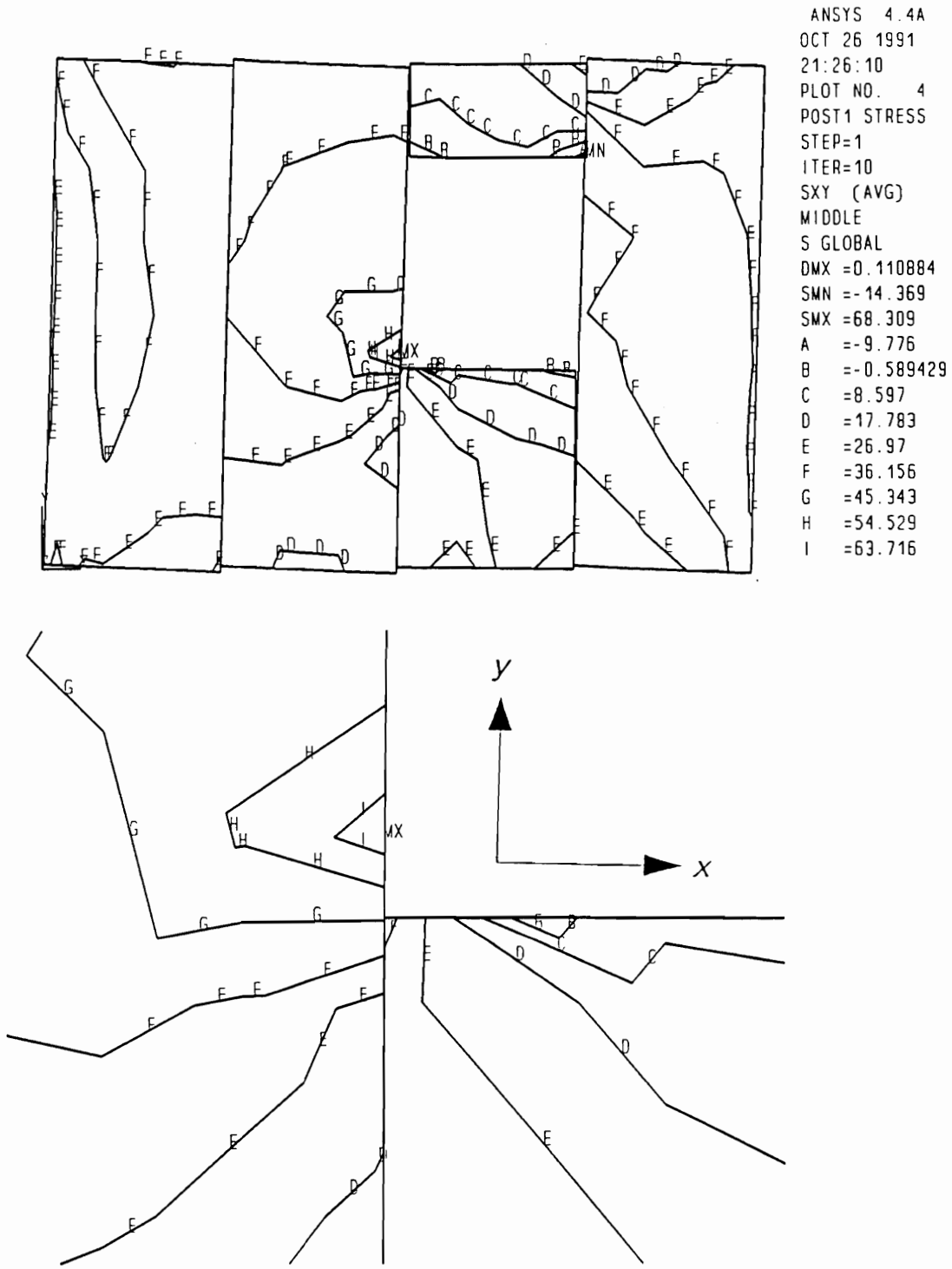

Figure 83. Stress σ_{xy} (psi) for the Plywood Sheathing of Wall 1, Stress Contours for (a) Full Wall and (b) Left Lower Window Corner.

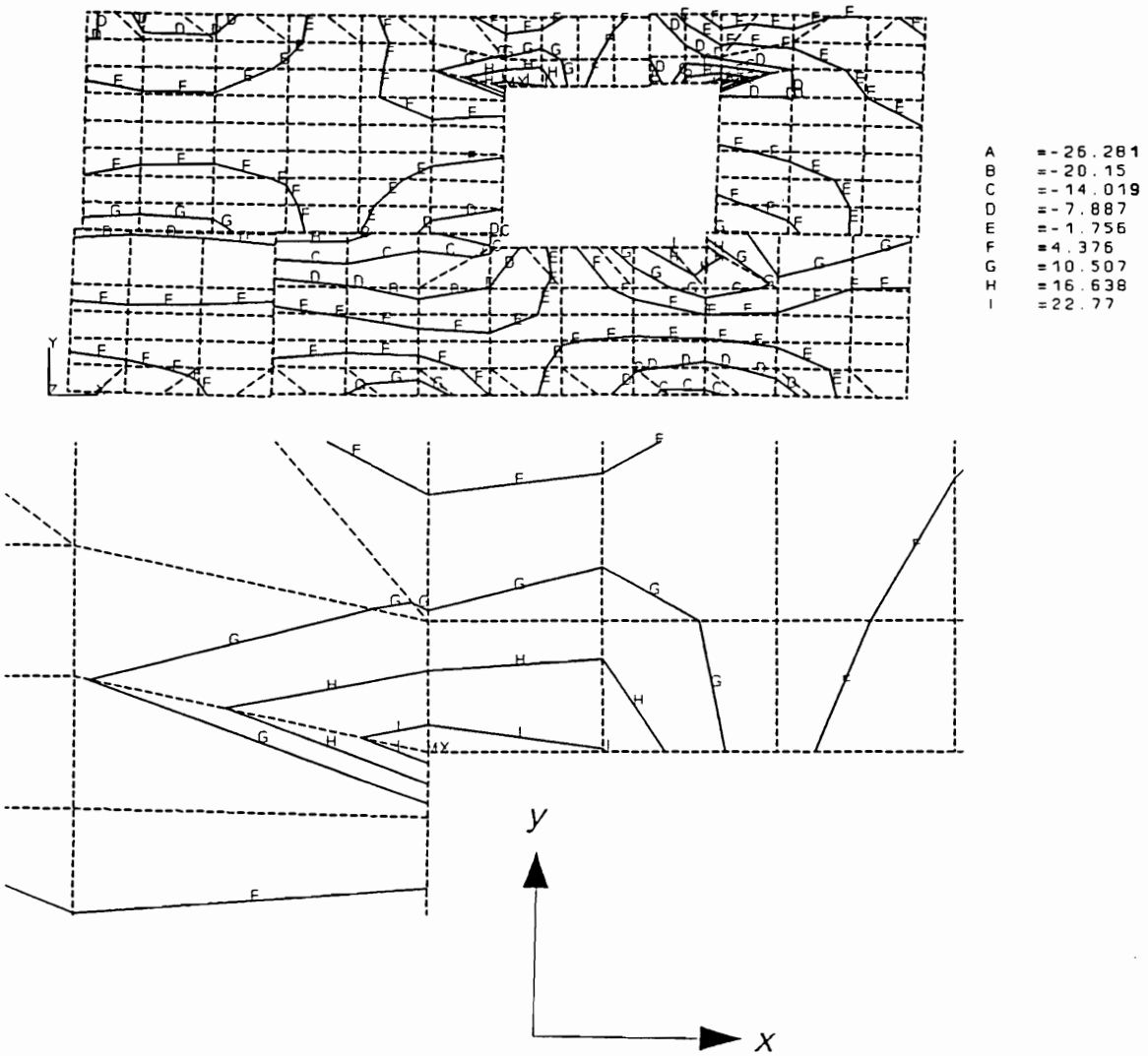

Figure 84. Stress σ_x (psi) in Gypsum Sheathing of Wall 1, Stress Contours for (a) Full Wall and (b) Left Upper Window Corner.

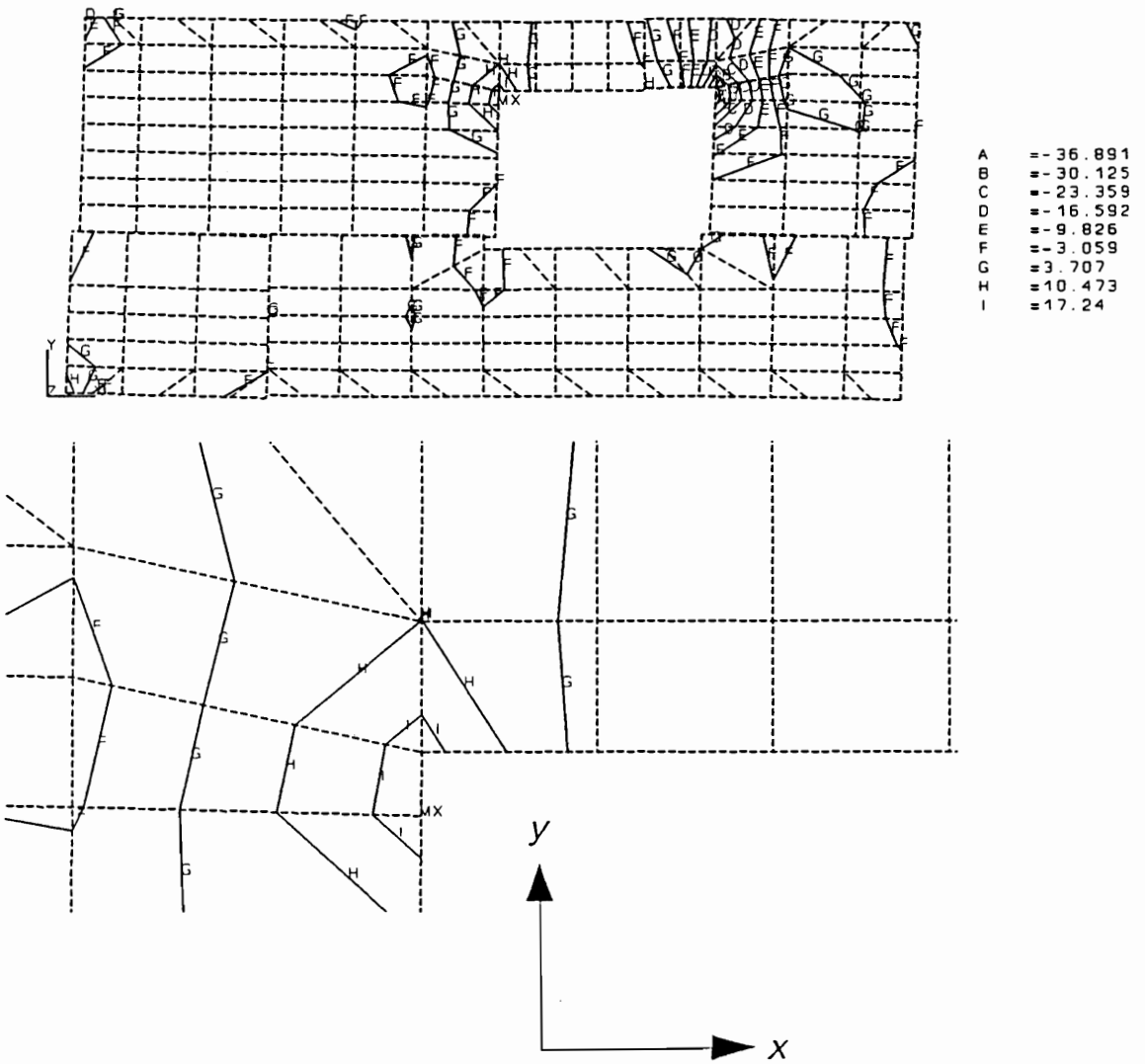

Figure 85. Stress σ_y (psi) in Gypsum Sheathing of Wall 1, Stress Contours for (a) Full Wall and (b) Left Upper Window Corner.

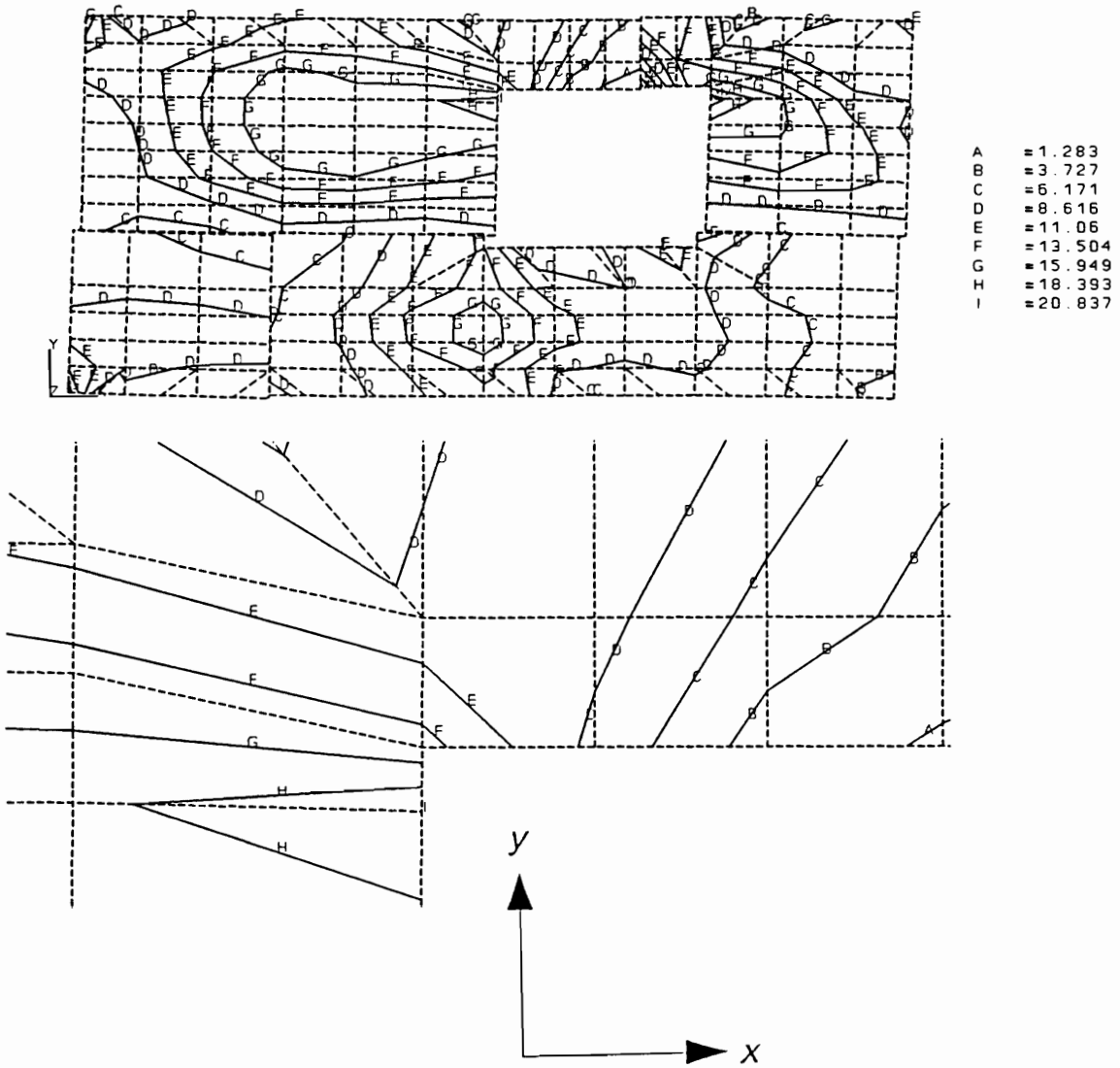

Figure 86. Stress σ_{xy} (psi) in Gypsum Sheathing of Wall 1, Stress Contours for (a) Full Wall and (b) Left Upper Window Corner.

number of stress tensor components. For the two-dimensional stress-state, the coordinate axes are two normal stresses in principal direction and a shear stress. A simplified form of the tensorial strength criteria is

$$F_{ij}\sigma_{ij}+F_{ijkl}\sigma_{ij}\sigma_{kl}=k \qquad i,j,=1,2,3 \tag{49}$$

and

$k<1$ no failure

$k\geq 1$ failure

Where: σ_{ij}, σ_{kl} = components of the stress tensor

F_{ij} = strength tensor of the second order

F_{ijkl} = strength tensor of the fourth order

Using the tensor property $\sigma_{ij}=\sigma_{ji}$ and the plain-stress condition $\sigma_{3j}=0$ the equation (49) can be rewritten

$$F_{1111}\sigma_{11}^2+F_{2222}\sigma_{22}^2+2F_{1122}\sigma_{11}\sigma_{22}+F_{1212}\sigma_{12}^2+F_{11}\sigma_{11}+F_{22}\sigma_{22}=k \tag{50}$$

Where: σ_{11} = normal stress in the direction 1 (x)

σ_{22} = normal stress in the direction 2 (y)

σ_{12} = shear stress in plane 12

F_{ij}, F_{ijkl} = strength tensor components

Using contracted notation (Jones, 1975), Equation (50) can be rewritten

$$F_{11}\sigma_1^2+F_{22}\sigma_2^2+2F_{12}\sigma_1\sigma_2+F_{66}\sigma_6^2+F_1\sigma_1+F_2\sigma_2=k \tag{51}$$

in which $F_{11}=F_1$, $F_{22}=F_2$, $F_{1122}=F_{12}$, $F_{1111}=F_{11}$, $F_{2222}=F_{22}$, $F_{12}=F_6$, $F_{1212}=F_{66}$. Notation for stress tensor components can be obtained by substituting symbol σ for F.

The strength tensor components for the plywood sheathing were estimated from the strength properties given by the Plywood Design Specifications (APA, 1989b) for dry conditions. Values were corrected for the principal

material directions using cross-sectional properties ratio. Since no information about the biaxial strength of plywood is given, this value must be estimated. From the work of Askhenazi and Ganov (1980) it follows that the biaxial strength of plywood in compression is about 15% lower than uniaxial compressive strength in the weaker plywood direction. Therefore, the value of biaxial strength of plywood was estimated to be 15% less then the compressive strength perpendicular to the face veneers. Shear through the thickness was used for shear strength. The values of the individual strengths for plywood used to compute strength tensor components are in Table 15.

Table 15. Strength Properties of Douglas-Fir Plywood Estimated from Plywood Design Specifications (APA, 1989).

Property	Value-psi (MPa)	Notes
Tension parallel	534 (3.71)	APA Table 3
Compression parallel	528 (3.64)	Species group 1, dry conditions.
Tension perpendicular	234 (1.62)	Stress level S-1.
Compression perpendicular	231 (1.61)	Values corrected for cross-sectional properties.
Biaxial compression	196 (1.37)	
Shear	76 (0.61)	

Strength tensor components can be calculated:

$$F_1=\frac{1}{X}+\frac{1}{X'}=\frac{1}{534}+\frac{1}{-528}=-2.128E-5$$

$$F_2=\frac{1}{Y}+\frac{1}{Y'}=\frac{1}{234}+\frac{1}{-231}=-5.55E-5 \qquad F_6=0$$

$$F_{11}=-\frac{1}{XX'}=-\frac{1}{534(-523)}=3.547E-6$$

$$F_{22}=-\frac{1}{YY'}=-\frac{1}{234(-231)}=1.850E-5 \qquad (52)$$

$$F_{66}=\frac{1}{S^2}=\frac{1}{76^2}=1.731E-4$$

$$F_{12}=\frac{1}{2P^2}[1-P(F_1+F_2)-P^2(F_{11}+F_{22})]=-1.1022E-6$$

Where:

X, Y	=	tensile strength in x and y-directions
S	=	shear strength
P	=	biaxial strength
X′, Y′	=	compressive strength in x and y directions

A short subroutine was written to incorporate the tensor strength criterion into the software as a part of the postprocessing. The criterion was applied to all elements representing plywood sheathing which allowed to evaluate every discrete point in the mesh for the stress combination. The values of the stress function for different locations of

the plywood sheathing are shown in Figure 87. The function has its maxima around window opening which coincides with values of individual stress tensor components. From Figure 87 it can be concluded that for a combination of the dead, snow and wind load, no plywood failure was detected.

The change of the values of the stress function is shown in Figure 88. The sharp increase of the function value below window followed by rapid decrease is due to the contact effect in which left gap below window is closing and right gap is opening.

The above calculation serves as an example of how the strength criterion can be applied in conjunction with the finite-element solution. The approach here is strictly deterministic and it is anticipated that stochastic approach will give more reliable data. The framing and gypsum sheathing can be evaluated in a similar manner.

If the material is considered as isotropic, the above criterion converges to the Huber-von Misses-Hencky criterion (Tsai and Wu, 1971) and is still applicable. This represents a significant simplification, since no biaxial strength is considered. However, as shown by Askhenazi and Ganov (1980) for orthotropic and anisotropic material, the Huber-von Misses-Hencky's criterion is not acceptable since it assumes no shape change under infinite hydrostatic pressure, which is not true for anisotropic materials. Therefore, multiaxial stress in wood and plywood cannot be evaluated with the more simple Huber-von Misses-Hencky's theory. Particleboards, flakeboards and wood composites with randomly oriented components can be treated as isotropic and more simple theories applied.

The use of the tensorial strength criterion as a part of the postprocessing procedure makes it possible to evaluate the stress function anywhere in the structure thus giving a designer more information about potentially weak points.

The decision about the failure depends on several factors

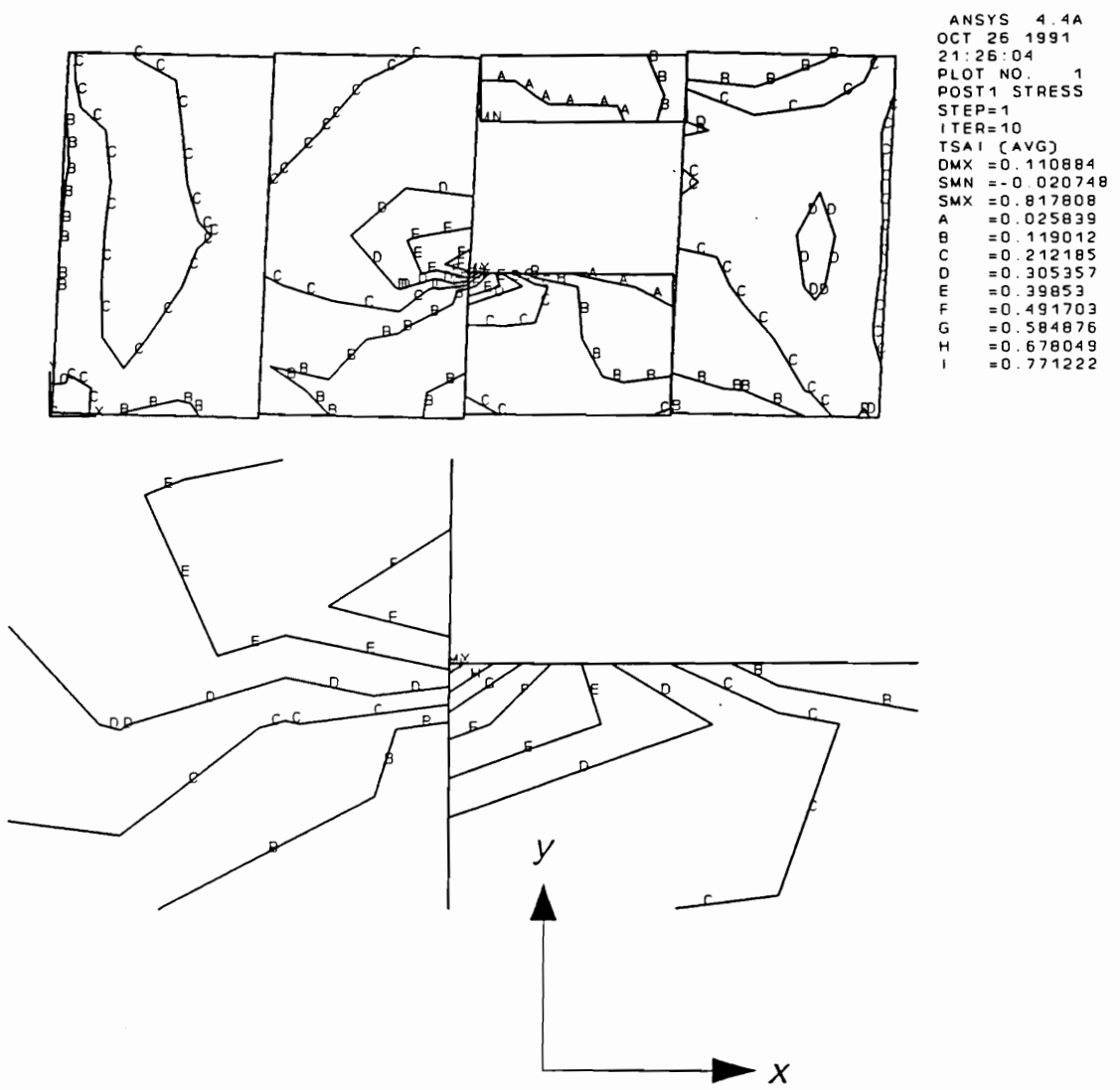

Figure 87. Contours for the Values of the Strength Theory Function of the Tensorial Strength Criteria for Plywood Sheathing of the Wall 1.

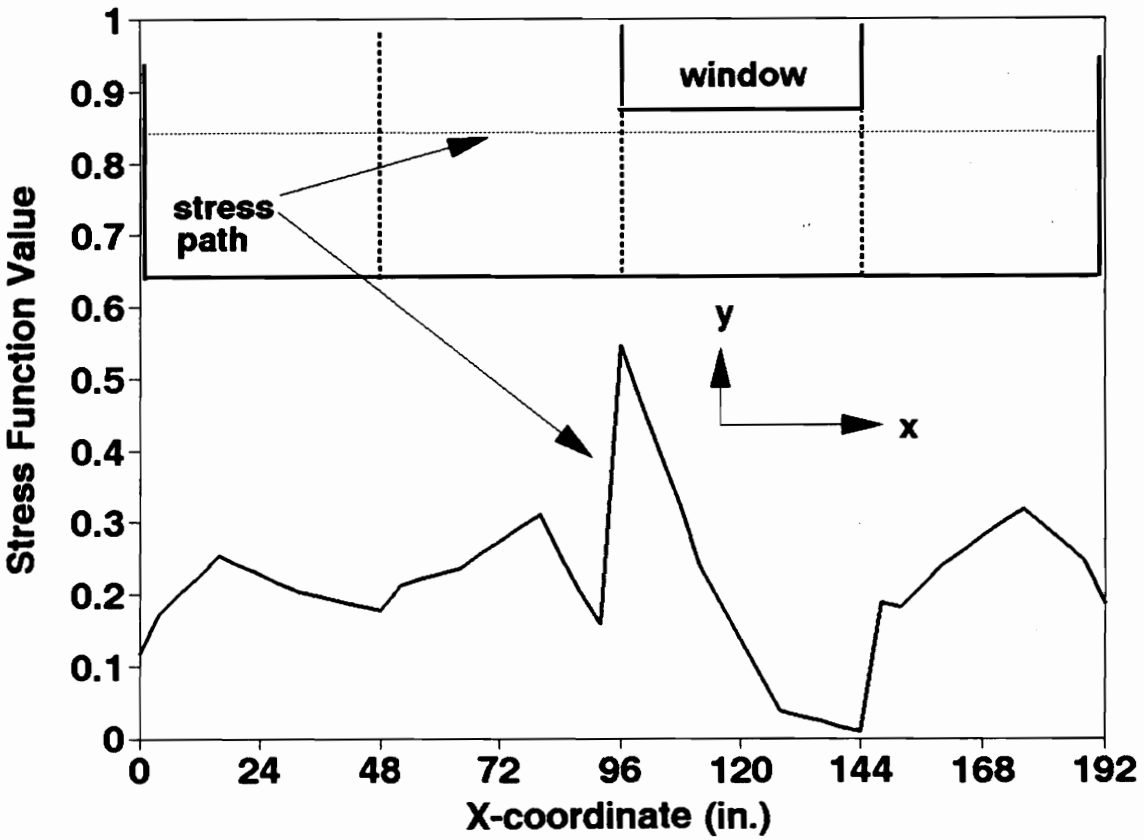

Figure 88. Values of the Strength Theory Function for Plywood Sheathing of Wall 1 as a Function of the Position.

such as element size, size of the area where a critical value of the stress function is exceeded, location of maximal stress and others including load sharing. To address the problem of failure correctly, the stochastic character of the loads as well as material properties must be recognized. Thus, the failure function is a function of random variables.

The distribution describing the probability of failure is a multivariate distribution consisting of marginal distributions each associated with one coefficient of the Equation (49). Finding the probability density function of each variable and the assessment of the statistical dependency among variables is a problem itself and will not be discussed here. The finite-element model, however, can be used to simulate the real situation by repeating the computation of internal forces for a randomly chosen vector of loads and material properties. Computed stresses serve as the input for Equation (49), whereas strength tensor components F_{ij}, F_{ijkl} must be determined using other techniques such as Advanced First-Order Second-Moment Method described e.g. by Thoft-Christensen and Baker (1982).

Nails

The nail connections are the main source of the nonlinear behavior in the structure. Connections are a major limitation in application of wood structures. In design, only the allowable force per connection is checked against the applied force. The allowable force represents the strength of the connection and is based on the yield model described by McLain (1991).

The shear resistance of the wood-stud walls is based on the experiments performed on full wall assemblies and is expressed as the allowable shear per unit wall length.

Thus, the strength of the individual connection is not directly used in shear wall design. This is due to the lack of a suitable analytical model which can be used to compute forces within the individual connection. The detailed model of the wall, however, can predict these forces. Moreover, it takes into account the nonlinear nail behavior and other nolinearities (such as gaps).

The distribution of the nail forces is influenced by the orientation of the sheathing which is shown in Figure 89. The mesh for plywood sheathing was refined at the bottom window corners to account for the stress concentration due to the contact stiffness.

The vectorial representation of the nail forces is shown in Figure 90 through Figure 92. The x-components of nail shear forces are concentrated around horizontal edges of panels and - Figure 90a and b. Some maxima can be observed in the vicinity of the gaps around window. The right bottom and left top gap tend to open thus loading nail connections in x-shear. Double arrows mean the presence of two nails at the geometrically identical location (each sheet is connected to the studs separately). The direction of forces is not important since shear resistance of the nail was considered independent on direction.

Similarly, for the y-direction forces are concentrated along the vertical panel edges as shown in Figure 91a and b. The gypsum sheathing has no continuous vertical gaps which results in sudden decrease of shear at the end of the vertical gap - Figure 91b.

The withdrawal forces are shown in Figure 92a and b. In this case, forces are concentrated in the plywood field due to the applied suction. Smaller vector length on the edges of plywood sheathing -Figure 92a means smaller forces per element but total reaction force is larger due to the larger amount of nails located at the panel edges. The forces in z-direction for nails connecting gypsum board to studs are

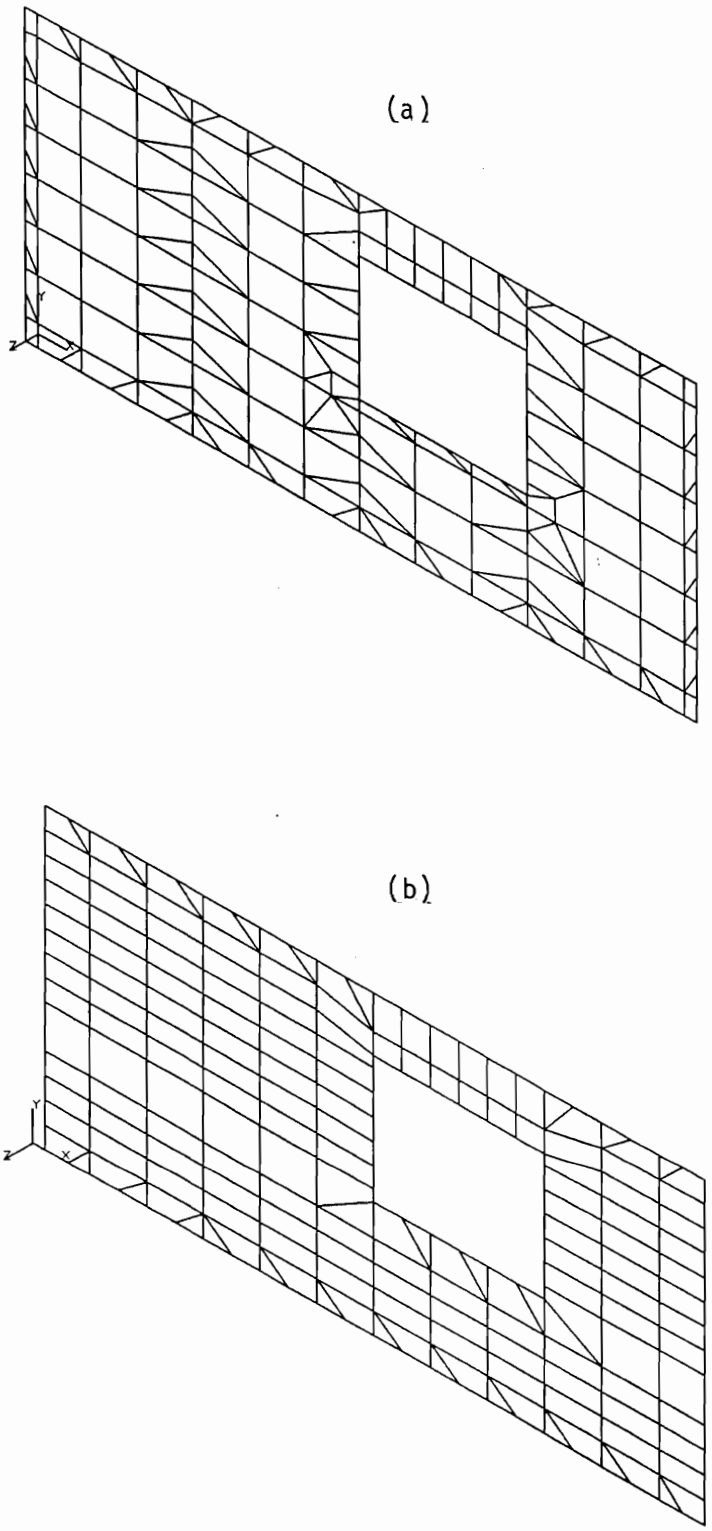

Figure 89. Finite-Element Mesh of (a) Plywood and (b) Gypsum Sheathing of Wall 1.

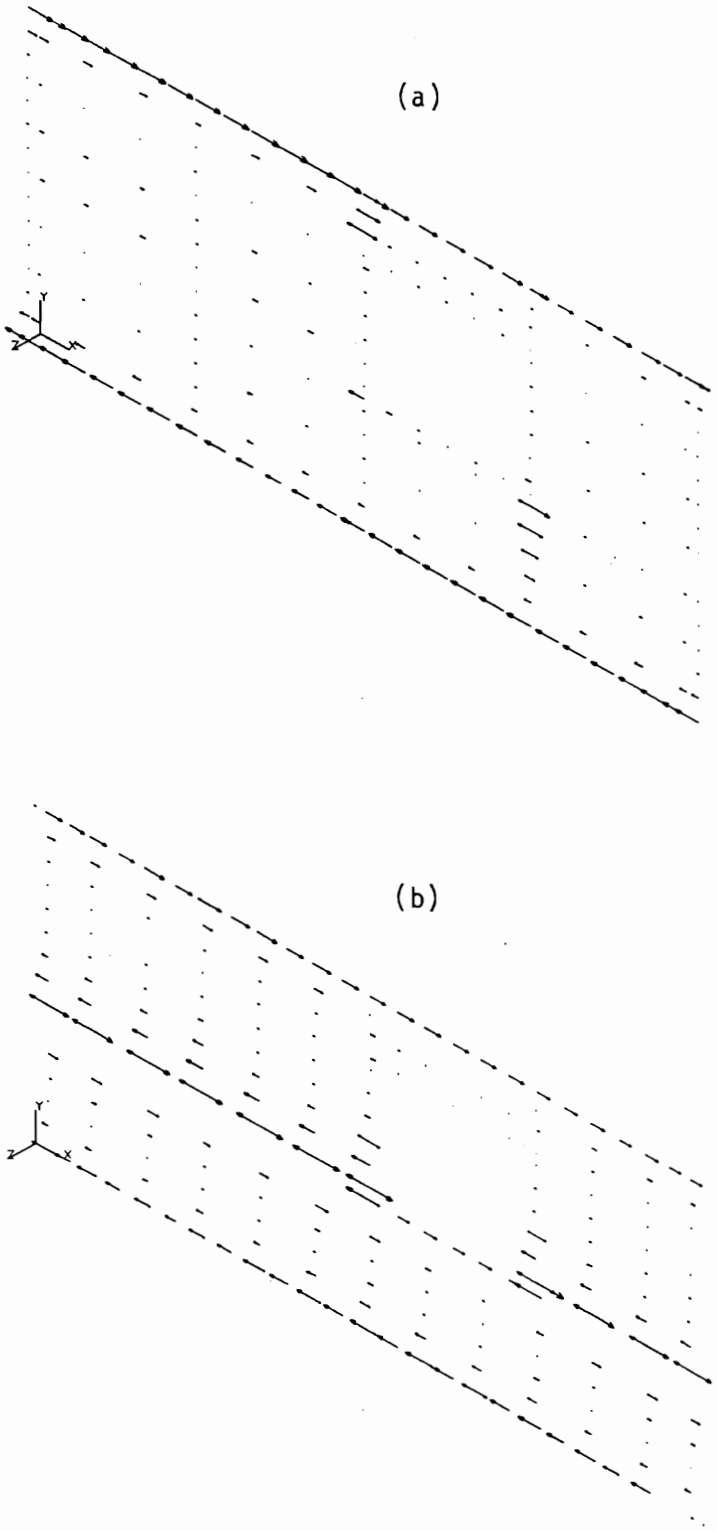

Figure 90. Nail Connection Forces in Global X-Direction between Framing and (a) Plywood, (b) Gypsum Sheathing.

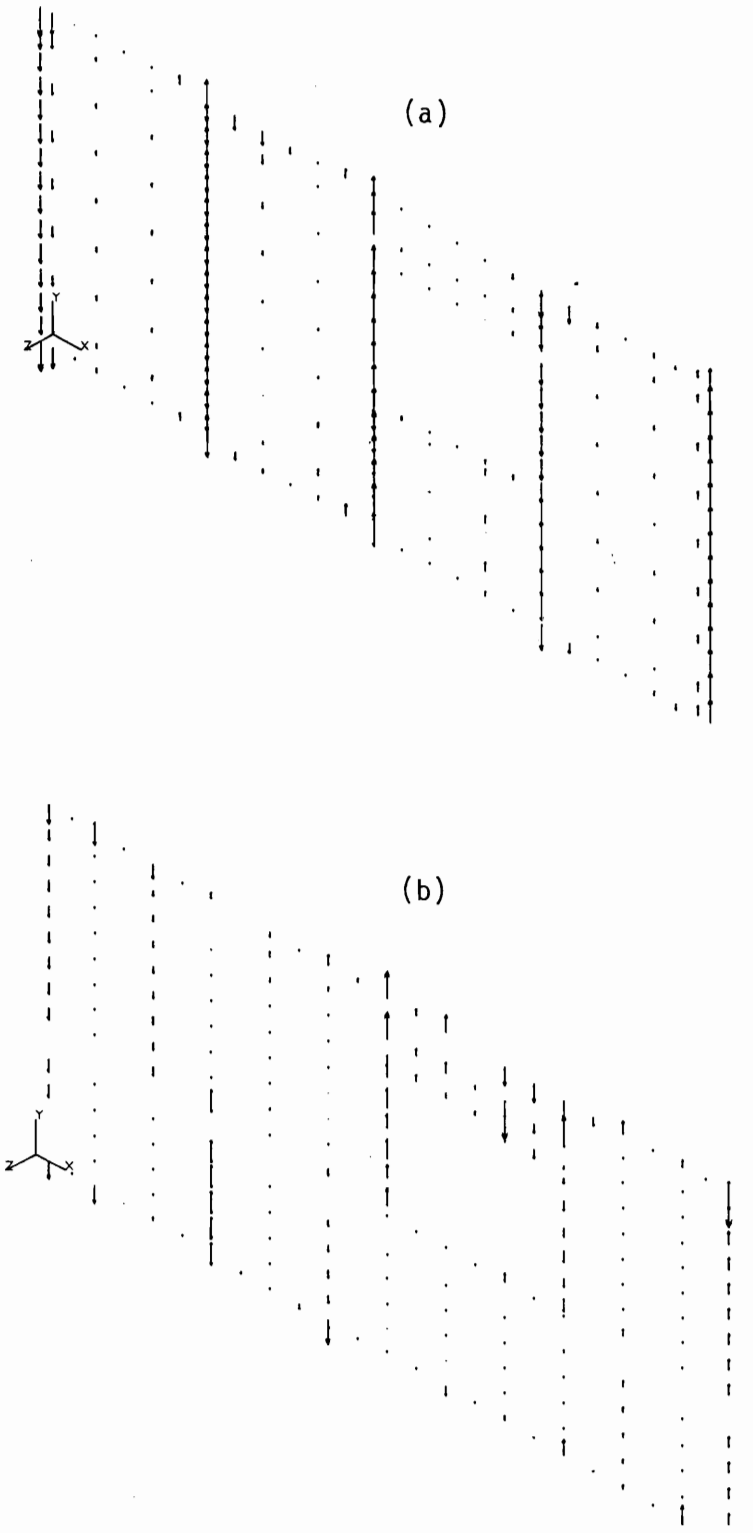

Figure 91. Nail Connection Forces in Global Y-Direction between Framing and (a) Plywood, (b) Gypsum Sheathing.

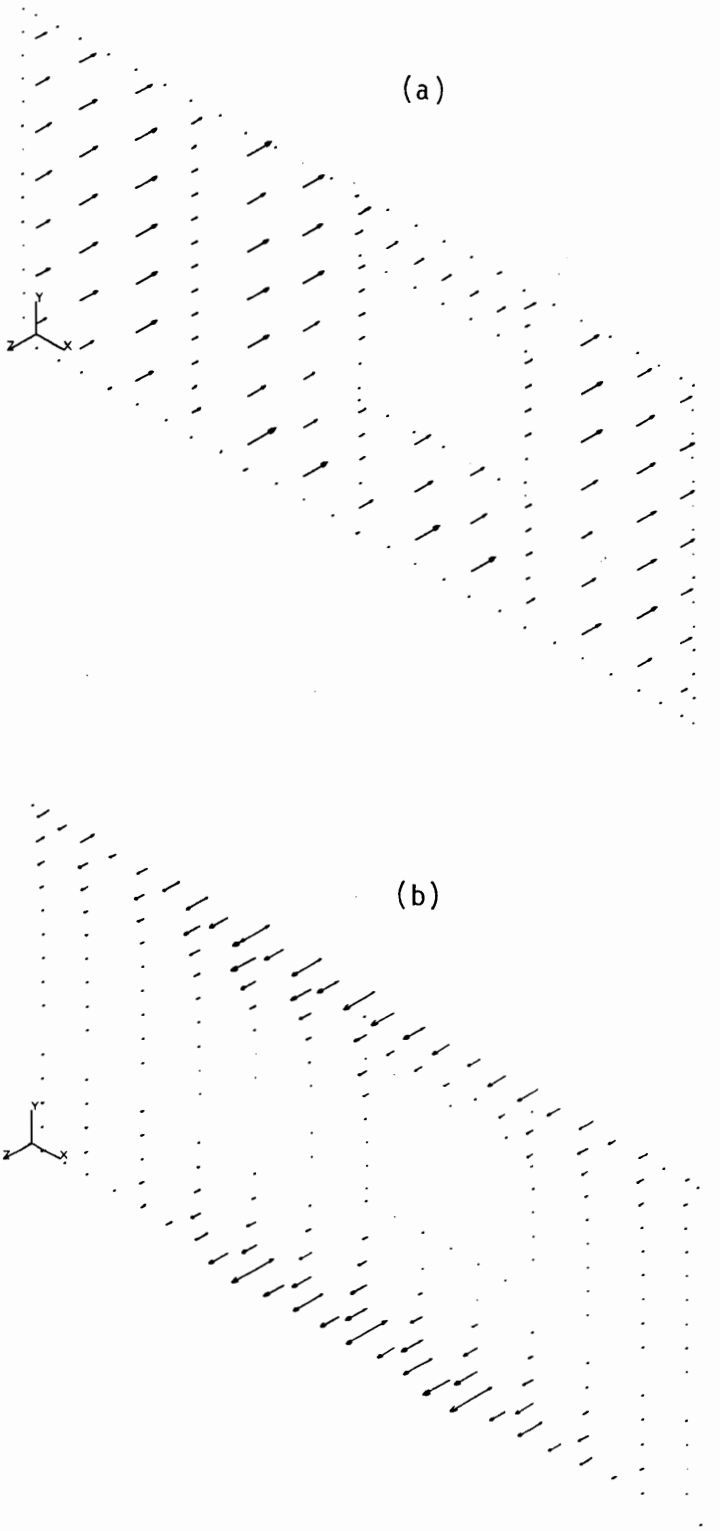

Figure 92. Nail Connection Forces in Global Z-Direction between Framing and (a) Plywood, (b) Gypsum Sheathing.

largest at the panel edges Figure 92b. No pressure was applied to gypsum but overall panel deformation causes the nail displacement in z-direction. Large forces on the gypsum edges may be due to the compression (contact) between gypsum and framing. The contact stiffness is several orders of magnitude higher than the withdrawal stiffness, which results in higher force. Also, the edge nails are close to the wall boundary and an influence of boundary conditions is possible.

The range of forces and deformations in nails is shown in Table 16. The results coincide with the findings of Gromala (1985) who estimated the slip between 0.001 and 0.01-in. (0.025-0.25-mm) for nail connections within wall and floor subassemblies. For a horizontally oriented gap in the middle of the wall the x-component of the force is relatively large, whereas for vertically oriented sheets maximums of the x-component occur at the top and bottom panel edge. The results coincide with the force distribution reported in works of Itani and Robledo (1984), Gupta and Kuo (1985) and others. Larger magnitudes of nail slips and forces in this case are due to the effect of combined loading, which to this time has not been fully investigated mainly because no suitable model existed.

The forces in the nail connections can be directly used to design the connections based on the provisions of National Design Specifications for Wood Construction (NFPA, 1986). Although the extreme values are relatively large, they do not exceed maximum allowable stress.

Table 16. Forces and Deformations for Nail Connections between the Framing and Sheathing for Wall 1.

Dir.	Plywood		Gypsum	
	Force lbs (N)	Deformation in (mm)	Force lbs (N)	Deformation in (mm)
x	0-75 (0-334)	0.0-0.018 (0.0-0.46)	0-54 (0-240)	0.0-0.032 (0.0-0.8)
y	0-95 (0-414)	0.0-0.029 (0.0-0.74)	0-60 (0-267)	0.0-0.016 (0.0-0.41)
z	0-21 (0-93)	0.0-0.001 (0.0-0.025)	0-96 (0-427)	0.0-0.005 (0.0-0.13)

x,y - shear deformation
z - withdrawal

Summary

The stress analysis of the substructures gives the insight into the mechanism of the structural performance of individual building components. The finite-element analysis can be coupled with design criteria such as strength theory or a value of allowable stress (e.g. for nail shear) which speeds up a process of evaluation of individual structural components.

The forces in individual connections can be computed and results can be directly used to design the substructure.

13. CONCLUSIONS

The three-dimensional nonlinear finite-element model of light-frame timber structure was developed and studied. Based on the results from the full-scale testing and analytical study, the following conclusions can be drawn:

1. The concept of superelements is applicable to those parts of structure which behave in linear manner. The roof and floor system can be analyzed as linear superelements.

2. The nonlinear behavior of walls can be effectively modeled using quasi-superelement models which incorporate the nonlinear shear behavior, bending and torsional wall stiffness as well as resistance to axial forces. The error in plate stiffness caused by the coarse mesh (higher stiffness with coarser mesh) does not significantly influence the full structure model. The model is sufficiently accurate to simulate the actual wall behavior.

3. The intercomponent connections can be represented by one-dimensional nonlinear load-deformation elements. Their load-deformation properties can be obtained from experiments or from detailed three-dimensional finite-element models. Several connections can be clustered into one finite-element node to account for the difference between the number of nodes and number of connections.

4. The model can be subjected to any combination of static loading. For load combination effect, these must act simultaneously and load superposition is not valid as a consequence of the nonlinear behavior.

5. The current design procedures for horizontal loads lead to erroneous results because the differences in wall stiffness are neglected. The rigid-beam model can be used to make a more accurate assessment of shear forces in the shear walls.

6. Load sharing among the shear walls is a function of shear wall stiffness, roof diaphragm action and intercomponent stiffness. The presence of the roof diaphragm and proper wall-to-diaphragm connections are essential. The bending stiffness of the transverse walls does not significantly affect the load sharing capability of the system. The currently used intercomponent connections satisfactorily transfer forces between structural components and further increase of their stiffness does not lead to a significant improvement in load sharing.

7. Results from the full structure analysis can be effectively used to design structural components such as walls or connections. Direct application of design specifications is possible or three-dimensional models of substructures can be analyzed. This makes it possible to carry out the stress analysis of the substructure components and compute the forces and displacements in the individual connections.

8. The loading conditions examined here were for static and quasistatic loads only. An evaluation of the dynamic performance of the light-frame structure by using the same method of equivalent substructures may be possible.

12. BIBLIOGRAPHY

Adams, N.R. 1972. Plywood shear walls. American Plywood Association Laboratory Report 105. American Plywood Association. Tacoma, WA. 33 p.

American Plywood Association (APA). 1988. Design/Construction Guide. Residential & Commercial. APA. Tacoma, WA. 55 p.

_____ 1989a. APA Design/Construction Guide. Diaphragms. APA Tacoma, WA. 27 p.

_____ 1989b. PDS Plywood Design Specification. Tacoma, WA. 28 p.

Anonymous. 1990. Survey of Current Business. US Department of Commerce/Bureau of Economic Analysis. 70(10):5,S-7.

Applied Technology Council (ATC). 1981. Guidelines for the design of horizontal wood diaphragms. ATC. Berkeley, CA. 184 p.

Askhenazi, E.K., and E.V. Ganov. 1980. Anizotropia konstructsionnykh materialov. Spavotschnik. Machinostroenie. Leningrad. 267 p. [in Russian].

Bathe, K.-J. 1982. Finite element procedures in engineering analysis. Prentice-Hall, Inc. Englewood Cliffs, New Jersey. 735 p.

Batoz, J.L., K.J. Bathe, and L.W. Ho. 1980. A study of three-node triangular plate bending elements. International Journal for Numerical Methods in Engineering. 15(6):1771-1812.

Bodig, J., and B.A. Jayne. 1982. Mechanics of wood and wood composites. Van Nostrand Reinhold Company. New York. 712 p.

Boughton, G.N. 1988. Full scale structural testing of houses under cyclonic wind loads. p.82-88. In Proceedings of The 1988 International Conference on Timber Engineering. October, 1988. Seattle, WA. Forest Products Research Society, Madison, WI.

Breyer, D.E. 1988. Design of wood structures. McGraw-Hill Book Company. New York. 680 p.

Cheung, K.G., R.Y. Itani, and A. Polensek. 1988. Characteristics of wood diaphragms: Experimental and parametric studies. Wood and Fiber Science. 20(4):438-456.

Chou, C. 1987. Modeling of nonlinear stiffness and nonviscous damping in nailed joints between wood and plywood. Ph.D. dissertation. Oregon State University, Corvallis, OR.

Cook, R.D. 1981. Concepts and applications of finite element analysis. John Willey & Sons. New York., N.Y. 537 p.

Corder, S.E., G.H. Atherton, and A. Polensek. 1966. Side-loaded tests of stuccoed frame walls. FRL report T-21. Oregon State University Corvallis, OR. 12 p.

_____, and D.E. Jordan. 1975. Some performance characteristics of wood joist floor panels. Forest Products Journal. 25(2):38-44.

Cramer, S.M., and R.W. Wolfe. 1989. Load-distribution model for light-frame wood roof assemblies. Journal of Structural Engineering. 115(10):2603-2616.

Deutsche Industrie Norm. DIN 1052. T1. 1969. Holzbauwerke. Berechnung und Ausfűhrung [in German]. Springer Verlag, Heidelberg, Germany.

Dolan, J.D. 1989. The dynamic response of timber shear walls. Ph.D. thesis. Dept. of Civil Engineering. University of British Columbia. Vancouver, BC. Canada. 318 p.

Dutko, P. 1976. Wood Structures [in Slovak]. ALFA. Bratislava. Czechoslovakia. 460 p.

Easley, J.T., M. Foomani, and R.H. Dodds. 1982. Formulas for wood shear walls. Journal of the Structural Division. Proceedings of ASCE. 108 (ST11):2461-2478.

Ehlbeck, J. 1979. Nailed joints in wood structures. Virginia Polytechnic Institute Rep. No. 166. Virginia Polytechnic Institute & State University, Blacksburg, VA. 147 p.

Forest Products Laboratory. 1965. Nail-withdrawal resistance of American woods. Forest Products Laboratory Research Note FPL-093. U.S. Forest Service Madison, WI. 5 p.

Ge, Y.Z., S. Gopalaratnan, and H. Liu. 1991. Effect of openings on the stiffness of wood-frame walls. Forest Products Journal. 41 (1): 65-70.

Gerald, C.S., and P.O. Wheatley. 1984. Applied Numerical Analysis. Addison-Wesley Publishing Company. Reading, MS. 579 p.

Glos, P., D. Henrici, and B. Schmelmer. 1987. Festigkeit von ein- und zweiseitig baplankten Wandelementen [in German]. Holz als Roh- und Werkstoff. 45(1):41-48.

Glos, P., D. Henrici, and H. Horstmann. 1990. Versuche mit großflächig geleimten Stabwerken [in German]. Holz als Roh- und Werkstoff. 48(9):333-338.

Gopu, V.K.A., and N. Kumar. 1988. Finite-element analysis of wood floor systems with GTSTRUDL. p.29-36. In Proceedings of The 1988 International Conference on Timber Engineering. R.F. Itani. Washington State University. Pullman, WA.

Gromala, D.S. 1985. Lateral nail resistance for ten common sheathing materials. Forest Products Journal. 36(9):61-68.

_____, and A. Polensek. 1982. Analysis and design of wall systems under axial and bending loads. USDA Madison, WI. 12 p.

_____, and A. Polensek. 1984. Light-frame wall research--Axial and bending loads. Housing Science. 8(4):383-394.

Groom, K.M. 1992. Nonlinear finite-element modeling of intercomponent connections in light-frame wood structures. M.S. thesis. Oregon State University, Corvallis, OR.

_____, and R. J. Leichti. 1991. Finite-element model of a nonlinear intercomponent connection in light-framed structures. p. 346-353. In 1991 International Timber Engineering Conference. September 1991. London, England. Vol. 4. Timber Research and Development Association. High Wycombe. England.

Gupta, A.K., and P.H.Kuo. 1984. Behavior of wood framed shear walls. Department of Civil Engineering. North Carolina State University. Raleigh, NC. 30 p.

_____, and G.P.Kuo. 1985. Behavior of wood-framed shear walls. Journal of Structural Engineering. 11(8):1722-1733.

_____, and G.P.Kuo. 1987. Wood-framed shear walls with uplifting. Journal of Structural Engineering. 223(2):241-259.

Hata, M., and H.Sasaki. 1987. Structural analysis of racking behavior of nailed stressed-skin panels and behavior of transmitted forces through nails. I. Mokuzai Gakkaishi. 33(1):12-18.

_____, S. Takino, and H. Sasaki. 1988. Structural analysis of racking behavior of nailed stressed-skin panels and behavior of transmitted forces through nails. II. Mokuzai Gakkaishi. 34(9):718-723.

Hayashi, K. 1989. Studies on methods to estimate the racking resistance of houses with wooden wall panels (Part 2 Theoretical study (1)). p 113-118. In Proceedings of The Second Pacific Timber Engineering Conference 1989, Vol. 2. September, 1989. Auckland, New Zealand. University of Auckland, Auckland, New Zealand.

Haynes, R.W. 1989. An analysis of the timber situation in the United States:1989-2040. Part I: The current resource and use situation. USDA-Forest Service. Washington, D.C. 281 p.

International Conference of Building Officials (ICBO). 1988. Uniform Building Code. ICBO. Whittier, CA. 926 p.

International Mathematics Subroutine Library (IMSL). User's Manual. IMSL Math/Library$^{T.M.}$. Version 1.1. January 1989. IMSL Houston. TX. 1151 p.

Institute for Standardization and Testing (UNM). 1984. Design of wood structures. CSN 73 1701. UNM Prague. Czechoslovakia. 92 p. [in Slovak]

Itani, R.Y., H.M. Morshed, and R.J. Hoyle. 1981. Experimental evaluation of composite action. Journal of the Structural Division. 107(ST3):551-565.

Itani, R.Y., and K.C. Cheung. 1984. Nonlinear analysis of sheathed wood diaphragms. Journal of Structural Engineering. 110(9):2137-2147.

Itani, R.Y., and F.M. Robledo. 1984. Finite-element modeling of light-frame wood walls. Civil Engineering for Practicing and Design Engineers. 3: 1029-1045.

Jenkins, J.L., A. Polensek, and K.M. Bastendorf. 1979. Stiffness of nailed wall joints under short and long-term lateral loads. Wood Science. 11(3):145-154.

Jones, R. J. 1975. Mechanics of composite materials. Hemisphere Publishing Corporation. New York. 355 p.

Kasal, B., M. Wang, and R. J. Leichti. 1991. A Nonlinear finite-element model for wood-frame stud walls. p.325-333. In 1991 International Timber Engineering Conference. Vol. 4. September, 1991. London, England. Timber Research and Development Association. High Wycombe, England.

Katakoa, Y. 1989. Application of supercomputers to onlinear analysis of wooden frame structures stiffened by shear diaphragms. p. 107-112. In Proceedings of The Second Pacific Timber Engineering Conference, Vol. 2. September, 1989. Auckland, New Zealand. University of Auckland. Auckland, New Zealand.

Kikuchi, N. 1986. Finite element methods in mechanics. Cambridge University Press. Cambridge. England. 418 p.

Kolar, V. 1982. Analytical Models of Geometrically Orthotropic Plates. Transportation Structures Design Institute. Brno, Czechoslovakia. 214 p. [in Czech]

Kohnke, P.C. 1989. ANSYS Engineering Analysis System Theoretical Manual. Swanson Analysis Systems, Inc., Houghton, Pennsylvania. 412 p.

Koželouh, B., and M. Najdekr. 1986. [Securing the 3-dimensional stiffness of the wood structure.] [In Czech]. Pozemni Stavby (12): 551-557.

Lafave, K. D. 1990. Experimental and Analytical Study of Load Sharing in Wood Truss Roof Systems. M.S. thesis. Washington State University. Pullman, WA. 120 p.

Laursen, H.I. 1988. Structural analysis. McGraw-Hill. New York. 475 p.

Lekhnitskii, S.G. 1987. Anisotropic Plates. Gordon and Breach Science Publishers. New York, N.Y. p. 534.

Liu, J.Y. and L.A. Soltis. 1984. Lateral resistance of nailed joints - A test method. Forest Products Journal. 34(1):55-60.

Loferski, J.R., and A.Polensek. 1982. Predicting inelastic stiffness moduli of sheathing to stud nail joints. Wood Science. 15(1):39-43.

Malmeister, A.K. 1966. Geometria teorii protschnosti. Mekhanika Polymerov (Polymer Mechanics). [in Russian]. 4 (11):519-534.

Malmeister, A.K., V.P. Tamuzh, and G.A. Teters. 1972. The strength of rigid polymer materials. Translation from Russian. US Department of Commerce. Washington, D.C. 486 p.

McLain, T.E. 1991. Engineered wood connections and the 1991 National Design Specification. Wood Design Focus. 2(2):7:10.

McCutcheon, W.J., R. L. Tuomi, R. W. Wolfe, and D.S. Gromala. 1979. Toward improved structural design of housing components. Housing: Planning, Financing, Construction. p. 734-749. In Proceedings of International Conference on Housing Planning, Financing, Construction. Miami Beach, FL.

Moody, R.C., and R.J. Schmidt. 1988. Lateral loading of wood frame houses - Analysis and performance. p. 62-72. In Proceedings of The 1988 International Conference on Timber Engineering, Vol. 1. October, 1988. Seattle, WA. Forest Products Research Society, Madison, WI.

Najdekr, M. 1989. Zur Analyse geleimter doppelschaliger Holztafel-Elemente [in German]. Holz als Roh- und Werkstoff 47:61-66.

National Association of Home Builders (NAHB) Research Foundation. 1965. Structural performance of wood frame load bearing wall panel system for the American Plywood Association. Research Report CR 185-A. NAHB Research Institute, Inc. Rockville, Maryland. 23 p.

National Forest Products Association (NFPA). 1986. National Design Specification for Wood Construction. Washington, D.C. 87 p.

Nelson, E.L., D.L. Wheat, and D.W. Fowler. 1985. Structural behavior of wood shear wall assemblies. Journal of Structural Engineering. 111(3):654-666.

Nicol-Smith, C.A. 1977. Two-way action of pitched roofs. Forest Products Journal. 5(5):55.

Ohashi, Y., and I. Sakamoto. 1988. Effect of horizontal diaphragm on behavior of wooden dwellings subjected to lateral load - Experimental study on a real size frame model. p.112-120. In Proceedings of The 1988 International Conference on Timber Engineering, Vol. 1. October, 1988. Seattle, WA. Forest Products Research Society, Madison, WI.

Okabe, M., N. Maruyama, and T. Arima. 1985. The effect of the structural performance of post and beam construction with wood-frame panels. I. Mokuzai Gakkaishi. 31(8):648-656.

Oliva, M.G. 1990. Racking behavior of wood-framed gypsum panels under dynamic load. Earthquake Engineering Research Center Report No. UCB/EERC-85/06. College of Engineering. University of California. Berkeley, CA. 49 p.

Pellicane, P.J., and J. Bodig. 1982. Comparative study of several testing techniques to evaluate nail-slip modulus. Special Report WSL-1. Colorado State University. Fort Collins, CO. 14 p.

Peterson, J. 1983. Bibliography on lumber and wood panel diaphragms. Journal of the Structural Division, Proceedings of the American Society of Civil Engineers. 109(ST12):2838-2852.

Phillips, T.L. 1990. Load sharing characteristics of three-dimensional wood diaphragms. M.S. thesis. Washington State University. Pullman, WA. 236 p.

Pierce, C.B. 1982. The analysis of load distribution between rafters in a traditional timber roof structure Part 2: Simulations under concentrated loads. Building Research Establishment Current Paper. CP 3/82. Princes Risborough, England. 10 p.

_____, and P.S.K. Harrod. 1982. The analysis of load distribution between rafters in a traditional timber roof structure. Part 1: Building and validating a computer model. Building Research Establishment Current Paper. CP 2/82. Princes Risborough, England. 15 p.

Polensek, A. 1975. Finite element method for wood-stud walls under bending and compression loads. Research Report F-914. Department of Forest Products. Oregon State University, Corvallis, OR. 69 p.

_____ 1976a. Nonlinear behavior of nailed wood-stud walls at service loads and overloads. p. 1938-1952. In Proceedings, Second International Conference on Mechanical Behavior of Materials. Federation of Material Society, Boston. Mass.

_____ 1976b. Finite element analysis of wood-stud walls. Journal of the Structural Division, Proceedings of American Society of Civil Engineers. 102(ST7):1317-1335.

_____ 1976c. Rational design procedure for wood-stud walls under bending and compression loads. Wood Science. 9(1):8-20.

_____ 1978. Properties of components and joints for rational design procedure of wood-stud walls. Wood Science. 10(4):167-175.

_____ 1982. Effect of construction variables on performance of wood-stud walls. Forest Products Journal. 32(5):37-41.

_____ 1983. Structural analysis of light-frame wood buildings. p. 189-205. In Structural Wood Research, State-of-the-Art and Research Needs. R.Y. Itani and F.F. Faherty (ed.). American Society of Civil Engineers. New York, NY.

_____. 1989. Personal communications.

_____, and G.H. Atherton. 1976. Compression-bending strength and stiffness of walls with utility grade studs. Forest Products Journal. 26(11):17-25.

_____, G.H.Atherton, S.E. Corder, and J.L. Jenkins. 1972. Response of nailed wood-joist floor to static loads. Forest Products Journal. 22(9):52-61.

_____, and K.M. Bastendorff. 1982. Wood-stud walls: stiffness of joints between studs and hardwood paneling. Forest Products Journal. 32(7):51-53.

_____, and K.M. Bastendorff. 1987. Damping in nailed joints of light-frame wood buildings. Wood and Fiber Science. 19(2):110-125.

_____, and Schimel B. 1986. Rotational restraint of wood-stud wall supports. Journal of Structural Engineering. 112 (6):1247-1262.

_____, and B. D. Schimmel. 1991. Dynamic properties of light-frame wood subsystems. Journal of Structural Engineering. 117(4):1079-1095.

_____, and R.H. White. 1979. Analysis of support restraint of wood-stud walls. ASCE Convention & Exposition. Preprint 3642. Atlanta. 17 p.

Reardon, G.F. 1989. Effect of cladding on the response of houses to wind forces. p. 101-105. In Proceedings of The Second Pacific Timber Engineering Conference 1989, Vol 2. September, 1989. Auckland, New Zealand. University of Auckland. Auckland, New Zealand.

Reddy, J.N. 1984. An introduction to the finite element method. McGraw Hill. New York. 495 p.

Sadakata, K. 1988. Study on evaluation of aseismatic performance of neoconventional wooden frame structures assembled by using highly ductile connection fittings. p. 73-81. In Proceedings of The 1988 International Conference on Timber Engineering, Vol. 2, October, 1988. Seattle, WA. Forest Products Research Society, WI.

Sasaki, Y., S. Miura, and T.Takemura. 1988. Non-linear analysis of semi-rigid jointed metal-plate wood-truss. Mokuzai Gakkaishi. 34(2):120-125.

Sazinski, R.J., and M.D. Vanderbilt. 1979. Behavior and design of wood joist floors. Wood Science. 11(4):209-220.

Schmidt, R.J., and R.C. Moody. 1989. Modeling laterally loaded light-frame buildings. Journal of Structural Engineering. 115(1):201-217.

Scholten, J.A. 1965. Strength of wood joints made with nails, staples, or screws. USDA Forest Service Research Note FPL-0100. Madison, WI. 16 p.

Smith, I. 1979. Design of simply supported stressed skin panels with a uniformly distributed transverse load. Timber Research and Development Association (TRADA) Research Report 2/79. Hughenden Valley. England. 60 p.

Stasa, F.L. 1985. Applied Finite Element Analysis for Engineers. Holt, Rinehart and Winston. New York, NY. 657 p.

Steward, W.G., J.R. Goodman, A. Kliewer, and E.M. Salsbury. 1988. Full-scale tests of manufactured houses under simulated wind loads. p.97-111. In Proceedings of The 1988 International Conference on Timber Engineering, Vol. 1. October, 1988. Seattle, WA. Forest Products Research Society, Madison, WI.

Sugyiama, H., N. Andoh, T. Uchisako, S. Hirano, and N. Nakamura. 1988. Full-scale test on a Japanese type of two-story wooden frame house subjected to lateral load. p.55-61. In Proceedings of The 1988 International Conference on Timber Engineering, Vol. 1. October, 1988. Seattle, WA. Forest Products Research Society, Madison, WI.

Takayanagi, H., K. Kemmochi, and R. Hayashi. 1990. The effect of elements on the rigidity and strength of wall panels subjected to racking loads. Mokuzai Gakkaishi. 36(8):679-688.

Thoft-Christensen, P., and M.J. Baker. 1982. Structural reliability theory and its application. Springer Verlag. New York, N.Y. 267 p.

Timoshenko, S., and S. Woinowsky-Krieger. 1987. Theory of plates and shells. McGraw-Hill. New York, NY. 580 p.

Tissell, J.R. and J.E. Elliott. 1990. Plywood Diaphragms. APA Research Report 138. American Plywood Association. Tacoma, WA. 55 p.

Tokuda, M. 1983. Mechanics of nail withdrawal resistance. I. Evaluation of normal stress exerted by the surrounding wood on a nail with a small load-cell. Mokuzai Gakkaishi. 29(9):566-571.

_____ 1985. Measurement of shearing forces induced on nails holding sheathing to frames in wall-racking tests. Mokuzai Gakkaishi. 31(1):39-42.

Tsai, S.W., and E.M. Wu. 1971. A general theory of strength for anisotropic materials. Journal of Composite Materials. (1): 58-80.

Tsujino, T. 1985. Bending analysis of nailed single stressed-skin panel by finite-element method. Mokuzai Gakkaishi. 31(11):896-902.

Tuomi, R.L. 1980. Full-scale testing of wood structures. p.45-62. Full-Scale Load Testing of Structures. ASTM STP 702. W.R. Schriever (ed.). American Society of Testing and Materials. New York, NY.

_____, and W.J. McCutcheon. 1974. Testing of a full-scale house under simulated snowloads and windloads. Research Paper. FPL 234. USDA Forest Service, Forest Productrs aboratory, Madison. WI. 32 p.

_____, and W.J. McCutcheon. 1978. Racking strength of light-frame nailed walls. Journal of the Structural Division. Proceedings of American Society of Civil Engineers. 104(ST7):1131-1140.

Turnbull, J.E., K.C. McMartin, and A.T. Quaile. 1982. Structural performance of plywood and steel ceiling diaphragms. Canadian Agricultural Engineering. 24(2):135-140.

Walker, G.R., G.F. Reardon, and G.N. Boughton. 1984. Testing houses for cyclone resistance. Proceedings of Northern Engineering Conference. Australia.

Wheat, D.L., M.D. Vanderbilt, and J.R. Goodman. 1983. Wood floors with nonlinear nail stiffness. Journal of Structural Engineering. 109(5):1290-1302.

_____, D.S. Gromala, and R.S. Moody. 1986a. Static behavior of wood-joist floors at various limit states. Journal of Structural Engineering. 112(7):1677-1691.

_____, D.C. Shock, and L.M. Wolf. 1986b. Nail slip in wood-joist floors. Forest Products Journal. 36(11/12):29-32.

Wolfe, R.W. 1983. Contribution of gypsum wallboard to racking resistance of light-frame walls. USDA Research Paper. FPL-RP-439. Madison, WI. 23 p.

_____, and M. McCarthy. 1989. Structural performance of light-frame roof assemblies. I. Truss assemblies with high truss stiffness variability. Research Paper FPL-RP-492. USDA-Forest Service, Forest Products Laboratory. Madison, WI. 41 p.

Yasumura, M., T. Murota, I. Nishiyama, and N. Yamaguchi. 1988. Experiments on a three-storied wooden frame building subjected to horizontal load. p. 262-275. In Proceedings of The 1988 International Conference on Timber Engineering, Vol. 1. October, 1988. Seattle, WA. Forest Products Research Society, Madison, WI.

Zienkiewicz, O.C. 1982. The Finite Element Method in Engineering Science. McGraw-Hill. London, England. 787 p.

APPENDICES

APPENDIX A
Drawings of the Experimental Building

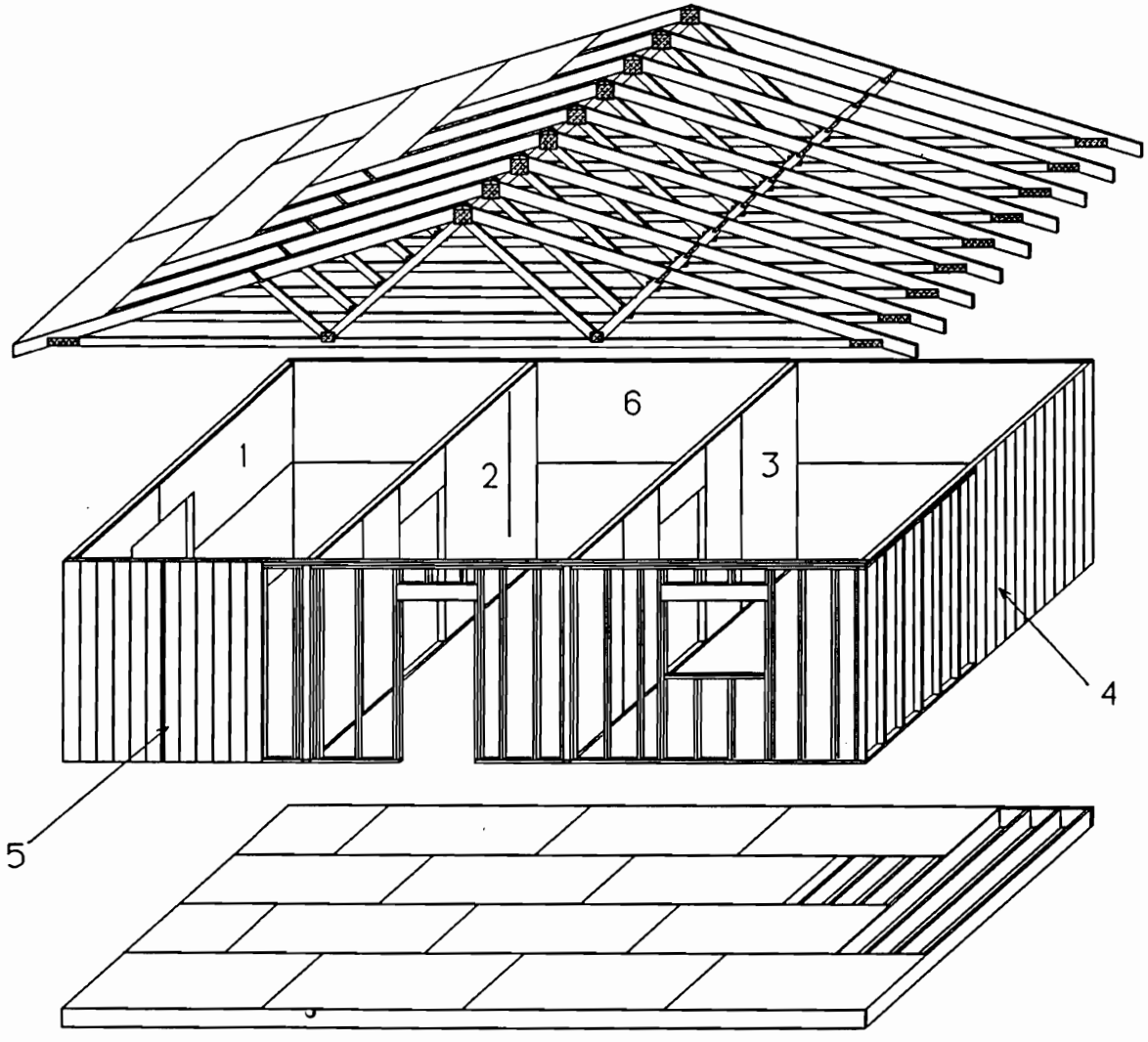

Figure A1. Three-Dimensional View of the Experimental Structure (Phillips, 1990).

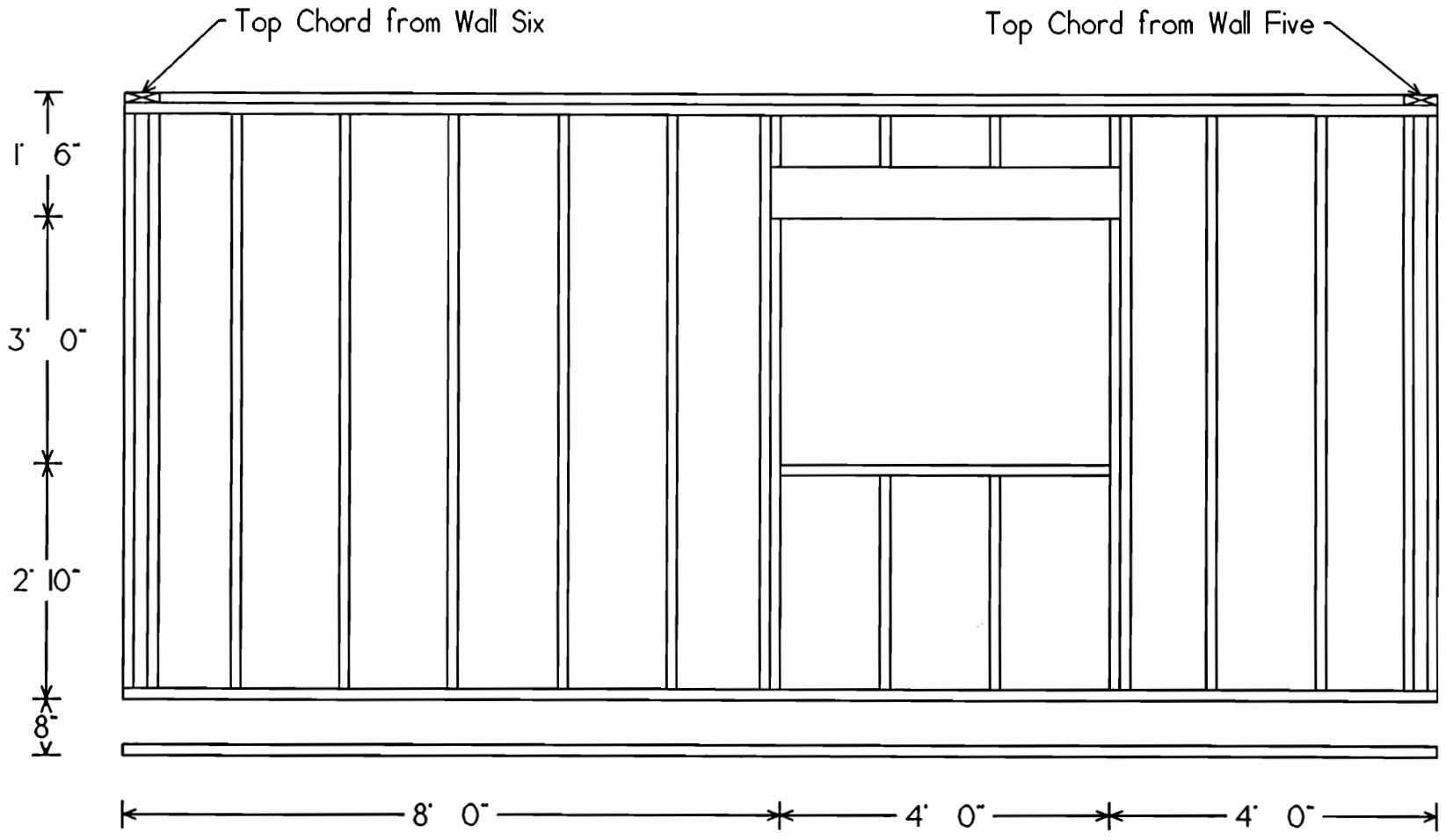

Figure A2. Framing of Wall 1.

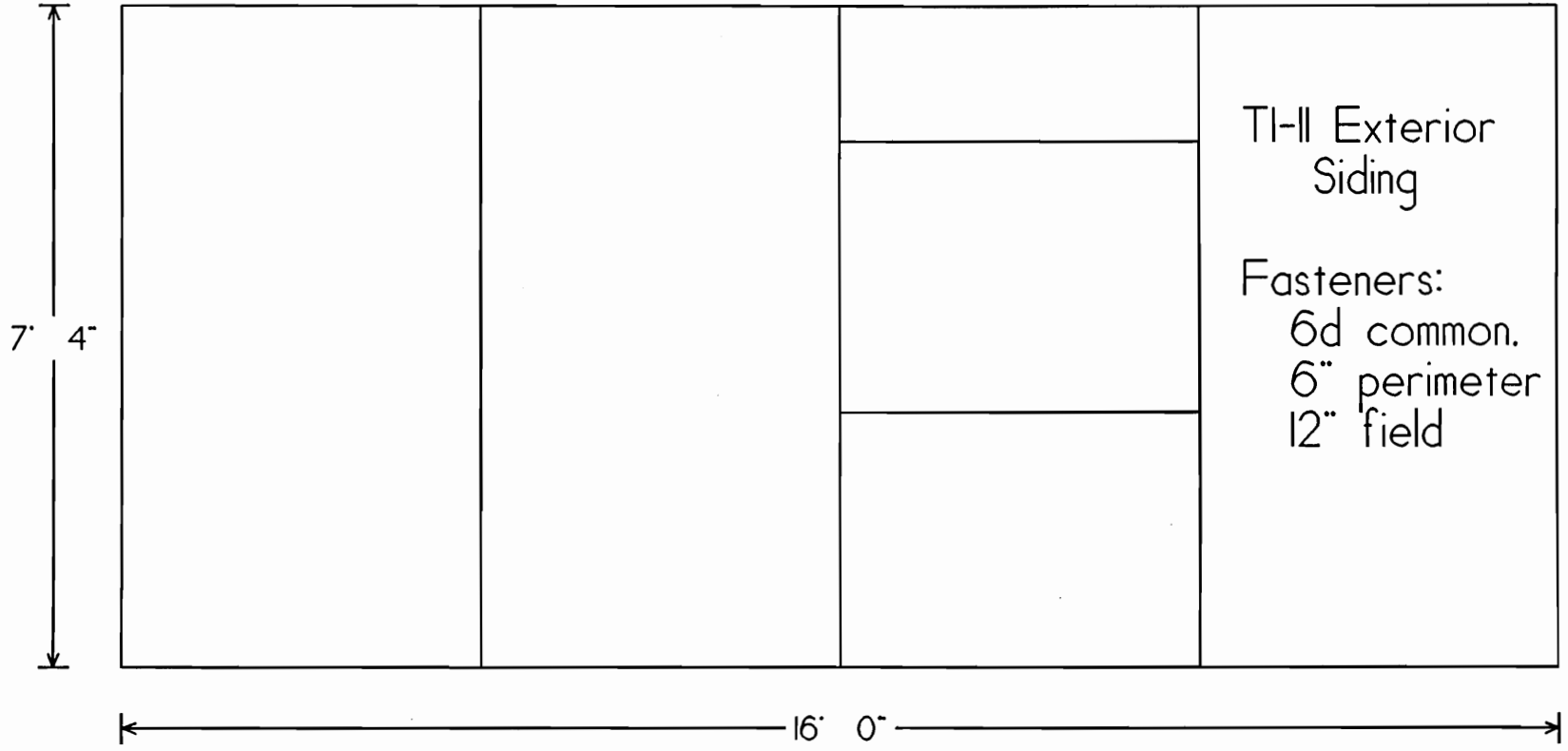

Figure A3. Plywood Sheathing of Wall 1.

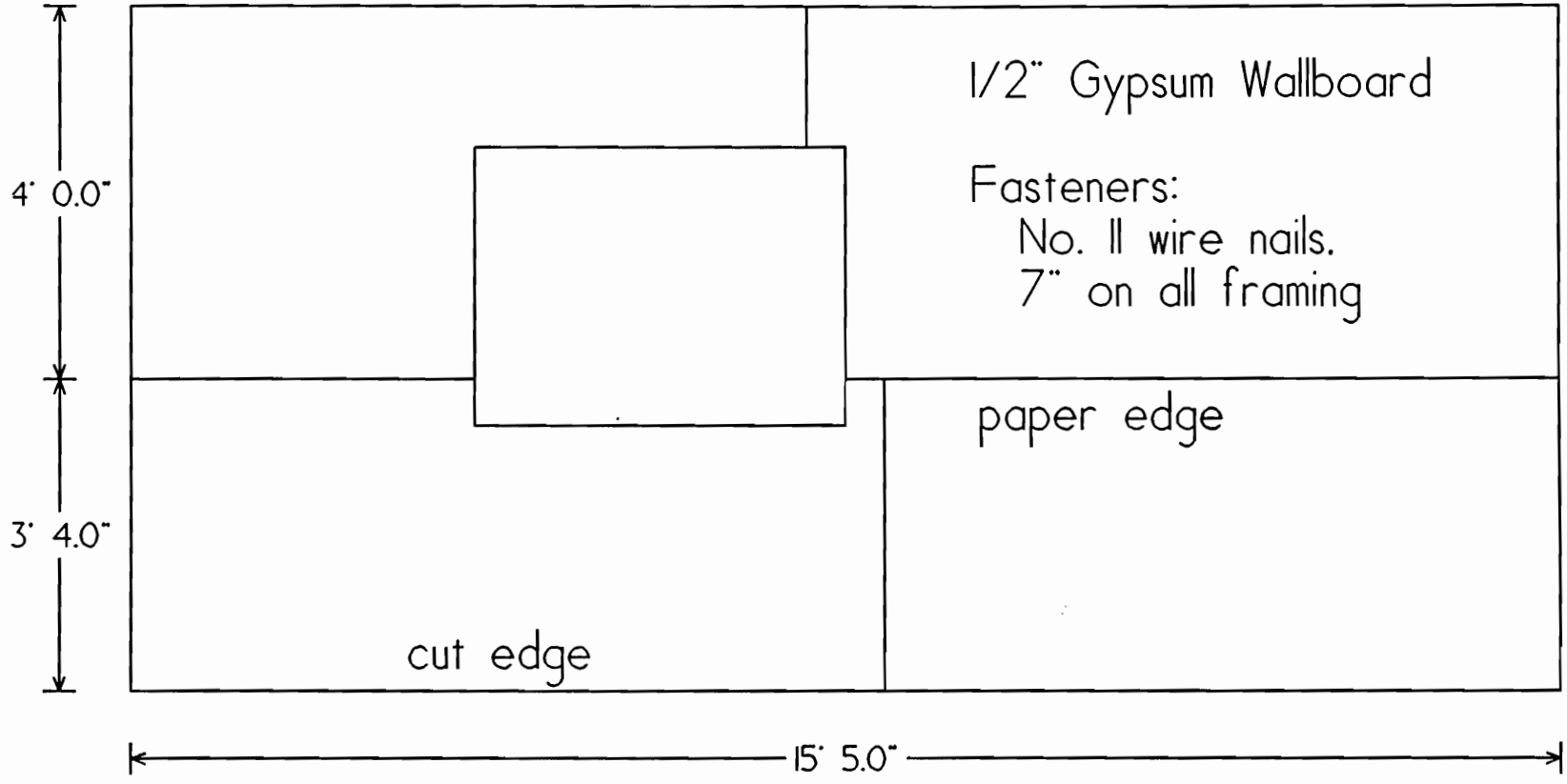

Figure A4. Gypsum Sheathing of Wall 1.

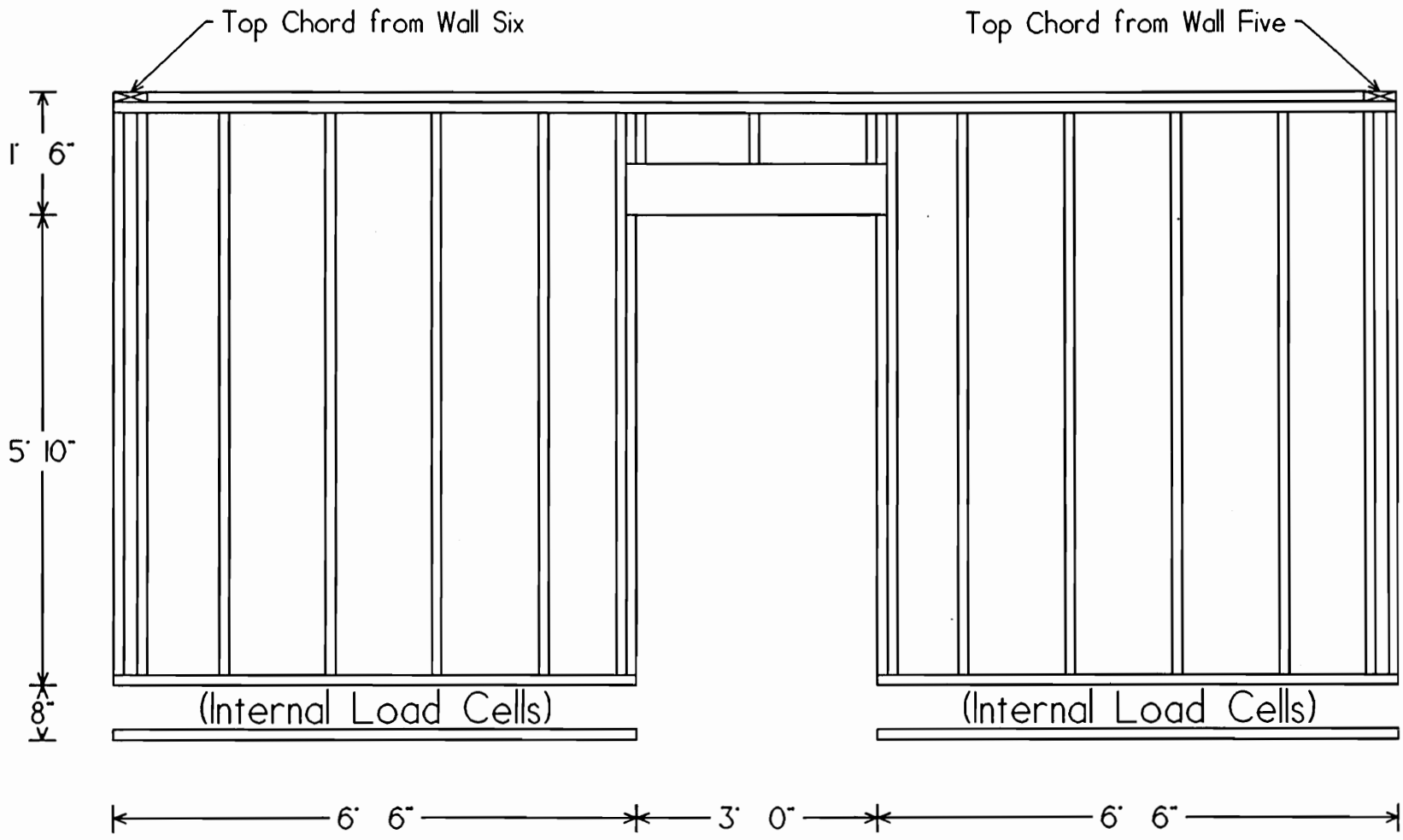

Figure A5. Framing of Walls 2 and 3.

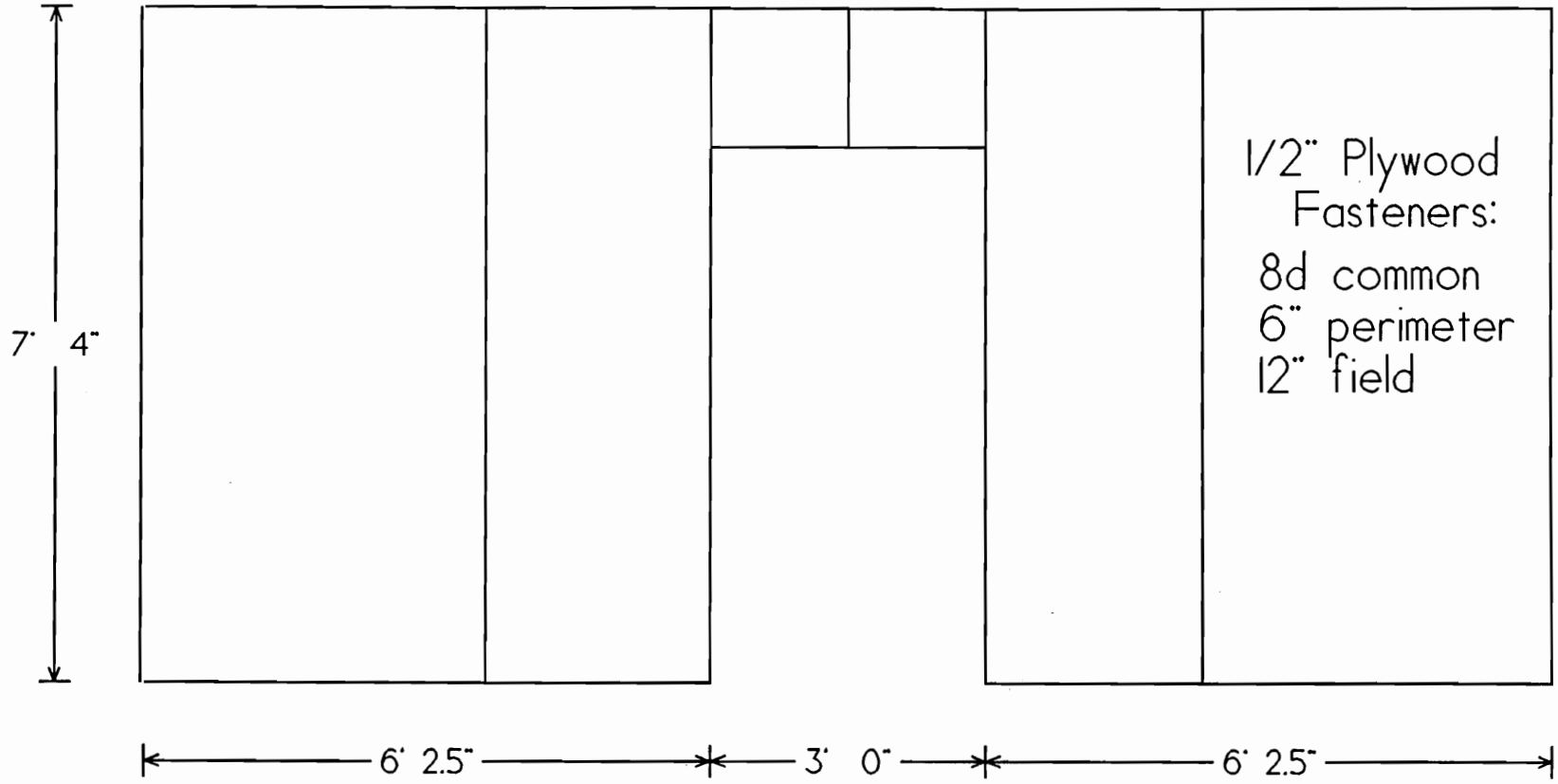

Figure A6. Plywood Sheathing of Wall 2.

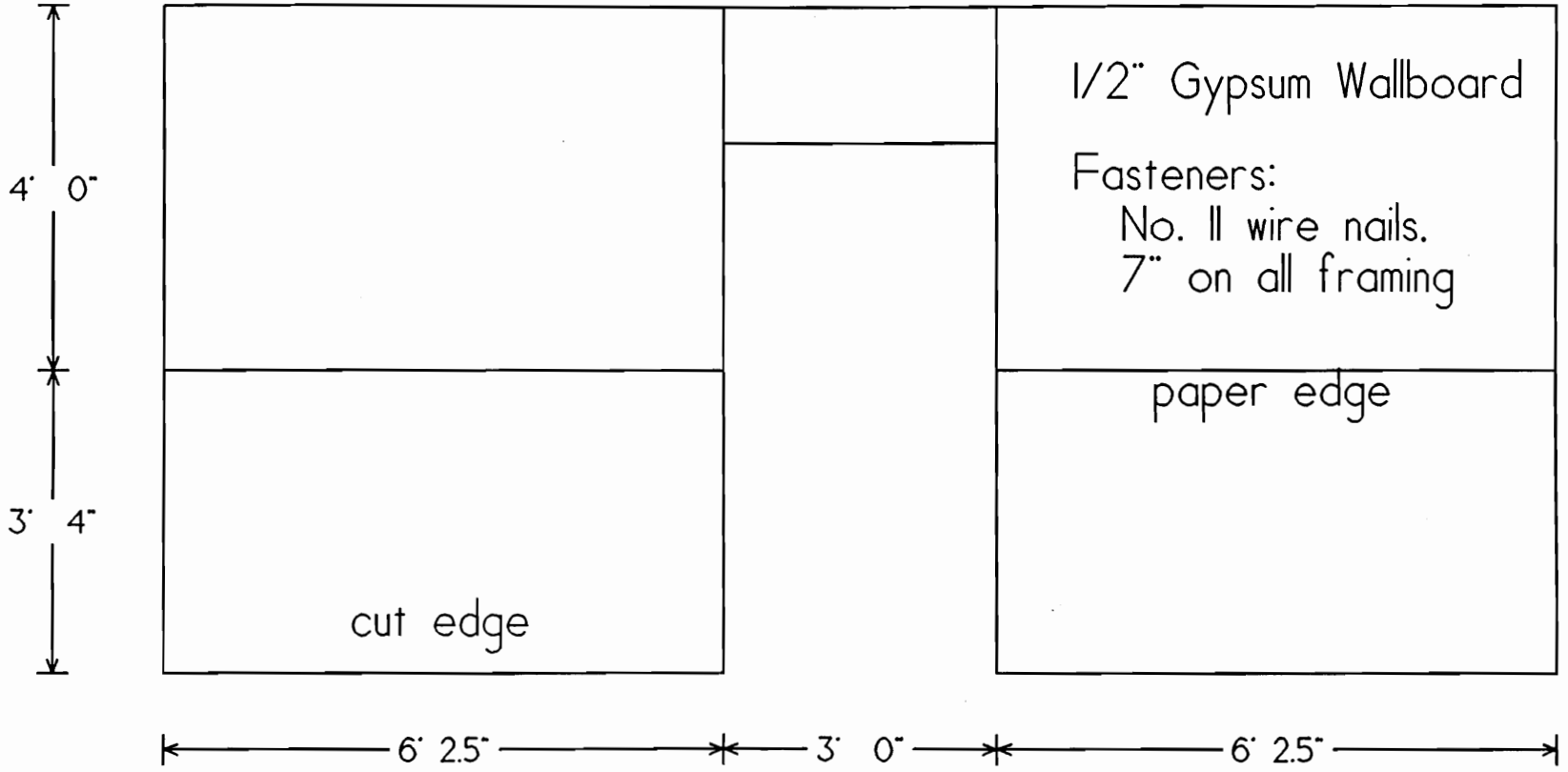

Figure A7. Gypsum Sheathing of Wall 3.

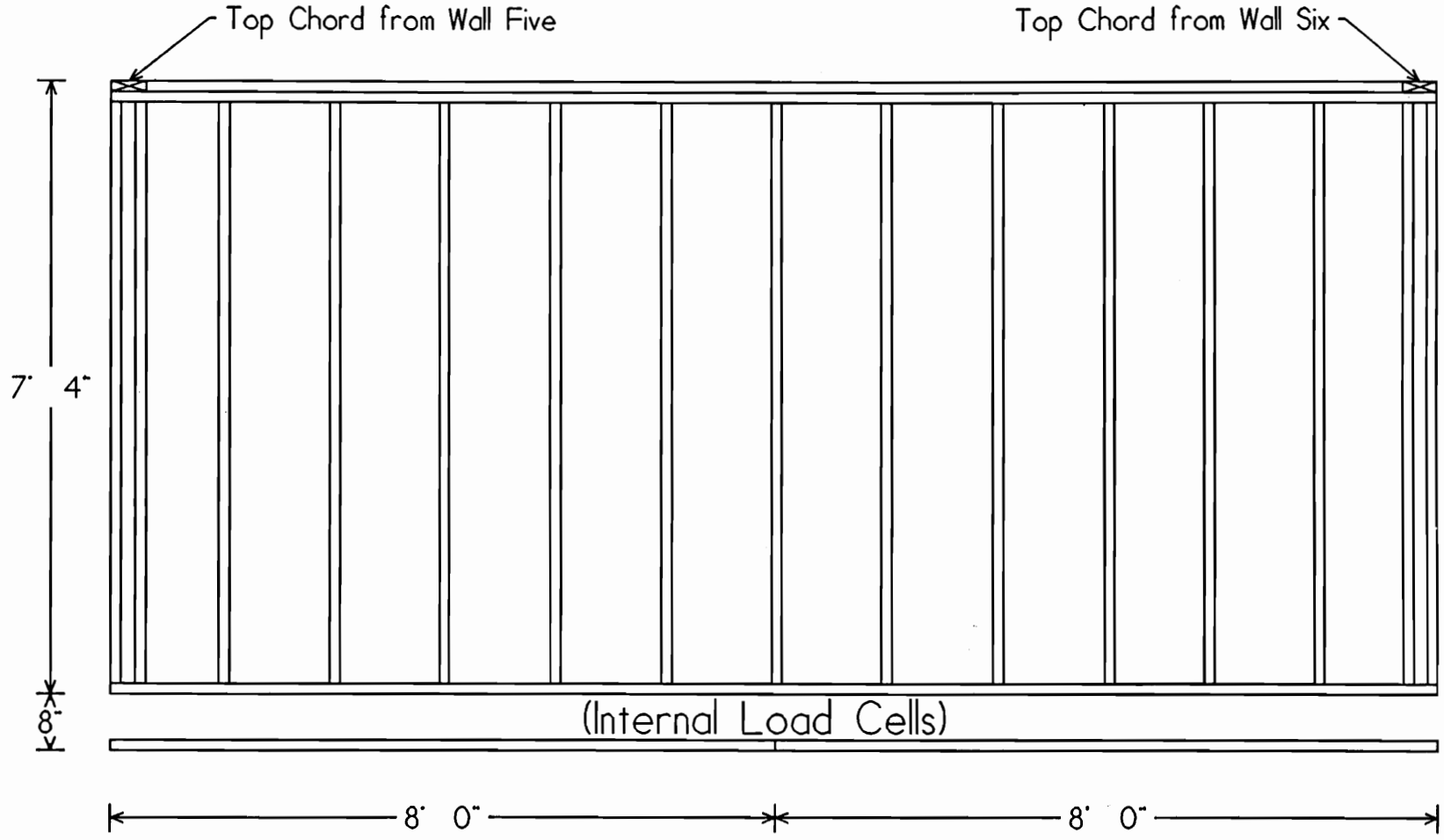

Figure A8. Framing of Wall 4.

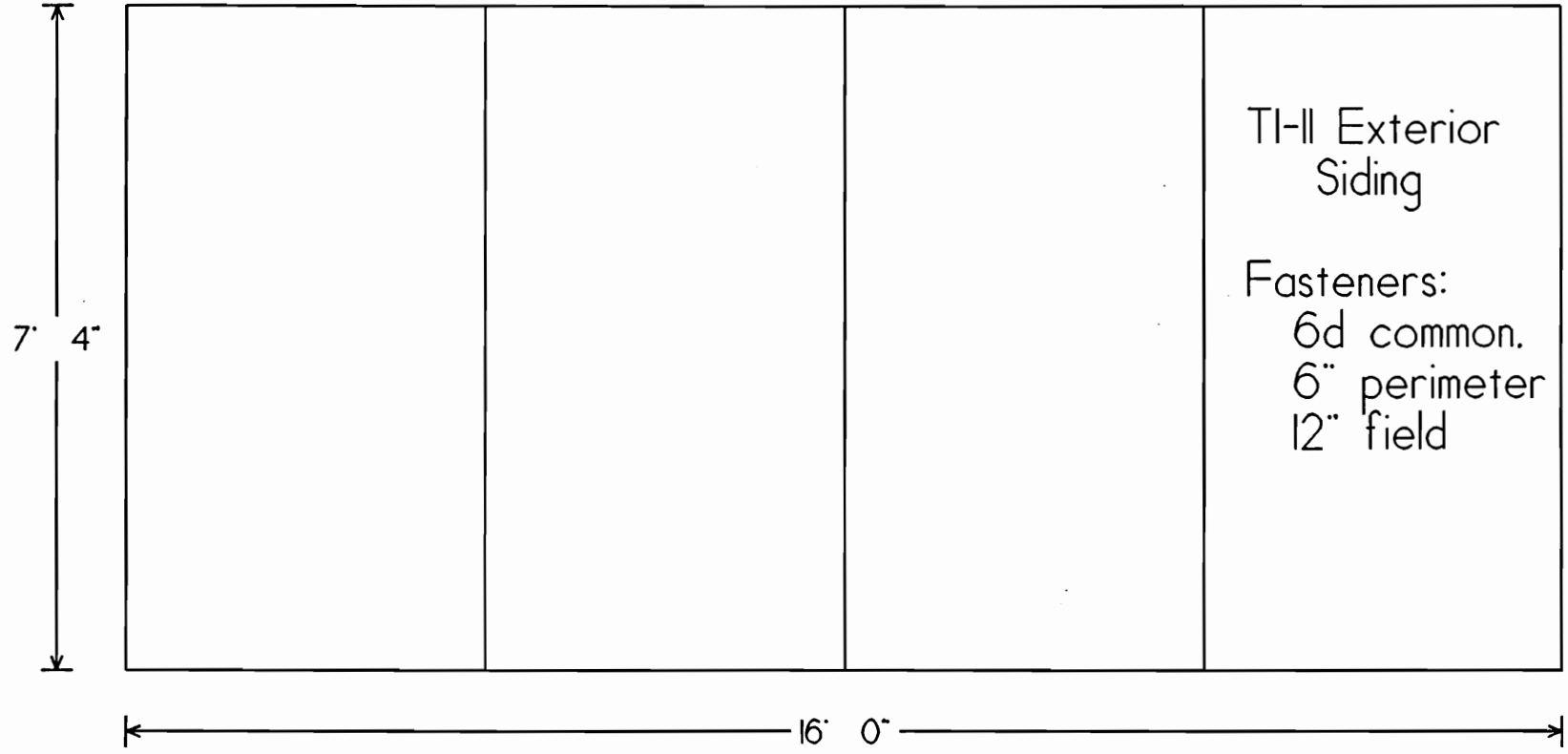

Figure A9. Plywood Sheathing of Wall 4.

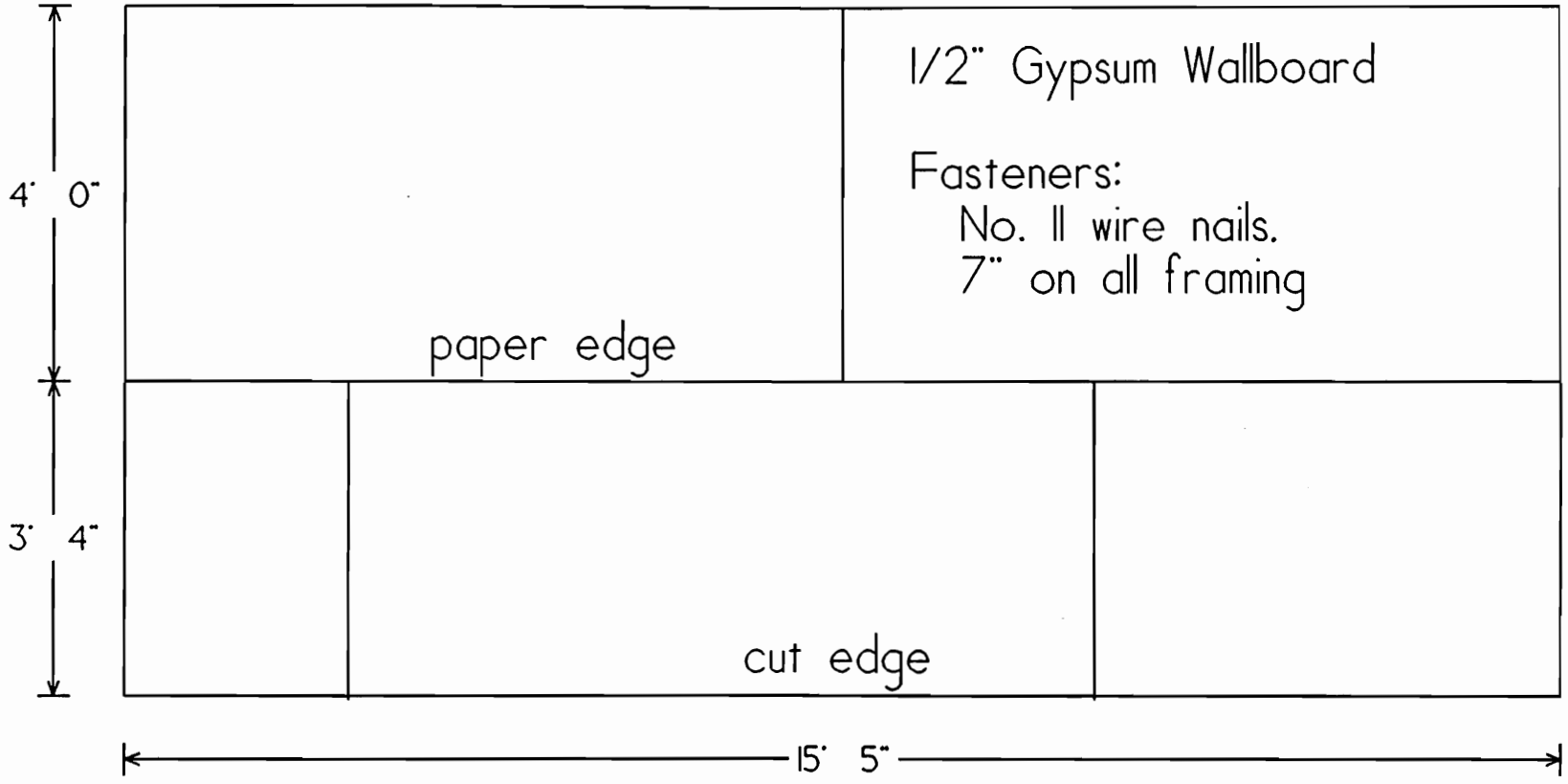

Figure A10. Gypsum Sheathing of Wall 4.

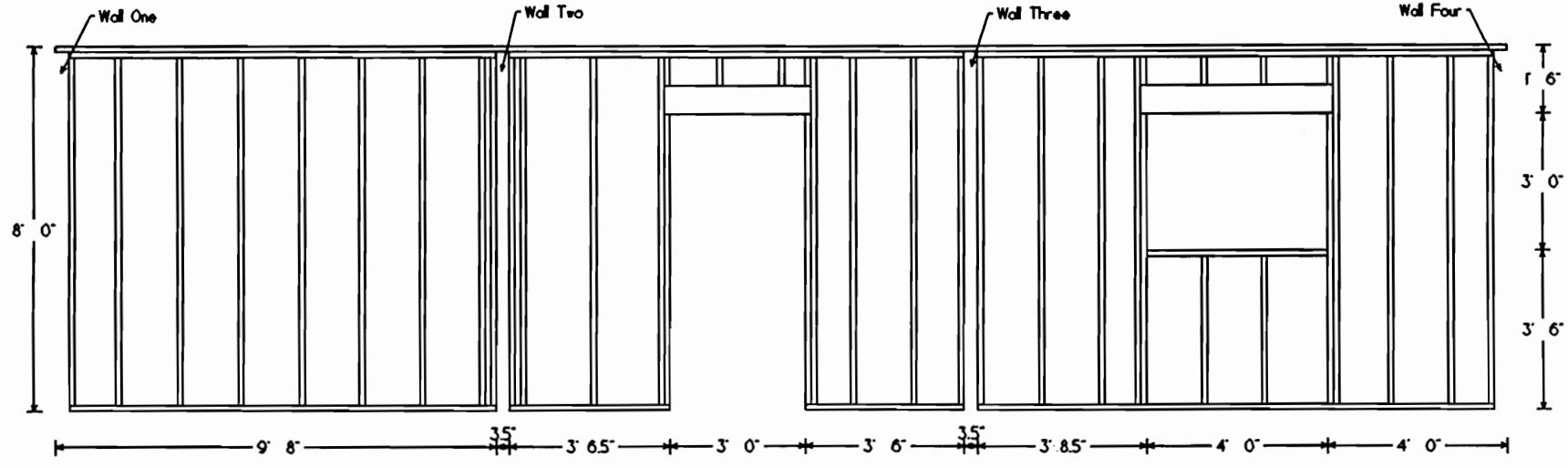

Figure A11. Framing of Wall 5.

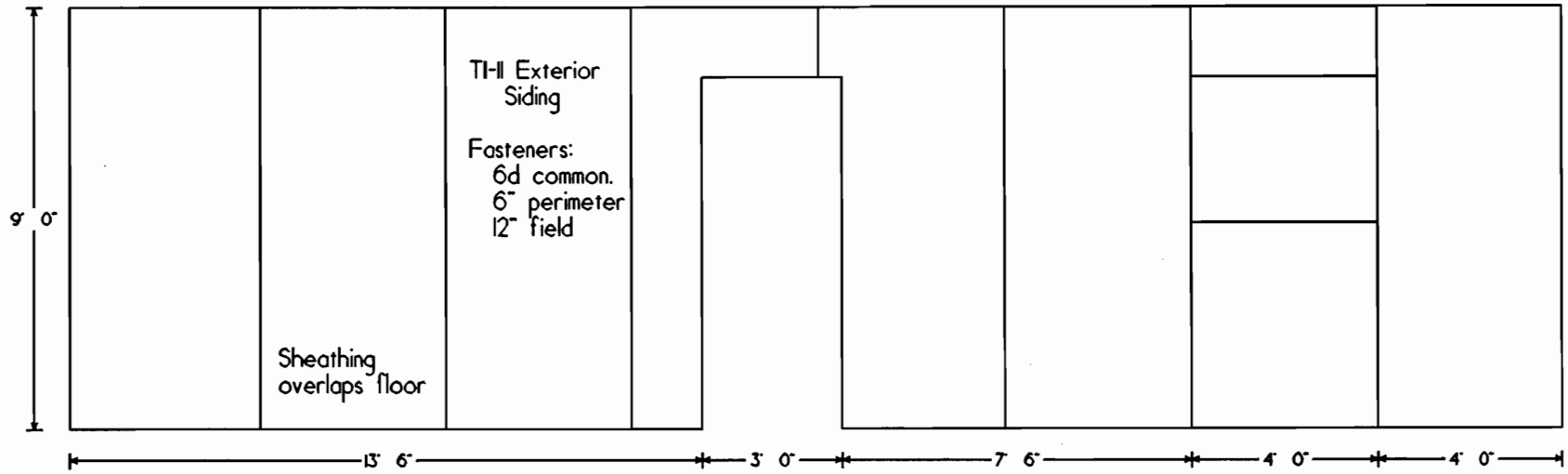

Figure A12. Plywood Sheathing of Wall 5.

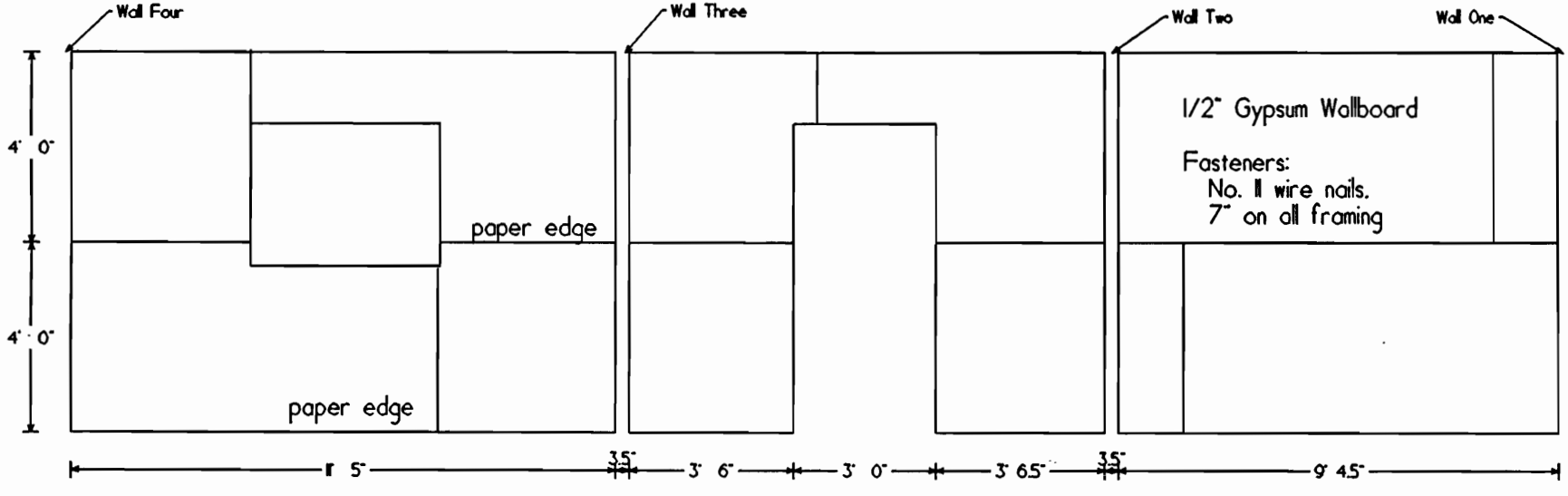

Figure A13. Gypsum Sheathing of Wall 5.

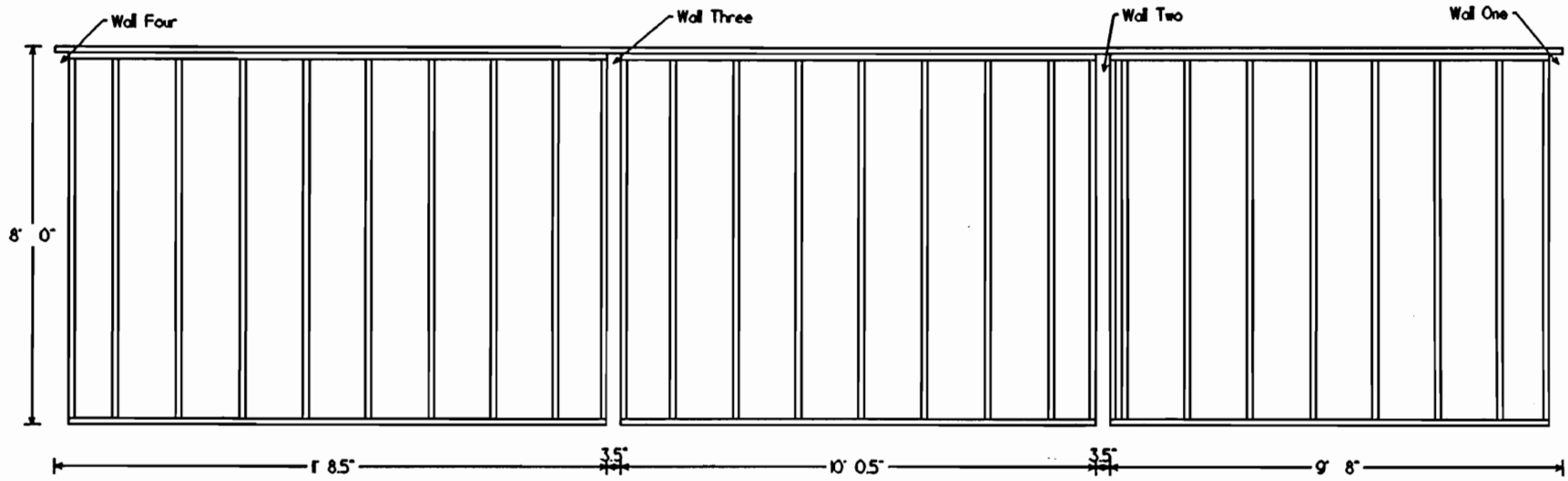

Figure A14. Framing of Wall 6.

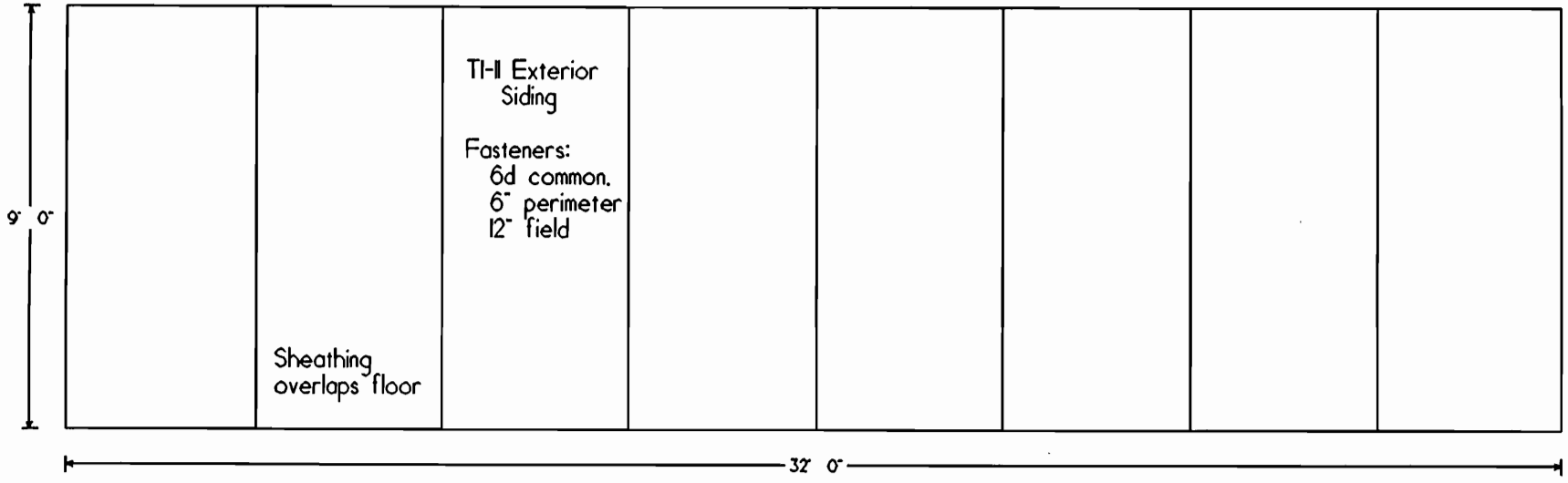

Figure A15. Plywood Sheathing of Wall 6.

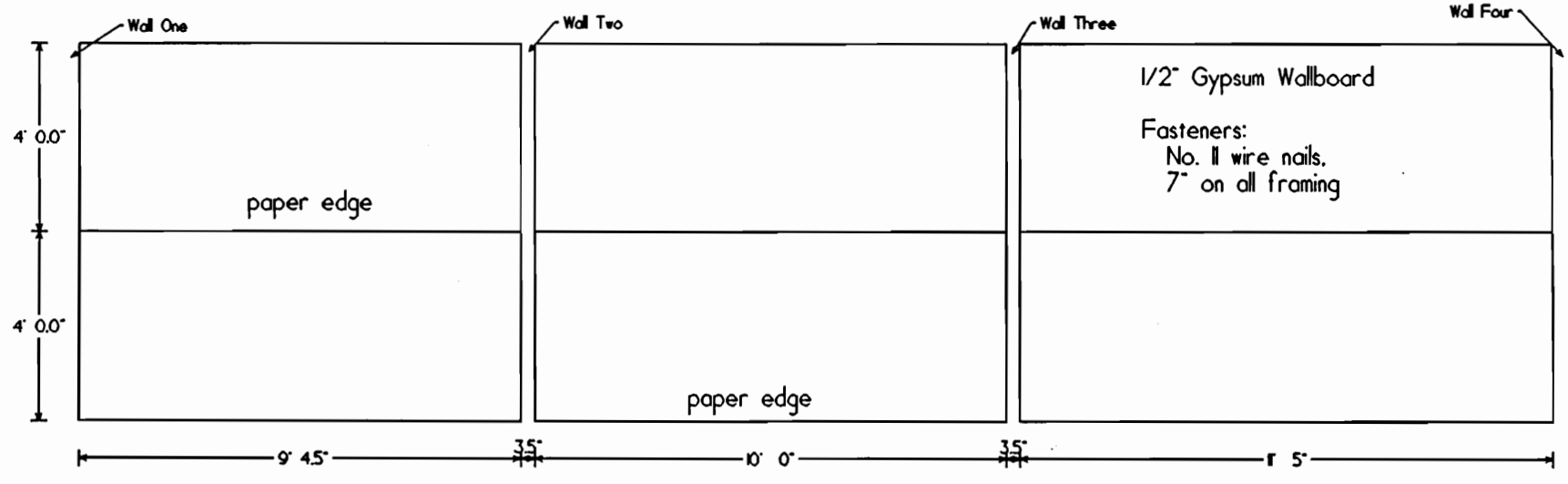

Figure A16. Gypsum Sheathing of Wall 6.

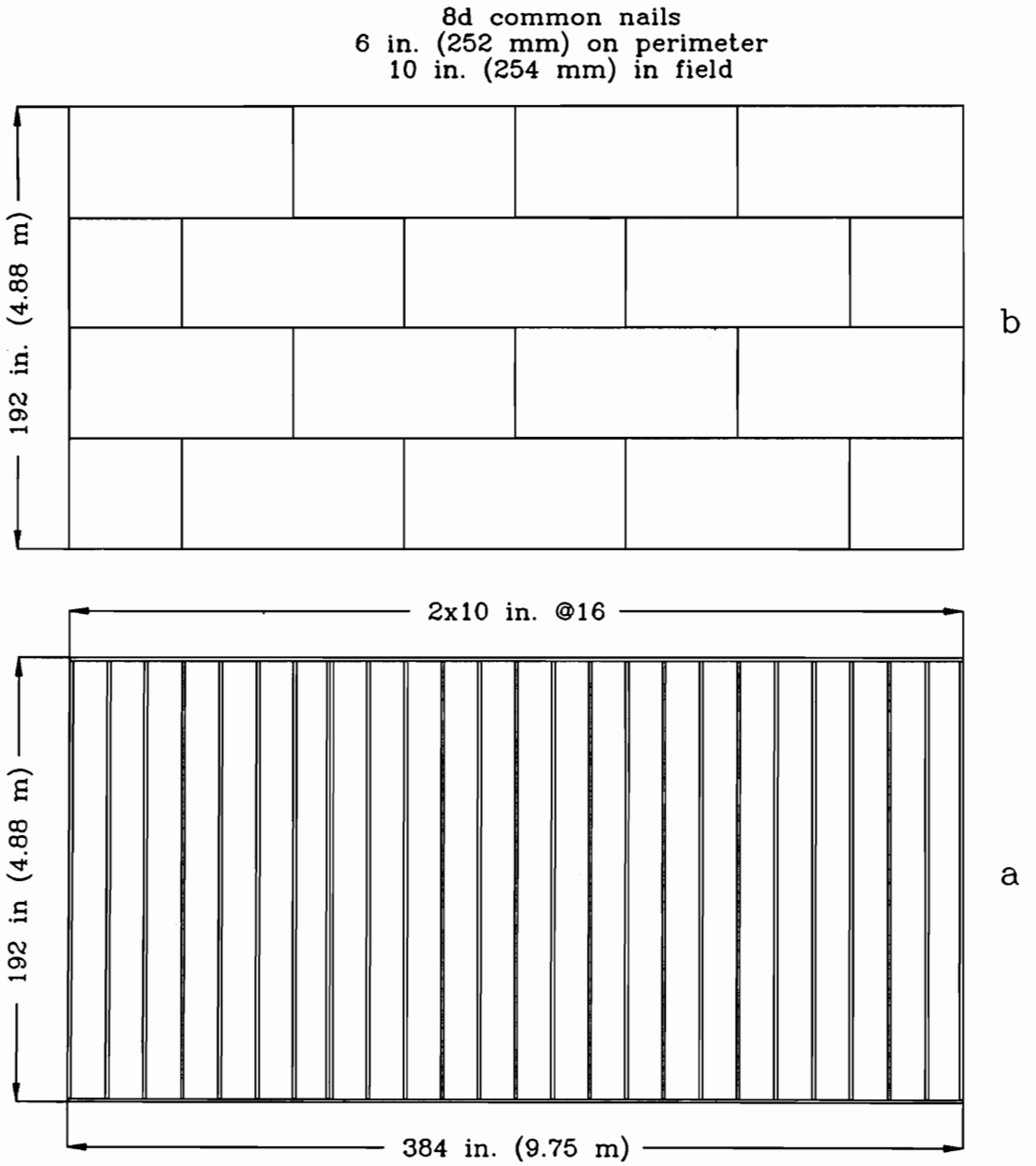

Figure A17. Floor, (a) Framing and (b) Sheathing.

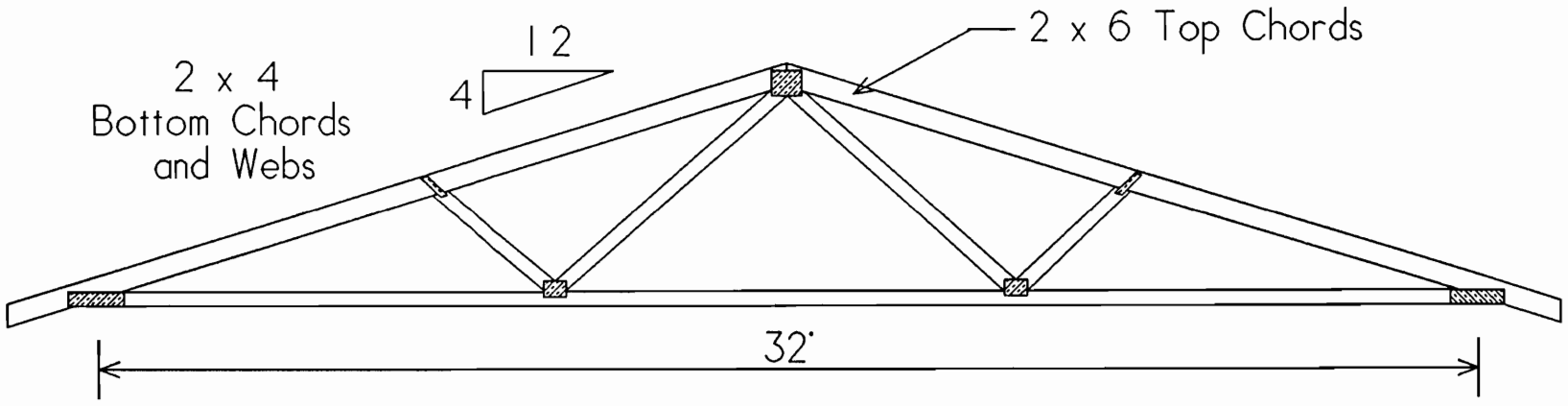

Figure A18. A Typical Roof Truss.

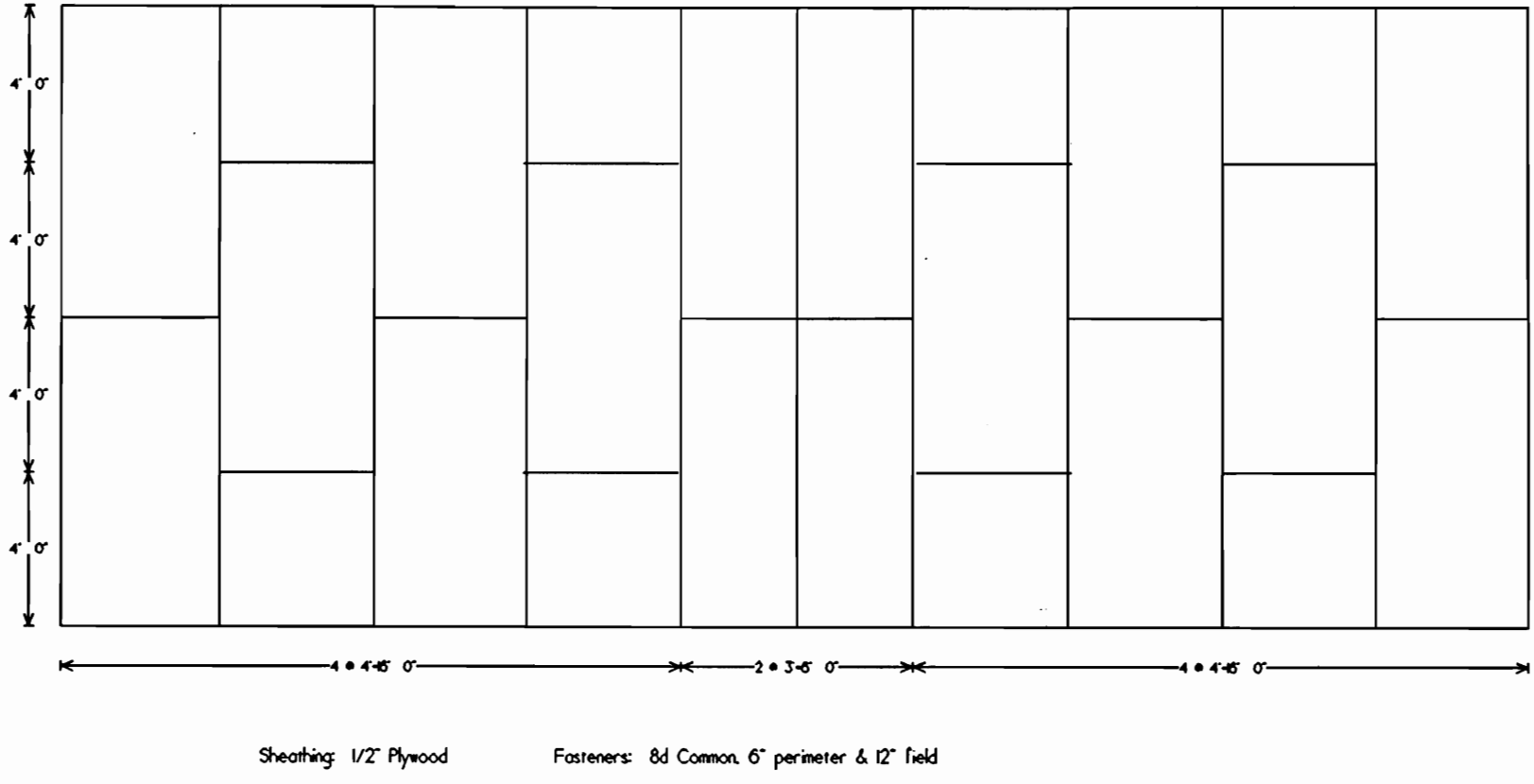

Figure A19. Plywood Sheathing of the Roof.

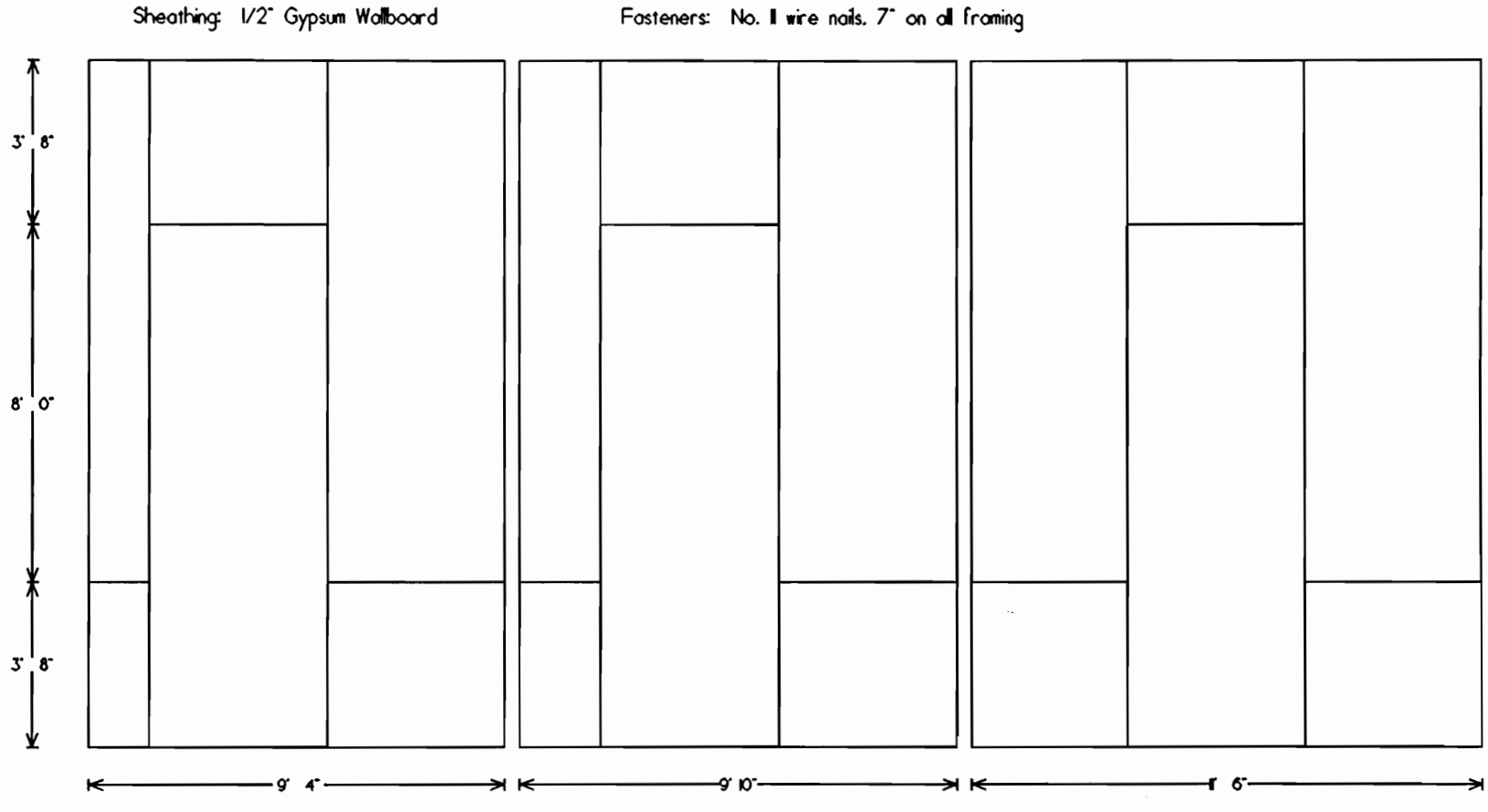

Figure A20. Gypsum Sheathing as Attached to the Bottom Truss Chords.

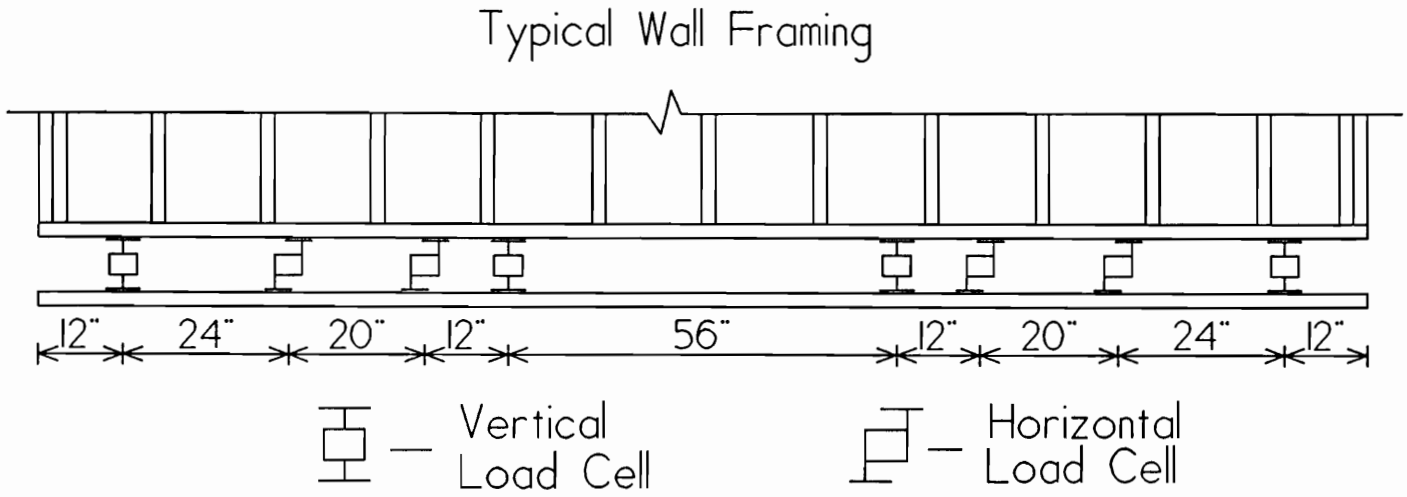

Figure A21. Load Cells between Floor and Walls 1 through 4.

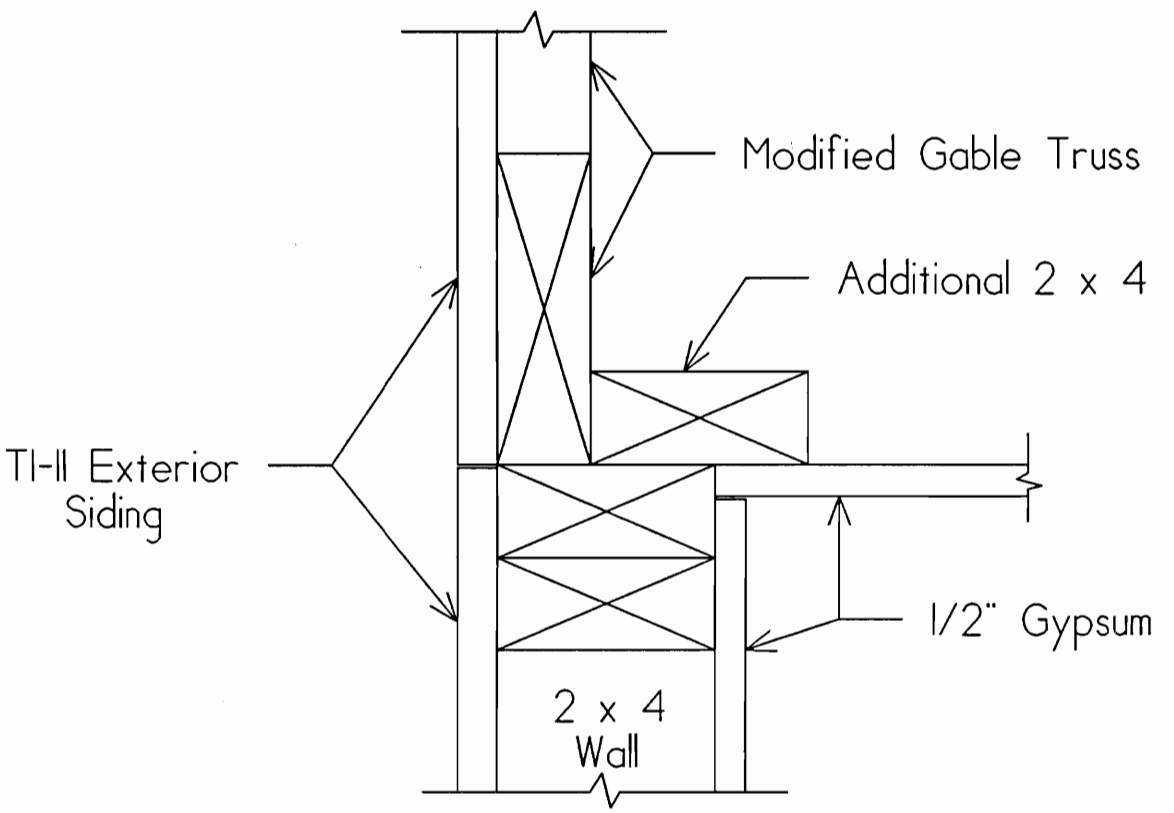

Figure A22. Connection between Walls and Roof.

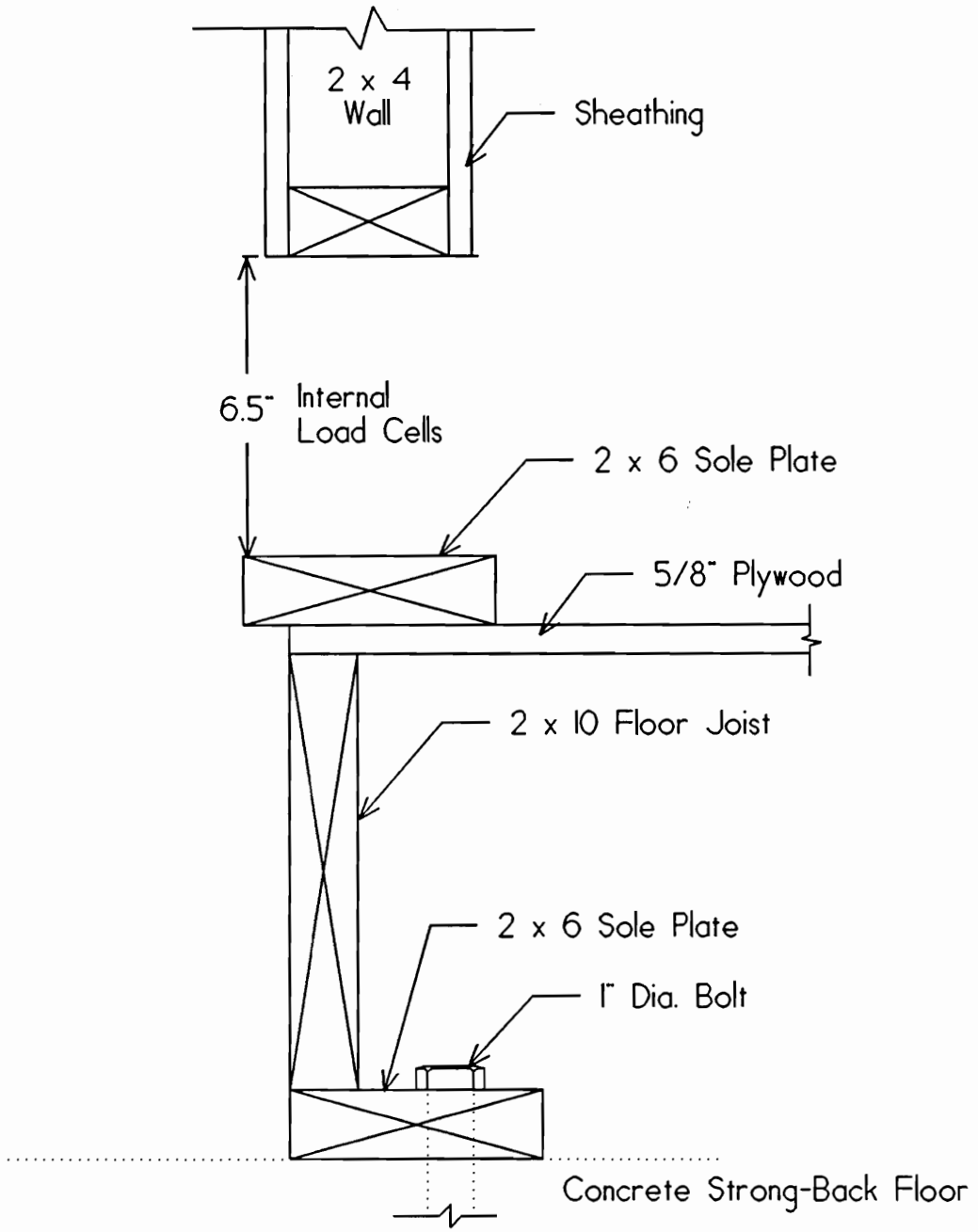

Figure A23. Connection between Floor and Wall 1 and 4.

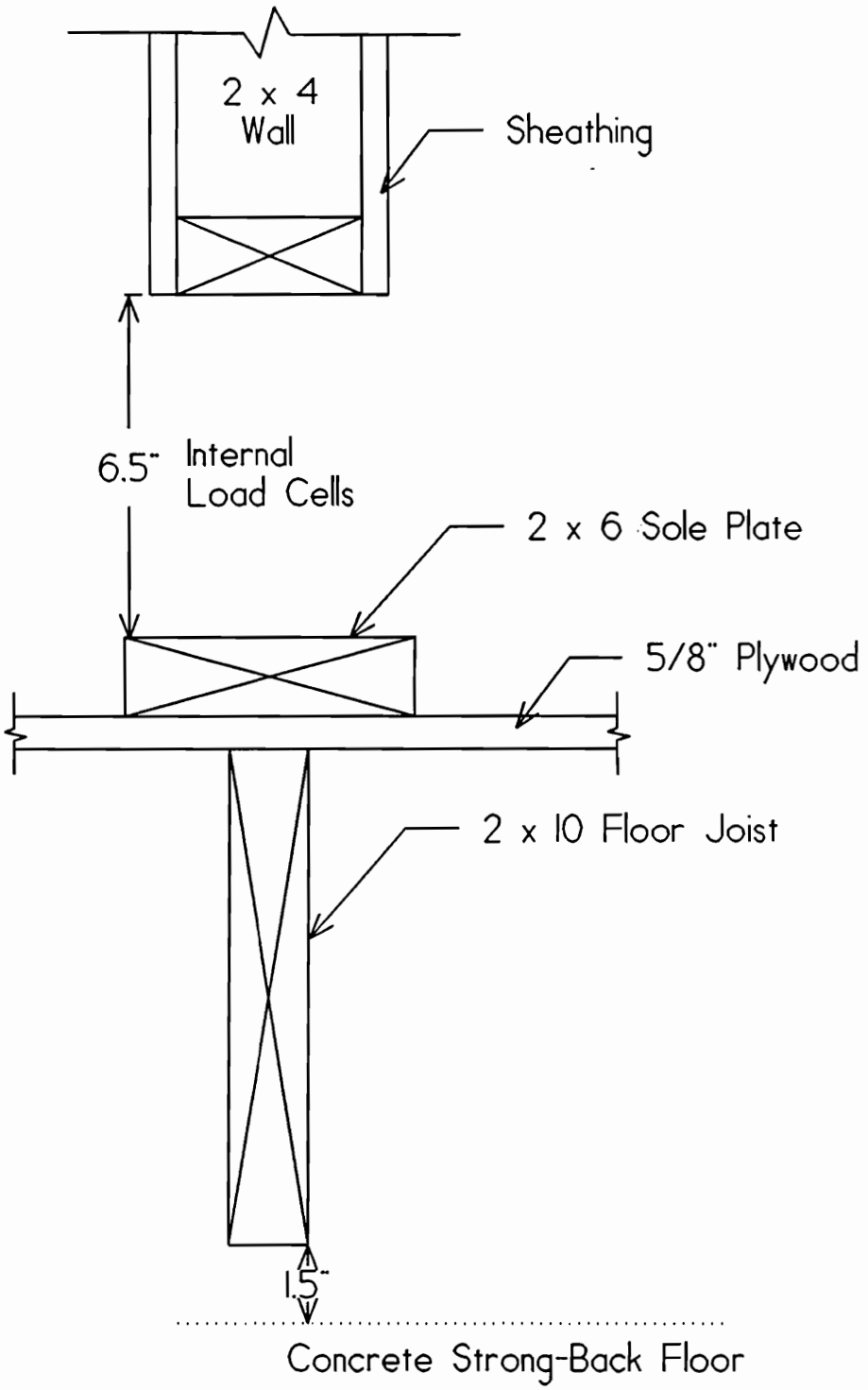

Figure A24. Connection between Floor and Partition Walls.

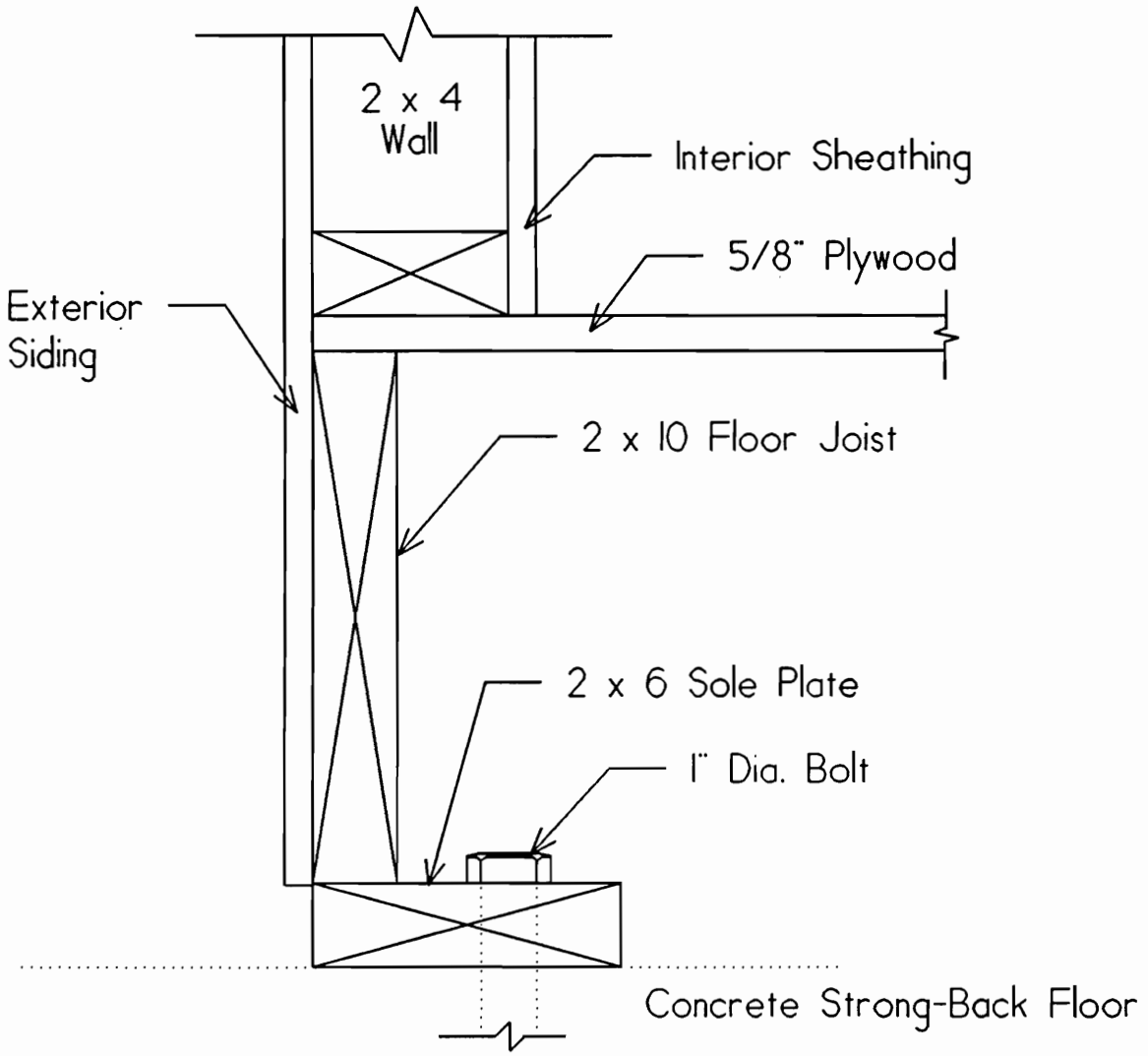

Figure A25. Connection between Floor and Walls 5 and 6.

APPENDIX B
Finite-Element Meshes of the Substructures

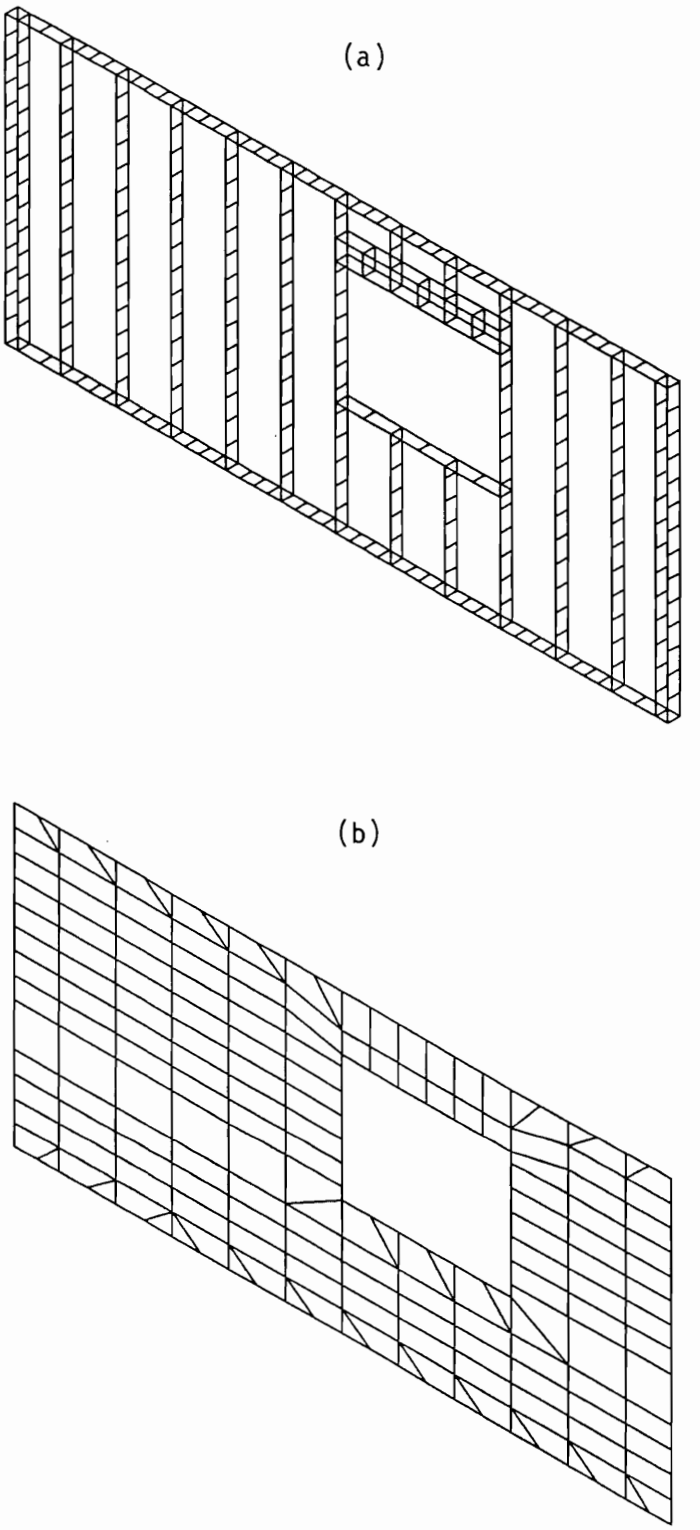

Figure B1. Finite-Element Mesh of Wall 1, (a) Framing and (b) Sheathing.

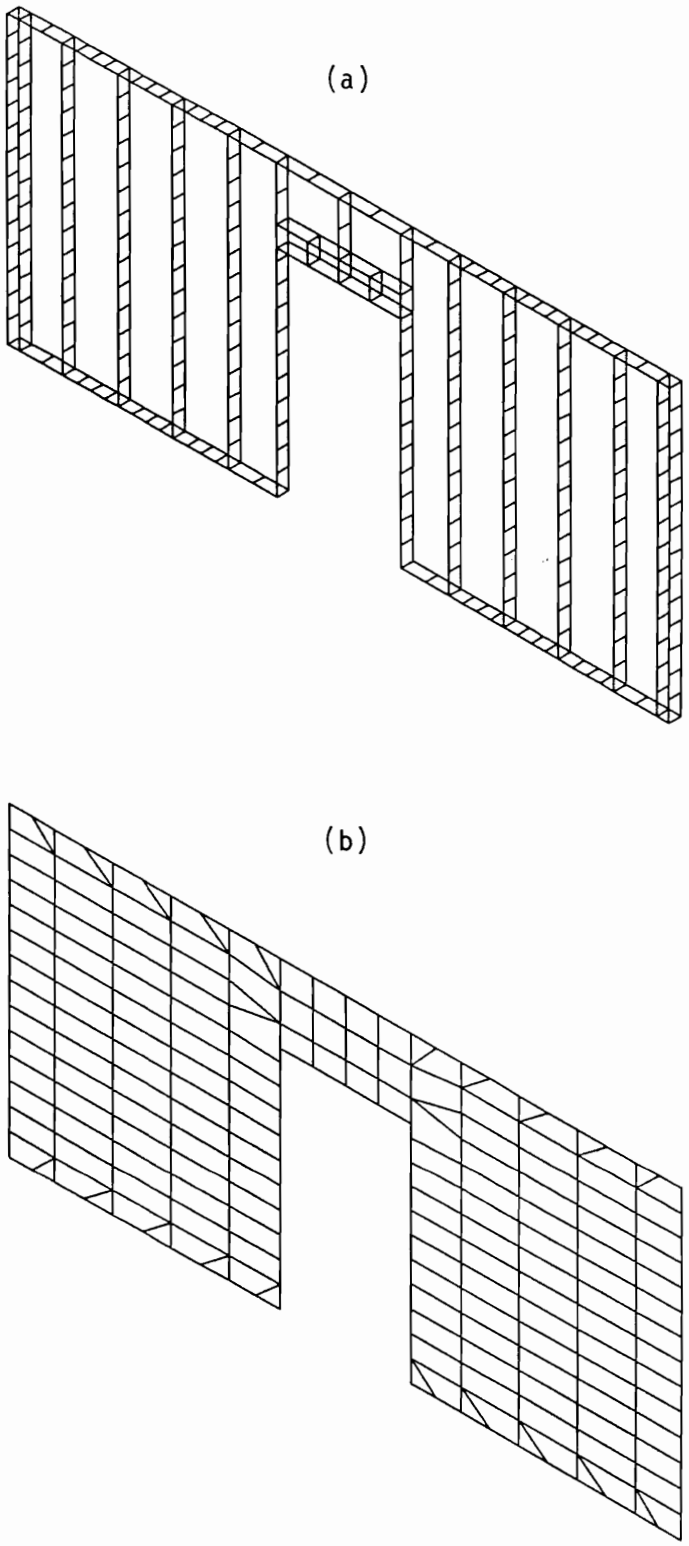

Figure B2. Finite-Element Mesh of Walls 2 and 3, (a) Framing and (b) Sheathing.

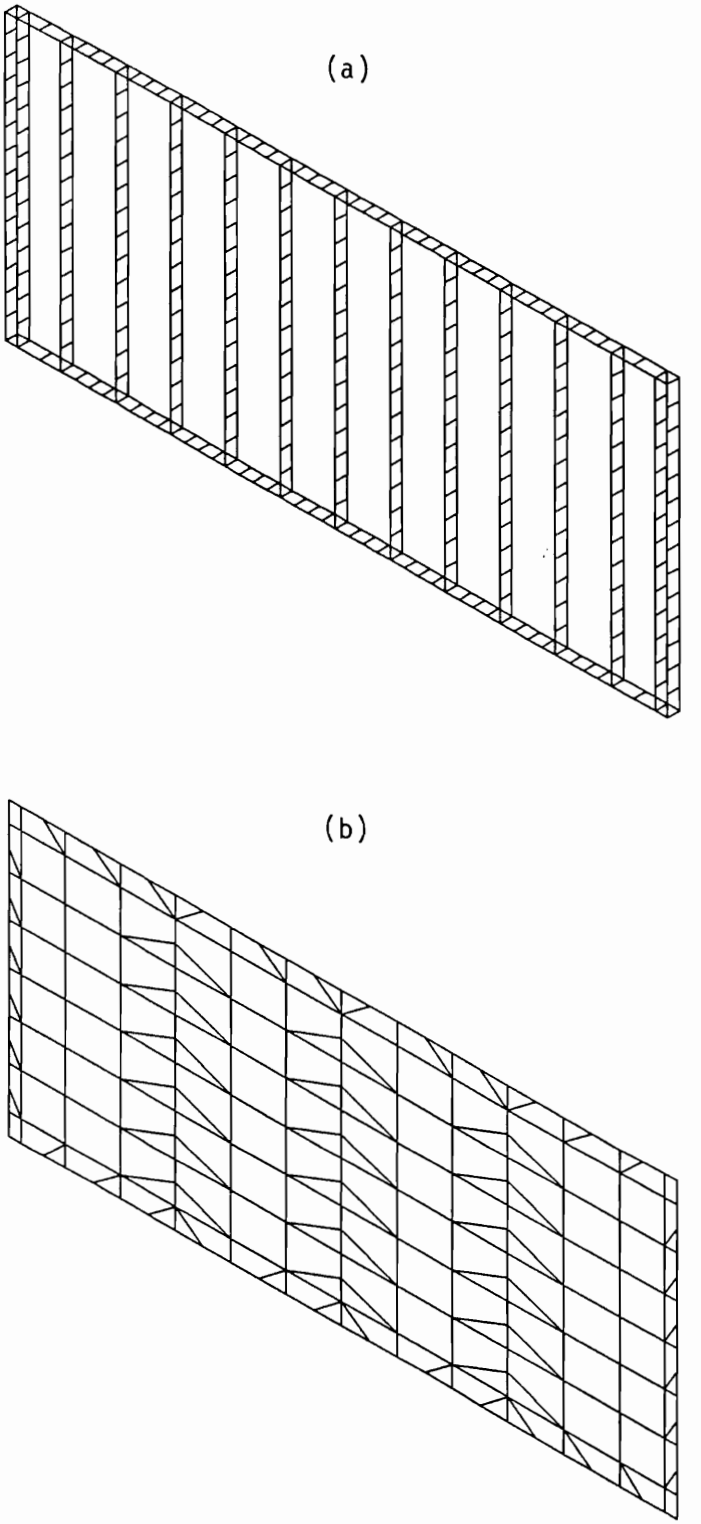

Figure B3. Finite-Element Mesh of Wall 4, (a) Framing and (b) Sheathing.

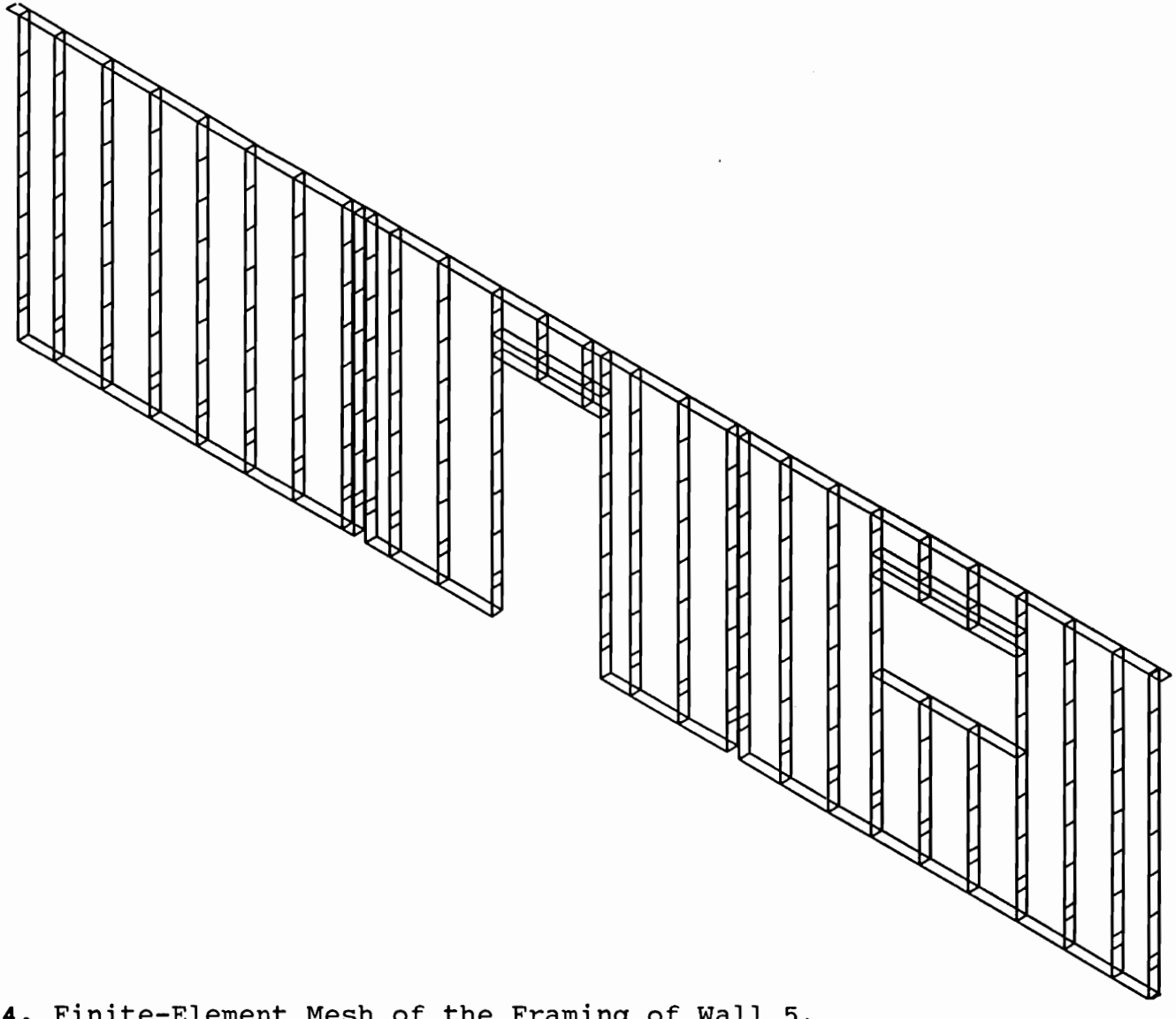

Figure B4. Finite-Element Mesh of the Framing of Wall 5.

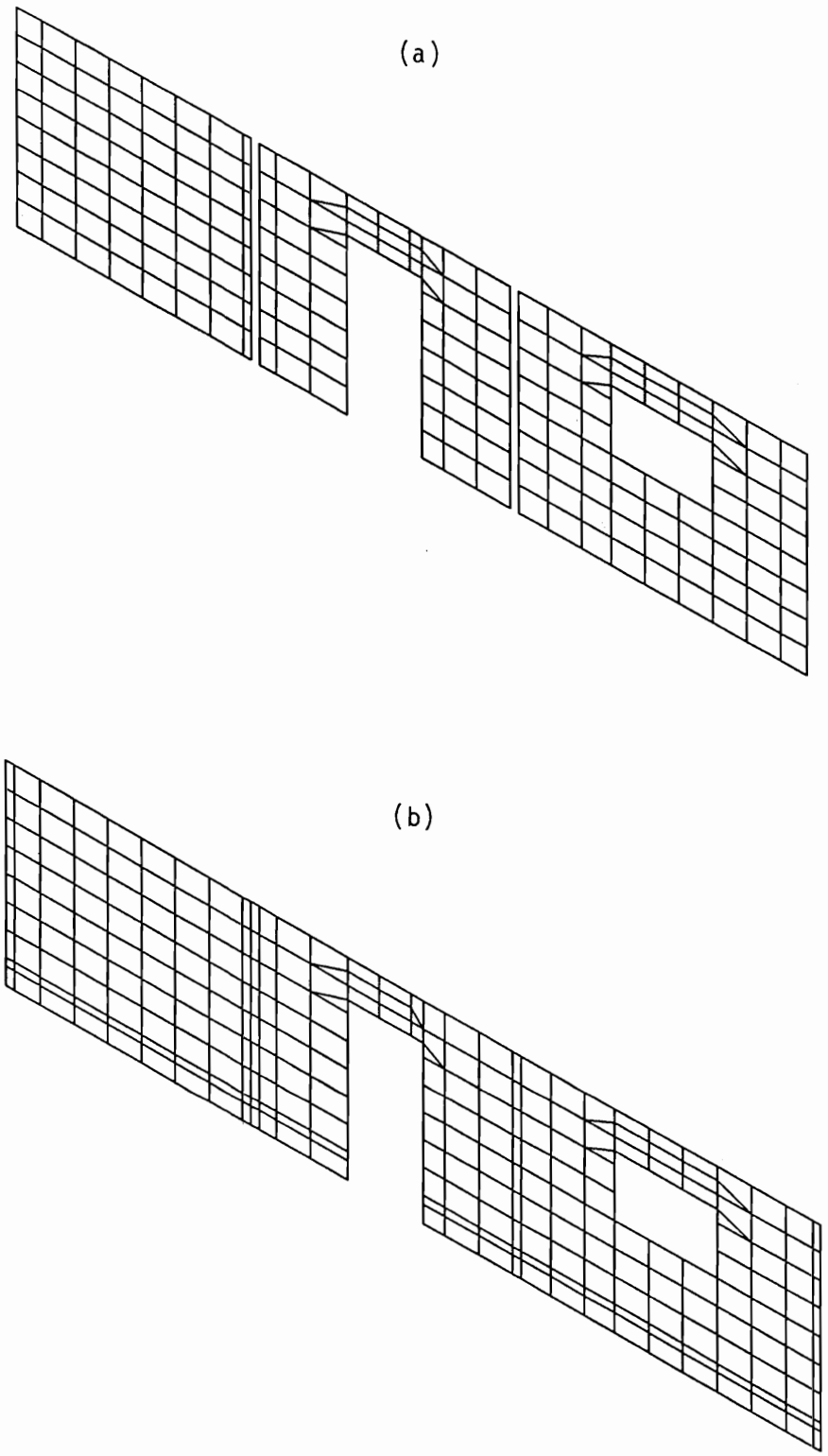

Figure B5. Finite-Element Mesh of the Sheathing of Wall 5, (a) Gypsum and (b) Plywood.

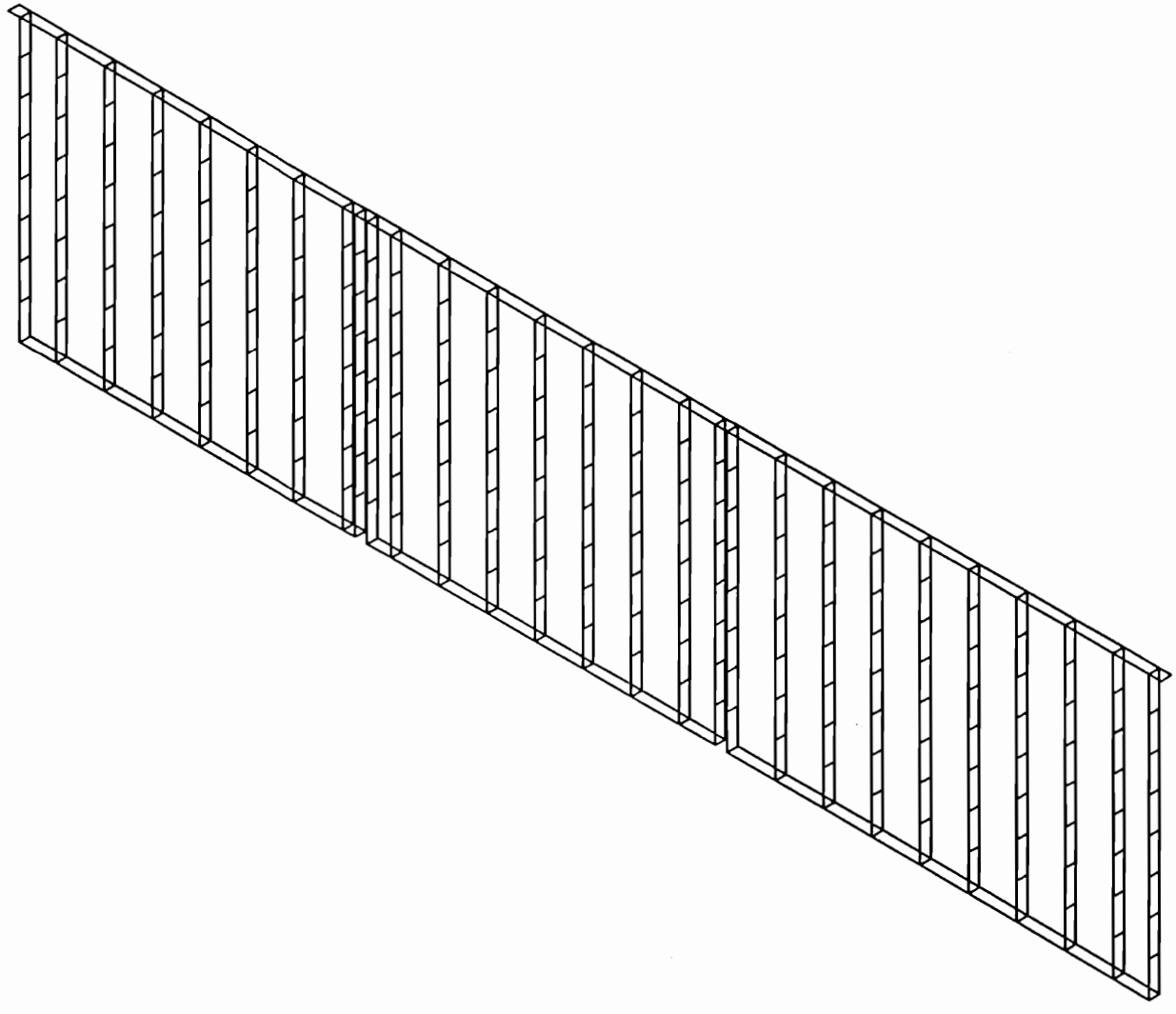

Figure B6. Finite-Element Model of Framing of Wall 6.

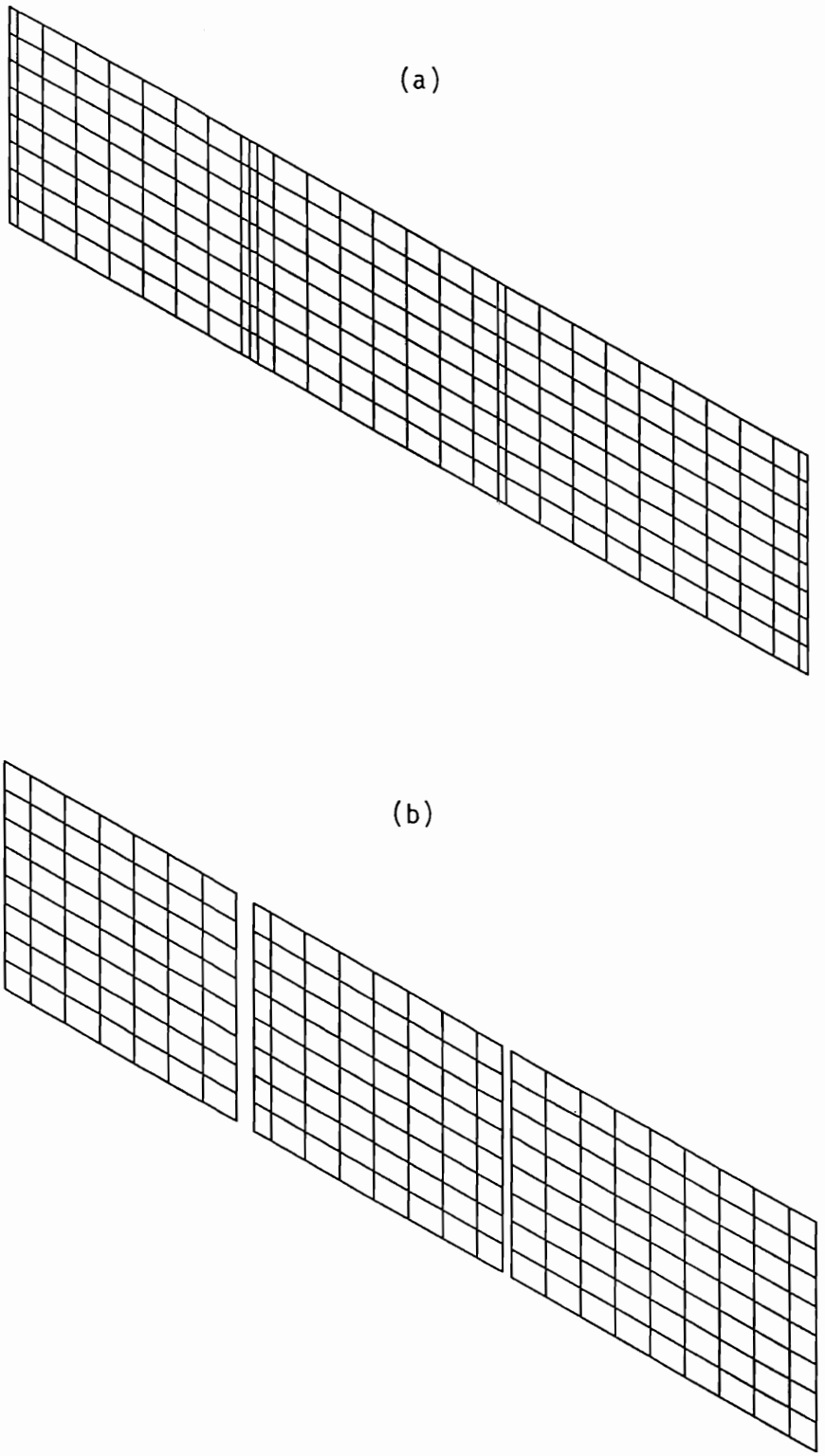

Figure B7. Finite-Element Mesh of the Sheathing of Wall 6, (a) Plywood and (b) Gypsum.

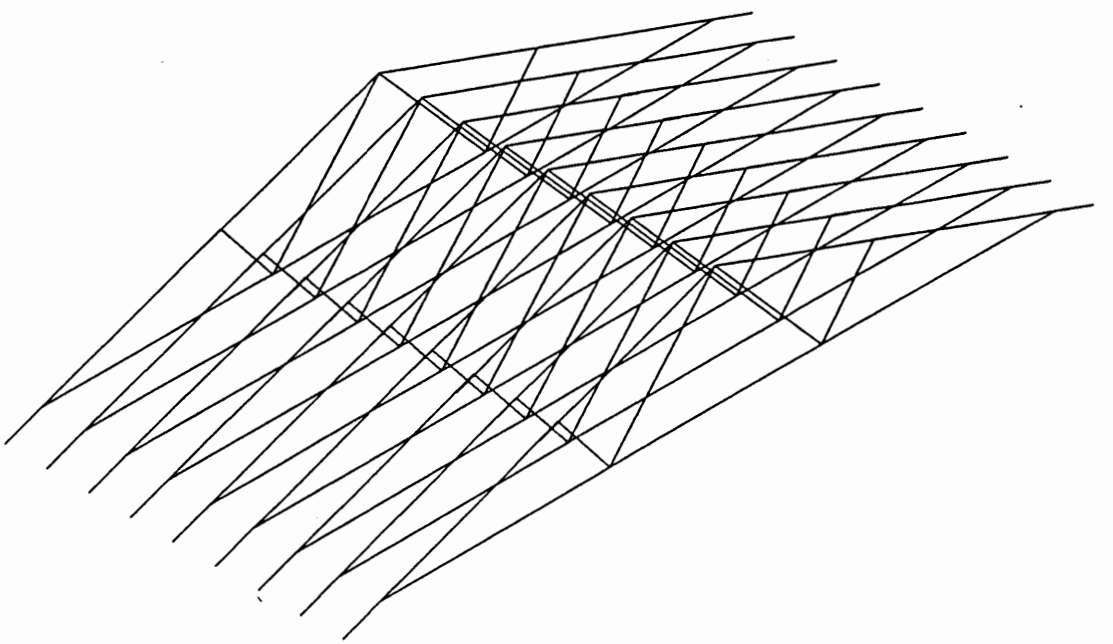

Figure B8. Finite-element Mesh of the Roof Truss.

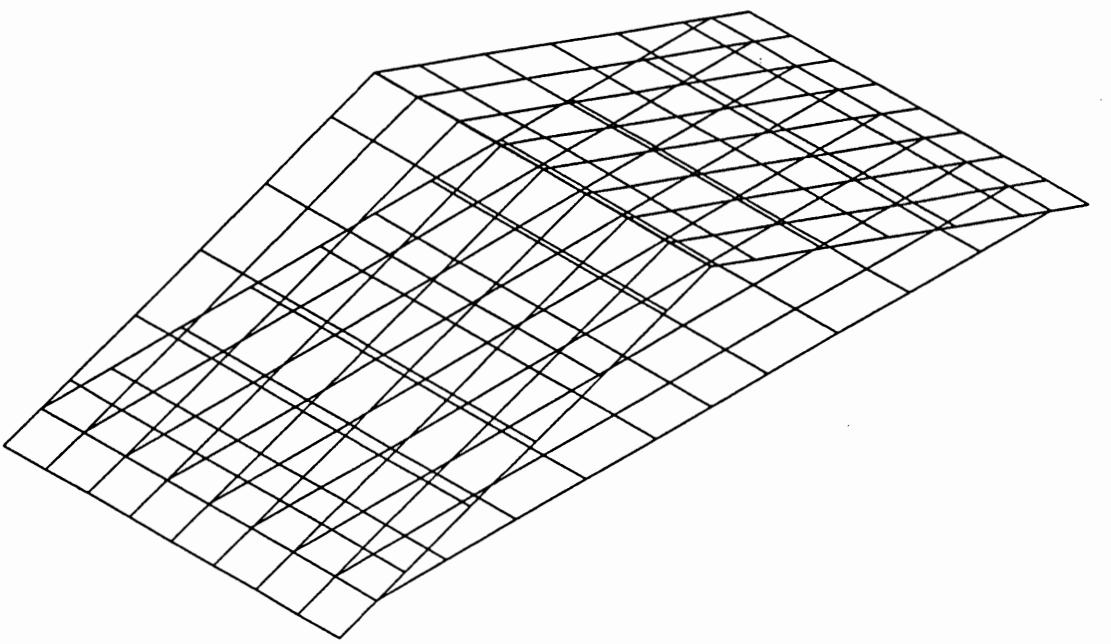

Figure B9. Finite-element Mesh of the Roof Sheathing.

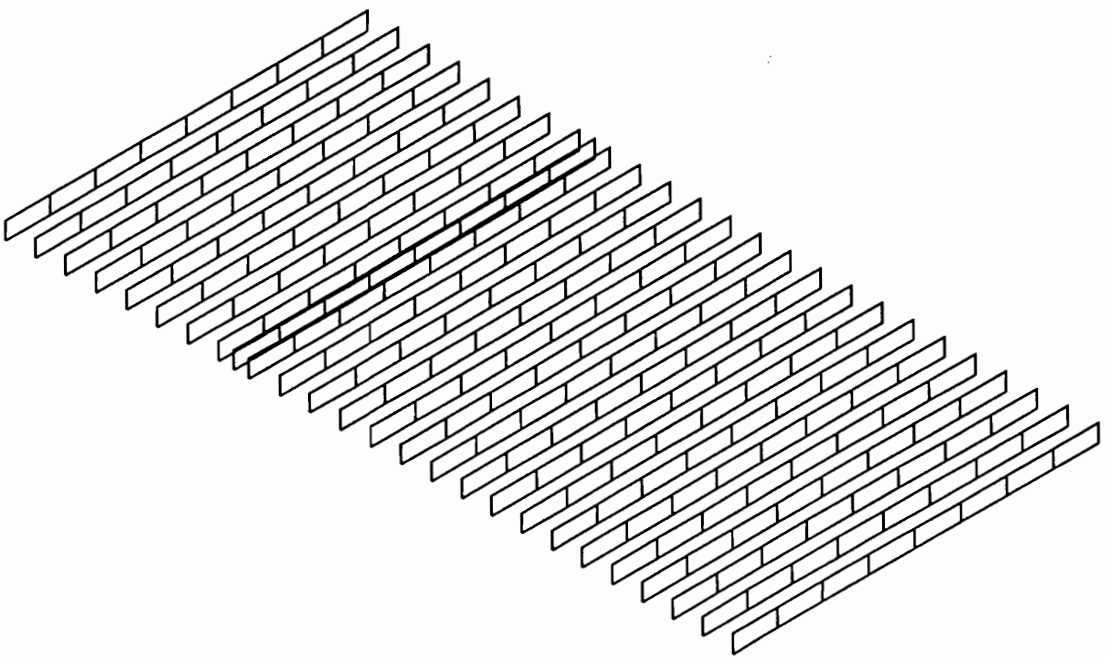

Figure B10. Finite-Element Mesh of the Floor Framing.

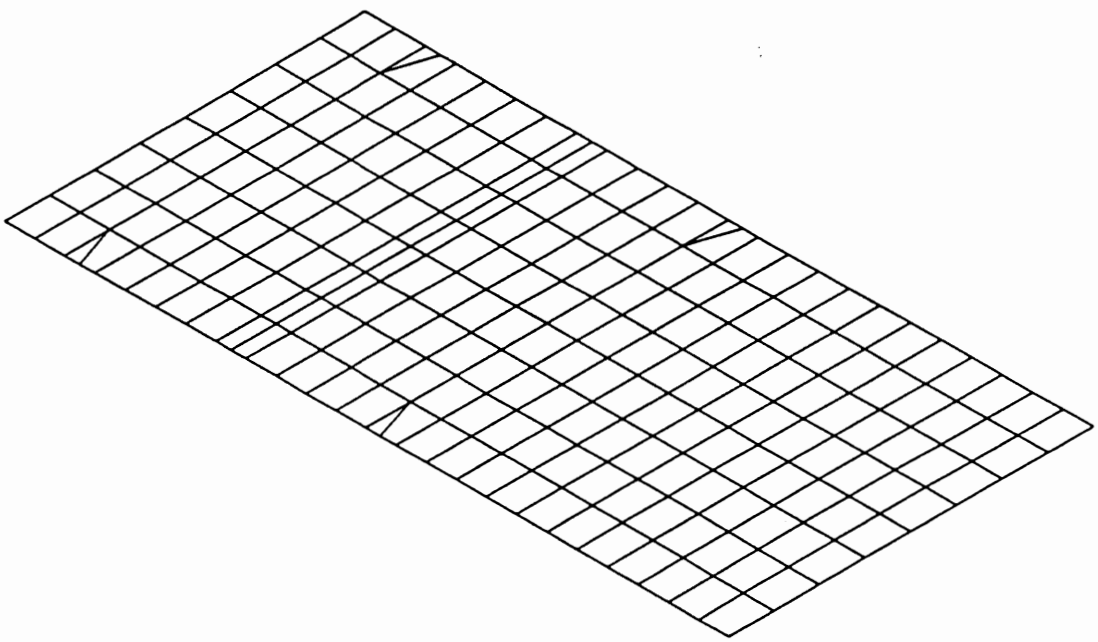

Figure B11. Finite-Element Mesh of the Floor Sheathing.

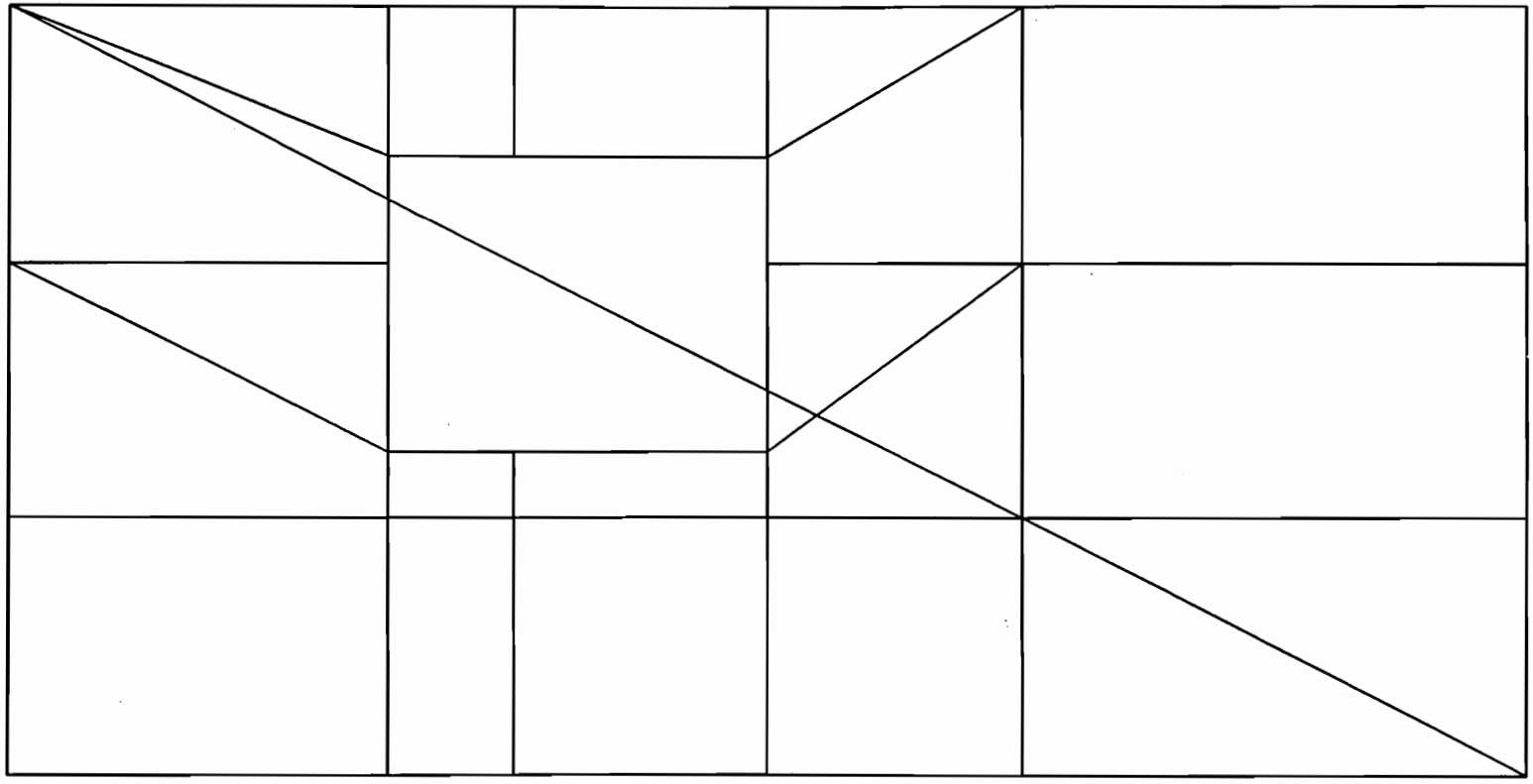

Figure B12. Finite-Element Mesh of an Equivalent Model of Wall 1.

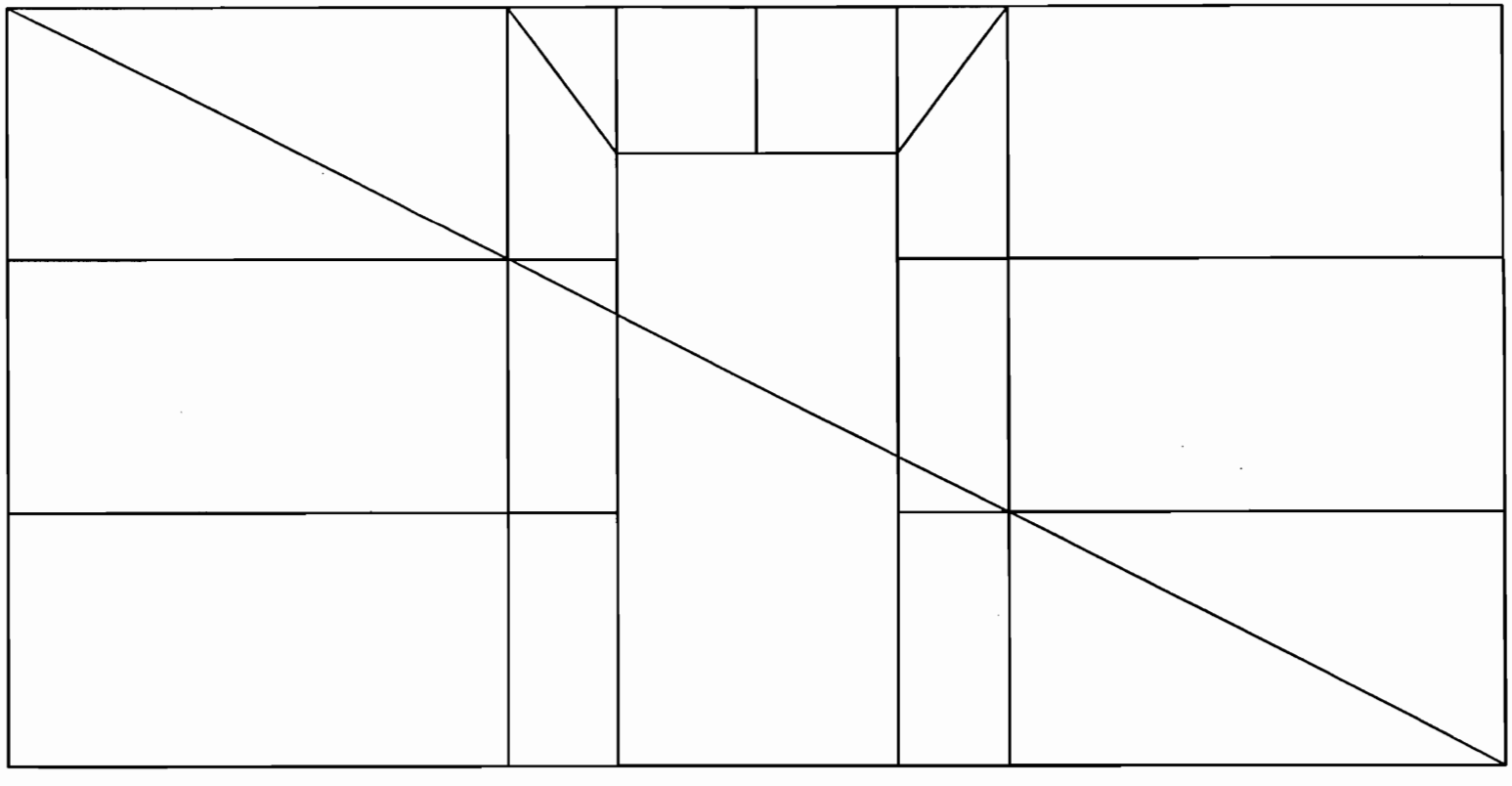

Figure B13. Finite-Element Mesh of an Equivalent Model of Walls 2 and 3.

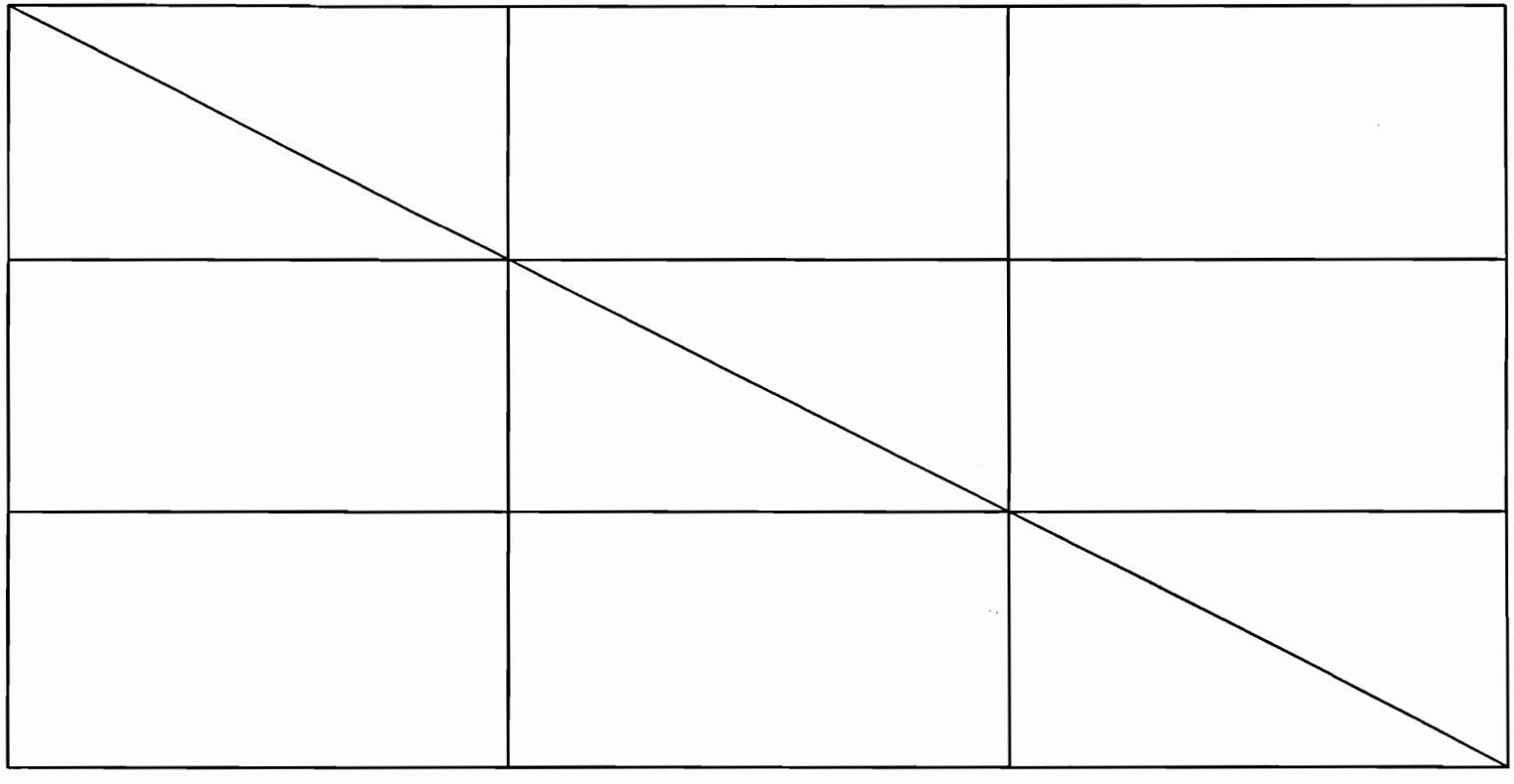

Figure B14. Finite-Element Mesh of an Equivalent Model of Wall 4.

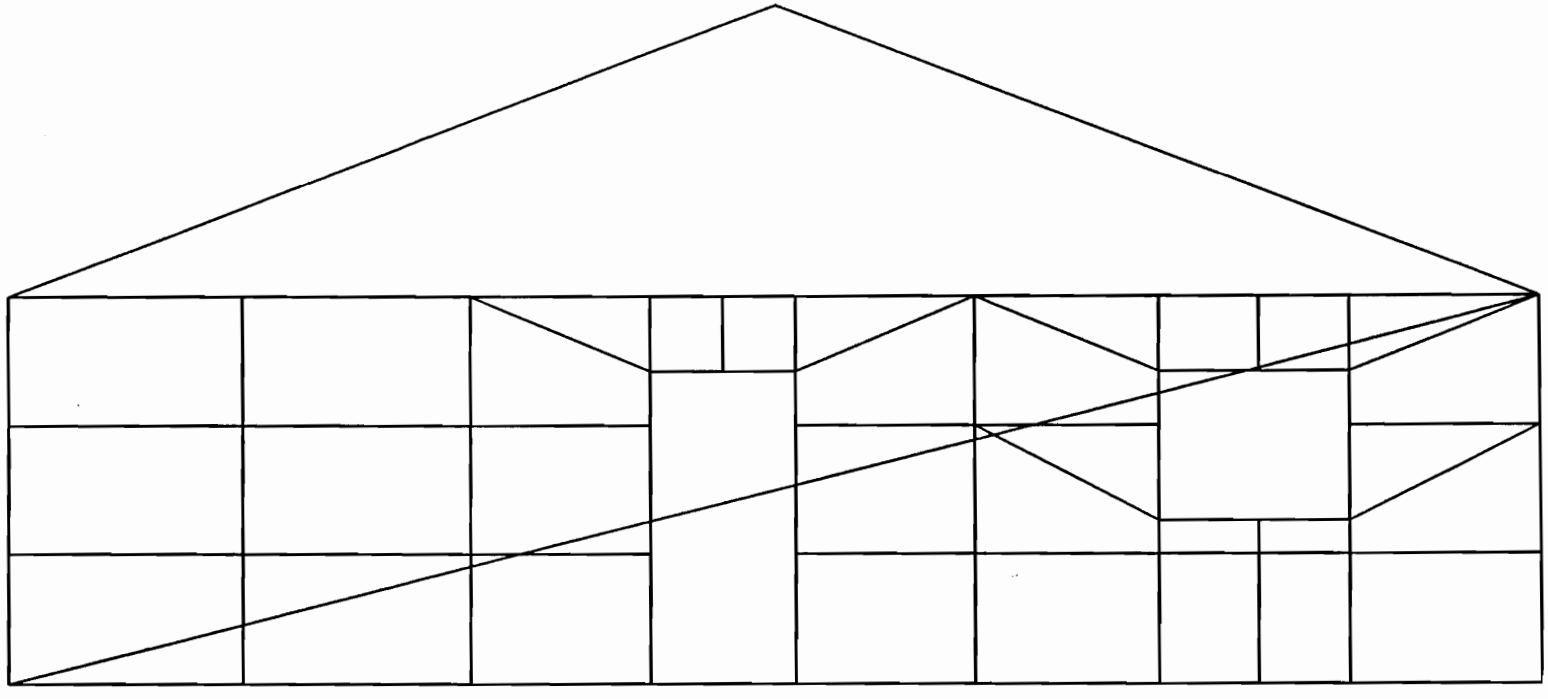

Figure B15. Finite-Element Mesh of an Equivalent Model of Wall 5.

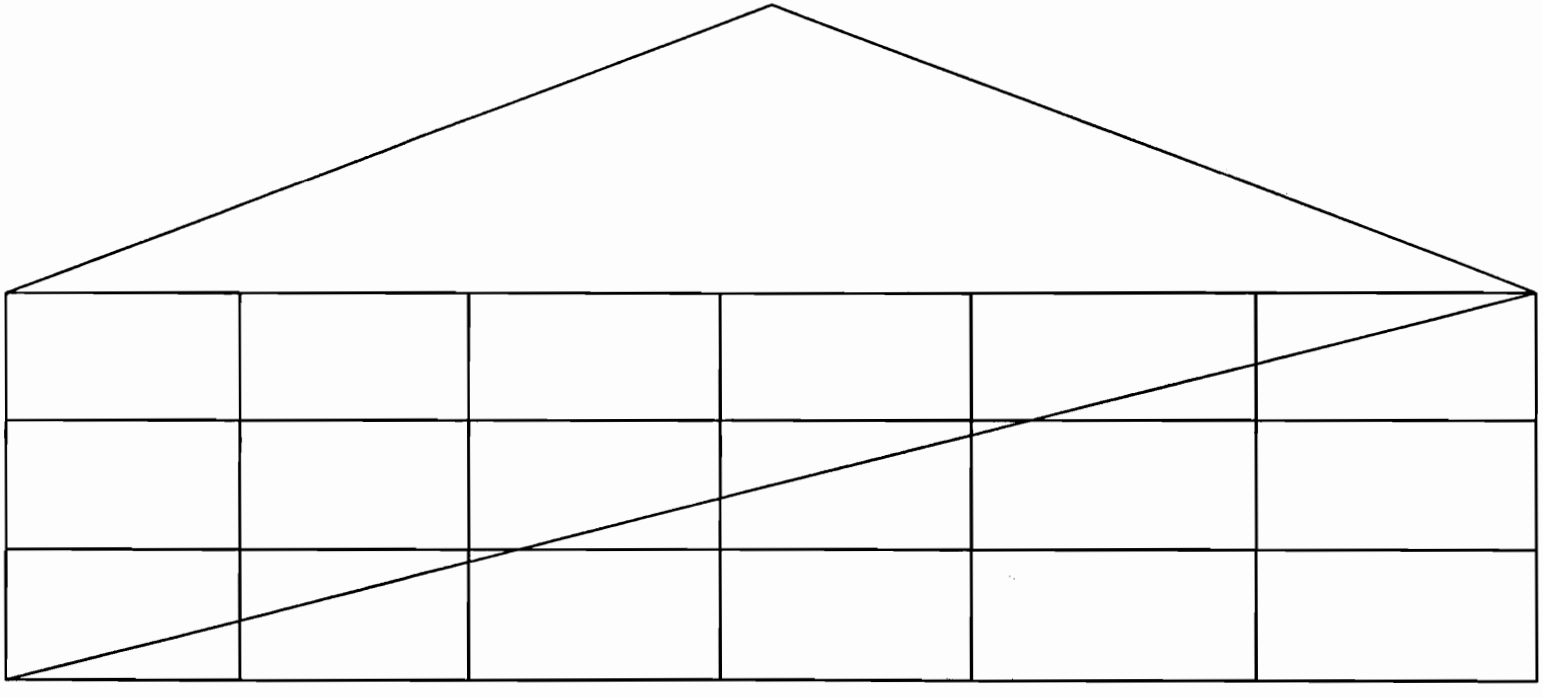

Figure B16. Finite-Element Mesh of an Equivalent Model of Wall 6.

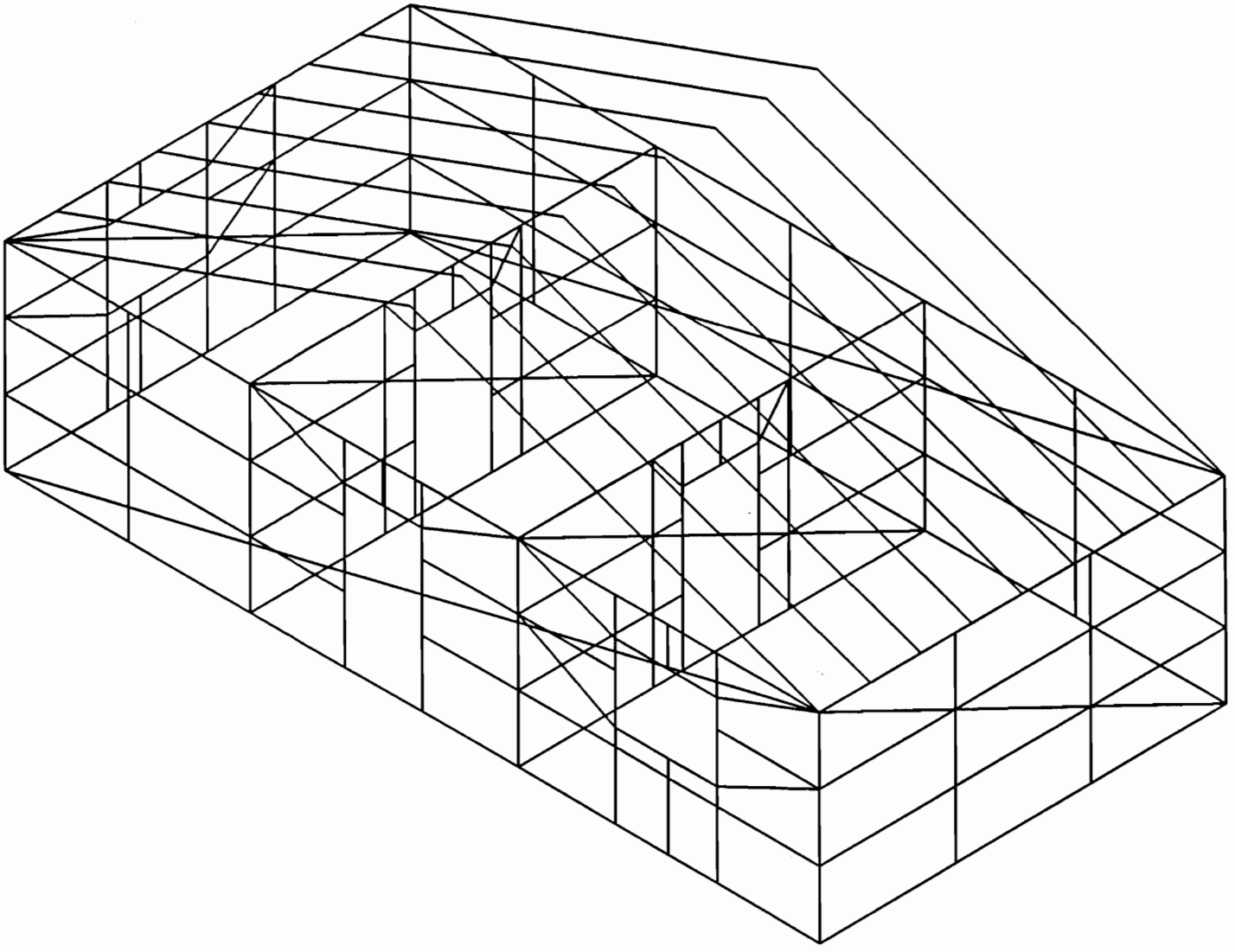

Figure B17. Coarse Finite-Element Mesh of the Full-Structure.

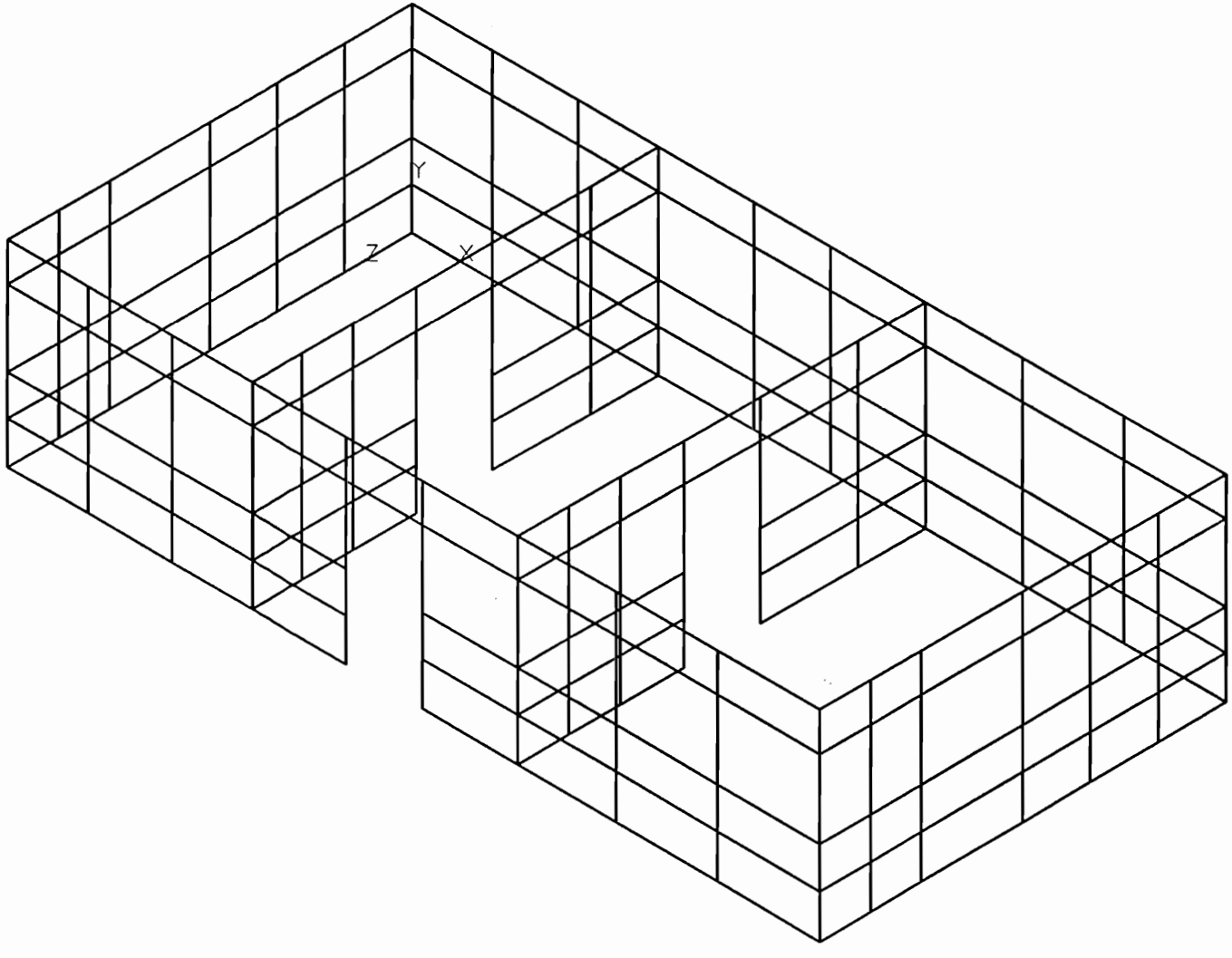

Figure B18. Refined Finite-Element Mesh of the Full-Structure.

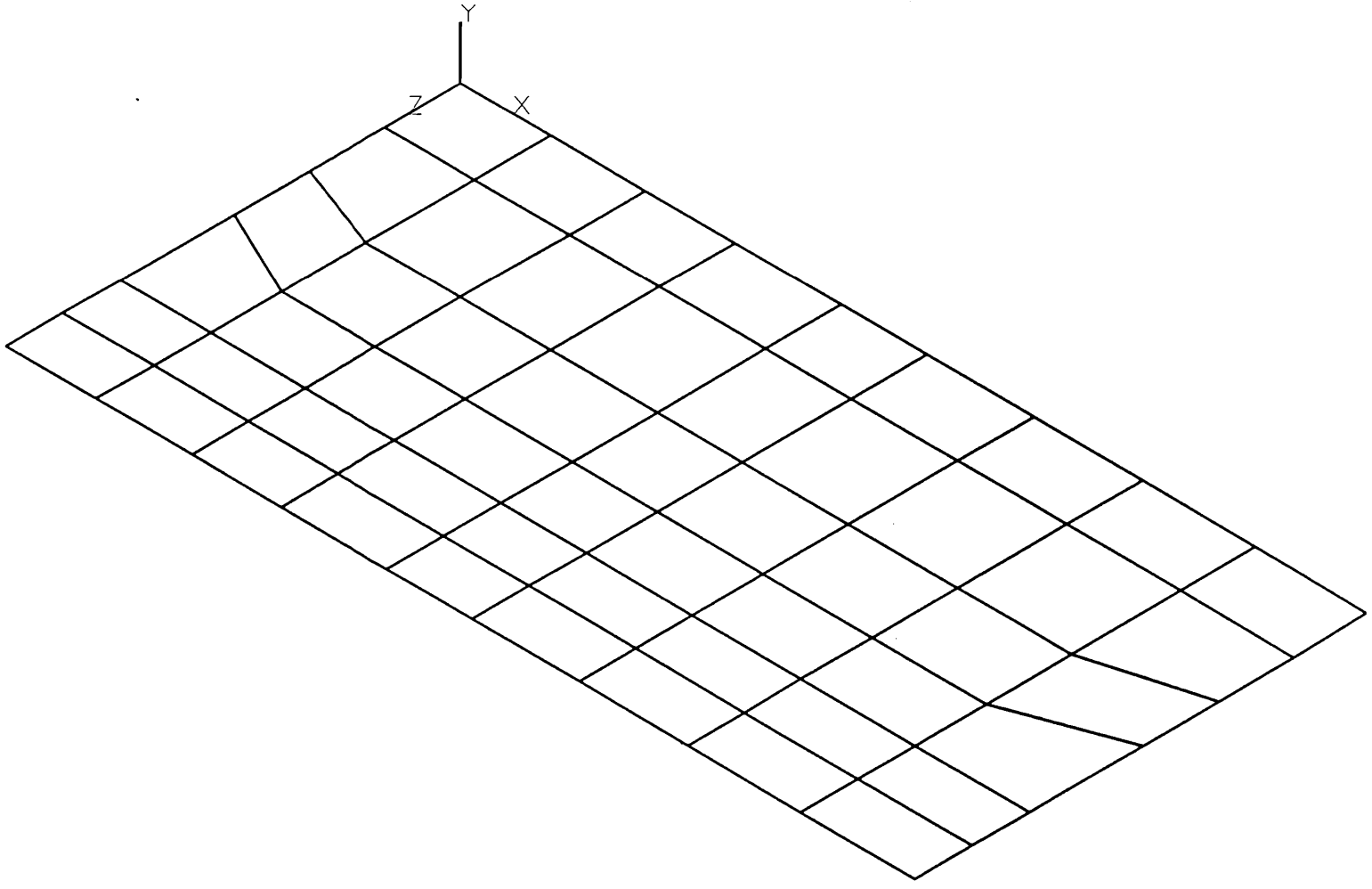

Figure B19. Finite-Element Mesh of the Floor Modeled as an Orthotropic Plate.

APPENDIX C

Computer Program for the Solution of Material Properties of an Orthotropic Plate

```
C     ****************************************************************
C     **  12/6/90 **  PLATE STIFFNESSES **  BOHUMIL KASAL        ***
C     ****************************************************************
C
C     THIS PROGRAM CALCULATES THE STIFFNESSES OF THE ORTHOTROPIC PLATE.
C     CALCULATION IS BASED UPON THE ANALYTICAL SOLUTIONS OF ORTH. PLATE
C     UNDER FOLLOWING BOUNDARY CONDITIONS AND LOADING:
C
C     1. SIMPLY SUPPORTED ON OPPOSITE EDGES, UNIFORM PRESSURE
C        REPEATED FOR BOTH PAIRS OF EDGES
C     2. SIMPLY SUPPORTED ON ALL EDGES, UNIFORM PRESSURE
C     3. OPPOSITE CORNERS SUPPORTED AND OTHER TWO LOADED BY SINGULAR
C        FORCE (PURE TORSION)
C     4. SIMPLY SUPORTED ON ALL EDGES AND LOADED BY SINGULAR FORCE
C        AT THE POSITION x,y
C
C     FIRST BENDING STIFFNESES ARE ESTIMATED USING SIMPLE BEAM
C     ANALOGY FROM THE B.C.1.  THEN B.C.2  IS USED
C
C     TORSIONAL STIFFNES IS OBTAINED FRON LOADING BY PURE TORSION.
C     SOLUTION ASSUMES THAT TORSIONAL STIFFNESS CAN BE CALCULATED
C     STRAIGHT FROM THE PURE TORSION CASE.
C     STIFFNESS IS CORRECTED TO ACHIEVE CONVERGENCY FOR ALL FOUR SIDES
C     SUPPORTED.
C     SOLUTIONS ARE OBTAINED FROM:
C     LEKHNITSKII,S.G.(1987) ANISOTROPIC PLATES (3RD ED.). GORDON AND
C     BREACH SCIENCE PUBLISHERS.534 PP. FOR A UNIFORMED PRESSURE CASE
C     AND DERIVED FOR THE PURE TORSION.
C
C==========================================================
C
      REAL W1,W2,W3,A,B,Q,P,EPS,PHI
      REAL MU2,DEF,W
      COMMON X4,X5,Y4,Y5,A,B,C,LOAD,Q,P,XP,YP,X3,Y3
      LOGICAL AL
C
C
C
C     W1=DEFLECTION FOR SIMPLE BEAM CASE AT x,y, SHORT SIDES SUPPORTED
C     W2=SAME AS W1                    LONG SIDES SUPPORTED
C     W3=DEFLECTION AT x,y , ALL FOUR EDGES SIMPLY SUPPORTED
C     W4=DEFLECTION AT X4, Y4  FROM FORCE P APPLIED AT XP, YP
C     W5=DEFLECTION AT THE CORNER FROM PURE TORSION AT X5, Y5
C       APPLIED FORCE IS 2xP5 AT EACH OPPOSITE CORNER
C     A=LENGTH        B=WIDTH     Q=PRESSURE          P=FORCE
C     X5,Y5=COORDINATES FOR THE TORSIONAL DEFLECTION W5 BY FORCE 2xP5
C          AT THE CORNERS
C     MU2
C     P  =FORCE FOR 4 SUPPORTED EDGES APPLIED AT XP, YP
C     Q  =PRESSURE
```

```
C     LOAD= IF=1 THEN PRESSURE, ELSE FORCE P AT XP, YP
C
C
      READ (1,*) W1
      READ (1,*) W2
      READ (1,*) W3,X3,Y3
C     READ (1,*) W4,X4,Y4
      READ (1,*) W5,X5,Y5,P5
      READ (1,*) H

C     READ (1,*) A,B,Q,P,XP,YP
      READ (1,*) A,B,Q
      READ (1,*) LOAD
      READ (1,*) MU2


C

      C=A/B
      W=0.
      A4=A*A*A*A
      B4=B*B*B*B
C     FROM BENDING TEST AS SIMPLE BEAMS (PRESSURE)
C
      D1=5*Q*A4/(384.*W1)
      D2=5*Q*B4/(384.*W2)
      WRITE (2,*) 'INITIAL GUESS'

      WRITE (2,*) 'D1=',D1,'D2=',D2

C     t o r s i o n
C     --------------
C     NOW COMBINED STIFFNESS IS BEING SOUGHT
C
C     SOLUTION IN POLYNOMIAL FORM FROM LEKHNITSKII IS USED TO
C     COMPUTE DK=TORSIONAL STIFFNESS (DK=G*H**3/12)
C
C
      A1=X5*Y5-B*X5/2-A*Y5/2+A*B/2
      DK=P5*A1/(2*W5)
      DFL=P5/(4*DK)*A*B
      D3=D1*MU2+2*DK
      WRITE (2,*) 'D3=',D3
      CALL DEFL (W,D1,D2,D3)
      WRITE (2,*) 'W=',W,'W3=',W3

C     IF LOAD IS SINGULAR FORCE P AT XP, YP AND DEFL W4, USE W4 AS
C     COMPARING CRITERION

C     INITIALIZE LOGICAL VARIABLE
      AL=.TRUE.
```

```
      IF (LOAD.NE.1) THEN
        WPRESS=W3
        W3=W4
      END IF


      K1=2
2     EPS=(W3-W)/W3
      IF (ABS(EPS).GT.1e-4) THEN
      IF (K1.EQ.0) THEN
              IF ((W3-W).LT.0.) THEN
                D3=D3+0.001*D3
                  ELSE
                   D3=D3-0.001*D3
              END IF
         K1=2
       END IF
       IF (AL) THEN
              K1=K1-1
              AL=.FALSE.
              IF ((W3-W).LT.0.) THEN
                D1=D1+0.001*D1
                  ELSE
                   D1=D1-0.001*D1
              END IF
       ELSE
              AL=.TRUE.
              K1=K1-1
              IF ((W3-W).LT.0.) THEN
                D2=D2+0.001*D2
                     ELSE
                        D2=D2-0.001*D2
              END IF
       END IF
      W=0.0
      WRITE (2,*) 'D1=',D1,'D2=',D2,'D3=',D3
      CALL DEFL (W,D1,D2,D3)
      WRITE (2,*) 'W=',W,'W3=',W3
         GOTO 2
      END IF
      WRITE (2,*)
      WRITE (2,*) 'SOLUTION FOR H=',H,'AND POISSON S RATIO=',MU2,':'
C
C     COMPUTING ELASTICITY PROPERTIES FOR THICKNESS H=1IN
C     AND POISSON'S RATION POI=0.7

      E1=12.*D1*(1-MU2*MU2)/(H*H*H)
      E2=12.*D2*(1-MU2*MU2)/(H*H*H)
      DK=(D3-D1*MU2)/2.
      G=12*DK/(H*H*H)

      WRITE (2,*)
```

```
      WRITE (2,101) 'D1=',D1,'E1=',E1
      WRITE (2,101) 'D2=',D2,'E2=',E2
      WRITE (2,101) 'D3=',D3,'G=',G
      WRITE (2,101) 'W=',W
      WRITE (2,101) 'W3=',W3
101   FORMAT (A3,1X,E12.6,4X,A4,1X,E12.6)

      END
```

```
C    THIS SUBROUTINE COMPUTES DEFLECTION OF THE PLATE UNDER DIFFERENT
C    LOADING AND B.C.  DOUBLE FOURIER SERIES SOLUTION IS USED.
C    CONVERGENCY CRITERION CAN BE CHANGED.
C

     SUBROUTINE DEFL (DEF,D1,D2,D3)
     COMMON X4,X5,Y4,Y5,A,B,C,LOAD,Q,P,XP,YP,X3,Y3
     REAL AMN,W,D1,D2,D3,A,B,C,X,Y,PI,DEF
     IF (LOAD.EQ.1) THEN
           X=A/2
           Y=B/2
             ELSE
                X=X4
                Y=Y4
     END IF
              X=X3
              Y=Y3


     MMAX=11
     NMAX=MMAX
     PI=3.141592654
     DO 10 M=1,MMAX,2
       DO 20 N=1,NMAX,2
         WOLD=W1
         PM=SIN(M*PI*X/A)
         PN=SIN(N*PI*Y/B)

C    THIS COEFFICIENT IS EQUALY VALID FOR PRESSURE AND SINGULAR FORCE

         W1=PM*PN/(D1*(M**4/C**4)+2*D3*N*N*(M*M/(C*C))+D2*N*N*N*N)
C         IF (LOAD.EQ.1) THEN

C    UNIFORM PRESSURE OVER THE SURFACE

            AMN=16.*Q/(PI*PI*M*N)
C           ELSE
C
C    SINGULAR FORCE AT THE POINT XP,YP
C
c              AMN=4*Q*SIN(M*PI*XP/A)*SIN(N*PI*YP/B)
C         END IF
            DEF=DEF+W1*AMN
20        CONTINUE
10   CONTINUE
           DEF=DEF*B*B*B*B/(PI*PI*PI*PI)

     RETURN
     END
```

EXAMPLE OF THE INPUT FILE

91.08	BENDING SOFT DIRECTION WALL4-FULL
0.0943	BENDING STRONG DIRECTION
0.09424 96 42.25	BENDING ALL 4 SIDES SUPPORTED , DEFLECTIONS AT X3, Y3
1 192 84.5 120	TORSION: DEFLECTION, X, Y, FORCE (1/2 OF THE LOAD!)
1	THICKNESS
192 84.5 0.1	LENGTH, HEIGHT (ALONG THE STUDS), PRESSURE
1	FLAG (ALWAYS 1)
0.07	POISSON'S RATIO

W1 deflection from the pressure,short sides supported	
W2	long sides supported
W3	all 4 sides supported
W4 X4 Y4 P4	4 sides supported, force P at points XP,YP and deflection measured at point X4, Y4
W5	X5 Y5 deflection at point X5,Y5 from pure torsion by load 2xP5 at the opposite corners NOTE: your force is then only 1/2 of the testing load!!! If deflection measured right below the force, X5=A and Y5=B (usually).
H	thickness (not necessary if pure torsion tested), but something must be input

A B Q P XP YP
LOAD TYPE (1-PRESSURE,0-SINGULAR FORCE)
POISSON'S RATIO
A-length
B-width
Q-uniform pressure
P-singular force applied at XP, YP
XP,YP-point where force P is applied

APPENDIX D

Finite-Element Formulation of Some Elements Used for the Full Structure Model

DERIVATION OF ELEMENT STIFFNESS MATRICES

Element stiffness matrices for elements used in the modelling of equivalent wall models are shortly discussed. Details of the derivation can be found elsewhere (Reddy, 1984; Stasa, 1985; Zienkiewicz, 1982 etc.). The model consists of several different element types superimposed over each other. This creates the complex behavior of the structure. Since the elements have different number of degrees of freedom per node, the appropriate positions at the global stiffness matrix must be established. This is accomplished by substituting zeros at the positions of nonexisting degrees of freedom. The finite-element software used for the model verification entails this possibility.

Truss Element

The governing differential equation for the truss element is in the form:

$$-\frac{d}{dx}\left(a\frac{du}{dx}\right)-f(x)=0 \qquad 0<x<l \qquad \textbf{(D1)}$$

where a=extensional stiffness (EA)
E=modulus of elasticity
A=cross sectional area
u=unknown displacement
f=distributed load

Variational formulation over a typical element with nodes 1 and 2 and length $h_e=x_{e+1}-x_e$ can be expressed in the form:

$$0=\int_{x_e}^{x_{(e+1)}} v[-\frac{d}{dx}(a\frac{du}{dx})-f]\,dx \qquad \textbf{(D2)}$$

where v=weight function

x_e=coordinate at end 1

x_{e+1}=coordinate at end 2

Using integration by parts, the order of equation is reduced and boundary terms obtained:

$$0=\int_{x_e}^{x_{(e+1)}} (a\frac{dv}{dx}\frac{du}{dx}-vf)\,dx+[v(-a\frac{du}{dx})]_{x_e}^{x_{(e+1)}} \qquad \textbf{(D3)}$$

with boundary terms

$$(-a\frac{du}{dx})\Big|_{x_e}=P_1^{(e)} \qquad (a\frac{du}{dx})\Big|_{x_{(e+1)}}=P_2^{(e)} \qquad \textbf{(D4)}$$

where $P_1^{(e)}$, $P_2^{(e)}$ = axial forces at node 1 and 2.

Using Lagrangian interpolation functions to approximate u(x) and v, finite-element model can be created:

$$u(x)=\sum_{j=1}^{n} u_j\phi_j^{(e)} \qquad v=\phi_i \qquad \textbf{(D5)}$$

and n=2 for two nodes

$$0=\sum_{j=1}^{n}(\int_{x_e}^{x_{(e+1)}} a\frac{d\phi_i}{dx}\frac{d\phi_j}{dx}dx)\,u_j-\int_{x_e}^{x_{(e+1)}}\phi_i f dx-P_1^{(e)}\phi_i(x_e)-P_2^{(e)}\phi_i(x_{(e+1)}) \qquad \textbf{(D6)}$$

Which is in the form

$$K_{ij}u_j=F_i \qquad \textbf{(D7)}$$

where K_{ij}=stiffness matrix

$F_i^{(e)}$=force vector and

$$K_{ij}=\sum_{j=1}^{n}\left(\int_{x_e}^{x_{(e+1)}} a\frac{d\phi_i}{dx}\frac{d\phi_j}{dx}dx\right)$$

$$F_i=\int_{x_e}^{x_{(e+1)}}\phi_i f dx-P_1^{(e)}\phi_i(x_e)-P_2^{(e)}\phi_i(x_{(e+1)}) \qquad \textbf{(D8)}$$

The Lagrangian interpolation functions can be found elsewhere (e.g. Reddy, 1984). For constant modulus of elasticity and cross sectional area over the element length, the well known form of the stiffness matrix is obtained:

$$\frac{EA}{l}\begin{bmatrix}1 & -1\\ -1 & 1\end{bmatrix} \qquad \textbf{(D9)}$$

The same stiffness matrix is used for a nonlinear connection element which can be non-dimensional (nodes i and j are coincident). In this case coefficient EA/l is replaced by K(u), where K(u) is a stiffness (force/displacement) and is a function of nodal displacement u defined as $u=u_i-u_j$.

Beam Element

Beam behavior can be described by fourth-order differential equation:

$$\frac{d^2}{dx^2}\left(b\frac{d^2w}{dx^2}\right)+f(x)=0 \qquad 0<x<L \qquad \textbf{(D10)}$$

where b=beam stiffness (EI)
w=beam deflection
f=transversely distributed load
E=modulus of elasticity
I=moment of inertia
x=coordinate on the beam

Variational formulation over a typical element is expressed in the form

$$0=\int_{x_e}^{x_{e+1}} v\left[\frac{d^2}{dx^2}\left(b\frac{d^2}{dx^2}\right)+f\right]\,dx$$

$$=\int_{x_e}^{x_{e+1}} \left[-\frac{dv}{dx}\frac{d}{dx}\left(b\frac{d^2w}{dx^2}\right)+vf\right] + \left[v\frac{d}{dx}\left(b\frac{d^2w}{dx^2}\right)\right]_{x=x_e}^{x_{e+1}} \qquad \textbf{(D11)}$$

$$=\int_{x_e}^{x_{e+1}} \left(b\frac{d^2v}{dx^2}\frac{d^2w}{dx^2}+vf\right)\,dx + \left[v\frac{d}{dx}\left(b\frac{d^2}{dx^2}\right)-\frac{dv}{dx}b\frac{d^2w}{dx^2}\right]_{x=x_e}^{x_{e+1}}$$

In the above equation essential and natural boundary conditions can be recognized as:

$$w \text{ and } \frac{dw}{dx} = \textit{essential boundary conditions}$$
$$b\frac{d^2w}{dx^2} \text{ and } \left(\frac{d}{dx}\right)\left(b\frac{d^2w}{dx}\right) = \textit{natural boundary conditions} \qquad \textbf{(D12)}$$

Essential boundary conditions represent deflection and rotation, whereas natural boundary conditions represent moment and shear force at the element endpoints. Replacing weight function v and deflection function w by Hermite interpolation functions in the form:

$$\phi_1^{(e)} = 1 - 3\left(\frac{\bar{x}}{h^e}\right)^2 + 2\left(\frac{\bar{x}}{h_e}\right)^3$$
$$\phi_2^{(e)} = -\bar{x}\left(1 - \frac{\bar{x}}{h_e}\right)^2$$
$$\phi_3^{(e)} = 3\left(\frac{\bar{x}}{h_e}\right)^2 - 2\left(\frac{\bar{x}}{h_e}\right)^3 \qquad \textbf{(D13)}$$
$$\phi_4^{(e)} = -\bar{x}\left[\left(\frac{\bar{x}}{h_e}\right)^2 - \frac{\bar{x}}{h_e}\right]$$

an approximation of the unknown deformation can be made. The bar over variable x means that the coordinate system was transformed from global coordinate into **local** coordinate system where element length l is between 0 and 1. The deflection w is approximated by

$$w(x) = \sum_{j=1}^{4} u_j \phi_j^{(e)} \qquad \textbf{(D14)}$$

where u_1=deflection at end 1
u_2=rotation at end 1
u_3=deflection at end 2
u_4=rotation at end 2

which leads to following form of eq. 11:

$$0=\sum_{j=1}^{4}\left(\int_{x_e}^{x_{e+1}} b\frac{d^2\phi_i}{dx^2}\frac{d^2\phi_j}{dx^2}\right)u_j^{(e)}dx+\int_{x_e}^{x_{e+1}}\phi_i f dx-Q_i^{(e)}$$

$$or \qquad \textbf{(D15)}$$

$$\sum_{j=1}^{4}K_{ij}^{(e)}u_j^{(e)}-F_i^{(e)}=0$$

where

$$K_{ij}^{(e)}=\int_{x_e}^{x_{(e+1)}} b\frac{d^2\phi_i}{dx^2}\frac{d^2\phi_j}{dx^2}dx$$

$$\textbf{(D16)}$$

$$F_i^{(e)}=-\int_{x_e}^{x_{e+1}}\phi_i f dx+Q_i^{(e)}$$

$K_{ij}^{(e)}$ is an element stiffness matrix, $F_i^{(e)}$ is a load vector and $Q_i^{(e)}$ are shear forces and moments applied at node i. The stiffness matrix $K_{ij}^{(e)}$ represents the known 4x4 matrix for b being independent on coordinate x. Vector $\{F^{(e)}\}$ is a vector of generalized forces represented by statically equivalent forces and moments due to the uniformly distributed load over the element. The 4x4 stiffness matrix can be expanded into 3-dimensional space and superimposed over the truss and torsional stiffness matrix (Laursen, 1988; Kohnke, 1989):

$$
\begin{bmatrix}
\frac{AE}{l} & & & & & & & & & & & \\
0 & \frac{12EI_z}{l^3} & & & & & & & & & & \\
0 & 0 & \frac{12EI_y}{l^3} & & & & & & & & & \\
0 & 0 & 0 & \frac{GJ}{l} & & & & & & & & \\
0 & 0 & \frac{-6EI_y}{l_2} & 0 & \frac{4EI_y}{l} & & & & & & & \\
0 & \frac{6EI_z}{l^2} & 0 & 0 & 0 & \frac{4EI_z}{l} & & & & & & \\
\frac{AE}{l} & 0 & 0 & 0 & 0 & 0 & \frac{AE}{l} & & & & & \\
0 & \frac{-12EI_z}{l^3} & 0 & 0 & 0 & \frac{-6EI_z}{l^2} & 0 & \frac{12EI_z}{l^3} & & & & \\
0 & 0 & -\frac{12EI_y}{l^3} & 0 & \frac{6EI_y}{l^2} & 0 & 0 & 0 & \frac{12EI_y}{l^3} & & & \\
0 & 0 & 0 & -\frac{GJ}{l} & 0 & 0 & 0 & 0 & 0 & \frac{GJ}{l} & & \\
0 & 0 & \frac{-6EI_y}{l^2} & 0 & \frac{2EI_y}{l} & 0 & 0 & 0 & \frac{6EI_y}{l^2} & 0 & \frac{4EI_y}{l} & \\
0 & \frac{6EI_z}{l^2} & 0 & 0 & 0 & \frac{2EI_z}{l} & 0 & \frac{-6EI_z}{l^2} & 0 & 0 & 0 & \frac{4EI_z}{l}
\end{bmatrix}
\qquad \textbf{(D17)}
$$

where I_y, I_z=moments of inertia around local y and z-axes

l=length of the element

J=polar moment of inertia

G=shear modulus

Plate Element

Governing equation for an orthotropic plate can be written in the form (Lekhnitskii, 1986):

$$D_{11}\frac{\partial^4 w}{\partial x^4}+2D_3\frac{\partial^4 w}{\partial x^2\partial y^2}+D_{22}\frac{\partial^4 w}{\partial y^4}=f(x,y) \qquad \textbf{(D18)}$$

where the variables were defined earlier.
Knowing that

$$M_{xx}=-\left(D_{11}\frac{\partial^2 w}{\partial x^2}+\nu_{12}D_{22}\frac{\partial^2 w}{\partial x^2}\right)$$

$$M_{yy}=-\left(D_{22}\frac{\partial^2 w}{\partial y^2}+\nu_{21}D_{11}\frac{\partial^2 w}{\partial x^2}\right) \qquad \textbf{(D19)}$$

$$M_{xy}=-2D_{12}\frac{\partial^2 w}{\partial x\partial y}$$

and denoting

$$D_3=\nu_{21}D_{11}+2D_{12} \qquad \textbf{(D20)}$$

and

$$D_3=\nu_{12}D_{22}+2D_{12} \qquad \textbf{(D21)}$$

we obtain

$$-\frac{\partial^2 M_{xx}}{\partial x^2}-2\frac{\partial^2 M_{xy}}{\partial x\partial y}-\frac{\partial^2 M_{yy}}{\partial y^2}=f(x,y) \qquad \textbf{(D22)}$$

Where M_{xx} = bending moment around y-axis
M_{yy} = bending moment around x-axis
M_{xy} = torsional moment
$f(x,y)$ = transversely distributed load

Multiplying eq.(21) by weight function v and using Gauss-Green theorem to carry the integration by parts we obtain (Kikuchi, 1985)

$$\int_{\Omega} \{M_{xx}(-\frac{\partial^2 v}{\partial x^2}) + 2M_{xy}(-\frac{\partial^2 v}{\partial x \partial y}) + M_{yy}(-\frac{\partial^2 v}{\partial y^2})\} \, d\Omega =$$
$$= \int_{\Omega} fv d\Omega - \int_{\Gamma} \{(-\frac{\partial M_{xx}}{\partial x} - \frac{\partial M_{yx}}{\partial y}) n_x + (-\frac{\partial M_{xy}}{\partial x} - \frac{\partial M_{yy}}{\partial y}) n_y\} \, v \, d\Gamma - \quad \textbf{(D23)}$$
$$- \int_{\Gamma} \{(M_{xx}n_x + M_{yx}n_y) \frac{\partial v}{\partial x} + (M_{xy}n_x + M_{yy}n_y) \frac{\partial v}{\partial y}\} \, d\Gamma$$

Where right hand side represents boundary conditions in terms of normal forces on moments specified on the boundary Γ and body forces over the volume Ω, and the left hand side is the expression from which a stiffness matrix is derived Knowing that

$$Q_x = \frac{\partial M_{xx}}{\partial x} + \frac{\partial M_{yx}}{\partial y} \qquad Q_y = \frac{\partial M_{xy}}{\partial x} + \frac{\partial M_{yy}}{\partial y} \qquad \textbf{(D24)}$$
$$M_x = M_{xx}n_x + M_{yx}n_y \qquad M_y = M_{xy}n_x + M_{yy}n_y$$

Where Q_x, Q_y M_x, M_y are surface tractions on boundary Γ Also

$$\overline{K}_{xx} = -\frac{\partial^2 v}{\partial x^2}, \quad \overline{K}_{xy} = \overline{K}_{yx} = -\frac{\partial^2 v}{\partial x \partial y}, \quad \overline{K}_{yy} = \frac{\partial^2 v}{\partial y^2} \qquad \textbf{(D25)}$$

in which quantities K_{xx}, K_{yy}, and K_{xy} represent virtual curvatures. Using eqn's. (24) and (23), eq. (22) can be expressed as

$$\int_{\Omega}(M_{xx}\overline{K}_{xx}+M_{xy}\overline{K}_{xy}+M_{yy}\overline{K}_{yy})\,d\Omega = \int_{\Omega} fv d\Omega + \int_{\Gamma}(Q_x n_x+Q_y n_y)\,v d\Gamma + \int_{\Gamma}\left(M_x\frac{\partial v}{\partial x}+M_y\frac{\partial v}{\partial y}\right)d\Gamma \qquad \text{(D26)}$$

Equation (25) can be rewritten more simply

$$\int_{\Omega} M_{ij}\overline{K}_{ij}d\Omega = \int_{\Omega} qv d\Omega + \int_{\Gamma} Q_i n_i v d\Gamma + \int_{\Gamma} M_i v_{,i} d\Gamma \qquad \text{(D27)}$$

At this point, interpolating polynomials must be chosen to approximate deflections w and weight function v.

The stiffness matrix can have a different form depending on the element shape and number of nodes. Each node has three degree of freedom (one translation and two rotations). The discussion about the choice of shape functions can be found elsewhere (Batoz et al, 1980; Bathe, 1982; Zienkiewicz, 1982).

Zienkiewicz (1982) presented the derivation based on the minimization of the total potential energy which can be more simply written as

$$\boldsymbol{K}^{(e)} = \int_{volume} \boldsymbol{B}^{T}\boldsymbol{D}\boldsymbol{B}dxdy$$

$$\boldsymbol{B}=\boldsymbol{L}\,\boldsymbol{N}$$

$$\boldsymbol{L}=\begin{bmatrix} \dfrac{-\partial^2}{\partial x^2} \\ \dfrac{-\partial^2}{\partial y^2} \\ 2\dfrac{\partial^2}{\partial x \partial y} \end{bmatrix} \qquad \text{(D28)}$$

where **N** = vector of the shape functions
L = operator defined above
D = elasticity matrix having form

$$\boldsymbol{D} = \begin{bmatrix} D_{11} & D_{12} & 0 \\ D_{21} & D_{22} & 0 \\ 0 & 0 & D_{33} \end{bmatrix} \qquad \textbf{(D29)}$$

which is the known matrix representing properties of the orthotropic continua in two dimensions.

With three degrees of freedom for each node (one translation, w and two rotations θ_x, and θ_y) 12x12 stiffness matrix will be obtained for four-node element and 9x9 matrix for three-node element.

2-D Elasticity Element

The two-dimensional stress state can be described by following equation

$$\sigma_{ij,j} + f_i = 0 \qquad \textbf{(D30)}$$

which is the equation of motion with zero inertia force. For two dimensions, equation (29) can be expanded

$$\frac{\partial \sigma_x}{\partial x} + \frac{\partial \sigma_{xy}}{\partial y} + f_x = 0$$

$$\frac{\partial \sigma_{xy}}{\partial x} + \frac{\partial \sigma_y}{\partial y} + f_y = 0 \qquad \textbf{(D31)}$$

where σ_x=normal stress in x-direction

σ_y=normal stress in y-direction

σ_{xy}=shear stress

f_x=x-component of body force

f_y=y-component of body force

Multiplying eq. (30) by weight functions w_1 and w_2 and integrating over the whole domain variational form can be obtained

$$0=\int_{\Omega_e} w_1 \left[\frac{\partial \sigma_x}{\partial x}+\frac{\partial \sigma_{xy}}{\partial y}+f_x\right] dxdy$$

$$0=\int_{\Omega_e} w_2 \left[\frac{\partial \sigma_{xy}}{\partial x}+\frac{\partial \sigma_y}{\partial y}+f_y\right] dxdy \qquad \textbf{(D32)}$$

Integrating by parts

$$0=\int_{\Omega_e} \left[-\frac{\partial w_1}{\partial x}\sigma_x-\frac{\partial w_1}{\partial y}\sigma_{xy}+w_1 f_x\right] dxdy+ \oint_{\Gamma_e} w_1 \left[n_x\sigma_x+n_y\sigma_{xy}\right] dS \qquad \textbf{(D33)}$$

where line integral $\oint$ represents surface tractions and n_x and n_y are x- and y-components of normal to the boundary Γ_e. Similarly for second equation

$$0=\int_{\Omega_e} \left[-\frac{\partial w_2}{\partial x}\sigma_{xy}-\frac{\partial w_2}{\partial y}\sigma_y+w_2 f_x\right] dxdy+ \oint_{\Gamma_e} w_2 \left[n_x\sigma_{xy}+n_y\sigma_y\right] dS \qquad \textbf{(D34)}$$

Approximating unknown displacements in x- and y-direction (u and v) by interpolation functions

$$u=\sum_{j=1}^{n} u_j\phi_j(x,y)$$
$$v=\sum_{j=1}^{n} v_j\phi_j(x,y) \qquad \textbf{(D35)}$$

and using constitutive equations relating stress and strain

$$\begin{matrix}\sigma_x\\ \sigma_y\\ \sigma_{xy}\end{matrix} = \begin{bmatrix} C_{11} & C_{12} & 0\\ C_{12} & C_{22} & 0\\ 0 & 0 & C_{33}\end{bmatrix} \begin{matrix}\epsilon_x\\ \epsilon_y\\ \epsilon_{xy}\end{matrix} \qquad \textbf{(D36)}$$

where C_{ij} is the elasticity matrix and ϵ_x, ϵ_y, and ϵ_{xy} are strains defined as

$$\epsilon_x=\frac{\partial u}{\partial x}, \qquad \epsilon_y=\frac{\partial v}{\partial y}$$
$$2\epsilon_{xy}=\frac{\partial u}{\partial y}+\frac{\partial v}{\partial x} \qquad \textbf{(D37)}$$

equations (32) and (33) can be written as

$$0=\int_{\Omega^e}\left[\frac{\partial\phi_i}{\partial x}\left(C_{11}\frac{\partial u}{\partial x}+C_{12}\frac{\partial v}{\partial y}\right)+\frac{\partial\phi_i}{\partial y}C_{33}\left(\frac{\partial u}{\partial y}+\frac{\partial v}{\partial x}\right)-\phi_i f_x\right]dx\,dy-\oint_{\Gamma^e}\phi_i t_x dS$$
$$0=\int_{\Omega^e}\left[\frac{\partial\phi_i}{\partial x}C_{33}\left(\frac{\partial u}{\partial y}+\frac{\partial v}{\partial x}\right)+\frac{\partial\phi_i}{\partial y}\left(C_{12}\frac{\partial u}{\partial x}+C_{22}\frac{\partial v}{\partial y}\right)-\phi_i f_y\right]dx\,dy-\oint_{\Gamma^e}\phi_i t_y dS \qquad \textbf{(D38)}$$

in which t_x and t_y are tractions having the form:

$$t_x=n_x\sigma_x+n_y\sigma_{xy} \qquad t_y=n_x\sigma_{xy}+n_y\sigma_y \qquad \textbf{(D39)}$$

Collecting terms containing u and v following expressions can be obtained

$$\begin{bmatrix} [K^{11}] & [K^{12}] \\ [K^{21}] & [K^{22}] \end{bmatrix} \begin{Bmatrix} \{u\} \\ \{v\} \end{Bmatrix} = \begin{Bmatrix} \{f^1\} \\ \{f^2\} \end{Bmatrix} + \begin{Bmatrix} \{t^1\} \\ \{t^2\} \end{Bmatrix} \tag{D40}$$

in which

$$\begin{aligned} K_{ij}^{11} &= \int_{\Omega^e} \left(\frac{\partial \phi_i}{\partial x} C_{11} \frac{\partial \phi_j}{\partial x} + \frac{\partial \phi_i}{\partial y} C_{33} \frac{\partial \phi_j}{\partial y} \right) dxdy \\ K_{ij}^{12} &= \int_{\Omega^e} \left(\frac{\partial \phi_i}{\partial x} C_{12} \frac{\partial \phi_j}{\partial y} + \frac{\partial \phi_i}{\partial y} C_{33} \frac{\partial \phi_j}{\partial x} \right) dxdy \\ K_{ij}^{22} &= \int_{\Omega^e} \left(\frac{\partial \phi_i}{\partial x} C_{33} \frac{\partial \phi_j}{\partial x} + \frac{\partial \phi_i}{\partial y} C_{22} \frac{\partial \phi_j}{\partial y} \right) dxdy \end{aligned} \tag{D41}$$

are the submatrices of the element stiffness matrix and

$$\begin{aligned} f_i^1 &= \int_{\Omega^e} f_x \phi_i dxdy \qquad f_i^2 = \int_{\Omega^e} f_y \phi_i dxdy \\ t_i^1 &= \oint_{\Gamma^e} t_x \phi_i dS \qquad t_i^2 = \oint_{\Gamma^e} t_y \phi_i dS \end{aligned} \tag{D42}$$

are distributed forces and surface tractions.

The size of the stiffness matrix is given by the element shape and shape functions used. Elements have two degrees of freedom at each node (displacement u and v) which leads to 6×6 and 8×8 stiffness matrix for triangular and rectangular element, respectively.